Newcastle University – School of Engineering

PhD Thesis

Design analysis of short neutral section through dynamic modelling of performance

John C Morris

Student number 120478279

September 2019

Abstract

UK railway overhead line electrification employs a feature known as 'short' neutral section which uses insulators spliced into the contact wire to separate the electrical phases, and they are known as a cause of reliability problems. This research proposes to develop, validate and apply a hitherto unexplored approach to studying short neutral section behaviour.

This research briefly initially examines the experience of British Rail with the introduction of the ceramic bead neutral section and its development during the 80s and 90s, and the subsequent introduction and development of a further proprietary type in the early 2000s, which is then assessed in detail.

Using information from Network Rail, the significant failures of the main types of neutral sections are examined over a 10 year period for which adequate data exists. European practice is briefly examined.

Current methods for analysing the interaction of pantograph and overhead lines are investigated, and the principles are adopted into a bespoke methodology implemented using proprietary software Ansys, rather than custom code as is current widespread practice. This methodology is constructed using finite element and multi-body principles and is successfully validated against 'benchmarks', in accordance with current European practice and standards.

Mathematical models of a neutral section are constructed using their physical characteristics and data captured in lab tests, and the behaviour against real UK pantographs is simulated using this method. Findings are again successfully validated against real line test data. Using the result, the sensitivity of the neutral section performance to particular parameters of its construction is tested, allowing opportunities for optimisation to be identified, and improvements proposed, successfully demonstrating a (previously untried) validated methodology for examining the neutral section problem. This work has answered all its research questions.

Acknowledgements

I'd like to thank:

Peter Dearman (then at Network Rail) for his suggestion and support for this particular research in the first place.

Richard Stainton, Phil Doughty, Anthony Roache, Geoff Norris and Andy Mackintosh of Network Rail for support, advice and access to internal Network Rail data.

Shamil Velji of RSSB.

Chris Bryan of Furrer + Frey, UK, and Charles Lateu-Smith of Network Rail, for access to Old Dalby test run data. Michael Kolbe and Jorg Heland of DBST for help with understanding the data.

Mark Robinson, Roberto Palacin, Cristian Ulianov, Peter Gosling and Jack Hale of Newcastle University School of Engineering for support and assistance.

Adam Beagles and Sam Hayes of Sheffield University, and Joao Pombo and Pedro Antunes of Huddersfield University.

Albrecht Brodkorb and Axel Schmieder of Siemens, Germany.

Paul Culnane of Arthur Flury, UK, for assistance

Roman Kovalev and Gennady Mikheev of Computational Mechanics Ltd, Bryansk, Russia.

For information on European practice: Guido v Kalsbeek, Jiri Simanek, Serdar Aydin, Daniel Davidovic, Branislav Jelkic, Andreja Mijalcic, Marco Filipe do Carmo Pereira dos Santos, Fernando Ribeiro Vendas, Danny Richards, Tsvetan Tomov.

Picture credits:

Noel Dolphin for Figure 3.14

Daniel Beardsmore for Figure 3.22

Barry Duffin for Figure C.2

Table of contents

List of Figures

List of Tables

Glossary

This is a selected glossary of specialist acronyms, terms and abbreviations used in this thesis. For a full set of definitions of rail electrification terms, see the International Electrotechnical Vocabulary (IEV) IEC 60050, chapter 811 Electric Traction, available online as 'Electropedia' at http://www.electropedia.org/iev/iev.nsf/index?openform&part=811.

A note on terminology

In the field of railway electrification different terms are used in UK, European and American English. In particular the term for overhead line equipment is variously OLE (and occasionally, and inaccurately, OHE or OHLE) in the UK, OCL (Overhead Contact line, mostly European) and 'Catenary' (mostly North American).

This latter term 'catenary' is also used in the UK to refer to the upper or supporting wire of the OLE, whereas in N. America and elsewhere internationally, this wire is known as a 'messenger'.

Given the ambiguities possible with these terms, together with the usage later in the thesis of the subscript 'c' to denote parameters associated with the contact wire, for the purposes of this thesis I have chosen to adopt the usage 'messenger' for the upper or supporting wire, and 'OCL' for the complete overhead line equipment.

It should be noted however that the other terms referred above are used variously throughout the works referenced in the text (including their titles), and their interchangeability should be acknowledged. Their meaning should be clear from the context.

ac	**Alternating current**	
AF	**Arthur Flury**	Swiss OCL component manufacturer http://www.aflury.ch/en/Default.aspx
APT	**Advanced Passenger Train**	British Rail initiative in late 1970s to develop a fast train for use on conventional lines, using tilting technology
BICC	**British Insulated Callender's Cables**	British manufacturer of OCL systems and components
BR	**British Rail**	Pre-privatisation (1995) UK rail network operator
	Brecknell Willis	British manufacturer of pantographs
CB	**Ceramic bead**	
CLC	**Cenelec**	European standardisation body responsible for standards in the electrotechnical field www.cenelec.eu
CW	**Contact wire**	
DB	**Deutsche Bahn**	German national railway operator and infrastructure owner
DBST	**Deutsche Bahn Systemtechnik**	DB Systemtechnik is the engineering office of DB, including particularly testing and measuring of overhead contact lines https://www.db-systemtechnik.de/dbst-en
dc	**Direct current**	
DfT	**Department for Transport**	

DNO	**Distribution network operator**	Part of the UK electricity supply system
DSM	**Dynamic simulation method**	Numerical method that uses a fixed set of input parameters describing a pantograph/overhead contact line system to calculate a set of output values representative of the dynamic behaviour of that system
EN	**European Standard**	
ENE TSI	**Energy TSI**	The TSI for the Energy subsystem
ERA	**European Railway Agency** **"the Agency"**	An agency of the European Union set up to create an integrated railway area by reinforcing safety and interoperability. From June 2016, following the entry into force of the technical pillar of the 4th EU Railway Package, the European Union Agency for Railways replaces and succeeds the European Railway Agency. http://www.era.europa.eu
FEM	**Finite Element Method**	A numerical technique for partial differential equations
F+F	**Furrer + Frey**	Swiss OCL system manufacturer, supplier and installer. Supplier to Network Rail of Series 1 OCL. https://www.furrerfrey.ch/en.html

	Future Railway	A collaboration between Network Rail and RSSB, established to support innovation in the delivery of the Rail Technical Strategy. It has cross industry support through the Technical Strategy Leadership Group. http://www.rssb.co.uk/future-railway-programme
GWEP	**Great Western Electrification Programme**	
IEP	**Inter City Express Programme**	Train procurement project managed by DfT, to provide new electric and bi-mode trains for East Coast and Great Western main lines.
MBS	**Multi-Body Systems**	The study of the dynamic behaviour of interconnected rigid or flexible bodies
N/S	**Neutral section**	
NR	**Network Rail**	Post-privatisation UK rail network operator
OCL	**Overhead Contact Line**	Alternative (mainly European) term for Overhead Line Equipment
ODTT	**Old Dalby Test Track**	Former name of Melton Rail Innovation & Development Centre, a Network Rail test facility in Leicestershire https://www.networkrail.co.uk/industry-commercial-partners/research-development-technology/ridc/ridc-melton/

OLE	**Overhead Line Equipment**	
OLEMI	**Overhead Line Equipment Master Index**	A Network Rail index of all OCL design drawings
ORR	**Office of Rail & Road**	An essential element of the post-privatisation railway industry, which (inter alia) regulates the rail industry's health and safety performance, holds Network Rail and High Speed 1 (HS1) to account and ensures that the rail industry is competitive and fair. (Prior to 2015 known as Office of Rail Regulator) http://orr.gov.uk/
R&DD	**Research and Development Division**	Part of the old pre-privatisation British Rail structure
RIDC	**Rail Innovation & Development Centre**	RIDC Melton is a Network Rail owned test facility in Leicestershire, formerly known as Old Dalby
RSSB	**Rail Safety & Standards Board**	An essential element of the post-privatisation railway industry, responsible for standards for safety and safe interworking. www.rssb.co.uk
RTRI	**Railway Technical Research Institute**	Japanese Rail Research establishment
SNCF	**Société Nationale des Chemins de Fer Français**	French state owned rail network operator

SPARK		Joint RSSB and UIC webtool providing access to rail research material www.sparkrail.org http://www.railway-research.org/
TNO	**Transmission network operator**	Part of the UK electricity supply system
TOC	**Train Operating Company(s)**	Post-privatisation UK rail industry bodies responsible for running franchised rail services, or as an 'open access' operator
TSI	**Technical Specification for Interoperability**	Technical documents underpinning the EU Railway Interoperability Directive, issued mostly as EU Decisions or Regulations
TSLG	**Technical Strategy Leadership Group**	A cross industry body facilitated by RSSB
UIC	**Union Internationale Chemin de Fer**	International Union of Railways www.uic.org
UNIFE	**Union des Industries Ferroviaires Européennes**	European rail supply industry trade association www.unife.org
VSD		Vehicle System Dynamics (International Journal of Vehicle Mechanics and Mobility). Official journal of the International Association for Vehicle System Dynamics (IAVSD) Published by Taylor & Francis www.tandfonline.com

Chapter 1 Introduction

1.1 Summary

This chapter describes the background to the research topic and basic premise behind it.

1.2 Background

The Department for Transport published the document "Britain's Transport Infrastructure: Rail Electrification" in July 2009 (Department for Transport, 2009). This document set out the commitment of the UK Government to the installation of 25kV ac overhead line electrification on more of the rail network in Britain. This followed a period of time in which the extent of new electrification construction in the UK had been essentially stagnant, with little or no technical development work having been undertaken (especially in comparison to mainland Europe). An industry wide effort is presently under way to develop a modern technical approach to electrification, and to address issues of performance, reliability and affordability. This approach is articulated in the Network Rail electrification Route Utilisation Strategy (Network Rail, 2009) and the Rail Technical Strategy development led by RSSB and FutureRailway (*The Future Railway, The Industry's Rail Technical Strategy* 2012).[1]

1.3 Context of problem – reasons for research

Overhead line electrification utilises robust current collection from the overhead contact line (OCL) by the means of train roof mounted collectors ('pantographs'). The quality of the current collection is conventionally measured by 'loss of contact', but also includes other considerations such as damage to pantograph and OCL components, and, in the longer term, excessive wear and tear. Discrete features in the OCL, provided to effect particular types of electrical functionality, can present discontinuities which can disturb the quality of the current collection. One such discrete feature is a 'neutral section', which provides a phase break between live sections fed by different electrical phases.

[1] A full explanation of abbreviations, acronyms, and a description of the organisations acting in the railway industry is given in the Glossary.

Single phase ac power is (conventionally) taken from the grid at about 25 to 30 mile intervals, and mid-way between these points a neutral (or 'phase break') section is needed to separate the live sections fed by the different (electrical) phases. For reasons of providing operational flexibility, neutral sections are often situated at the supply point locations as well.

Two fundamentally different means of providing this neutral section functionality are available:

- A 'long' neutral section (or 'carrier wire') employs a series of conventional OCL overlaps to provide a relatively smooth transition for the pantograph from sections which are (electrically) live, to floating, and back to live sections again; it can be up to 200m long, and hence is difficult to locate conveniently in the congested UK rail infrastructure (Network Rail, 2013b);
- A 'short' neutral section is constructed from discrete insulating components inserted directly into the contact wire of the OCL, is typically less than 10m long, and hence can be located much more conveniently.

For these reasons short neutral sections of various types were developed in the very early days of UK electrification, and have been mostly used ever since. However experience indicates that they are notoriously unreliable, requiring more intensive maintenance than any other OCL feature, and perform poorly, leading to poor quality current collection and pantograph damage. This is a contributing factor to a widespread perception of the poor overall reliability of overhead line electrified railways. (Network Rail, 2014a)

It is thought that these (perceived and real) performance and reliability issues of neutral sections create a tendency to avoid or minimise their usage; to pursue feeding arrangements with longer electrical sections, and hence fewer neutral sections. Longer feeding sections lack operational flexibility, and need expensive 400kV grid connections. It is anticipated that shorter feeding sections, connected at 132kV (say) would be cheaper, and would facilitate greater operational flexibility (RSSB, 2011a; Department for Transport, 2012a). Additionally they would contribute to the potential implementation of electrical feeding scenarios using 'Smart Grid' type technology, where flexible feeding is made possible by a greater number of smaller feeding sections (Khayyamim *et al.*, 2015; MERLIN, 2015).

'Smart Grid' is a compound term used to describe a package of technologies but in this context would include micro-generation, energy capture and storage and intelligent real time switching between sources of power supply, using a wide implementation of modern telecommunications and IT infrastructure (Palfreyman and Hewings, 2013). It is generally seen as beneficial to electric railways, but the facility for switching between multiple sources of supply would imply the need for more frequent neutral sections (except where inverter fed systems are proposed).

Consequently it is thought that avoiding short neutral section usage is compromising better electrification installations, and therefore opportunities exist for benefits to be realised from developing a technical solution which imparts greater confidence.

In addition to the use of neutral sections as true 'phase breaks', in the recent work on reducing the cost of electrification, a number of studies (RSSB, 2011b; RSSB, 2011a; Department for Transport, 2012a) have highlighted the cost of rebuilding bridges in order to create suitable electrical clearances for the live OCL. Many of these suggest a form of 'discontinuous electrification' where the bridges remain in situ, but the problem of electrical clearances is addressed by running the OCL 'earthed' through the bridge, and the lead in and out of this earthed section is in fact an adaptation of the neutral section. This, if adopted, would create an additional demand for a reliable and robust neutral section design.

1.4 Areas of study – methodology of research

The aim of this research is to investigate if a methodology to identify a short neutral section with sufficiently improved performance and reliability can be proposed, which would enable its usage in flexible feeding scenarios, without any perceived performance penalty.

Historically neutral section designs have been developed based primarily on static analysis of their construction, function and performance. However, their behaviour in practice is affected mostly by dynamic issues, instigated by the energy inputs as the pantograph passes. It is proposed to re-evaluate the factors of neutral section design when considered in the context of current day techniques for dynamic simulation and analysis of pantograph/OCL interaction, and that these techniques might be brought to bear on the neutral section problems.

Neutral section design practice will be studied, predominantly from the UK, but with some consideration of overseas practice with emphasis on Europe. Types of UK short neutral sections used by Network Rail will be looked at, and their development and improvement as issues are identified and considered. Experience of their performance will be looked at to determine how successfully performance and reliability issues have been addressed, including the definition of performance criteria.

The necessary question of what the real performance criteria actually are, and how they should be measured, will be addressed. This will lead to questions of pantograph/OCL interaction, and, although this has been widely studied elsewhere, it is mostly concerned with 'open route'[2] situations, and it is thought very little attention has been given to the theoretical study of discrete features such as neutral sections.

This will involve research into current practices in modelling and measuring OCL pantograph interaction, and current work undertaken by various parties in conjunction with European high speed rail developments.

A significant amount of work has been undertaken recently in Europe in conjunction with the extension of high speed rail in Europe. As part of compliance with the requirements of the Interoperability Directive (EU, 2008), as transposed into UK law (*Railway (Interoperability) Regulations*, 2011), there is a regulatory need to assess current collection quality (i.e. the behaviour of the pantograph/OCL 'couple'), as defined in Technical Specifications for Interoperability (TSIs), and this has led to a greater interest in the understanding of this interface. (Further information on Interoperability and TSIs is given in Appendix A.)

The application of the multi-body dynamics modelling methods (often proprietary to manufacturers), currently used to model pantograph/OCL interaction forces for prediction of current collection quality, will be assessed for their applicability to studying neutral section performance and reliability. These techniques and methodologies may be useful to a greater or lesser degree to investigate the OCL/neutral section interaction.

It is anticipated that the dynamic influence of individual components, or features of the construction of the neutral section, can be identified, and options for tuning these

[2] That is, where there are no special features in the track or OCL, e.g. switches, crossings, overbridges, neutral sections, etc.

characteristics to contribute to an optimisation of performance and reliability can be proposed and verified. (Morris, 2013)

1.5 Prospects for benefits realisation and exploitation

Specific outcomes of this research are anticipated as:

- Analysis of short neutral section design characteristics in UK, Europe and elsewhere;
- Assessment of criteria used to assess pantograph/OCL interaction behaviour and reliability;
- Analysis of performance and reliability of short neutral sections;
- Influence of the neutral section design characteristics on performance and reliability;
- Assessment of dynamic analysis methods (multi-body and others) used to model forces for current collection quality prediction, and their applicability for studying neutral section performance and reliability;
- The results from analytical behaviour of a typical neutral section when subjected to dynamic analysis; and
- Proposals for areas of development to improve performance and reliability of short neutral sections.

The wider benefits to industry are anticipated as improvements to performance and reliability of short neutral sections, and hence whole life costs and attractiveness of electrified railways; shorter feeding sections in the electrified rail network, with accompanying flexibility, facilitating application of 'Smart Grid' technology; and finally, furnishing a methodology to assess other discrete features, e.g. crossovers, section insulators, overbridges, etc.

This has informed the development of the following research questions:

- Do short neutral sections have sufficiently similar characteristics that can be captured in a generic model?
- Can the current state of art methods for simulating pantograph/OCL interaction be adapted to study the neutral section behaviour?
- Can this simulation of behaviour be used to perform a parametric analysis on the neutral section?

- Could this parametric analysis identify any improvements to the form of the neutral section?

1.6 Structure of this thesis

This thesis is structured as follows. Chapter 2 contains a general description of railway electrification and the arrangements for power supply and overhead contact lines, insofar as is necessary background to the remainder of the thesis. Chapter 3 describes some history of the development of short neutral sections and the recent and current practice in the UK, and the performance history is discussed. Some reference to practice elsewhere in Europe is made. Chapter 4 introduces the techniques of pantograph/OCL dynamic interaction analysis, arriving at the current state of art. In Chapter 5 the development of a specific Ansys based pantograph/OCL dynamic simulation method is described, and its successful validation, in incremental steps, against current European Standards. Chapter 6 describes the creation of a model of the Arthur Flury single rod neutral section, currently in wide use on Network Rail, and its inclusion within the dynamic simulation method that has been developed. Chapter 7 describes a limited amount of parametric analysis carried out using this method, whereby certain characteristics of the neutral section are adjusted systematically with the intent of arriving at a 'theoretical' better performing version. One improvement of note is identified. Some practicalities of implementation are discussed. In Chapter 8 a summary of work done is provided, and a critical analysis of its execution is made. Some considerations for further work are included. Appendices A to D contain additional background detail.

Chapter 2 Overhead Line Electrification Background

2.1 Summary

This chapter describes briefly overhead line electrification and the function and characteristics of a neutral section within that, insofar as is necessary to understand the rest of this thesis.

This chapter introduces the concept of rail electrification, and then demonstrates how the 25kV overhead line system has become the dominant system at the present time, and for the foreseeable future. The physical characteristics of this system are described and explained (including that of the neutral section), introducing some of the technical constraints and issues, and, finally, demonstrating how an effective neutral section function is fundamental to the operation of this system. This therefore sets the focus of this research into its context.

2.2 Overhead line electrification

Rail electrification refers to the provision of a facility by which railway trains and vehicles are powered electrically, by means of an 'off-board' electric power supply (i.e. not an 'on-board' system such as batteries).

Thus an electric railway is characterised by the trackside electrical power supply equipment, and the means of transferring this power to the moving trains, typically by means of either overhead contact lines and train mounted pantographs, or ground level conductor rails and train mounted shoe-gear.

Consequently an electrified railway incorporates a significant amount of additional infrastructure over and above a railway where trains/vehicles are powered by self-contained on-board energy sources such as diesel, LPG or even steam (from coal).

2.3 Brief history of ac and dc electrification in UK and Europe

The earliest rail-ways were horse drawn, but it was the application of steam power to locomotives in the 1820s that caused the rapid expansion in railways to occur from that date onwards.

Proposals to replace steam with electric traction had been around since 1880s, in both the UK and continental Europe. A variety of ingenious methods were proposed and used to effect the supply of electricity from the trackside to the moving rail vehicles, gaining in sophistication as train speeds increased. But by the early 1900s two distinct forms had emerged; ground level conductor rails, with current being collected by shoe gear on the rail vehicle (bogie), and tensioned overhead contact lines, with the current being collected by roof-mounted bow collectors or pantographs (The IET, 2010).

The electrical voltages in use, both on trackside supply and on-board the vehicles, contributed to the practicability of both systems. Ground level conductor rail, being largely exposed, required lower voltages for safety. Overhead contact lines, being less accessible to persons, allowed higher voltages. And higher voltages meant lower currents for the same power, and hence smaller, lighter conductors, lower voltage drop and losses, and permitted longer electrical feeding lengths (i.e. the distance between trackside feeder points), reducing the amount of trackside electrical equipment required. This is the basis of the economic argument that ultimately governs the choice of system (The IET, 2010).

The balance of the economic arguments facing one or other of the fundamental systems changed due to developments in material science, particularly insulating materials and eventually the development of power semiconductors.

The lower voltages of conductor rail systems (~500-600V) fed directly into the early traction motors. The higher voltages allowed by overhead lines also fed directly into traction motors, up to the level of insulation afforded by the technology of the time. At voltages above this level, a transformation to a lower on board voltage was required. Some early locomotives used rotary converters for this purpose, but the need for on board transformers forced the higher voltage systems to adopt alternating current, which allowed these voltages to be used with (initially) dc traction motors of around 1,000V dc (The IET, 2010).

In the 1950s, electrification in the UK had resolved into two forms: 650V dc by conductor rail, mainly on the Southern Region lines, radiating south from London; and 1,500V dc overhead line systems, on the Great Eastern lines from London Liverpool St and Fenchurch St, and the Manchester - Sheffield - Wath trans-Pennine route.

By the late 1950s however, subsequent to successful trials and implementation in France, overhead electrification at 25,000V ac 50Hz (i.e. 'industrial frequency') was adopted for the UK for all new electrification (British Transport Commission, 1955). The 'difficult' development of the UK rail electrification policy is well described in Michael Duffy's technical history of electric traction (Duffy, 2003).

At the same point in Europe, significant strides had been taken for electrification, and significant amounts of 1,500V dc existed in France and Holland, 3,000V dc in Belgium, Spain, Italy and Eastern Europe, and a variety of systems in Germany and Scandinavia.

It might be thought that given the laws of physics and roughly equal economic circumstances, all the various railways in Europe would have converged on similar systems. But this isn't so. Many countries with extensive systems remained wedded to their 1,500/3,000V dc systems (due to the cost of conversion) whilst others, notably Germany, Austria and Switzerland adopted a 15,000V ac 16 $^{2}/_{3}$ Hz system, delivering the benefits of a higher transmission voltage, necessitating the use of transformers on the train, hence its being ac, with the benefit of the low frequency being suitable for dc series wound traction motors (Ch.1.2 of *15 kV AC railway electrification*, 2016; Kiessling *et al.*, 2016).

It is worth noting that no other European (or world) railway has adopted ground level conductor rail systems on such an extensive scale as the (quasi-main line) network as in UK. Even using shrouded side and bottom contact systems it is largely restricted to metro and urban rail networks. The restriction to lower voltages (~750V dc) was influential in the economic calculation (notwithstanding a few higher voltage systems such as 1,200V on Manchester - Bury in UK and in Hamburg, Germany).

The economic balance between the systems can be seen to be based upon where the transformer/rectifier from the ac distribution system was located (and consequently the quantum of such equipment needed).

Up until the 1990s the economic arguments for the systems went thus:

For a high voltage ac system:

transformer rectifiers on the train, to feed the traction motors

For a low voltage dc system:

transformer rectifiers on the trackside.

Consequently, for high voltage ac, the economic sensitivity was to numbers of trains, and for low voltage dc, to quantum of route miles. Therefore a system with low route mileage and high number of trains, such as a metro or urban system, favoured low voltage dc, and a system with long route length, but relatively fewer trains (such as East Coast or West Coast main line in UK) favoured high voltage ac.

Since the 1990s, and into the current century, the use of ac traction motors with modern solid state power electronics drives has distorted the balance even further. Now all trains, both ac and dc, have expensive and complex on board equipment, with the additional burden for dc systems of expensive and extensive trackside equipment as well. (The IET, 2010)

It is not surprising therefore that for the first time the conversion of UK's southern region third rail dc system to ac overhead line is being contemplated, and is supported by research undertaken by RSSB (RSSB, 2011c) for which a positive economic case is being made. Furthermore it is the case in UK that 650V dc third rail systems are out of favour on safety grounds, in fact the ORR policy, without actually prohibiting it, includes "… a presumption against the reasonable practicability of new-build or extended DC third rail in view of the safety requirements duty holders must satisfy in order to justify the use of third rail." (ORR, 2015b)

So, essentially by the turn of the century, European main line electrified railways resolved into three distinct systems:

- 25kV ac 50 Hz overhead line
- 15kV ac 16 $^{2}/_{3}$ Hz overhead line
- 1,500/3,000V dc overhead line

Other than extensions to the 650/750V dc system in the south and around Merseyside, in UK all new mainline electrification since 1959 has been of the 25kV ac overhead line system. Since that date approximately 5,000 single track kilometres of electrification (stkm) have been added to the network. The current Department for Transport (DfT) plans for the future include an extensive amount of electrification, approximately 2,750 stkm before 2019 (Department for Transport, 2009), to which a further 200 stkm by 2019 was added by the time the High Level Output Statement (HLOS) for Control Period 5 (Department for Transport, 2012c) was published, although some of this was later

'paused' and deferred into the next control period, CP6 (2019-2024) (Hendy, 2015) (Butcher, 2015)[3].

The DfT has determined against continued extension of the third rail dc system, on safety grounds (ORR, 2015b) except for some very closely defined exceptions, and so, in the UK, the future of main line rail electrification would seem to be ac overhead line.

2.4 Current 25kV ac OCL predominance in Europe

In mainland Europe the situation at present (given allowances for the validity dates of the information) is as shown on Table 3.1 in Chapter 3. AC electrification, of one form or another, accounts for approx. 60% of the networks, whilst the extension of electrification and new projects (particularly those for high speed) are virtually all 25kV or 15kV ac. (EU, 2017a; International Energy Agency, 2019)

2.5 Traction power supply systems

2.5.1 Background

This section describes the power supply and electrical feeding arrangements that are typical for a UK 25kV ac electrified railway.

Although in the early days of railway electrification power generating facilities were often owned and operated by the railway company, since the 1950s modernisation plan of British Rail and the widespread adoption of 25kV 50 Hz on British railways, supplies have been taken from the electricity supply industry, via the national grid. (The National Grid and the Central Electricity Generating Board - CEGB - having been set up in 1940.)

The national grid transmits electrical energy from a range of generating sources, at a range of voltages covering 66kV, 132kV, 275kV and 400kV. Electricity privatisation and de-regulation has altered some of the terminology used to describe the actors in the electricity generation, transmission and distribution field, and also adjusted the boundaries between them. Currently electricity transmission and distribution is handled by Transmission Network Operators (TNOs) and Distribution Network Operators (DNOs). TNOs typically operate the 275kV and 400kV networks, DNOs the

[3] The Railways Act 2005 requires the DfT to set targets for Network Rail, and monitor performance, against 5-year 'Control Periods', referred to as CP5, CP6 etc.

lower voltages. (Incidentally, in Europe, different values for standard transmission and distribution voltages are found.)

2.5.2 'Classic 25kV systems'

What follows below is a description of a typical classic 25kV arrangement in the UK. This arrangement is the basis for the major feeding design of an electrified railway on classic 25kV principles – it is aspirational and a 'target', and is adjusted to suit the particular conditions of route topography and other circumstances. For instance the joining and diverging of electrified routes require adjustment to the nominal scheme, as does the local availability of convenient TNO/DNO supplies at suitable voltages and suitable security and capacity.

A transmission or distribution network delivers at high voltage 3 phase. An electrified railway (conventionally) requires a single phase supply, and consequently a single phase supply is taken from/across two phases of the TNO/DNO supply. In order to provide relatively high redundancy, two separate circuits supplying two separate 25kV transformers are then provided. These transformers supply a 25kV 'busbar'.

The busbar is used to supply, via circuit breakers, the OCL for tracks going east and west (say) of the feeder station location. The east and west feeds are kept separate and so the schematic of a typical 2 track feeder station looks as shown in Figure 2.1 below.

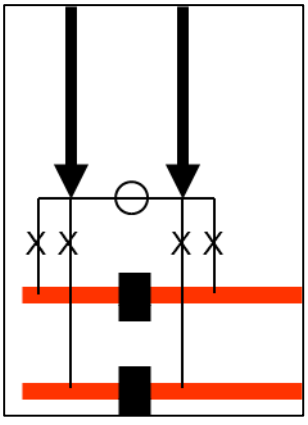

Figure 2.1 Schematic diagram of a 2-track 25kV feeder station showing the two incoming feeds (arrows), the track feeds and circuit breakers ('X's) and the neutral sections (black blocks)

In practice a 25kV feeder station is usually a secure compound containing a variety of both railway and TNO/DNO owned apparatus, consisting variously of outdoor and indoor equipment (the latter inside buildings or cubicles). The equipment inventory would include: supply transformers, circuit breakers, disconnectors, isolators, busbars,

current and voltage transformers, protection relays, meters, SCADA outstations, uninterruptible power supplies, etc.

The general arrangement of trackside switching stations and other facilities along a route is known as 'Major Feeding' and is captured on a Major Feeding Diagram (MFD). A major feeding diagram would typically indicate the routes electrified (not individual tracks) the feeder points, and the mid-points where neutral sections are located. An MFD would be used to establish 'alternate feeding' scenarios for when one (or more) of the feeders is unavailable. A typical example (taken from Great Western mainline electrification) is shown in Figure 2.2.

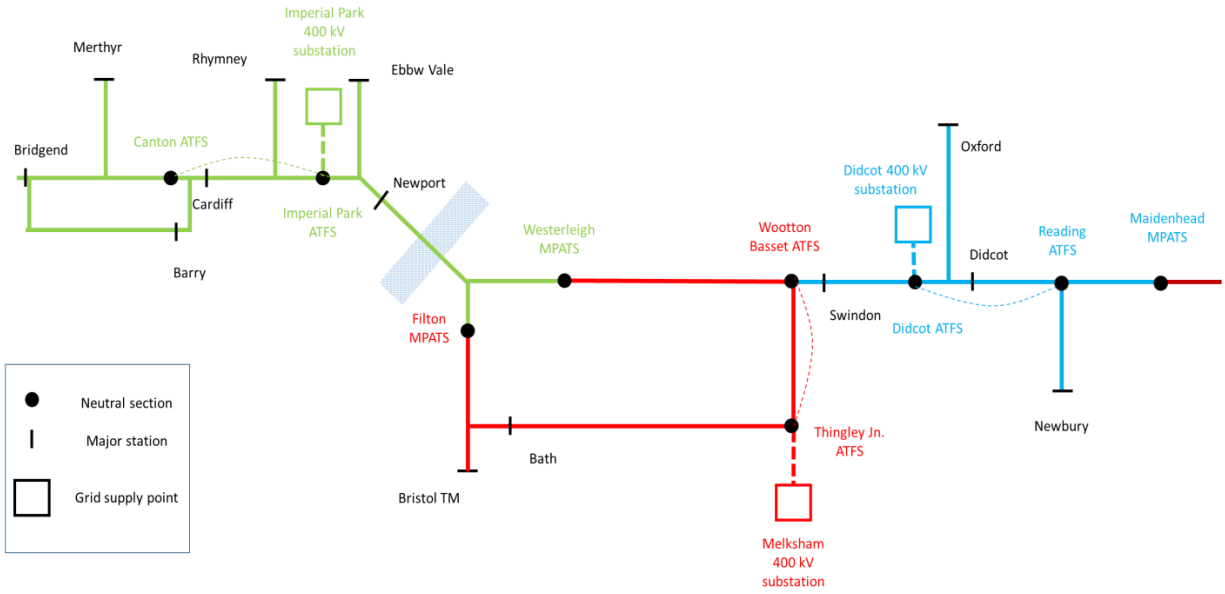

Figure 2.2 Typical major feeding diagram of a 25kV electrification scheme relating to Great Western Electrification Project (Network Rail, 2012d; Morris and Giddins, 2015).

Feeder stations might typically be spaced around 25 miles (40km) apart, although the actual spacing in practice is dependent upon both the availability of TNO/DNO power lines, and the power demands of the train and train service, which requires feeding arrangements which keep voltage regulation (and other technical criteria) within limits as required by TSIs (see Appendix A) and British and European standard BS EN 50163 (British Standards Institution, 2004).

The usual objective of major feeding design is to provide sufficient electrical energy to the nominated train service (timetable, train types, motoring pattern, and frequency), whilst maintaining prescribed limits of voltage regulation, unbalance, etc, all the while providing the ability to deal flexibly with perturbations and outages.

The supplies from each TNO/DNO source must be kept separate to avoid paralleling of the supply network, and comply with conditions of the supply, whether from the same

phase pairs or not. Consequently adjacent feeder stations can only feed either side of themselves up to a point nominally mid way between them, where an electrical break must be provided. This is usually known as a Mid-Point (switching station or track section cabin). The arrangement of a mid-point is shown in Figure 2.3 below, approximating to that of a feeder station without the incoming supplies.

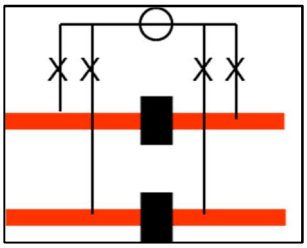

Figure 2.3 Schematic diagram of a 2-track 25kV mid-point switching station. Note the comparison to the feeder station in Figure 2.1 and the omission of the incoming feeds

To complete the picture, in between the feeder station and the Mid-point , an intermediate switching station (known as an Intermediate Track Sectioning Cabin) is often included, to provide the functions of: switching, sectioning, paralleling; and protection.

A typical arrangement is shown in Figure 2.4 below.

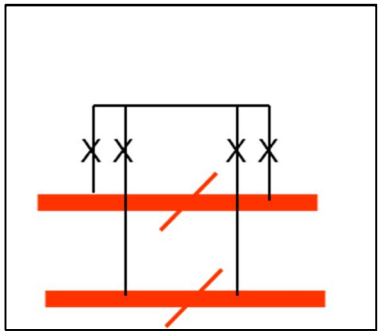

Figure 2.4 Schematic diagram of a 2-track 25kV Intermediate Track Sectioning Cabin Note the difference to the feeder station and mid-point, in that the neutral sections are replaced by overlaps (the oblique lines) which allow a pantograph to pass without interrupting collection of current.

Note that in an intermediate Track Sectioning Cabin (TSC), the bus section breaker is omitted entirely, and all four feeds (for the two track example shown) are 'commoned'. In addition, and significantly, the neutral section occurring in the feeder station and mid-point situations, is replaced by overlaps, which allow the pantograph to experience continuous current collection as it transits.

Putting all this together, the schematic for a typical feeder station to feeder station section of two track railway will look like as shown in Figure 2.5 below:

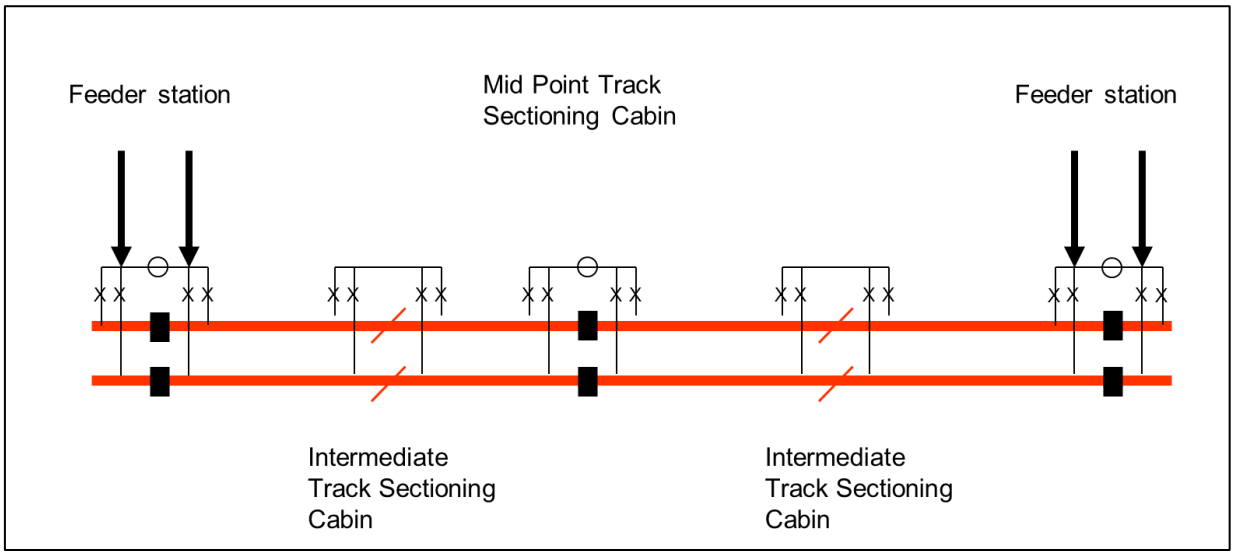

Figure 2.5 Schematic detail of a 25kV major feeding diagram, showing the disposition of Feeder Stations, Mid-point TSC and Intermediate TSC over a feeder station to feeder station length (approx. 25 miles), and the location of neutral sections (black blocks)

The remaining detail to be addressed is not part of the trackside system, but is the OCL. The OCL at the switching stations must replicate the functionality of the switching station, but at the same time it must allow the smooth, uninterrupted passage of pantographs.

At intermediate locations, this can be accommodated with an 'insulated overlap', allowing smooth passage of the pantograph, with facility to pass from one electrical section to another, but maintaining continuity of current collection, as contact with the next section is made before contact with the last section is broken (see further detail in section 2.7).

At mid-points or feeder stations however, this continuity of current collection cannot be maintained, as it would (momentarily) connect the electrical supplies derived from different TNO/DNO supplies, and hence a distinct electrical 'break' must be provided.

This is achieved through a particular discrete piece of OCL called a phase-break section or more commonly a 'neutral section' (N/S). This effectively consists of insulated pieces inserted into the contact wire, along which a pantograph can run (without damage) but experiencing a break in current collection(see Figure 2.6). For security, two such insulators are provided in sequence, separated by an earthed section between. Typically in the UK, (but less prevalent on mainland Europe) at the same time, track side transponders trigger on board receivers on the train to open the train main circuit

breaker and hence it draws no current whilst passing through the NS. This is known as automatic power control (APC).

A neutral section is also used for system separation sections. These occur where two different electrical systems exist either side of it, either different voltages/frequencies (e.g. 25kV 50 Hz and 15kV 16 $^{2}/_{3}$ Hz) or for administrative or billing purposes (e.g. at a national border or rail network ownership boundary).

Fuller details of the specific characteristics of overhead line equipment features are given in section 2.7 within this chapter.

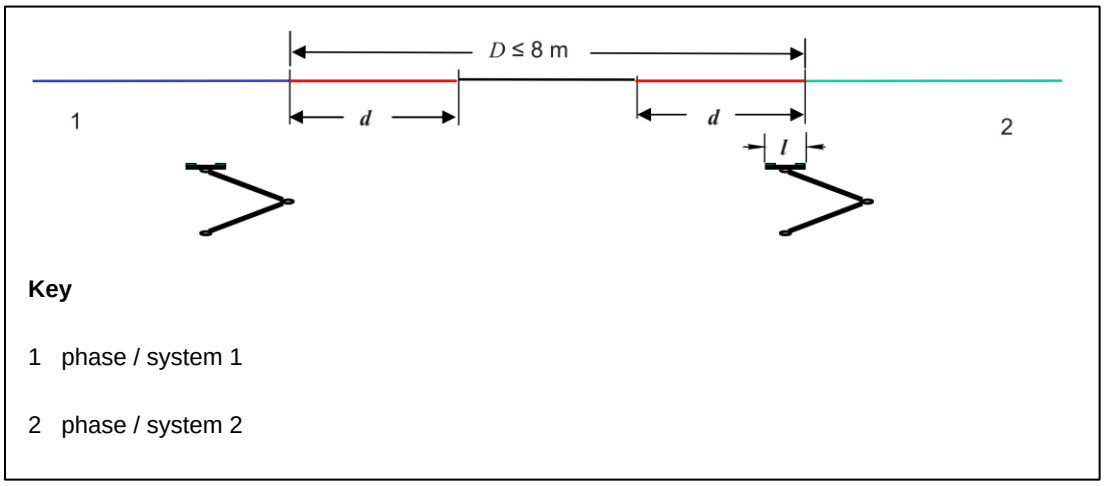

Figure 2.6 Graphic of a neutral section electrical schematic, from BS EN 50367 (British Standards Institution, 2012b). The dimensions 'D' and 'd' are specified such that locomotives with two pantographs raised can transit the neutral section safely.

Having passed through the train's transformer, the electric current is returned to the feeder station via the running rails. The low voltage (LV) terminal of the supply transformer secondary is connected to earth at each feeder station.

2.5.3 The return circuit

The return circuit, and the earthing and bonding regime that goes with it to provide safety in the rail environment, is a particularly complex aspect of 25kV electrification, but as it is not relevant to the particular issues being addressed here, no detail is presented. However, to appreciate the difference between the 'classic' and more recently developed 'auto-transformer' systems, it is first necessary to describe some aspects of the booster transformer and return conductor (BT/RC) system.

The Booster Transformer and Return Conductor (BT/RC) system is an attempt to address the issues associated with electromagnetic interference in lineside telecommunications and signalling circuits caused by the 'rail return' aspect of the conventional power supply system described above.

In this BT/RC system, in order to supplement the return current path via the running rails, a return conductor – a conductor supported on the OCL masts at height – is connected in parallel to the running rails. In order to 'encourage' the current (or at least a very large part of it) to use this parallel return path in preference to the running rails, a series of Booster Transformers are used to draw the current from the rails, and into the Return Conductor.

A Booster Transformer is a 1:1 ratio current transformer, whose primary is in series with the OCL 25kV circuit, and secondary is in series with the Return Conductor. Hence the 25kV line currents induce an equal and opposite current in the RC, this being the return current, and so causing this current to be drawn from the rails and into the RC.

Conventionally BTs are installed on UK networks at about 2 mile intervals, and connections to the RC to the rails at points approximately midway between the BTs.

This is an electrical feature of the power supply (and return circuit) but its relevance to the OCL (and current collection) comes from the need for the BT primary to be in series with the 25kV circuit. This means that a physical break in the electrical continuity of the OCL must be created, and around which the BT primary is connected. The electrical schematic of this is shown in Figure 2.7 below, which illustrates the supply current path to, and return path from, the train, via the OCL, rails and BT/RC.

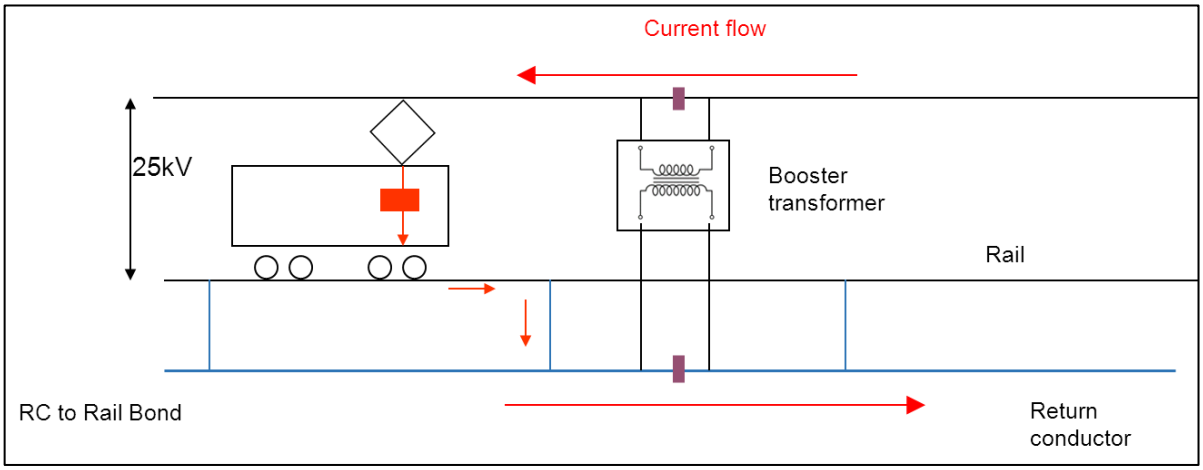

Figure 2.7 Graphic of a Booster Transformer and Return Conductor system showing current flow to and from trains thorough OCL, rails and BT/RC

The actual construction of the electrical break in the OCL is usually implemented by means of an 'insulated overlap', which has been described above in relation to the intermediate track sectioning sites and their connections to the OCL.

An advantage of the BT/RC system is that it removes return current from the running rails, and provides a level of immunisation (from induced voltages) to lineside

telecommunications and signalling circuits (in copper at least). The disadvantage is that the insertion of the BTs into the circuit has a significant impact on increasing impedance of the system, contributing to increased voltage drop and electrical losses.

2.5.4 'Auto-transformer' systems

A system that has gained favour across Europe (and the world) in the last 25 years was proposed by the introduction on the early French high speed LGV (Ligne a Grand Vitesse) lines, and now is common for 25kV high speed lines, and is being more widely applied across 'conventional' lines as well in the UK, is the 'Auto-transformer' system.

The system has the advantage of effectively utilising a 50kV transmission voltage from the supply point/feeder by the use of 'negative' 25kV feeders along the trackside, carried on the masts, which give the effective 50kV when used against the 'positive' 25kV in the OCL. For this reason the system is also sometimes known as the 25-0-25 system (the rail return being the '0' element of that nomenclature). Compared with a classic 25kV system this has the advantage of halving the currents, reducing interference, or of doubling (virtually) the power able to be transmitted at the same currents, with the overriding feature that the train still 'sees' 25kV at the pantograph, and so is completely inter-workable with classic lines.

The disadvantage is the provision of the 25kV parallel negative feeders, the provision of the autotransformer stations along the track (at 5 or 10km intervals) and the significantly higher (virtually double) inventory of equipment and plant in the trackside switching stations, i.e. both positive and negative busbars are required, with associated circuit breakers, disconnectors etc., see Figure 2.8. Some of the AT system feeder station sites can be extremely large, as a consequence; for example a proposed site for HS2[4] is planned at approximately 175m by 125m (Howard, 2013).

The ability of the AT system's effective 50kV transmission voltage to transmit greater power allows for the use of a fewer number of higher rated feeder stations. Typically feeder stations may be spaced at 40 mile intervals rather than the 25 miles seen in classic systems, illustrated by the current proposals for Great Western electrification in

[4] HS2, High Speed 2, is a project to construct a new high speed (350 km/h) railway from London to initially Birmingham, and ultimately Manchester and Leeds in the UK. Planned to open in stages between 2026 and 2033

UK , where the whole of the route from London Paddington to Cardiff is fed from just 4 supply points (Hewings, 2015).

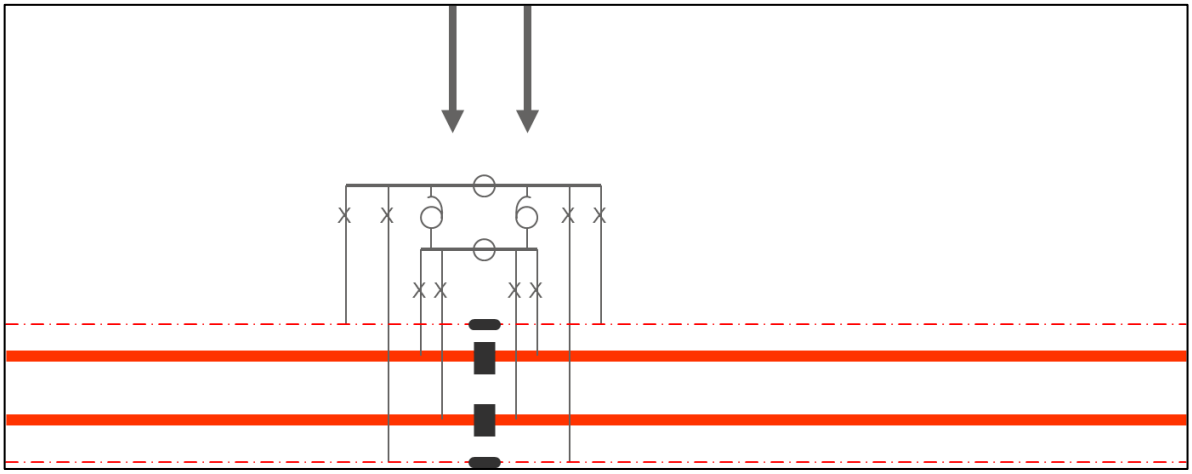

Figure 2.8 Schematic of a 25kV AT system feeder station, showing greater amount of equipment compared to a classic 25kV feeder station

The necessarily more complex major feeding arrangement of an AT system is shown (typically) in Figure 2.9 below. This may be compared to that for the classic system, shown in Figure 2.5 above.

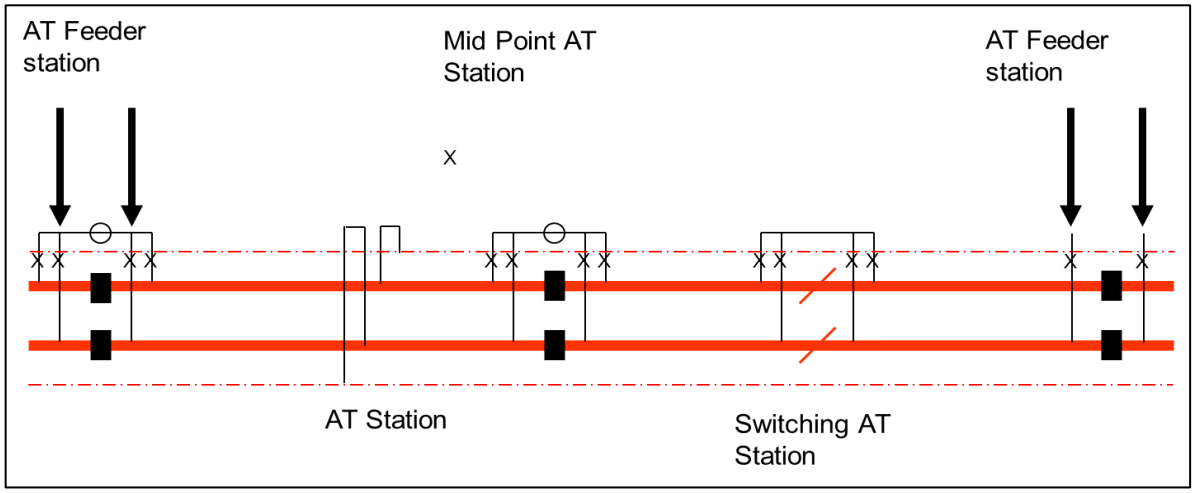

Figure 2.9 Schematic of a 25kV AT system major feeding diagram, showing the disposition of ATFS, MPATS and ATS over a FS to FS length (approx. 40 miles), and the parallel -25kV feeder (dotted)

The terminology for an AT system's components is adopted from the classic system, thus there is:

ATFS	Autotransformer Feeder Station
MPATS	Mid-Point Autotransformer Site
ATS	Autotransformer Site

As with the classic system, feeder stations and mid-points are equipped with neutral sections to allow an 'alternate' feeding scenario to be implemented in the event of any one of the supply points being unavailable.

Consequently, it can be seen that the increasing adoption of the 25kV auto-transformer system leads to a number of interesting consequences including (amongst others) the use of fewer wider spaced but higher power feeder stations. Feeding lengths are longer, feeder stations are bigger and more expensive, and neutral sections are fewer in number.

2.6 Pantographs

Current for electric traction is collected by a pantograph on the roof of the locomotive or multiple unit. The pantograph head is a bow shaped collector, 1.6m wide (in the UK) overall, with carbon collector strips (1, 2 or 3) across the head, and which make contact with a contact wire suspended over and along the track. The pantograph head is supported with a parallel linkage mechanism which allows it to raise and lower whilst keeping the head in the same attitude. The pantograph head applies a static force of variously 70N, 90N or 110N to the contact wire depending on the network parameters, but in any case European Standards (British Standards Institution, 2012b) and TSIs[5] (EU, 2014a) are standardising on 90N for the future.

[5] TSIs (Technical Specifications for Interoperability) are described in Appendix A.

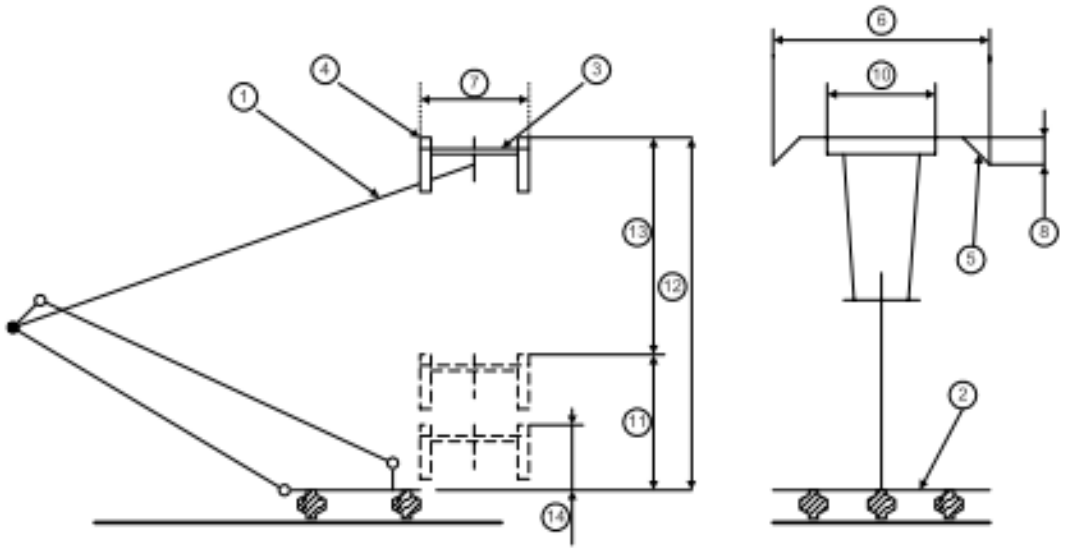

Figure 2.10 Pantograph diagrammatic representation showing the parallel linkage mechanism, and the pantograph head and collector strips. Source BS EN 50206-1 (British Standards Institution, 2010).

Figure 2.11 Typical pantographs (source Faiveley)

Most modern pantographs are of (at least) a two-stage construction, where the main frame accommodates major variations in contact wire height, e.g. at level crossings and bridges, and the head suspension movement accommodates minor variations due to the differences in compliance of the OCL throughout the length of the spans. Additionally most modern pantographs are of the 'asymmetric' arrangement shown in Figure 2.10 and Figure 2.11 (Ch 10.6 ofKiessling *et al.*, 2016; *Pantograph*, 2019).

The majority of pantographs in use on UK infrastructure are of Brecknell Willis (BW) manufacture. A number of older Stone Faiveley AMBR types, with both 2-strip and 3 strip heads, still exist on the older rolling stock/EMUs used on the Anglia Region for services out of London Liverpool St. The Eurotunnel services through the Channel Tunnel, and other high speed trains using the HS1 high speed line to the Channel Tunnel use either Faiveley GPU, or later Faiveley CX type pantographs.

The remainder of both multiple unit and locomotive pantographs running on Network Rail infrastructure are various ages and types of Brecknell Willis manufacture. The full details of their development and differences between them are described in (Hartland and Cullingford, 2013). The summary below in Table 2.1 is taken from the Network Rail technical specification for the Series 1 OCL procurement tender (Network Rail, 2010b), with some additions. New rolling stock is being introduced continually and the current UK trend for these seems to be BW HSP Mk II for conventional multiple units, and BW HSX 250 for higher speed (e.g. Hitachi IEP) trains.

Table 2.1 Brief summary of UK Pantograph types and usage based on Network Rail data, with some additions

Pantograph type	Train configuration	Max speed (m/hr)	Rolling stock classes
BR Brecknell Willis – High Speed	4, 8, 12 car EMU	100	321, 350, 357, 360 & 375
	Single loco, power cars	125	90, 92, 390
	Double headed locos	80	90, 92
Brecknell Willis – Low Height (HSP)	4, 8, 12 car EMU		319
Faiveley AMBR	3 car EMU	75	313, 314, 315
	4, 8, 12 car EMU	100	317
	Single loco, power cars	100	86
	Double headed locos	80	86
Faiveley monoband CX	5, 6, 10, 12 car EMU	125	395
Brecknell Willis – High Speed HSX 250	5, 9 car EMU	140	800, 801, 802

2.7 The overhead contact line (OCL)

2.7.1 Types of overhead line

The contact wire (CW) is the conductor supported over the track from which the trains collect current via contact with the pantograph's collector strips. It is a solid copper or copper alloy conductor of typically 100-120mm^2 cross sectional area (for ac systems) and is circular with a groove on either side. This is to allow the contact wire to be supported by clamps without fouling the smooth passage of the pantograph head beneath.

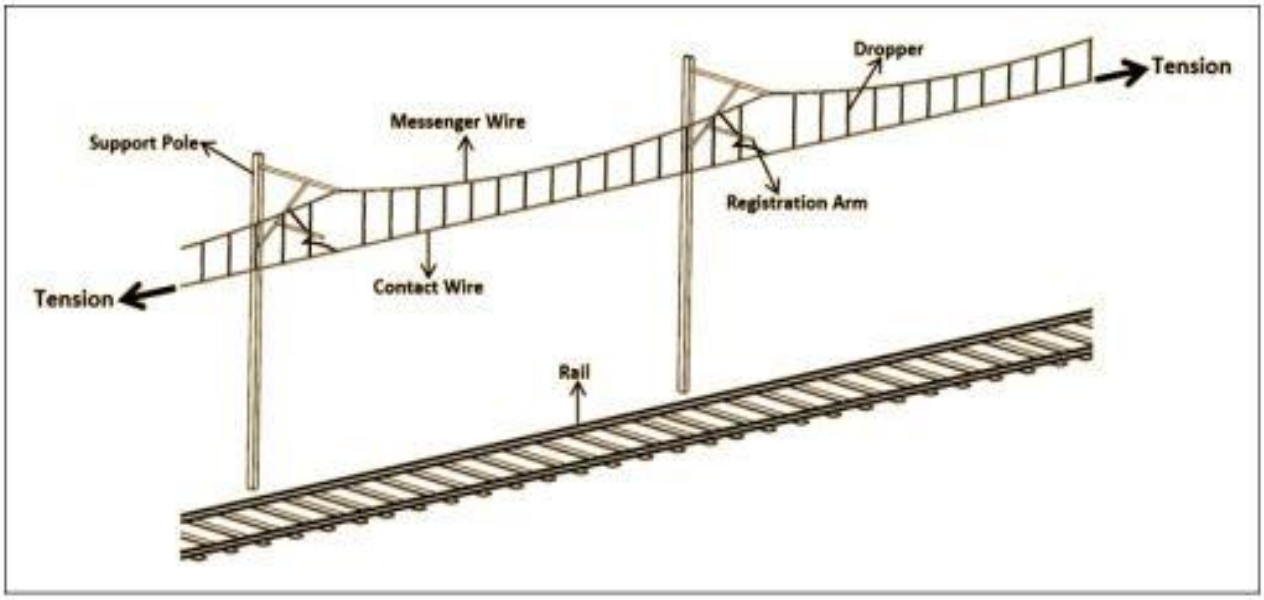

Figure 2.12 Typical overhead line equipment layout showing simple catenary supported on single track cantilevers

The usual material for contact wire is hard drawn copper. Alloys such as cadmium copper and silver copper are used where higher mechanical strength, to support higher tensions, is required, but is more expensive. This is significant, as, in order to create an economic distance between support points, the contact wire can be required to sustain significant mechanical tensions.

Notwithstanding its being tensioned, in order to avoid the contact wire sagging excessively between support points, and to allow a greater distance between those supporting points, the contact wire profile is maintained by being supported from a messenger or carrier wire, known as a 'catenary' in UK (see glossary). The contact wire is supported from the messenger by hangers which are known as 'droppers' in the UK. The catenary is usually a stranded conductor, often a form of bronze, and is often tensioned to a similar extent as the contact wire. Droppers in UK have been solid stainless steel wire, up until relatively recently, when flexible stranded bronze wires are in favour. See Figure 2.13 and Figure 2.15.

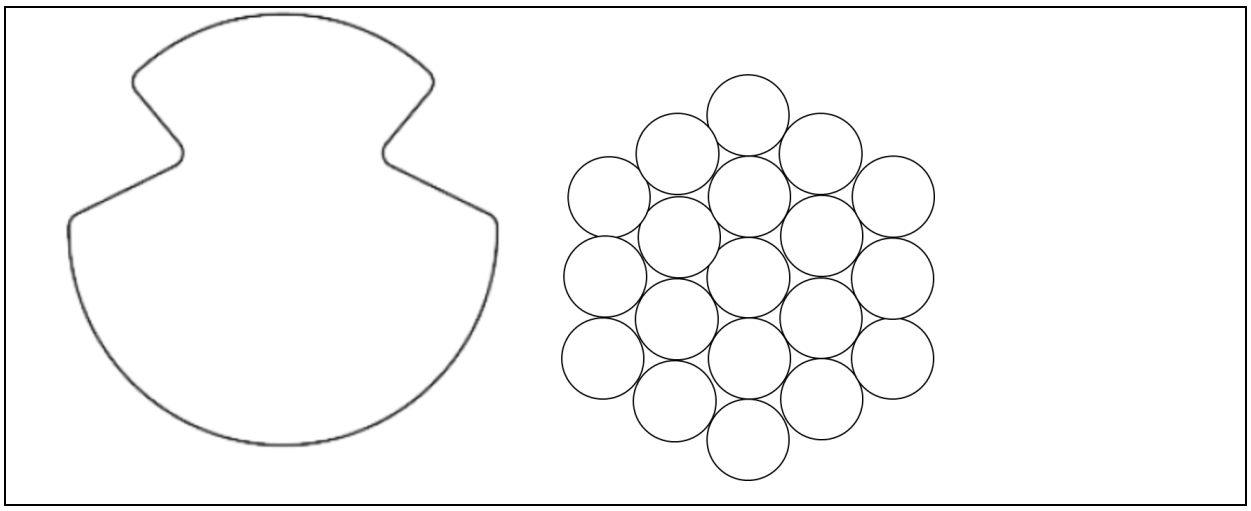

Figure 2.13 Typical CW and messenger wire cross sections showing grooved CW (left) and 19 strand messenger (right). Not to scale

The amount of sag in the catenary wire depends on the unit weight and tension, and knowing these the accurate lengths of the droppers can be calculated to deliver the desired profile of the contact wire. In many cases a sagged profile of the CW is provided, to improve current collection dynamics, see Figure 2.14. The sag or 'pre-sag' as it is called, is usually around 1/1000th of the span length.

The system of catenary, droppers and contact wire together are known as the Overhead Line Equipment (OLE) or more commonly in Europe, Overhead Contact Line (OCL). (The term 'catenary' to refer to the overhead line system is now out of favour, see Glossary.)

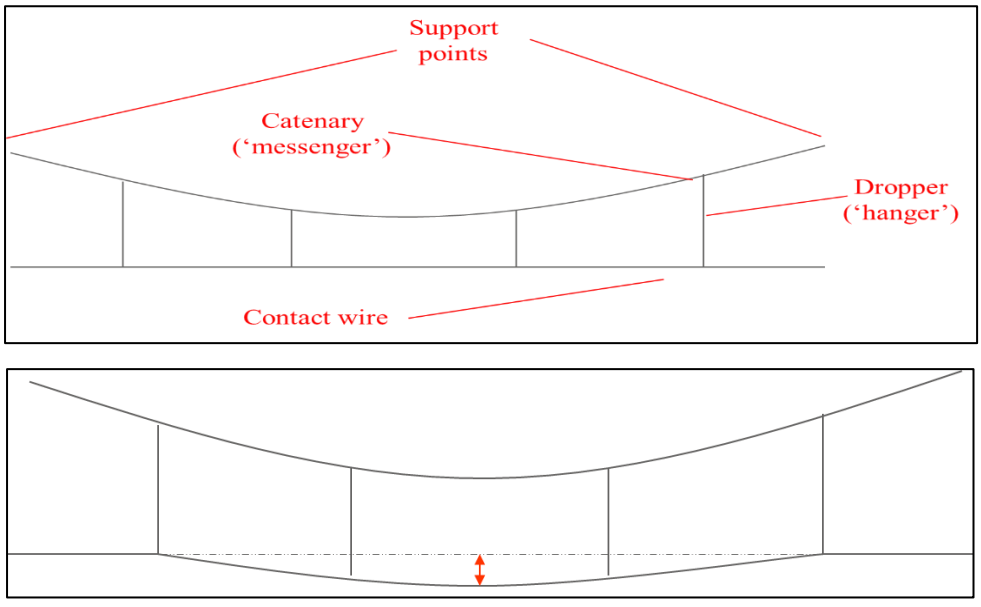

Figure 2.14 Typical 'simple' OCL geometry showing major components. Level CW (above) and pre-sagged CW (below)

Figure 2.15 Typical flexible dropper showing connections to messenger and contact wire. Source (Arthur Flury, 2019)

In the early days of UK rail electrification (i.e. 1950s) all components were made of copper or non-ferrous materials, but in later years, more use has been made of cheaper materials such as galvanised cast iron, steel and aluminium.

The most important criterion in judging OCL is the quality of the current collection. The equipment forms part of a passive dynamic system, being a series of masses and springs and dampers (although in practice very little damping), which can be excited by an input of energy from the passage of a pantograph.

The characterisation of 'quality of current collection' is essentially the avoidance of loss of contact, or at the least, the restriction of losses of contact to very short durations. The reason quality of current collection becomes an issue, is due to the essential economic configuration of the OCL, with an attempt to improve the economics of the system by the use of longer spans between support points. This produces a difference in stiffness or compliance at the mid-point of the span relative to the support point, and hence the effect on dynamic behaviour.

Other configurations of OCL have been used other than the simple single messenger, single CW construction described above, in order to produce a system with better dynamic behaviour, and hence current collection performance, at higher speeds.

'Compound' equipment uses an additional or 'auxiliary' messenger wire between the main catenary and the CW, and hence two sets of droppers. This gives the effect of supporting the CW by a series of smaller spans, and also introduces more damping,

which is beneficial if multiple pantographs are in operation, however it is heavier and more expensive.

'Stitched' equipment is ostensibly cheaper and simpler than compound equipment, involving the use of what amounts to a short length of auxiliary messenger at each support point, which has the effect of improving the 'compliance' of the OCL at this point, to a value closer to that at the mid span. But this type of equipment is very difficult to install and adjust, although it is in favour on a lot of the continental systems.

Stitched and compound catenary suspension systems are indicated on Figure 2.17 and Figure 2.16 below.

Some other systems, particularly those for dc systems where current are much higher, use double messengers, or double contact wires, or both.

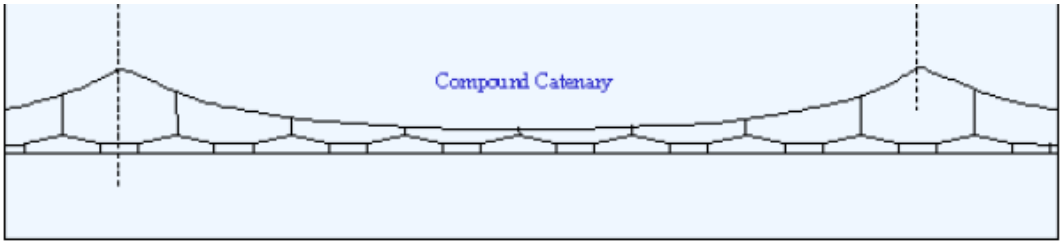

Figure 2.16 Compound catenary graphic showing how CW is supported from an auxiliary catenary, which in turn is supported from the main catenary. Source Quora.com

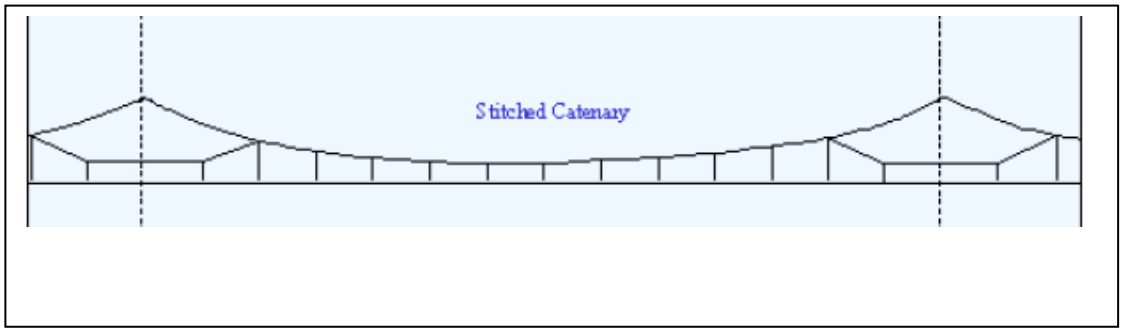

Figure 2.17 Stitched catenary graphic showing how CW is supported from a 'stitch wire' around the support point. Source Quora.com

Because of the importance of the quality of the current collection offered by a particular design of OCL, especially as higher speeds were anticipated, computer programmes have been developed to simulate and predict the dynamic behaviour, based on models of the OCL and the pantograph. This will be returned to in Chapter 4.

2.7.2 Tensioning arrangements

As the profile of the CW, and hence the dynamic behaviour of the OCL, depends upon the tensions in the conductors, arrangements were developed which allowed for automatic tension adjustment of these conductors with temperature. For a fixed termination system, the tension will increase as the temperature drops and the conductors (which being non-ferrous have a reasonably high coefficient of expansion) contract. This may lead to high tensions infringing factors of safety at low temperatures, or low tensions leading to excessive sags and infringement of electrical clearances at high temperatures.

Automatic regulation of conductor tensions is conventionally achieved by use of a system of weights and pulleys (known as a 'balance weight'). This allows the OCL to expand and contract (within limits) and maintain a (reasonably) constant mechanical tension. A consequence of this is twofold: one the supporting arrangement for the conductors over the track has to allow the along track movement caused by the expansion and contraction; and secondly, there are limits to the amount of such expansion and contraction that can be so accommodated, thus restricting the length of each individually tensioned conductor. For a fixed termination OCL, the length of each discrete conductor is only limited by the practical constraint of the amount of conductor normally contained on a single drum (approximate 2 miles, 3.2km). But for an automatically tensioned conductor, the above constraint reduces this to about 1 mile, 1.6km, or less.

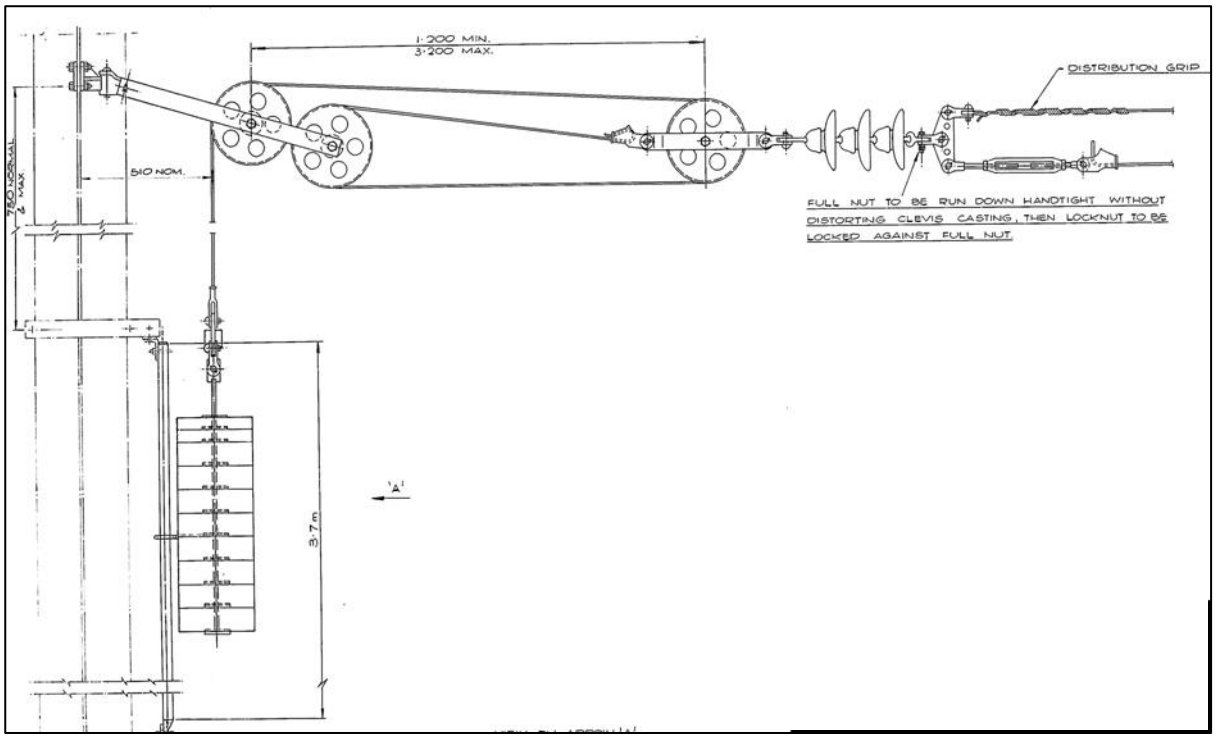

Figure 2.18 'Balance weight' tensioner graphic showing how weights and 3:1 pulley arrangement apply tension to the contact wire and catenary wire. Source Network Rail OLEMI drawing 1/105/100/A3

For this reason, 'overlaps', which are the particular OCL features where one discrete length of conductor overlaps with the next, are spaced much closer. The overlap itself is a specific arrangement of conductors, such that the pantograph sees an uninterrupted collection of current as it passes from one OCL to the other. The length of OCL between one balance weight arrangement and another (effectively between overlaps) is known as a 'tension length'. See Figure 2.19.

The overlaps are conventionally constructed with two separate tension lengths of OCL running parallel in one (or sometimes two) spans, typically separated by ~400mm laterally, and with each graded in height so the pantograph runs from one CW, to both together, then onto the next tension lengths contact wire. Inclusion of insulators in the 'out of running' portions allow the overlap to be insulated, i.e. maintaining separate electrical sectioning in each tension length, but briefly providing continuity during pantograph passage, see Figure 2.20.

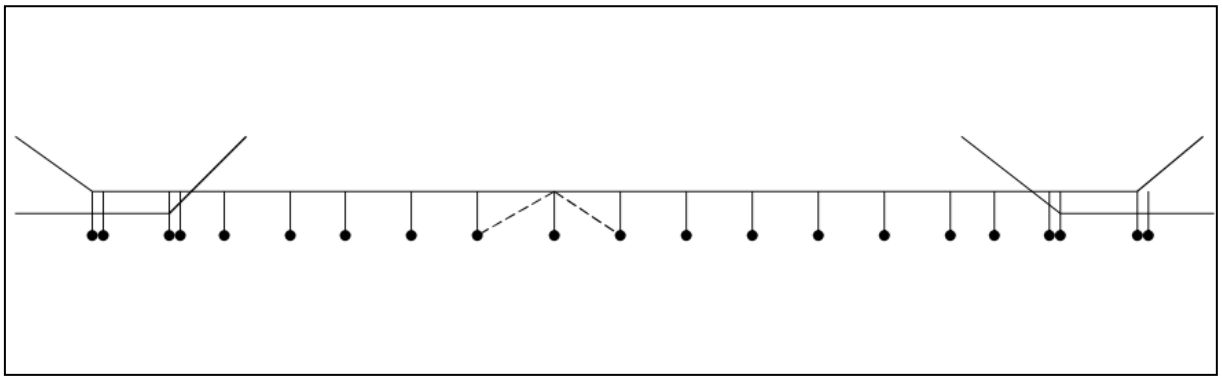

Figure 2.19 Tension length/overlap graphic showing how OCL is terminated at tensioning arrangements at overlaps, at each end of a section (approx. 1.5 km long). Also shows Mid-point Anchors.

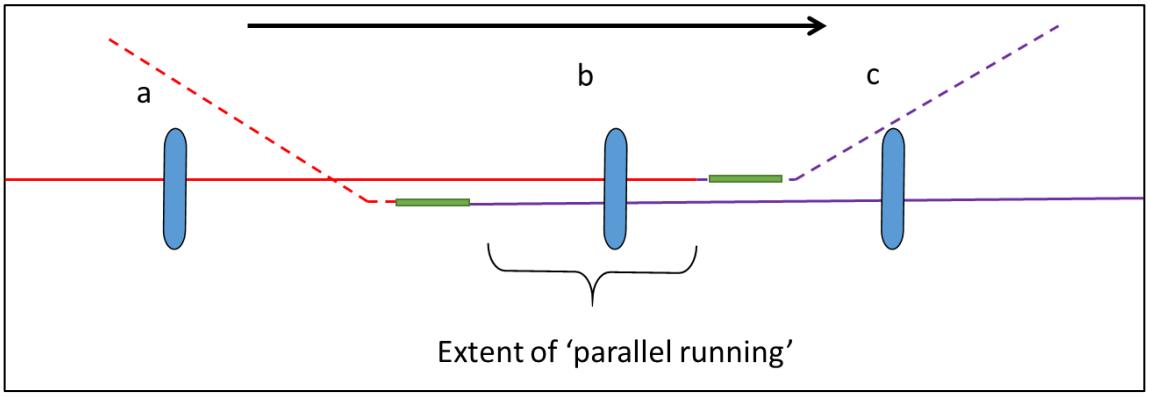

Figure 2.20 Insulated overlap arrangement showing the passage of the pantograph from (a) 'red' electrical section, through (b) parallel running, and (c) 'purple' electrical section. Green blocks are insulators. Note the section of parallel running when both sections are connected.

Some systems replace the weights and pulleys with hydraulic or spring tensioning units, and spring tensioners are at the present time the method of choice for Network Rail Series 1 and Series 2 OCL developments, see Figure 2.21.

Figure 2.21 Spring tensioner equipment used on Network Rail series 1. (source Pfisterer)

2.7.3 Supporting arrangements

At each support point, two functions need to be provided: the messenger wire needs to be supported (and hence the weight of all the other equipment hanging off it, via

droppers); and the contact wire (and usually the messenger as well) needs to be 'registered', i.e. maintained in a horizontal position at a fixed distance either side of the projected track (and hence pantograph) centre line. As the CW is tensioned (as has been noted) this usually involves 'pulling off' the CW by means of an arm, known as a 'registration arm'.

The position of the wire either side of the centre line is known as its 'stagger', and it usually follows one of two forms.

On straight track, in order to spread the wear of the pantograph head carbon collector strip evenly, the stagger alternates from side to side at successive registration points, the characteristic 'zig-zag' pattern.

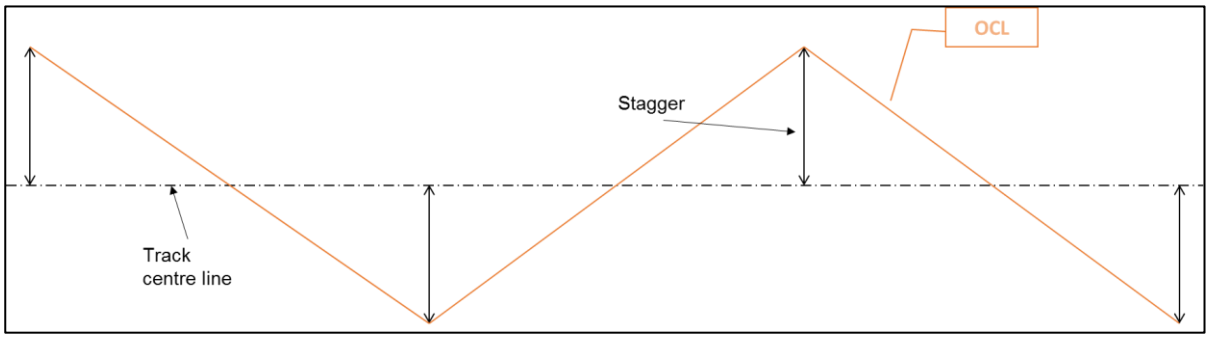

Figure 2.22 Stagger scheme on straight track showing how OCL is offset alternately either side of the track centre line

On curved track, the stagger is to the outside of the curve, and of such a dimension that at the mid-point of the span the CW is approximately back on the track/pantograph centre line.

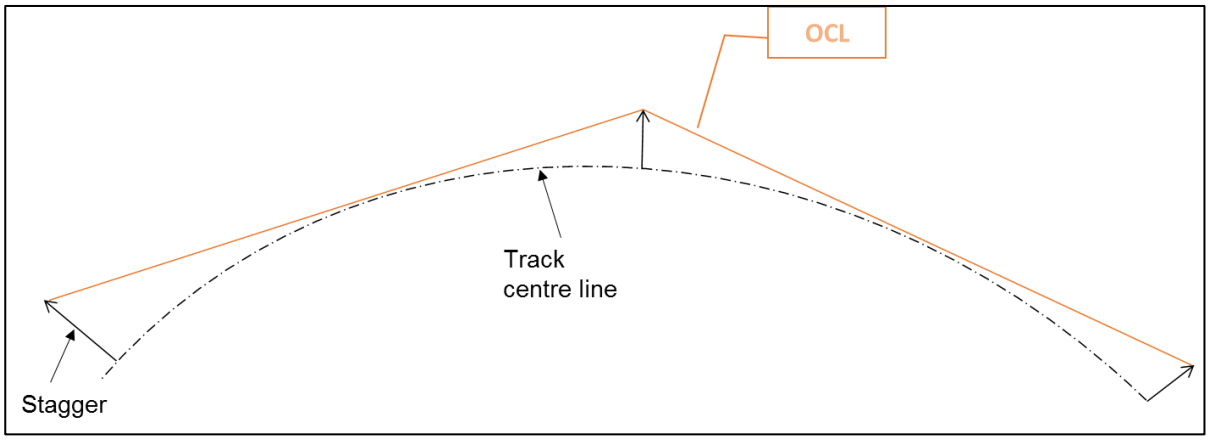

Figure 2.23 Stagger scheme on curved track showing how OCL is offset to outside of the track centre line

The development of a robust stagger regime is a complex matter, involving as it does the assessment of the vehicle and pantograph sway, track and OCL tolerances, the movement due to along track rotation of OCL, and the effects of wind ('blow-off'), plus track alignment, cant and curvature. There is no need to go into further detail here, as these matters are not significant to the subject of this research, but more information can be found in the literature (Baxter, 2015; Keenor, 2016; Kiessling *et al.*, 2016) and the European standard BS EN 50367 (British Standards Institution, 2012b).

The support points are therefore usually support and registration points. The exact arrangement of these depends on the type of supporting structure used, but the essential requirements are that they should, inter alia:

- Accommodate the along track movement (temperature expansion or contraction) of the equipment without adversely affecting the regulation of the tension;
- Allow for the unrestricted passage of the pantograph, including any pantograph sway or CW uplift that could occur; and
- Provide the necessary level of insulation of the live parts from earthed parts or parts in another electrical section.

Types of supporting structure are generally influenced by the physical space available in the railway footprint, the number of electrified tracks to be accommodated (and their spacing) and the ground conditions for the foundations.

Usually the most cost effective form is sought, but this should include the cost of erection as well as material costs (in railway construction, the logistics of installation is often the more significant element of construction cost).

It is generally found that the most cost effective form of supporting structure is the single track cantilever, used singly or in combinations (see Figure 2.24 and Figure 2.25). In this form of support, a live cantilever frame is supported from a single column mast, the frame being hinged at the mast, so as to allow the frame to rotate along track to accommodate the expansion and contraction of the OCL with temperature. The cantilever frame supports the messenger wire, and provides a fixing for the registration arm to create the stagger. Other forms of supporting structure are also widely used, including portal frames, headspans, two track cantilevers, and attachments to bridge and station structures.

Figure 2.24 Single track cantilever photograph

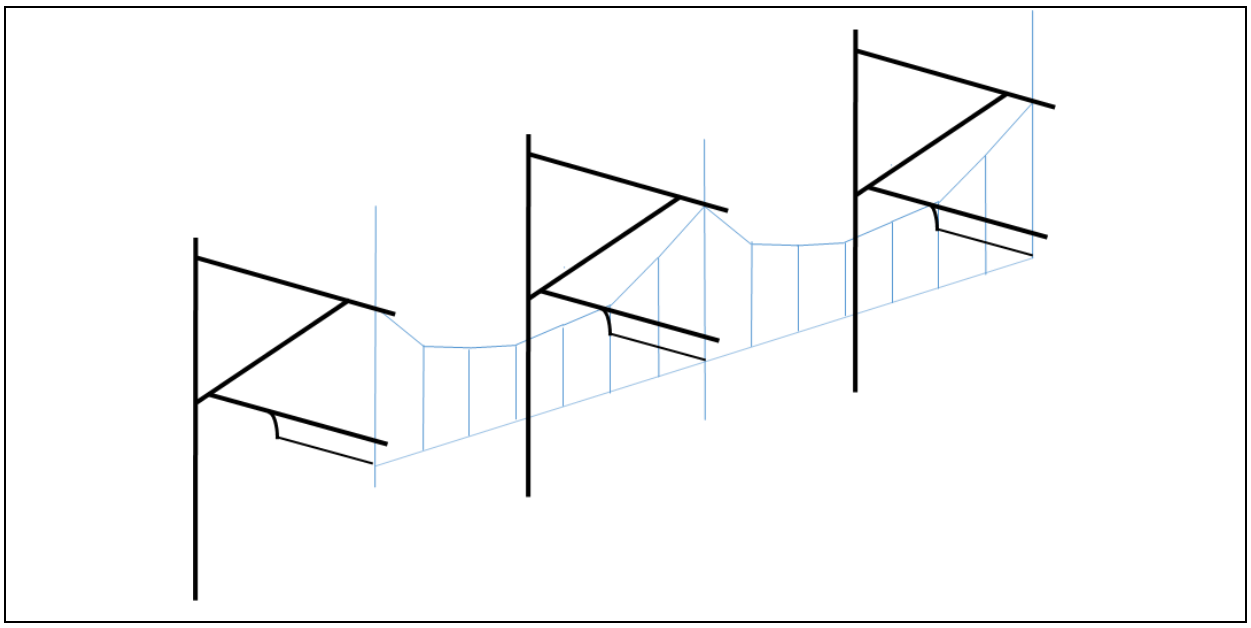

Figure 2.25 Single track cantilevers

The advantages of the single track cantilever are:

- Uses simple mast without welding or fabrications;
- Low loading on the ground leads to small foundations;
- Hinged at mast means large radius of rotation , which has minimal effect on tensions when rotated to accommodate along track expansion and contraction;
- Clear demarcation between live and earthed parts.

2.7.4 Sectioning arrangements

In order to provide the operational flexibility for the electrified railway, the electrical supply to the OCL over the various tracks is split into sections connected together by switches (normally closed) and which allow for some, or all, of these sections to be

energised as situations demand. In normal operations all sections naturally are energised but for maintenance, either of the OCL itself or of other railway infrastructure, or to deal with particular incidents or out of course occurrences, the switches can be operated, either manually or by remote control, to energise only the electrical sections required and permit others to be de-energised, and earthed for safety.

A typical sectioning arrangement is shown in Figure 2.26 below, which is an extract from an actual sectioning diagram. The different colours indicate the different electrical sub-sections. In this case the sub-sections are kept separated by section insulators.

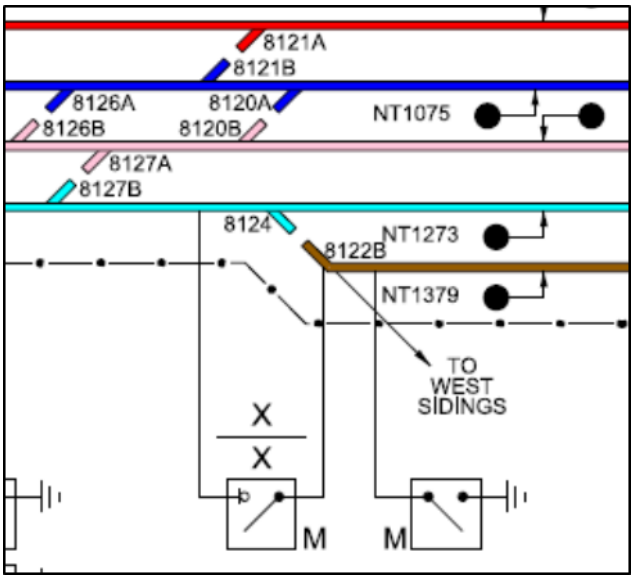

Figure 2.26 Extract from sectioning diagram (Network Rail, 2013c) showing how OCL on different tracks is electrically separate, and switches provided to connect across the breaks where crossovers occur. Other features shown are signals and point numbers.

As has been described above, when speaking about insulated overlaps (see Figure 2.20), although creating a potential electrical break, there must be continuity of current collection as a pantograph passes, and hence the functionality of an overlap is included even in a discrete sectioning device such as a section insulator. A section insulator is an OCL component whereby an insulator is inserted into the CW, and skids or runners are used to allow the pantograph to pass, and, by overlapping of the skids, to allow continuous collection of current as the pantograph passes, see Figure 2.27.

Figure 2.27 A typical section insulator (in this case a low voltage dc type) showing the overlapping copper skids which allow the pantograph to continue to collect current whilst passing across. Source (Arthur Flury, 2019)

A neutral section is another type of sectioning device, but with the specific absence of the 'continuity of current collection' functionality, and is described fully in the next chapter.

2.7.5 Current types of OCL in UK

A variety of OCL types are in current use in the UK, as have been installed and modified over the 60+ years of overhead electrification. Refer to previously mentioned sources (Dolphin, 2014; Doughty, 2015; Keenor, 2016) for details, but summarised here as shown in Table 2.2.

Table 2.2 Brief summary of UK OCL types

OCL type	Conductors	Usage
Mk3a, Mk3b	7/2.95 AWAC[6] messenger 107mm^2 CW	Northern part of WCML, all of ECML, Midland Main Line, Anglia, etc.
Mk3d	19/2.1 Bz messenger 107mm^2 CW	Modern upgrade of Mk3b with a bronze messenger and flexible copper droppers, used on southern ECML, and elsewhere.
UK1	19/2.1 Bz messenger 120mm^2 CW	140 m/hr capable design installed on WCML upgrade (south end).
GEFF	Various ex dc 'heavy' conductors	Furrer + Frey modern design to replace old ex-dc equipment on Great Eastern lines.

[6] Alumoweld/aluminium conductor. Alumoweld is a trade name for an aluminium coated steel core wire used in transmission industry.

OCL type	Conductors	Usage
Series 1	19/2.1 Bz messenger 120mm^2 CW	140 m/hr capable design developed by Furrer + Frey for Great Western Main Line
Series 2	19/2.1 Bz messenger 107mm^2 CW	Essentially a 'modern' version of Mk3d, 110 m/hr capable

Chapter 3 Current and Recent Neutral Section Performance

3.1 Summary

This chapter describes the investigation into current neutral section practice in UK and Europe in which the development of neutral section types and technology in the UK is described, leading to a description of current practice in UK, and currently experienced performance and reliability problems. Some comparison is made with European practice.

3.2 Early 25kV ac electrification in UK

As has been described previously in Chapter 2, the introduction of 25kV ac electrification onto the network of British Railways in the UK starting in the late 1950s, brought with it the fresh technical problems of separation between the different phases of electrical supply at adjacent and successive supply points. This was not a problem that existed in the then prevalent 1,500V dc system.

The technical and economic case for the conversion to 25kV ac was made, based, in large part, on drawing on French railway experience (British Transport Commission, 1955) and the technical aspects of the early UK 25kV ac electrification equipment and installation also followed this French practice (Duffy, 2003).

In a series of papers presented at a conference in London in 1960, a great deal of explanation was given to the descriptions of, and technical backgrounds to, the various technical decisions adopted (British Transport Commission, 1960). One such paper includes descriptions of the proposals for the neutral sections (British Transport Commission, 1960, Paper 6). The type of arrangement chosen for the phase separation sections for applications above 60 miles/hr was the type named at the time as the 'carrier wire' type neutral section, the first time such a description had been used.

A carrier wire neutral section is constructed from a series of overlaps, arranged in sequence, and where the successive overlaps allow the pantograph to transition smoothly from one live section, to a floating section, and then, depending on the particular type of construction, either back to the next live section, or onto an earthed section, and then via a further 'floating' section, onto the next live section. Thus, a

carrier wire neutral section can consist of 3, 4 or 5 sections, and 2 or 4 overlap spans, the choice of which of course will affect the overall length of the installation.

One of the variable characteristics of a 'carrier wire' type neutral section is the number of overlap spans in the sequence, implying whether earthed as well as 'floating' sections are included. This impacts obviously on the overall length of the complete installation, which itself becomes a factor that is relevant to the running of trains with multiple pantographs (i.e. multiple units coupled together) and the spacing of those pantographs. This is due to the possibility of separate pantographs connecting floating sections to different live sections at the same time.

In the case of these early 25kV ac carrier wire neutral sections, the arrangement was of a type that could be described as 4-span, and is shown schematically in Figure 3.1 below.

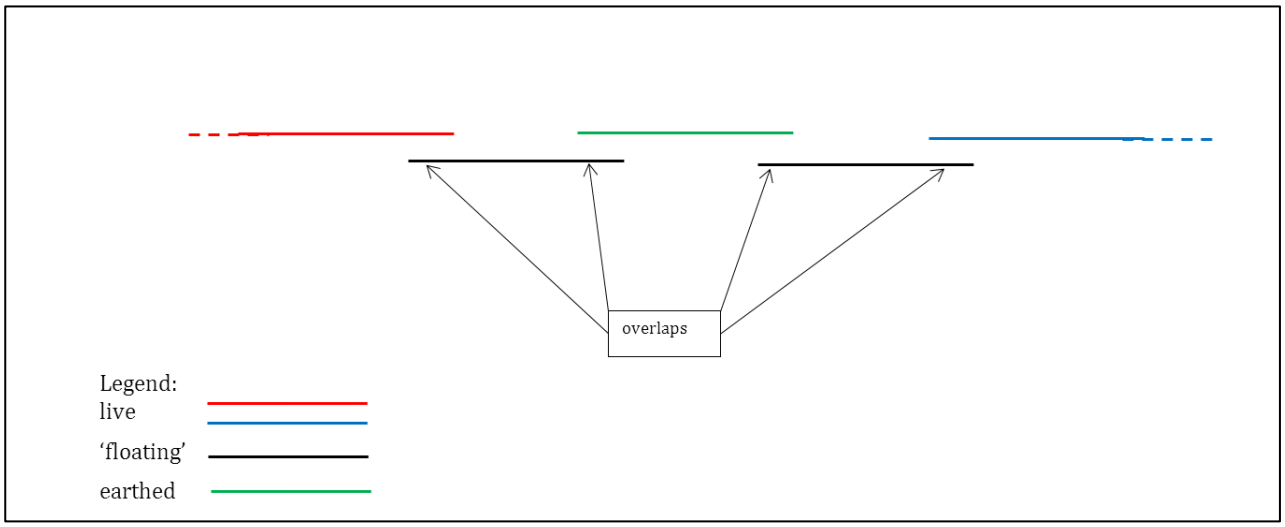

Figure 3.1 Electrical schematic of carrier wire neutral section (early UK 25kV ac carrier wire neutral section showing the 4 overlap construction).

In practice all four overlaps are consecutive (and are formed by a single additional overhead line equipment, known as the 'carrier wire'), see Figure 3.2

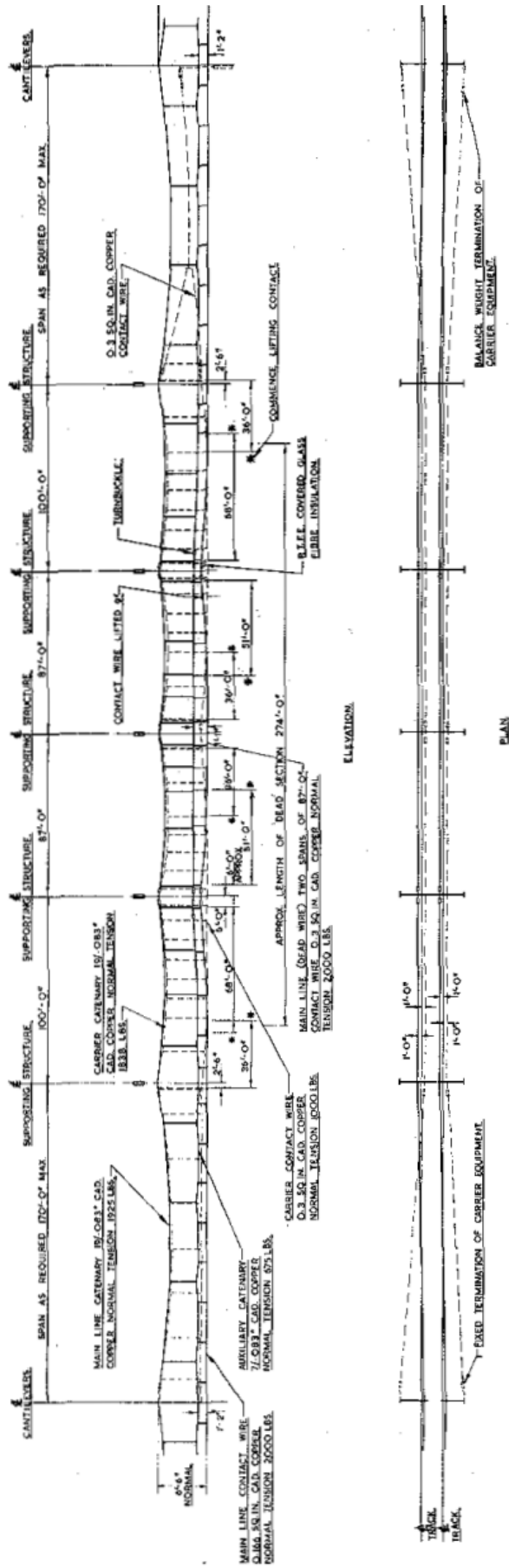

Figure 3.2 Arrangement of carrier wire neutral section (early UK 25kV ac carrier wire neutral section showing the 4 overlap construction). Source (British Transport Commission, 1960)

Other characteristic features of the carrier wire neutral section that were thought worthy of mention in the 1960 conference papers were:

- Allowance was made for both pantographs on a locomotive to be raised
- Overall dead section length was 270 feet (85m)
- Overlap spans of 100 feet (31.5m) and 87 feet (27.5m) were used

In order to reduce the impact of the length of the carrier wire neutral section, extremely short overlap spans were used, which could only be made to perform practically if either half tension conductors or heavier conductors were used, due to the need for a particular value of natural 'rise' of the conductor to be achieved.

Subsequently in the early wave of new 25kV ac electrification construction, and the eventual conversion of pre-existing 1500V dc to 25kV ac electrification in the UK, in the late 1950s and early 1960s, a number of such carrier wire neutral sections were installed at locations around UK.

It is interesting to note how quickly the interest in a shorter, more conveniently located form of neutral section arose. This appears to have been prompted by increasing acknowledgment of the spatial constraints rather than any performance issues *per se* (BICC, c.1966/67).

3.3 The first 'short' neutral sections

Short neutral sections using the 'skidded' ceramic bead insulators were introduced onto British Rail in about 1963 (Bradwell and Wheeler, 1974), as an alternative to the then prevalent carrier wire or section insulator form of neutral section, and were used from late sixties through the seventies until the early 80s, with the essential features remaining unchanged. (In the UK this was in the Mk1 and Mk3, 3a and 3b OCL systems.) The neutral section was manufactured and marketed by UK company BICC, and also appeared in other parts of the world where BICC did business, e.g. India, South Africa, Latin America, etc (see Figure 3.3 for example of how BICC 'marketed' this innovative short neutral section).

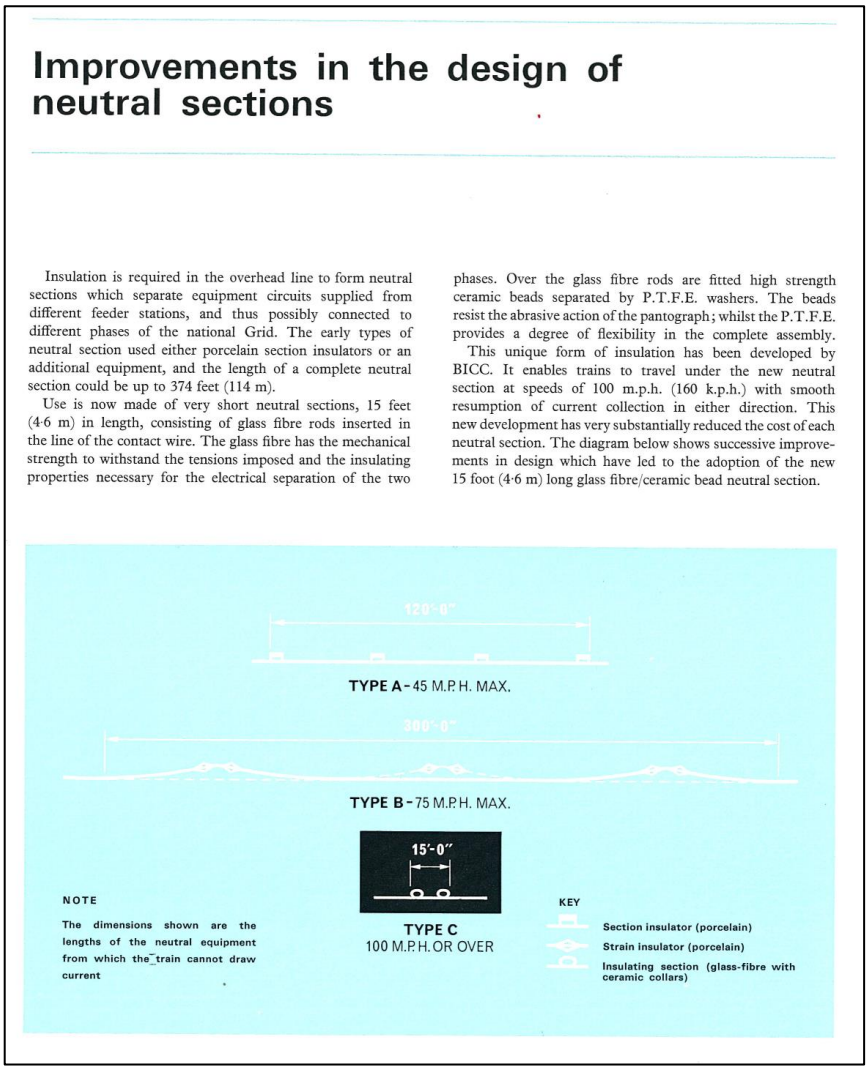

Improvements in the design of neutral sections

Insulation is required in the overhead line to form neutral sections which separate equipment circuits supplied from different feeder stations, and thus possibly connected to different phases of the national Grid. The early types of neutral section used either porcelain section insulators or an additional equipment, and the length of a complete neutral section could be up to 374 feet (114 m).

Use is now made of very short neutral sections, 15 feet (4·6 m) in length, consisting of glass fibre rods inserted in the line of the contact wire. The glass fibre has the mechanical strength to withstand the tensions imposed and the insulating properties necessary for the electrical separation of the two phases. Over the glass fibre rods are fitted high strength ceramic beads separated by P.T.F.E. washers. The beads resist the abrasive action of the pantograph; whilst the P.T.F.E. provides a degree of flexibility in the complete assembly.

This unique form of insulation has been developed by BICC. It enables trains to travel under the new neutral section at speeds of 100 m.p.h. (160 k.p.h.) with smooth resumption of current collection in either direction. This new development has very substantially reduced the cost of each neutral section. The diagram below shows successive improvements in design which have led to the adoption of the new 15 foot (4·6 m) long glass fibre/ceramic bead neutral section.

Figure 3.3 Ceramic bead neutral section source: (BICC, c.1966/67)

The details of interest are as follows: the insulators manufactured from ceramic beads threaded onto a glass fibre core, with an overall external diameter of 15.4 mm are used. The connections between the ceramic bead insulators and the contact wire are effected by the aluminium bronze end fitting of the insulator, which is glued to the glass fibre rod, and the contact wire cast aluminium bronze splice, which fits into a fork in the insulator end fitting, and is secured by pins. The contact wire is secured into the end fitting by set screws acting along the top of the contact wire profile (see Figure 3.4).

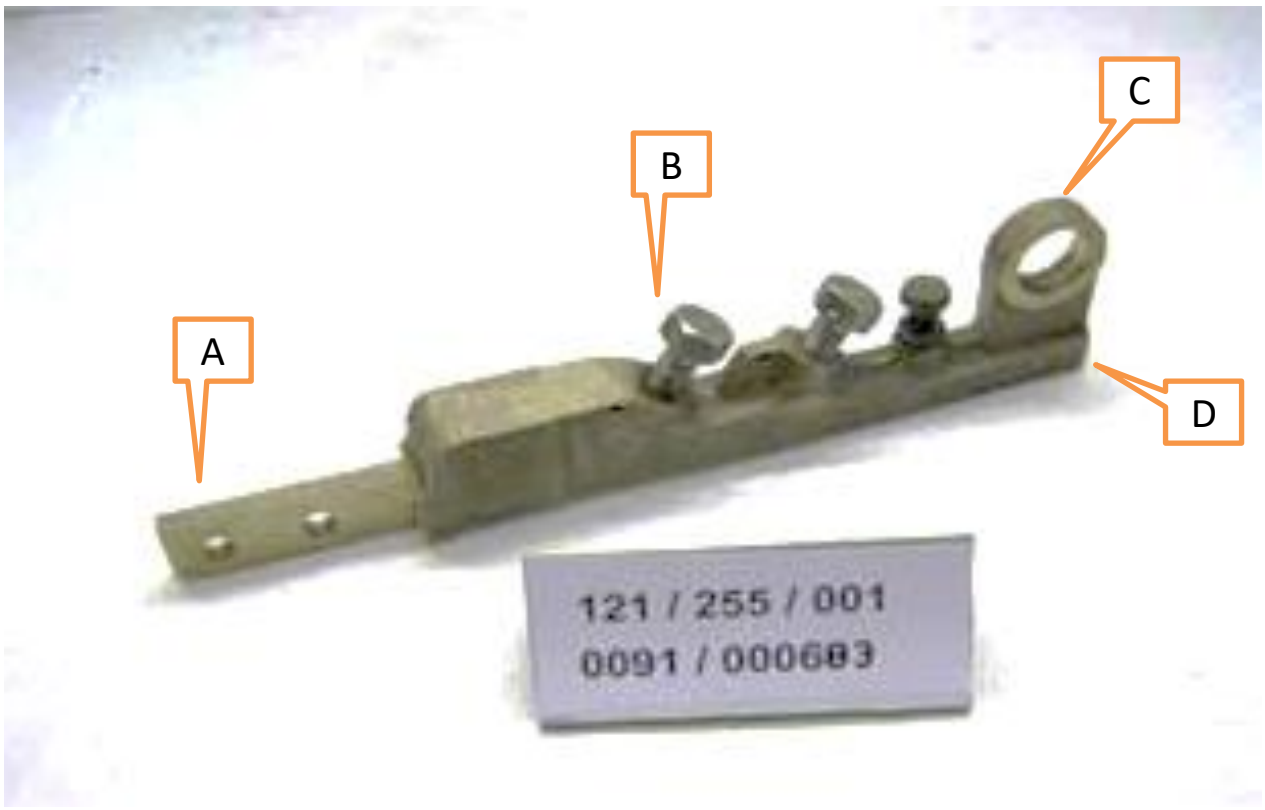

Figure 3.4 Ceramic bead neutral section end fitting/splice. Key: A – tongue for connection to ceramic bead insulator end fitting (see bottom RH of Figure 3.5), B – set screws for restraint of CW, C – connection for spring dropper, D – CW end. Source (Unipart Rail, 2015)

Skids (sometimes referred to as 'gliders') carry the pantograph head carbon collector strips across the discontinuity presented by the splices, and four anti-torsion spring droppers support the contact wire end fittings, to maintain the skids and fittings in a vertical attitude. Other aspects, which do not directly affect the pantograph/OCL interface, include the support of the arc catchers from a 'top hat' shaped arrangement, which is itself supported from the anti-torsion spring droppers. Most of the components were manufactured by BICC Jointing Systems Division at Prescot, Lancashire. The original anti-torsion spring droppers were formed from two concentric tubes, one inside the other, and the spring being provided by a rubber bellows element. At some point, due to problems with rubber bellows perishing, this type of springing was replaced by an improved design consisting of a stainless steel coil spring, with machined stainless steel end fittings.

By 1969, six years of satisfactory performance with these neutral section insulators at speeds up to 160 km/h had been achieved (Goldring *et al.*, 1969).

The preparations for the introduction of the Advanced Passenger Train (APT) in the late 1970s had indicated poor performance at these neutral sections at 200 km/h (125 miles/hr), where they generally ran adequately in 'normal' 160 km/h (100 miles/hr)

operation. At the same time there is mention of chipping of pantograph carbons (by misaligned skids) and cracked ceramic beads (Wheeler *et al.*, 1979).

Although not all the background information is available in the present moment, from these reports a picture emerges of two parallel workstreams to address this; one of development of the existing design and one of fundamental re-design.

The development activities revolved around fitting improved lightweight skids. High speed photography measured the uplift of the neutral section with the passage of the pantograph at various speeds and also observed the dynamic movements within the neutral section itself. (Wheeler *et al.*, 1980) and (Wheeler *et al.*, 1979).

A variety of different modifications to the design of the ceramic bead insulator themselves, to prevent bead cracking, PTFE spacer erosion and damage etc. were proposed, implemented and assessed in operation (Wheeler *et al.*, 1978) (Wheeler, 1975) (Bradwell and Wheeler, 1974). However, the minute detail of these failures and remedies is less useful than the general conclusion made by BR that the search for a feasible form of ceramic bead insulator was probably a fruitless task, and that more radical alternatives were necessary.

Equally, developments in finessing the design of the skids, which carry the pantograph carbons past discontinuities at the splice joint between the ceramic bead insulator end fitting and the contact wire, were undertaken (Evans, 1980b) and (Evans, 1980a). This also included variation in the shape and size of arcing horns, but the high speed photography (Wheeler *et al.*, 1980) (Wheeler *et al.*, 1979) indicated that the improvements were minimal. Indeed the 'lighter' skids, being of a longer length, infringed on the insulating creepage distance along the ceramic bead insulator, which in itself initiated failures by electrical tracking. These tests also indicated that the high flexibility of the ceramic bead insulator (with its glass fibre core) was a problem, and also identified that 800N was the 'low frequency' force that would initiate a chip in a pantograph carbon ((Wheeler, 1980) gives 1200g as the acceleration required for chipping). The APT pantograph test indicated peak low frequency forces at neutral section of between 270N and 550N at 200 km/h (Wheeler, 1980).

The requirement for 200 km/h operation with APT (and as it turned out subsequently, other types of trains), and the poor ability of existing designs, enhanced or not, to accommodate this with the same performance as other pantographs at 160 km/h, triggered a consideration of a more fundamental re-design (Wheeler, 1980).

In the early 1980s, prompted by anticipated demands for regular speeds of 200 km/h (125 miles/hr), and the deficiencies described above BR R&DD undertook research to ascertain whether 'a fundamental appraisal of the neutral section design unfettered by the technological constraints of the 1960s could avoid these problems altogether'.

Their report (Wheeler, 1980) describes the outcome of this research, and the details of a proposed new 'skidless' neutral section which addressed many of the problems described above. The features developed for this neutral section included a proposal to eliminate the skids from the design by eliminating the 'cumbersome' end fittings. These were replaced by the actual end fitting of the ceramic bead insulator (a glued ferrule) being a copper rod of similar profile to the contact wire profile, which could be spliced to the actual contact wire by a newly found form of splice (known at the time as a KP splice, from the original supplier, German OCL component manufacturer Karl Pfisterer) which transferred the tensile load through teeth gripping the grooves of the contact wire (see Figure 3.5 and Figure 3.6). This transferred the load along a line of action much closer to the neutral axis of the contact wire than the previous form of splices, and hence inserted a much smaller couple and hence deformation into the connection. This kind of splicing arrangement did not need skids, thereby creating a double advantage, no skids and no (or lesser) distortion of the contact wire profile.

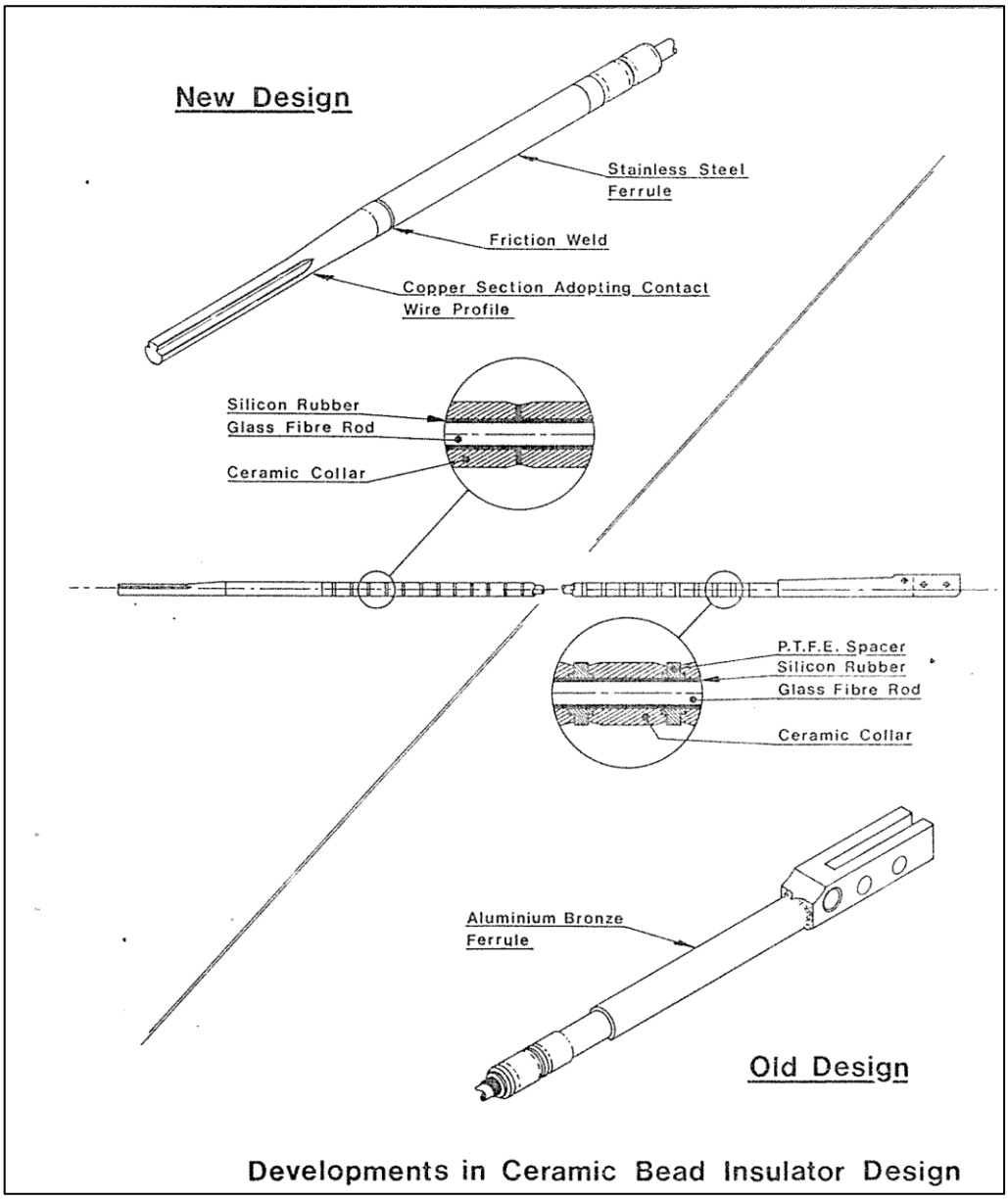

Figure 3.5 Graphic showing development in 'skidless' ceramic bead insulator from (Jones, 1984a)

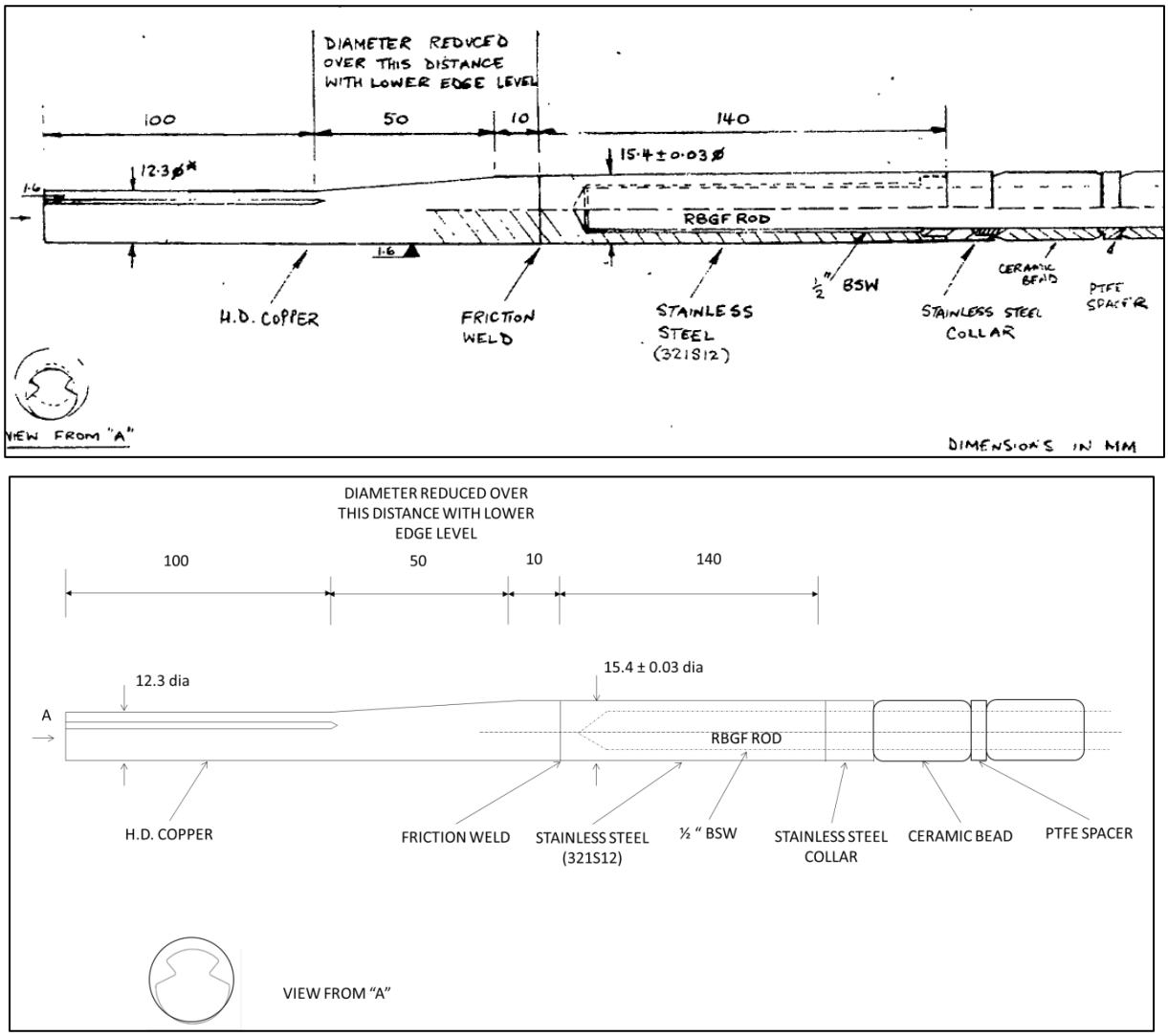

Figure 3.6 Detail of development of ceramic bead insulator splice showing (top) poor quality original scan from (Wheeler, 1980), and (bottom) reproduction sketch with clearer annotation

Other developments included:

- Elimination of the anti-torsion droppers, as the design of the end fitting allowed a degree of rotation without interfering with pantograph passages;
- New design of arcing horns;
- The elimination of PTFE spacers between the ceramic beads;
- New design of single piece arc catchers suspended by adjustable droppers.

After development from the prototype a production version was tested at Whitmore on the WCML, and after satisfactory results was installed at Murthat, also on the WCML, where it was tested at higher speeds using the APT equipped with a Brecknell Willis pantograph. The tests were satisfactory, a highest speed of 232 km/h was achieved, and the highest pantograph force recorded was 300N. Subsequently the skidless design of

ceramic bead neutral section was introduced into BR's standard OCL designs in 1983, and a campaign of replacement (at least for the higher speed lines) started (Jones, 1984b). 'Production' versions of the skidless neutral section (BR drawing 1/109/802/A1) differed from the research prototype in that an anti-torsion spring dropper was retained at the extremities of the unit, as problems were still being experienced with contact wire twist.

Subsequent design modifications between 1984 and 1995, introduced from service experience, replaced the single piece arc catcher support with a more readily adjustable two piece unit, and this was suspended by swinging links, rather than adjustable wire droppers, closer to the original BR R&DD proposal. See Figure 3.7 and Figure 3.22 (right).

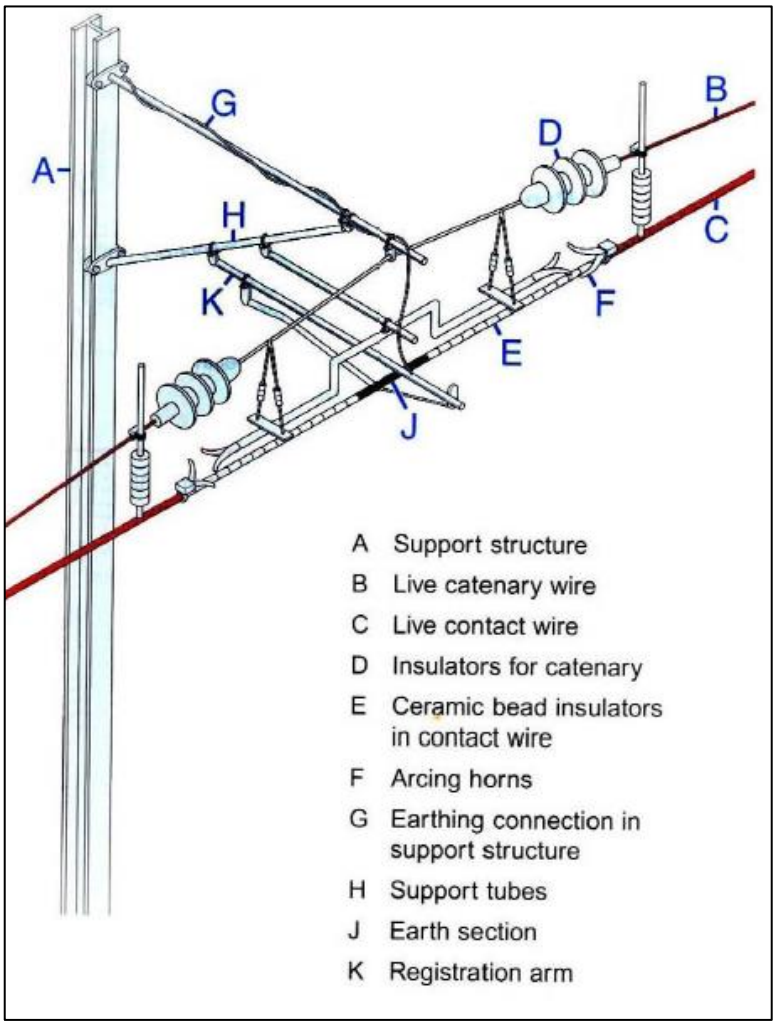

Figure 3.7 Diagram of skidless neutral section from (*GE/RT8000/AC Railway Rule Book: Module AC; AC Electrified Lines*, 2003)

3.4 Recent and current UK practice

Since the mid-1980s the skidless ceramic bead neutral section has been the predominant style installed in the UK network, but when a variety suitable for use with 120mm^2 contact wire was required for West Coast Route Modernisation in the late 1990s, its continued unreliability, and the sharper focus of attention paid to the OCL failures since privatisation triggered Network Rail to undertake investigations into alternative designs. In keeping with the prevailing policy of the times, the approach taken was to seek a proprietary item with a proven track record of performance, rather than set off on an 'in-house' technical development path.

The selected manufacturer was Arthur Flury (AF) of Switzerland; however the 'standard' design chosen, NS25-UK-10 (webpage: Arthur Flury (2011), required some modification to suit both UK condition and the demands of the Network Rail OCL engineers. (Although this approach came in for some criticism internally within Network Rail (Network Rail, 2012b), for undermining the manufacturers accountability.)

These first UK AF neutral sections were installed in large (193mm^2) CW systems in Anglia region, and then in conventional 107mm^2 and 120mm^2 systems in around 1999. The design was a conventional AF 25kV type, in use elsewhere in Europe and around the world. It consisted of two parallel PTFE covered rods, terminated in non-ferrous end fittings, skids and integrated arcing horns. Two sets of these were mounted symmetrically around the support point, supported at the CW/rod end fittings by adjustable droppers, see Figure 3.8.

Details of the construction of the original 'standard' AF NS25-UK-10 neutral section are shown in Figure 3.9, and details of the twin rod end fittings in Figure 3.10 (which also shows spreader bars used in transport and installation, but which are subsequently removed).

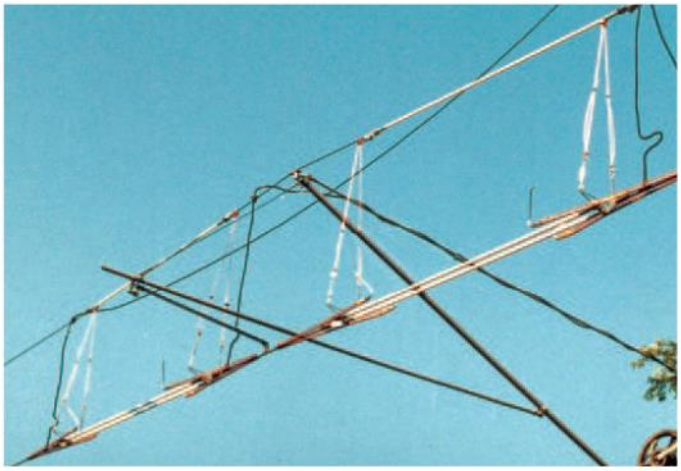

Figure 3.8 Photograph of Arthur Flury 2 rod neutral section from (Arthur Flury, 2011)

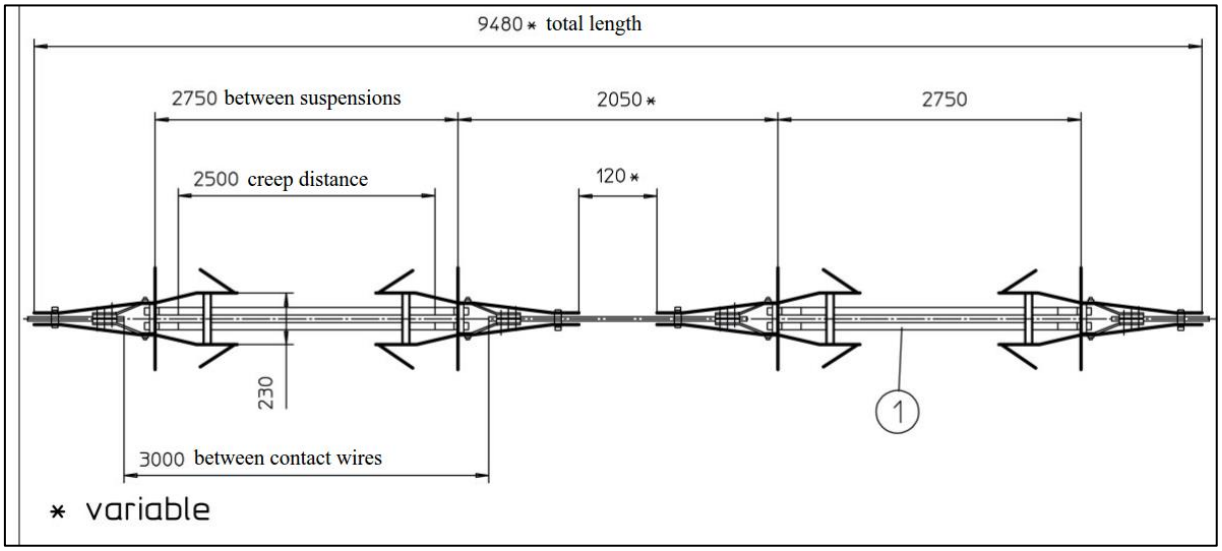

Figure 3.9 Plan view of Arthur Flury 2 rod neutral section from (Arthur Flury, 2011)

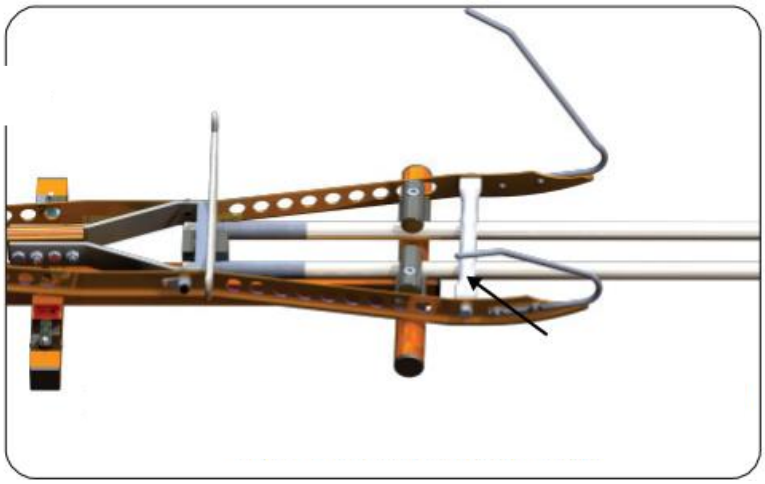

Figure 3.10 Detail of twin rod end fitting and skids (from (Arthur Flury, 2011))

The history and the rationale of the changes that were made to the design are documented in an internal Network Rail memorandum (Network Rail, 2012a) and conversations with the author of that document, together with discussions with the Network Rail engineers both centrally and in the regions 'at the coal face' responsible for delivering performance on the operating railway, have added further detail, although the complete rationale is not fully visible from the documentary record available.

The original standard AF neutral section design featured twin parallel PTFE covered glass fibre insulator rods, with skids to allow the pantograph head to negotiate smoothly across the insulator/contact wire connection. The use of twin parallel rods allowed a smaller glass fibre rod diameter which kept the neutral axis of the insulator close to that of the CW, reducing the bending due to the CW tension being transferred across an offset axis. The use of two rods however necessitates the use of an end fitting that cannot be negotiated by the pantograph head without the use of skids. Thus this design reverted to a pre-1980s concept (i.e. of using skids) that was abandoned when the BICC skidless ceramic bead insulator was introduced (see section 3.3).

The subsequent development of the AF neutral section essentially involves Network Rail prompting the manufacturer to undertake a variety of design improvements and developments (Network Rail, 2012a), although this is the action that drew criticism from Chris Gibb the author of a report (Network Rail, 2012b) into serious neutral section related incidents at Wembley, for muddying the waters of accountability of the original manufacturer for the performance of his product.

In a brief summary the changes introduced, and their consequences can be identified as:

- Initial experience of the West Coast (WC) indicated the 'standard' AF twin rod design did not perform well at 125 m/hr;
- Network Rail encouraged AF to develop a design with a single rod and without skids (2002);
- A subsequent version included rotating insulators (to allow wear to be spread evenly around the insulator circumference) using a stainless steel ratchet bolt (2003);
- Failures of stainless steel ratchet bolt initiated a move to titanium bolts (2008);
- Further failures of CW at the 'lead-in' end splice initiated the introduction of a 'lever arm' into the neutral section, and a further modification to the titanium ratchet bolts (2010) (Arthur Flury, 2014);
- Failures of CW splices led to a revised design of CW splice from AF, requiring a campaign of retro-fitting (Network Rail, 2012c);

The significant item here is the initiation of the development into a single rod, skidless adaptation of the original AF design. This neutral section has been characterised as having been 'assembled' rather than designed (Arthur Flury (UK), 2018). This version is now the dominant version of neutral section used extensively on Network Rail infrastructure. (This version is referred to as NSR25 on some, but not all, Arthur Flury documents, but is rarely referred to by this designation in Network Rail circles.) A general arrangement of this neutral section is shown in Figure 3.17, and a greater detail of one half (the neutral section being essentially symmetrical about the centre line) is shown in Figure 3.18.

The criticality of the neutral section failures prompted various lines of research by Network Rail with universities, technical specialist and others. One such report (IXC, 2014) investigated and drew attention to a number of issues, and from which made some recommendations. It observed:

- There are significant gaps in the knowledge about neutral sections in the UK network;
- Dynamic testing and modelling of neutral section has not been undertaken (or is not visible or available);
- Only static FEM analysis has been used on the critical components (splices, ratchet bolts etc.);
- The single rod type is only used in the UK;
- UK OCL is significantly more elastic (vertical stiffness) than the equivalent overseas varieties of OCL;
- Most pantograph/OCL dynamic simulation is directed towards the concept of 'current collection', and not the effect of pantograph passage on the wear and stresses and strain in individual components.

A variety of recommendations were made, those of which are relevant here:

- Undertake controlled testing and modelling of both components and systems;
- Adopting or collaborating with the main European research bodies active in this field, e.g. Polimi, IST Lisbon, SNCF;
- Install a highly instrumented neutral section in the line to measure strains at various points and components;

- Implement a full size neutral section laboratory test rig for receptive testing of pantograph passages (not known to exist elsewhere in Europe).

It can be seen that some of the questions addressed here in this research overlap with some of these observations and recommendations, although they are not directly related. It is understandable that IXC would arrive at many of same conclusions. Their report did not prompt this research.

Subsequent incidents caused ostensibly by fatigue failures of the contact wire inside the splice have led to further investigations, which are currently ongoing, but initial findings might indicate that the introduction of the lever arm itself is the cause of the fatigue problems (Network Rail, 2014b; Network Rail, 2014e; Network Rail, 2014d). Some regions of Network Rail have reverted to a neutral section without lever arm (Network Rail, 2015c). Figure 3.12 and Figure 3.13 show the fitting of the lever arm modification. Note that this is very similar in principle to the 'transition structure' developed by RTRI for rigid conductor beams and described more fully in Chapter 4 and (Kobayashi *et al.*, 2008a) and (Kobayashi *et al.*, 2008b).

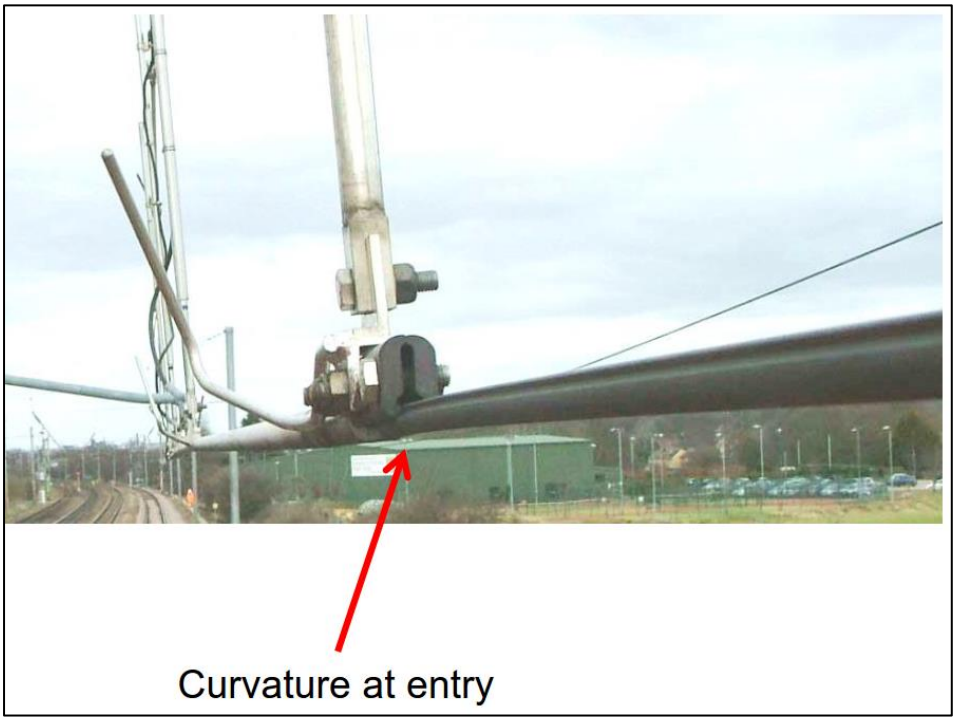

Figure 3.11 'Ramped' entry to CW splice of AF neutral section from (Arthur Flury, 2014)

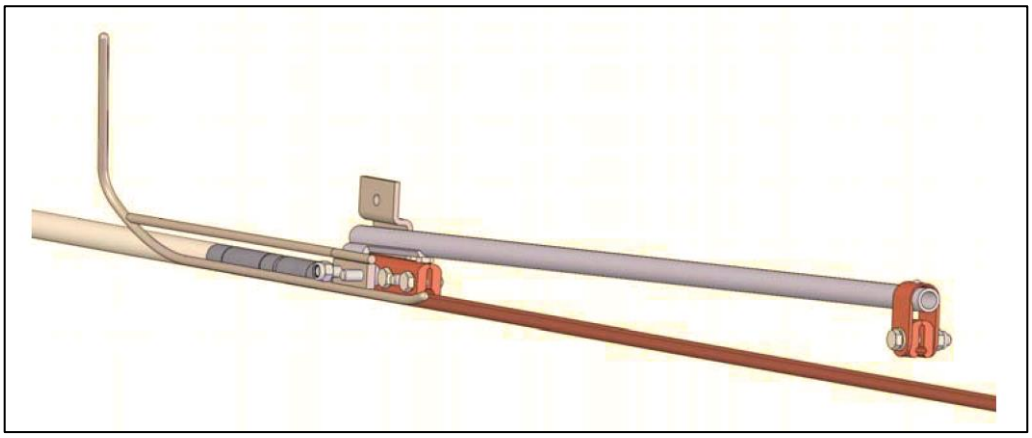

Figure 3.12 Fitting of the lever arm modification to AF neutral section from (Network Rail, 2013e)

Figure 3.13 Photograph of lever arm modification as installed (Arthur Flury, 2014). Direction of running from right to left

Figure 3.14 Photograph of Arthur Flury single rod neutral sections in adjacent tracks. Note the absence of lever arms. From (Dolphin, 2014)

Although, not fully relevant to the fundamental issue of this thesis, (i.e. the performance of a neutral section) the above history does indicate interesting aspects of the design development of such a piece of equipment. It demonstrates the complex nature of the neutral section and the need to balance the conflicting functionalities and characteristics of its component parts with the behaviour of the whole, and that the optimisation of component parts does not result in the optimisation of the whole.

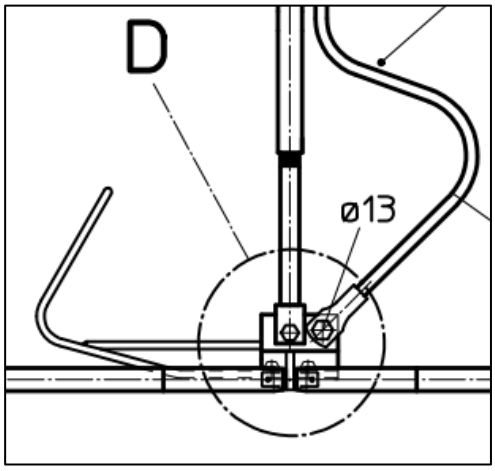

Figure 3.15 Detail of single rod connection and anti-torsion dropper (from AF drawing 655-936-504) (Arthur Flury, 2019)

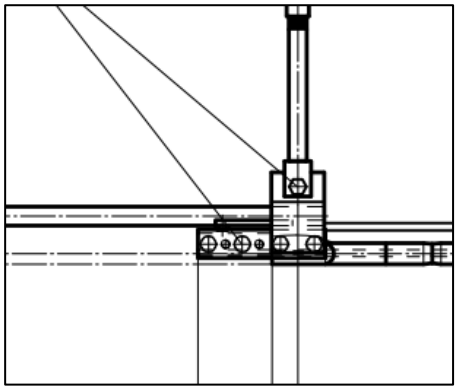

Figure 3.16 Detail of single rod CW connection and anti-torsion dropper (from AF drawing 655-936-504) (Arthur Flury, 2019)

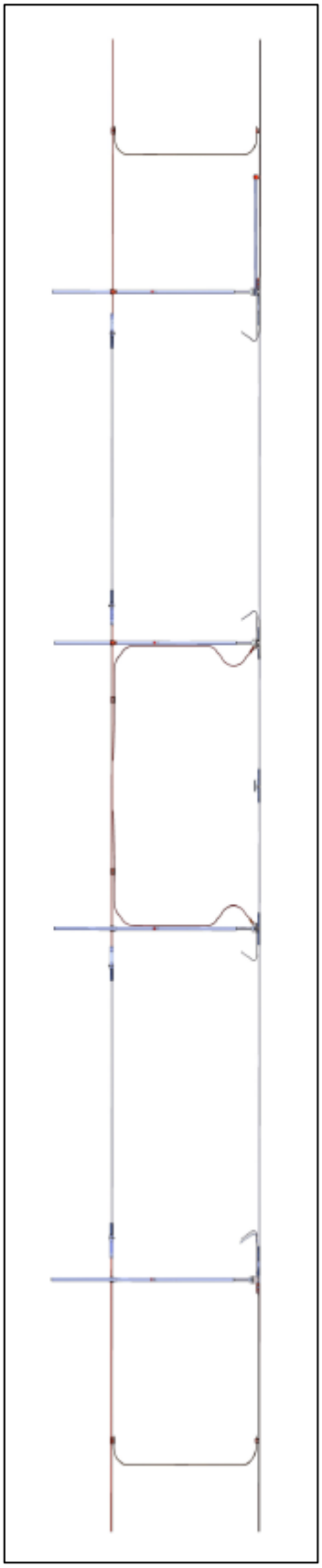

Figure 3.17 General arrangement of AF single rod neutral section (Arthur Flury, 2019) Note this is a later type modified by manufacturer to place the messenger insulators inside the spring droppers.

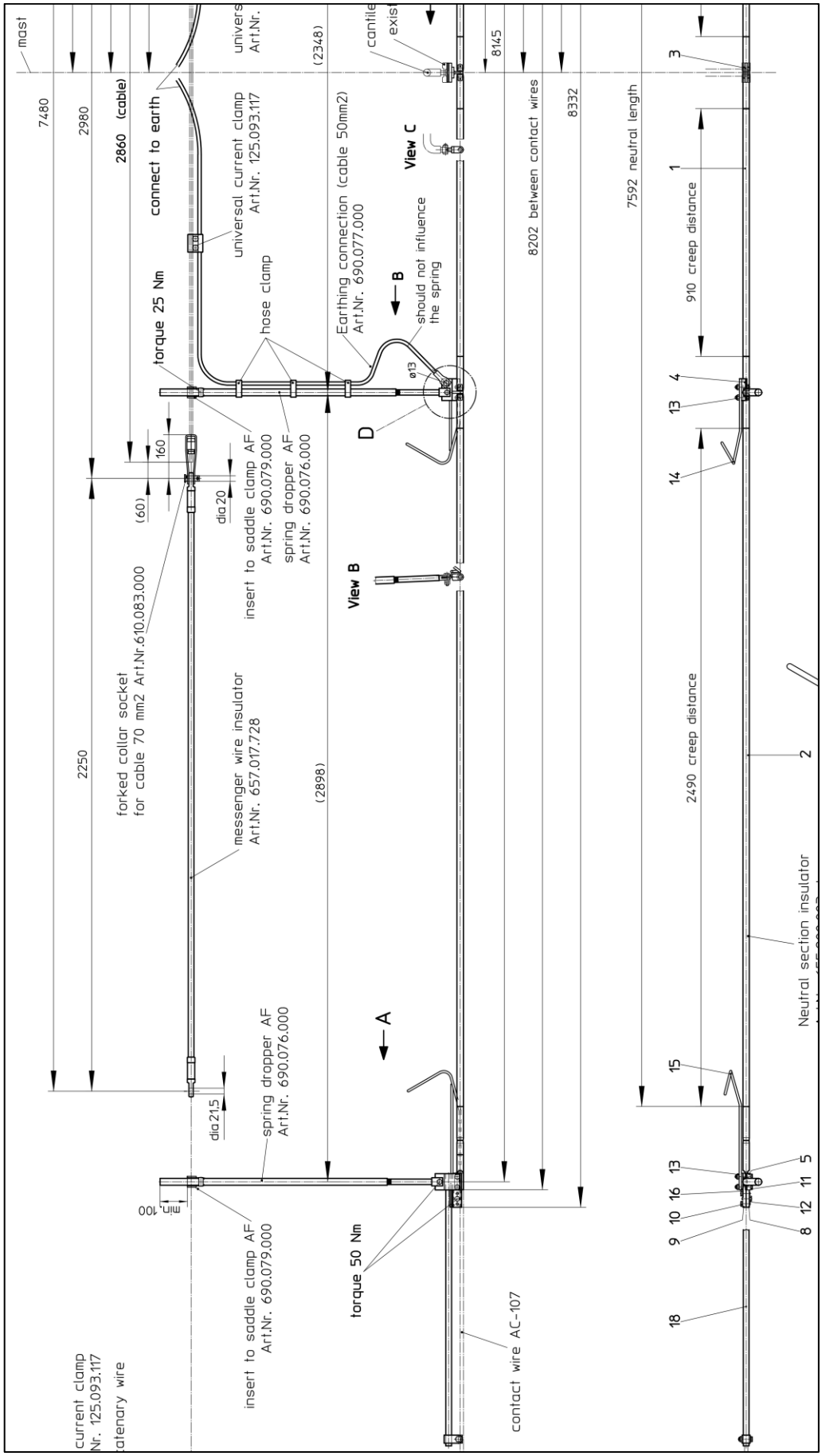

Figure 3.18 Detail of half of AF single rod neutral section (assembly is essentially symmetrical) From AF drawing 655-936-504 (Arthur Flury, 2019) Note this is a later type modified by manufacturer to place the messenger insulators inside the spring droppers.

3.5 Current European practice

As described above, a neutral section is required to effect a phase separation in ac electrified railways, where the supply is taken from the public network. Many electrified railways in Europe use the direct current dc system, which does not need or use a neutral section. In addition, the 15kV 16 $^{2}/_{3}$ Hz system, in the Germanic countries and Scandinavia, does not make great use of neutral sections as with this form of ac power supply the feeding sections can be interconnected, and often are.

At the present time, the size of the ac electrified network across Europe (includes EU and selected non-EU countries, excluding Russia) is as shown below in Table 3.1. Note that this data is indicative, due to different baseline dates for some countries data, and only 'main line' railways being included. This data is fundamentally based on 2014 data, sources (EU, 2014b; NeTIRail, 2015; UIC, 2015), and some national railways own websites, updated with more recent 2019 information (EU, 2019; UIC, 2019).

Table 3.1 Statistics of extent of rail electrification in Europe and systems in use

	Total route km	Electrified km	25kV[7] ac	15kV ac	3kV dc	1.5kV dc	750V dc
Austria	5,058	3,527	93	3,434			
Belgium	3,605	3,102	302		2,800		
Bulgaria	4,030	2,870	2,870				
Czech Republic	9,456	3,215	1,374		1,796		
Germany	39,219	20,746	36	19,124	24	204	1,358
Denmark	2,407	632	632				
Estonia	1033	132			132		
Greece	2,238	532	532				
Spain	16,870	10,123	3,323		6,800		
Finland	5,944	3,330		3,330			
France	30,581	16,741	10,225			6,520	
Croatia	2,604	970	970				

[7] Includes 2 x 25kV AT system as well

	Total route km	Electrified km	25kV[7] ac	15kV ac	3kV dc	1.5kV dc	750V dc
Hungary	7,892	3,138	3,138				
Ireland	1,919	108				108	
Italy	17,037	12,217	923		11,294		
Lithuania	1,911	152	152				
Luxembourg	275	262	262				
Latvia	1,853	245			245		
Netherlands	3,050	2,310	120			2,190	
Poland	18,513	11,779			11,779		
Portugal	2,544	1,629	1,629				
Romania	10,770	4,029	4,029				
Sweden	10,074	8,131		8,131			
Slovenia	1,208	610			610		
Slovak Republic	3,630	1,585	700		885		
United Kingdom	14,449	6,125	4,391			20	1,714
Norway	4,264	2,489		2,489			
Switzerland	4,061	4,061		4,061			
Montenegro	239	214	214				
FYROM	699	234	234				
Serbia	3,809	1,275	1,275				
Turkey	10,207	4,166	4,166				
TOTALS		130,679	41,590	40,569	36,365	9,042	3,072
PERCENTAGES		100%	31.8%	31.0%	27.8%	6.9%	2.4%

On the ac networks in UK and mainland Europe, neutral sections of a variety of types have been employed. Only 25kV networks are considered, as the 15kV 'Germanic' style of power supply uses a dedicated railway high voltage distribution network which allows all lines to be fed from a synchronised mesh, which does not require the adjacent

supplies to be separated (*15 kV AC railway electrification*, 2016). The type and circumstances of neutral sections in use by these networks is indicated in Table 3.2 below. The source of this information is from a variety of sources, some published, based on data, and some anecdotally or based on assumption or inference, and therefore is of a variable accuracy, and in some places incomplete. The information should therefore be seen as indicative. Those ac lines which are high speed[8] tend to use the 'long' or carrier wire neutral section as described previously, particularly as this is a requirement of the TSI (EU, 2014a) and the related European standards EN 50367 (British Standards Institution, 2012b). The use of short neutral sections is limited to slower speed applications, including, going forward, the UK where a recent Network Rail decision has limited them to line speeds of below 160 km/h (Network Rail, 2011c).

Details of short neutral section usage in (most) European countries using 25kV ac electrification are shown in Table 3.2, where data was readily available (including only those networks with greater than 1,000 km of 25kV route).

Table 3.2 Usage of neutral sections in Europe 25kV electrified lines (only showing those with significant route km, for which data is available)

Country	25kV ac route km	Neutral section usage
Bulgaria	2,861	Use twin rod type short neutral sections by Siemens or Arthur Flury (but longer than 8m), but require all trains to lower pantographs while transiting.
Czech Republic	1,374	Use the short neutral section made by the company EZ (Elzel), in use at 100 km/h. Experience is reportedly 'good'.
France	10,062	About 300 neutral sections, in 2011, about half on high speed (LGV) lines, so assumed to be 'long' types. Of the 'short type most are 30m long using section insulators, usually Galland, at 160 km/h. Some limited experience of Arthur Flury single rod at 200 km/h, but only 1 or 2 installed.
Hungary	3,012	*Data not available*
Portugal	1,629	A recent short (<8m) neutral section uses section insulators and a floating centre section, at 120 km/h on the Linea de Norte. Section insulators are of either Galland or Arthur Flury manufacture. Previously a longer (~30m) version was used. For speeds above 160 km/h, only overlaps are used.

[8] EU defines high speed as lines or sections of lines on which trains can go faster than 250 km/h at some point during the journey, EU (2014b) 'Transport in Figures, Statistical Pocketbook 2014'. Luxembourg: Publications Office of the European Union.

Country	25kV ac route km	Neutral section usage
Romania	4,029	*Data not available*
Spain	3,100	Anecdotally, all the 25kV lines in Spain are part of the high-speed network (AVE) and all neutral sections on running lines are of the 'long' type. Some short neutral sections may exist on low speed and operational connections.
United Kingdom	3,160	*See fuller detail in Table* 3.11 *and section 3.7.3*
Serbia	1,275	Some BICC ceramic bead types (with skids) are installed Belgrade – Bar section, at 120 km/h. Some local manufactured 'copies' are used. Currently considering AF single rod for use in (Chinese design) OCL for new 200 km/h project, Belgrade to Subotica (Hungary).
Turkey	3,330	High speed lines (up to 250 km/h) use long (>402m) overlap type neutral sections; Conventional lines at 160 km/h (maybe some at 200 km/h) use proprietary neutral section (Siemens or Arthur Flury), often in conjunction with a section insulator either side
TOTALS		

The data has been acquired from multiple sources including correspondence with helpful colleagues in the countries concerned (mentioned in 'Acknowledgements').

As can be seen, the types of short neutral section employed across Europe (including UK) are a mixture of directly sourced proprietary items from recognised manufacturers and suppliers of proprietary overhead line electrification components, and 'local' modifications and adaptations of these. Short neutral sections in Europe tend to be of proprietary manufacture, and the following manufacturers supplying the European market indicated below have been identified.

- Siemens AG Germany
- Arthur Flury AG Switzerland
- Galland-SAS France
- EZ (Elzel) Czech Republic
- Balfour Beatty/BICC UK
- MedSil Russia

Additionally TID Power (China) are known to supply silicone rubber or PTFE coated GRP insulator rods, but do not supply complete neutral sections.

Details of the standard offering neutral section from these manufacturers is available in their technical literature. Details of the local modifications and adaptations are more difficult to obtain.

The only neutral sections in use in Europe that are genuinely 'short' – i.e. comply with the less than 8.0m requirement of EN 50367 – are the Arthur Flury twin and single rod units (described in 3.4), and the Siemens twin rod 8WL5545 (see Figure 3.22 photograph left). Their use, other than UK, seems to be limited.

Other installations of 'short' (sic) neutral sections actually are longer than 8.0m but seem to be identified as such by the railway administrations, differentiated from the long and indeed very long installations made up solely from overlaps, and across which trains can pass without speed restrictions. The definition of 'short' seems to be predicated on the use of a discrete sectioning component in the arrangement, sometimes a section insulator, sometimes a single neutral section component. They are shorter than the 'split' neutral section (~142m) which is the third option offered in EN 50367. (The phrase 'Neutral Section' seems to be used loosely, in some cases, such as in UK and in this research, it refers to the complete installation, made up of two insulating breaks, where in other cases (e.g.Galland-SAS, 2016) just one of these insulators is a 'neutral section'.) These arrangements are made up variously, and some are shown in Figure 3.19.

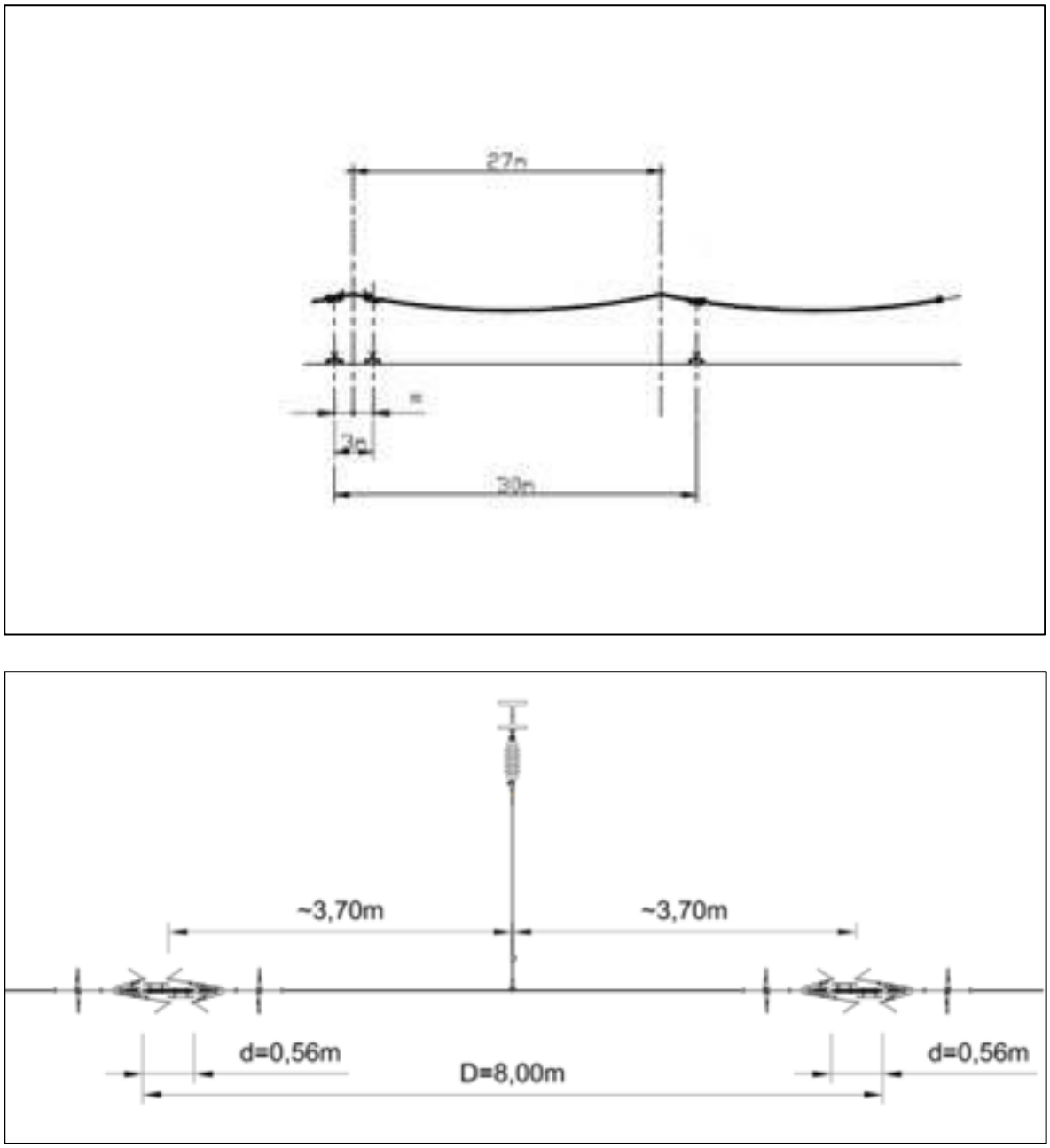

Figure 3.19 Examples of European neutral section installations (top) French 30 m with section insulators (SNCF, 2019) (bottom) Portuguese 8m neutral section with section insulators (Infrastruturas de Portugal, 2019)

It is not part of this work to scrutinise the definition of short, nor the benefits or otherwise of neutral sections of various lengths, in relation to multiple pantograph performance. The length of 8m is the minimum quoted pantograph separation in the table of permissible pantograph separations on multi pantograph trains, quoted in 4.2.13 of ENE TSI, and only then for speeds less than 80 km/h. The ENE TSI and EN 50367 are complementary, and were drafted to be so.

Most railway administrations accept some speed limitations on the use of 'short' neutral sections. In France (SNCF, 2019) the experience with short neutral sections with section insulators of various makes (mostly Galland and Arthur Flury) at 160 km/h is mixed, and their main priority is to find ways to install the 142m split neutral sections with overlaps, which is much preferred for reliability. In Czech Republic (Simanek, 2019) the short neutral section made by the company EZ is found to deliver a good experience, but speeds are relatively low at 100 km/h. In Portugal (Infrastruturas de Portugal, 2019) for speeds less than 160 km/h, typically 120 km/h a short neutral section created from two section insulators is used. In Serbia (Institute of Transportation (CIP) Belgrade, 2019) speeds generally are low, 120 km/h or even less, but experience with short neutral sections seems good, and they are favoured due to their minimal impact on signal placement, and train performance.

Also noted that many of the short neutral section installations use a 'floating' centre section, rather than earthed (either is allowed in the TSI/EN). Clearly an earthed centre section cannot be used where section insulators are employed, unless extra sections are introduced to prevent a direct earth fault being created, see Figure 3.20 and Figure 3.21 of a multi section neutral section using Galland components of around 14m (but not used in France).

Figure 3.20 Galland short neutral section installation not used in France. Source (Galland-SAS, 2016)

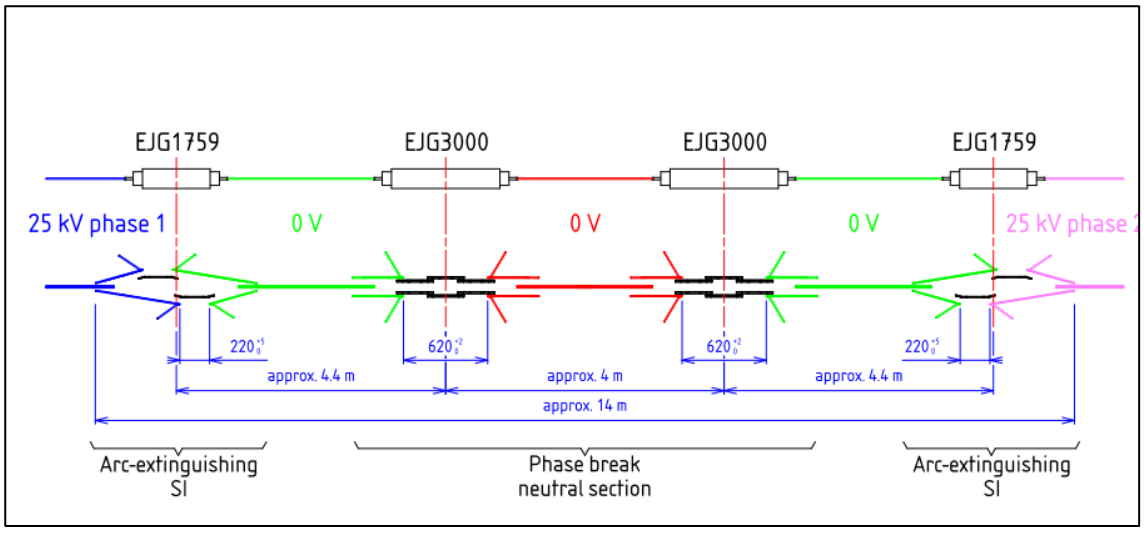

Figure 3.21 Galland short neutral section schematic showing use of devices called neutral section and section insulators (AUS Ltd, 2019)[9]

Overall, it would seem, even on this limited survey of European practice, that the UK, if not quite unique in its usage of short neutral sections, is at a different order of magnitude in terms of numbers of units used at speeds in the 160 – 200 km/h region, and under a high number of pantograph passages, see Table 3.11 later in this chapter. This usage may be seen as ambitious.

A comparative inspection of all the above types of short neutral section confirms the empirical observation that all true 'short' neutral sections have essentially the same features and form of delivering the primary functionality and indeed most of the secondary functionality, with some interesting variations in the details of their construction. These similarities and differences are examined in the next section.

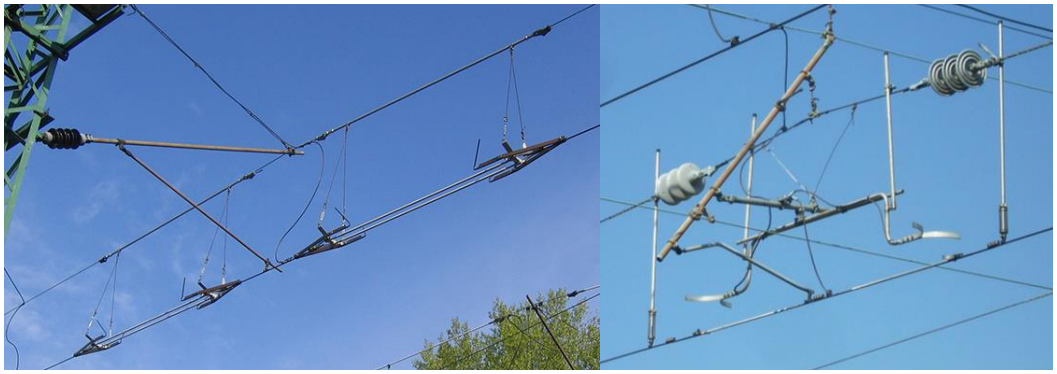
Figure 3.22 Photographs of neutral section examples left Siemens, right BICC(source Beardsmore). See also Figure 3.8 and Figure 3.14

[9] AUS Ltd are UK distributors of Galland-SAS products

A comparison of the major dimensions of the types of neutral section which are implemented as single discrete assemblies is shown in Table 3.3. It can be seen that one of the most significant features and points of difference is in the length of the insulating rods, and in particular the 'creepage' length (defined as the shortest distance along the surface of the insulating material between two conductive parts). In the case of an in-running insulator such as these, the creepage length has to be understood on consideration of the reduction created by skids, runners, arcing horns, and, when a pantograph passes, the along track dimension of the pantograph head. In the examples shown in the Table, there is greater than 2:1 difference between the longest and shortest. Some of this, but not all, is accounted for in pantograph head dimensions.

Table 3.3 Comparison of major dimensions of different neutral section types showing those which are marketed as complete assemblies

Manufacturer	Type	Drawing No.	Overall length	Insulator creepage length	Air gap	'earthed' length
BICC	Skidless (short)	109/807/A1	3982	1090	200 (to arc catcher horns)	762
BICC	Skidless (standard)	109/807/A1	4267	1260	200 (to arc catcher horns)	762
BICC	Skidless (long)	109/807/A1	5457	1854	200 (to arc catcher horns)	762
Arthur Flury	NS25UK10, 2 x rod	UK1-121-557 sh 1	9400	2500	1700	120 - 200
Arthur Flury	NSR single rod	655-936-514	8144	2490	2250	2348
Siemens	8WL5545	C-5992-AK-D7300-K111	7200	2010	1500	300

In the UK pantograph along track dimension is traditionally 260 or 400mm (RSSB, 2014a), but modern OCL for TSI compatible lines is designed for 650mm. For comparison, the values of electrical creepage distance[10] determined from the relevant European standards (British Standards Institution, 2017) for a 25kV system (with U_{Ni} =

[10] The shortest distance along the surface of insulating material between two conductive parts

170 or 200kV[11]) is given in Table A.7 of that standard as 880mm. So the worst case would be a creepage length of 1530mm.

It is not the intention of this study to address issues of electrical performance of the neutral section, being restricted as it is to dynamic behaviour, but the significantly greater overall length of the AF neutral section is noteworthy.

Other efforts have been made elsewhere in Europe to address the 'neutral section problem', or rather that of phase separation, and the need to deploy phase separation sections. The amount of work reported into neutral section developments and its contribution to overall OCL system performance is however limited. The Ifzone project (Acevedo *et al.*, 2011) in Spain considered only the very long (>1,000m) neutral section used in Spanish high speed lines (AVE). The main conclusion was the re-arrangement of the traction electrical feeding arrangements to minimise the occurrence of neutral sections, or the use of a switched neutral section whereby a shorter (albeit still around 400m, and not 'short' in the definition used in the European standards) was employed and the central, nominally un-energised, section was switched between one power supply and the next as the train passed, using fast acting semi-conductor devices. Work in France for SNCF (Bastian *et al.*, 2011) identifies the significant cost to the railway of disruption caused by the 'lack of respect' by train drivers of the power switch off requirements approaching neutral sections. A programme of investigation of possible remedies is described, although all are related, in one way or another, to electrical switching based solutions, both to back up the train power switch off, if the driver fails to implement, or to provide a switched neutral section which would not need auto power down to transit.

Furrer + Frey (Saxena and Gilgen, 2011) described work on a neutral section for Delhi Metro which is implemented in a rigid conductor beam situation and relates to the specific issues surrounding the implementation of a neutral section using the solid conductor beam arranged as a sequence of very short overlaps, which is possible with the conductor beam, as it is not tensioned. No in line insulators are used.

Little other material on neutral section development is available.

---

[11] Where U_{Ni} is the rated impulse voltage value characterising the specified withstand capability of insulation against transient overvoltages

3.6 A generic model of a short neutral section

The de facto industry standard approach to delivering the primary and secondary functionality for a true 'short' neutral section, as defined as <8.0m in the European standards, (described electrically in the diagram in Figure 3.25) based on the review of the proprietary European manufacturers' products, has been captured in two diagrams shown below in Figure 3.23 and Figure 3.24. (It has been seen above how some administrations colloquially refer to some neutral sections of greater than 8.0m as 'short', but this is not in accordance with the strict definition in EN 50367.)

Conceptually all the designs follow the primary functionality shown in Figure 3.23, with some differences in detail. In order practically to support the elements providing the primary functionality, further features need to be included, shown in Figure 3.24 as secondary functionality. Not all proprietary neutral section types have these secondary features, and where they do, there is more variation in detail than in the primary functionality. The primary functionality meets the requirements of the neutral section as defined in the relevant European and International standards, as described in section 3.8 later.

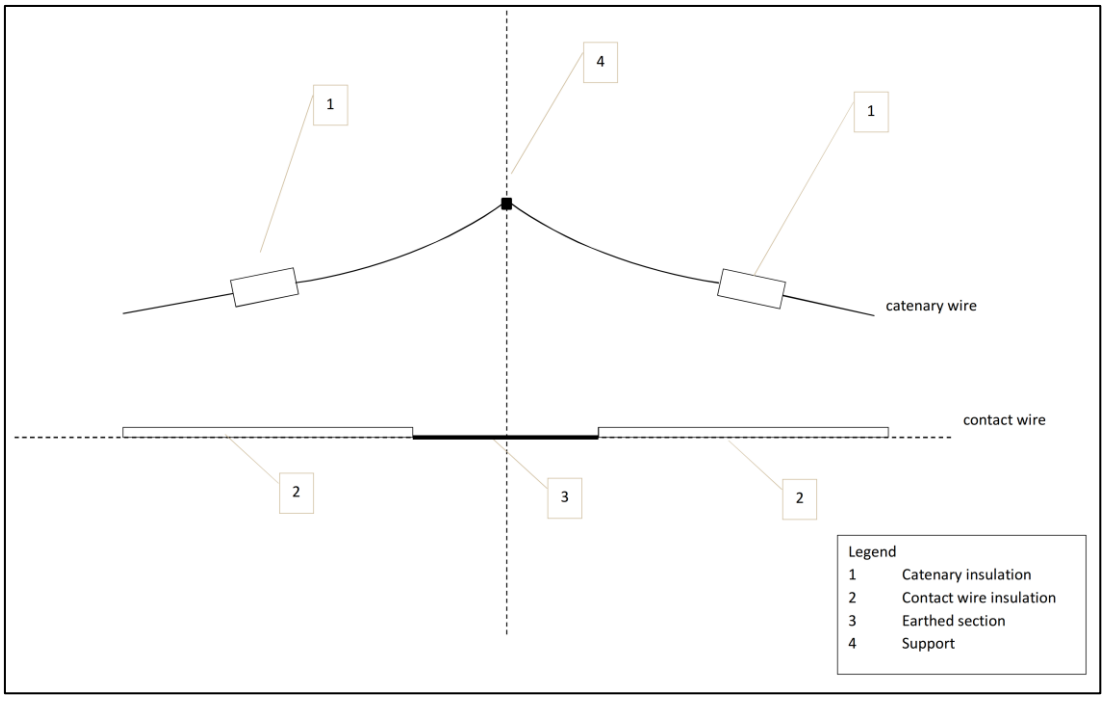

Figure 3.23 Generic neutral section primary functionality

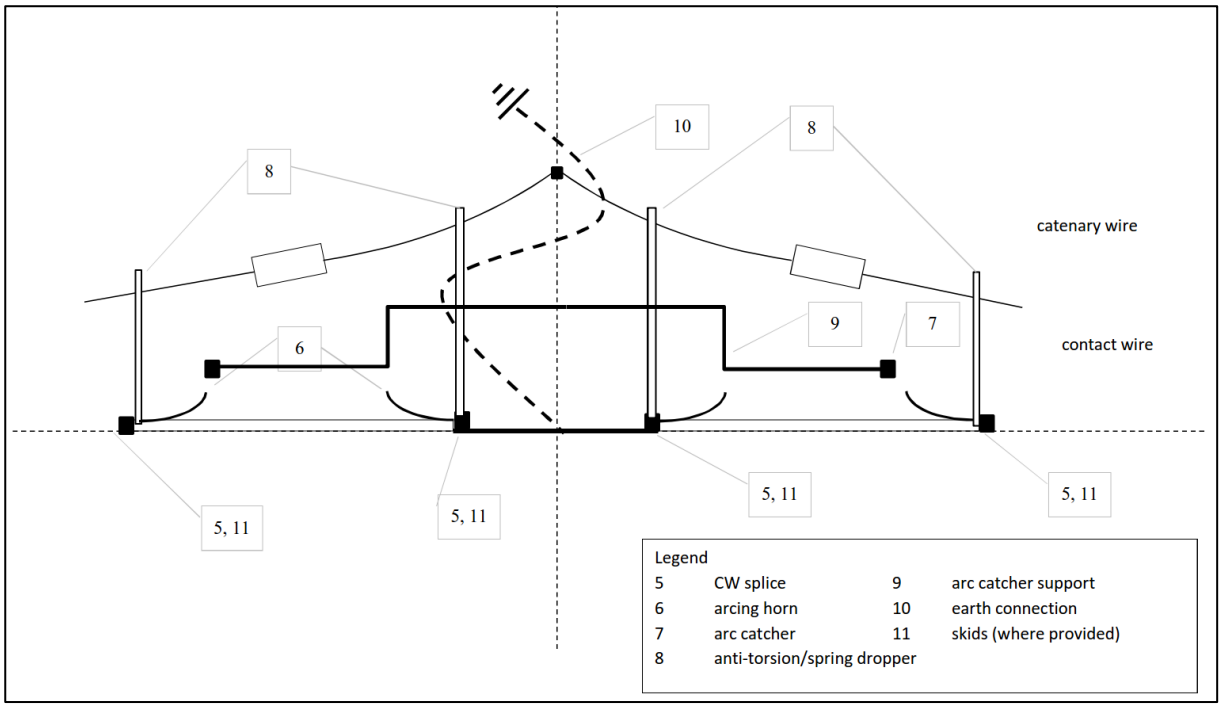

Figure 3.24 Generic neutral section secondary functionality (see Table 3.4)

The characteristics of the features are shown below in Table 3.4.

Table 3.4 Generic neutral section features (see Figure 3.23 and Figure 3.24)

Item	Feature	Functionality	Note
1	Messenger insulation	Primary	
2	Contact wire insulation	Primary	'in running' insulator makes contact with the pantograph head
3	Earthed section	Primary	Where provided
4	Support	Primary	
5	Contact wire splice	Secondary	Connects the CW to the insulator
6	Arcing horn	Secondary	Directs electrical arcs (if drawn) away from the insulator
7	Arc catcher	Secondary	Catches the arc from the arcing horns and directs to earth (where provided)
8	Anti-torsion/ spring dropper	Secondary	Maintains the whole assembly in the correct vertical orientation
9	Arc catcher support	Secondary	(where provided)
10	Earth connection	Secondary	(where provided)
11	Skids ('gliders')	Secondary	Carries the pantograph head past the discontinuities at the CW/insulator splice

What is referred to here as secondary functionality, can be considered as those features of the design and/or construction of the neutral section which are optional depending on choices and decisions of the manufacturer, based on the particular features of its construction, and which will not necessarily appear on every design of neutral section.

On the basis of this, it would seem appropriate for these models shown in Figure 3.23 and Figure 3.24 to be considered as the basis for a 'generic' model of a neutral section design arrangement, which could be used as the starting point for analysis, and which will permit aspects of its behaviour to be identified.

3.7 Current UK neutral section performance and reliability

3.7.1 More recent UK experience

The original premise of this research, i.e. short neutral section performance and possible optimisation, was proposed as a subject for this research by a senior Network Rail electrification engineer; this background has been described in Chapter 1.

Direct access to the Network Rail central electrification engineering team personnel, and good cooperation from them in access to, and provision of, data, reports and documentary information, and access to their current thinking and relevant workstreams, has allowed a better understanding of specific UK neutral section performance and reliability issues.

Neutral sections have always had 'performance implications' and traditionally have had the most onerous maintenance regime of all elements of the UK OCL system; typically six monthly 'hands on' inspections, compared to 2, 4 or 6 yearly for most other elements of the OCL (Network Rail, 2015d).

As part of the regulatory oversight regime, Network Rail submits an annual return of performance every year to the regulator (ORR), and in greater detail at the end of each 5 year control period (ORR, 2017b). Infrastructure 'incidents' causing train delays in excess of 500 minutes[12] are reported and published, broken down by infrastructure asset type (ORR, 2015a), (Network Rail, 2014a). The data reporting regime in Network Rail and ORR has not been consistent over the years, and for the purpose of this research a representative period of 9-10 years from 2006 to 2015, for which a reasonable quality and granularity of data is available, has been taken for analysis.

The headline data for the years 2006-2014 are shown in below, and, as can be seen, train delay minutes attributed to OCL failure as a cause run at about 3% of all Network Rail infrastructure caused reported train delay minutes. The detailed make up behind this data is available from Network Rail, for the years 2006-2010, and to a less detailed extent for earlier and later years, and can be analysed for the OCL incidents and those

[12] For recent years this has changed to 300 minutes

attributed to neutral section failure as the cause (Network Rail, 2011a). The analysis is shown in Table 3.6 below.

Table 3.5 Historical Network Rail delays due to OCL causes for the analysed time period 2006-2015

Reporting year	Minutes delay due to all infrastructure causes	Minutes delay due to OCL / 3rd rail causes	Minutes delay due to OCL incidents >500 mins
2006/07	10,491,906	336,596	192,715
2007/08	9,458,292	214,086	135,804
2008/09	8,776,680	214,291	155,658
2009/10	8,123,647	242,817	112,235
2010/11	8,914,451	249,121	151,179
2011/12	8,364,987	224,859	143,396
2012/13	8,817,320	320,595	208,322
2013/14	9,518,924	299,957	152,920

Table 3.6 OCL incidents causing train delays >500 minutes

	OCL incidents >500 mins		Neutral section incidents >500 mins			
Year	Number incidents	Total minutes	Number incidents	% of all OCL	Total minutes	% of all OCL
2006/07	69	192,715	6	8.70%	19,084	9.90%
2007/08	63	135,804	5	7.94%	7,061	5.20%
2008/09	66	155,658	5	7.58%	21,349	13.72%
2009/10	46	112,235	4	8.70%	18,200	16.22%
2010/11	61	151,179	2	3.28%	1,344	0.89%
2011/12	50	143,396	5	10.00%	26,158	18.24%
2012/13	52	208,322	1	1.92%	12,468	5.98%
2013/14	61	152,920	3	4.92%	18,784	12.28%
2014/15			3		17,488	

NOTE 1: incidents due to bird strikes and vegetation incursion are included but those proved to have been caused by defective train operating company (TOC) equipment, outside parties, vandalism and those arising as a direct result of extreme weather conditions are excluded.

NOTE 2: the sources of the above data in and Table 3.6 are from (ORR, 2015a), (Network Rail, 2014c) and (Network Rail, 2014a), to which additional depth of data was added from the responses received from a Freedom of Information request to Network Rail (Network Rail, 2015a).

NOTE 3: the cost associated with these train delay minutes is not available, although is recorded within Network Rail. Under the terms of Network Rail licence and the TOC's franchise agreements, payment are calculated for compensating TOCs for infrastructure caused train delays (and TOC on TOC delays), based on total aggregated delay minutes for all trains affected. The cost of the train delays due to the above incidents is not known, it varies by route, TOC and many other factors. Figures of £100-200 per minute are typical. As an indication, the West Coast report mentioned below quotes a figure of "between £500k and £1,500k" for Schedule 8 cost[13] of a failure between Rugby and Euston (Network Rail, 2012b).

These particular incidents and failures are examined below, but as an example of the importance with which these failures were held, is indicated by two particular incidents at Wembley, on the West Coast Main line from Euston to the North, in 2009 and 2010, causing in excess of 13,000 train delay minutes each, and which attracted serious Network Rail senior management attention (Network Rail, 2012b). Network Rail central engineering resources were actioned to address this issue.

The report for the ORR prepared by Network Rail on these West Coast Main Line performance issues (cited above) identified particularly the neutral section as the feature of the OCL causing the greatest contribution to unreliability, and criticised Network Rail OCL engineers for failure to transfer performance risk for this critical component to the original manufacturer.

The Network Rail annual return to the regulator for 2014 (Network Rail, 2014a) highlighted neutral section performance, stating:

"There was a significant increase in the number of AC traction power incidents causing delay due to equipment design, which increased by 23 percentage points, from 15 per cent in 2012/13 to 38 per cent in 2013/14. This was caused by design issues associated with a particular specification of neutral section (an OHL[14] asset used to separate different electrical supply points)." (Network Rail, 2014a).

---

[13] Schedule 8 is an automatic mechanism for ensuring that Network Rail and train operators are held financially harmless for delays that they cause to each other. The ORR sets the targets and the rates. A formula drives the payments, based upon who caused the delay, how bad the delay was, and how much fare box revenue is estimated to have been lost

[14] OHL: Overhead Line

3.7.2 Theoretical failure modes

This and other incident data, discussions with Network Rail OCL engineers and input from a variety of Failure Modes and Effects Analysis (FMEA) workshops and studies, indicates that the following failure modes shown in Table 3.7 exist, or are likely.

Table 3.7 Neutral section failure modes

1	Misaligned skids damaging pantograph carbons
2	Cracked/misaligned beads (in Balfour Beatty/BICC type) damaging pantograph carbons
3	(Fatally) damaged pantograph carbons initiate a dewirement downstream from the neutral section
4	(Fatally) damaged pantograph carbons causes a dewirement at a neutral section
5	Misaligned arcing horns damage pantograph carbons
6	Misaligned arcing horns/arc catchers fails to trap an arc (when drawn) and arc destroys the neutral section
7	Seized/stiff anti-torsion tube spring causes damaged pantograph carbons
8	Failure of contact wire splice causes neutral section to part

Insofar as the cause of failure is misalignment of a component, i.e. skids or arcing horns, etc., then this misalignment can itself be caused by either:

- Poor initial set up and installation;
- Excess force or impact from a previous pantograph passage.

It can also be deduced that some of the failures described above can be seen as a cascade, where a fault triggered by one pantograph passage becomes the trigger for an incident at a later pantograph passage. This may be a pantograph on a following train, or a second pantograph on the same train (as in multiple unit operation).

The above data has been extracted from two separate Fault Tree Analyses (by Arthur Flury and by Network Rail) which are not consistent or compatible, and so the above summary has been generated, in advance of a consolidated one becoming available. Additional data has been taken from the Network Rail standard for applying risk based maintenance to OCL asset types, (Network Rail, 2015d), which indicates that there are

35 number failure codes for the four neutral section types considered, indicating a significant interest in the failures.

3.7.3 Failure/incident analysis

The analysis of the incidents shown in and Table 3.6 above will provide some useful insight. The criteria for the analysis have been developed as below, and has been taken from the Network Rail incident reports and investigation, so far as they are available. These are the actual types of neutral section of which there are 4 types, 2 types of BICC (skidded and skidless) and two types of Arthur Flury (twin rod skidded and single rod skidless); the type of contact wire (107mm^2 and 120mm^2) and the line speed of the installation of the neutral section of the failure. It is recognised that this data has been filtered by the over-500 minutes criteria established by the ORR for Network Rail reporting and oversight, and that in some ways, this is arbitrary, as it can be imagined that some 'potential' over-500 minutes failures might be identified by a routine OCL maintenance patrol and rectified prior to their causing any (significant) delays. But the volume and quality of the data is broadly suitable for these purposes. The summary of the incidents shown in Table 3.6 broken down by the above criteria is shown in Table 3.8 and Table 3.9 below. Sources (Network Rail, 2011a; Network Rail, 2014a; Network Rail, 2014c; Network Rail, 2015a; Network Rail, 2015b; RIA, 2016).

Table 3.8 Neutral section failures by neutral section type, 2006-2015

Neutral section type	No. incidents	Minutes delay
BICC skidded ceramic bead	--	--
BICC skidless ceramic bead	17	49,033
AF 2 x rod skidded		
AF skidless single rod	16	91.359
Unknown type (data insufficient)	4	4,410

The analysis by line speed is shown below in Table 3.9. Note that the line speed is the speed of the track on which neutral section installed, not necessarily the speed of the train causing the incident. 51% of all incidents, and 83% of all delay minutes are caused by incidents on lines of 100 m/hr or over. Table 3.11 indicates a population of only 105 units of neutral section for this speed range, giving a train delay impact of over 900 minutes per unit over the analysis period.

Table 3.9 Network Rail Neutral section failures by line speed, 2006-2015

Line speed	No. incidents	Minutes delay
0 – 74 m/hr	5	5,491
75 – 99 m/hr	11	29,734
100- 125 m/hr	17	95,441

The data from Table 3.8 can be further broken down to indicate the 'worst offending' incidents by neutral section type. It can be seen that the AF type are responsible for most of the incidents with the bigger delays. It is believed that all the 16 AF neutral section incidents (bar one) were associated with line speeds of 100 m/hr or more. (These line speed ranges are different to those shown in Table 3.11, as no incidents were found on the 149 neutral sections installed on slow speed lines of 40 m/hr or less.)

Table 3.10 Network Rail neutral section failures by type and minutes delay, 2006-2015

		Minutes delay				
		500-1,000	1,000-2,000	2,000-5,000	5,000-10,000	Over 10,000
Type	total incidents					
BICC skidless CB	17	7	4	3	2	1
AF single rod skidless	16	4	2	3	4	3

This data has been assembled from multiple sources within Network Rail, including published asset stewardship information, statutory reports to the ORR, internal Network Rail incident tracking data, and is of a variable level of detail and granularity. This analysis by line speed in Table 3.11 is less reliable than the other data, as not all incident reports confirm on which line (of many) the neutral section was located, and some assumptions have been made.

Table 3.11 Network Rail neutral section population by line speed approximate numbers, due to varying validity dates of different sources of information.

Network Rail neutral section population by line speed				
	line speed (m/hr)			
	0-40	41-99	100+	Totals
Network Rail zone				
Anglia	10	73	37	120
London North Western	60	77	27	164
London North Eastern	62	56	11	129
Scotland	11	48	30	89
Western	6	7	0	13
TOTALS	149	261	105	515

The overall population of neutral sections, on the Network Rail network, at a date around 2015 (but not exact due to varying validity dates of different sources of information) is given in Table 3.11. Sources are (Network Rail, 2018; Railway Codes, 2018). The overall total, with the same caveat on accuracy, is around 515. Although exact numbers of the different types are difficult to obtain with certainty, due to ongoing (and overlapping) programmes of replacement of earlier types with the AF single rod, it is understood that a reasonable rule of thumb is that all the neutral sections on lines with line speeds of 100 m/hr and above are now the AF single rod type. Two track main lines, whatever speed, are also likely to be AF single rod. The remainder are mostly BR/BICC skidless ceramic bead types. No AF twin rod types remain (Network Rail, 2013d; Network Rail, 2014e). At the end of 2010 the numbers of AF neutral sections were quoted as 156, (based on 121 on LNW[15] route, 4 on LNE[16] route and 31 on Anglia route) (Network Rail, 2010a). There is a likelihood that some skidded BR/BICC types remain on very low speed and lightly used lines.

Not all the 37 incidents included in the statistics for the period of interest 2006 - 2015 are found to be genuine neutral section incidents. A number (four) have been removed

[15] London North Western, essentially the West Coast Main Line and branches
[16] London North Eastern, essentially the East Coast Main Line and branches

from the statistics shown in Table 3.6, as they are found not to be neutral section incidents (some high speed section insulators use ceramic bead insulators and can be misreported as 'neutral sections', some incidents at neutral section locations, but not affecting or caused by the neutral section, can be misreported, etc). There are 33 genuine neutral section incidents over 500 minutes train delay in the 2006 -2015 period.

As far as can be determined, given the quality and availability of the records, the causes of the (16) AF neutral section incidents are shown in Table 3.12.

Table 3.12 Network Rail Arthur Flury neutral section incidents by reported cause, and train delay minutes, 2006-2015.

ID	Cause	No.	Total delay minutes
1	CW fatigue at splice/lever arm	4	24,930
2	CW splice failure	2	800
3	Torsion rod (spring dropper) failure	1	1,616
4	Earthed cable connection	1	1,388
5	Neutral section parted at CW-insulator end ferrule connection	4	44,825
6	'skid assembly' (?)	3	3,371
7	Other (not known)	1	4,703

The two greatest contributors are items 1 and 5, which have been identified previously. Item 1 is the fatigue failure of the CW as it enters/leaves to lever arm, and was the cause of the two large incident s at Tallington and Retford (Network Rail, 2013f; Network Rail, 2014f). As has been described, this has led to the removal of lever arms in many cases. Item 5 is the failure of the stainless steel ratchet bolt, which has prompted the campaign change to replacement by the titanium version. The splice failures (item 2) are probably the material quality issue in splices which prompted a change in material specification (CuNi1Si to CuNi3Si and then back again), and 3 bolt to 4 bolt variety. The reference to 'skids' in the three of type 6 is not clear, it is unlikely that there are any skidded neutral section left, and may be a misreport from a first responder of a splice failure.

The summary and analysis above in Table 3.6 and Table 3.8, is based upon the best interpretation of the data that could be made, and is qualified. It has been admitted by Network Rail that the level of forensic investigation and record keeping subsequent to

an incident is not always satisfactory, the main emphasis being on the reinstatement of normal rail services (Network Rail, 2016).

What is immediately noticeable is that over the analysis period for which the data applies, the new, replacement neutral section, the AF skidless single rod, has been responsible for more incidents and minutes delay than its predecessor type. This bearing in mind that due to the campaign changes, the newer type would be more widely found in 'vulnerable' locations where it had replaced the BICC skidless type.

3.8 Neutral section functionality in standards

The primary functionality, for the purposes of this research, has been taken as the function described in the various European level technical standards in the subject: BS EN 50119 (British Standards Institution, 2009), BS EN 50317 (British Standards Institution, 2012a), BS EN 50318 (British Standards Institution, 2002), BS EN 50367 (British Standards Institution, 2012b) and the Energy Technical Specification for Interoperability[17] (TSI) (EU, 2014a).

Clause 3.15 of BS EN 50367 (British Standards Institution, 2012b) gives the definition of separation section or neutral section as:

> *"section of a contact line provided with a sectioning point at each end to prevent successive electrical sections, differing in voltage, phase or frequency being connected together by the passage of current collectors"*

This is shown schematically in figure A.3 of that standard (show below in Figure 3.25).

[17] For further explanation on TSIs, see Appendix A

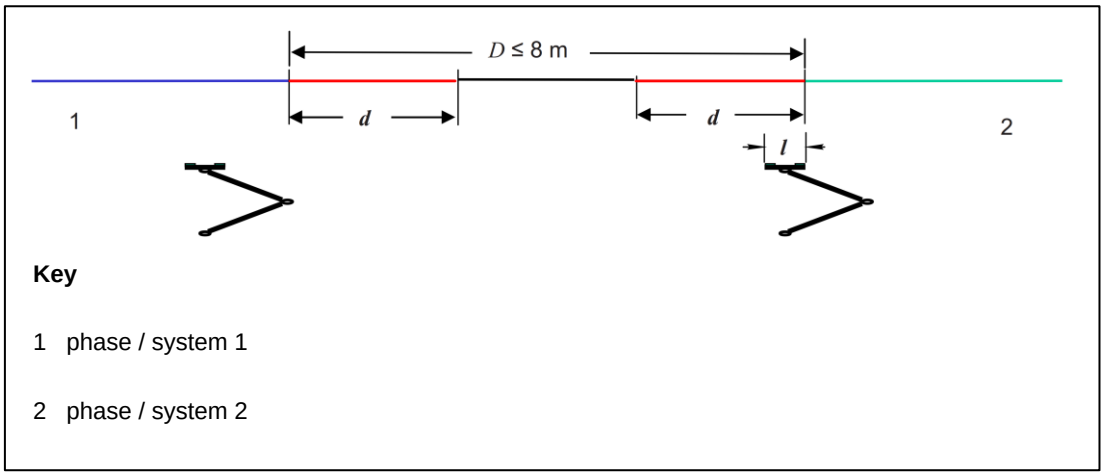

Figure 3.25 Short neutral section schematic taken from BS EN 50367:2012 (British Standards Institution, 2012b)

In Figure 3.6, the dimensions *D, d* and *l* represent:

D overall length of the un-energised section (not necessarily earthed)

d length of the insulator section

l length of the pantograph head

Additionally Figure 3.26 is an enlargement of a Functional Block Diagram (FBD) of the functionality of a neutral section taken from a FMEA study workshop held by Network Rail. Further details of reliability engineering assessment of OCL and an electrification FBD are given in (Morris and Giddins, 2015). This can be mapped onto the electrical feeding scheme described in Chapter 2.

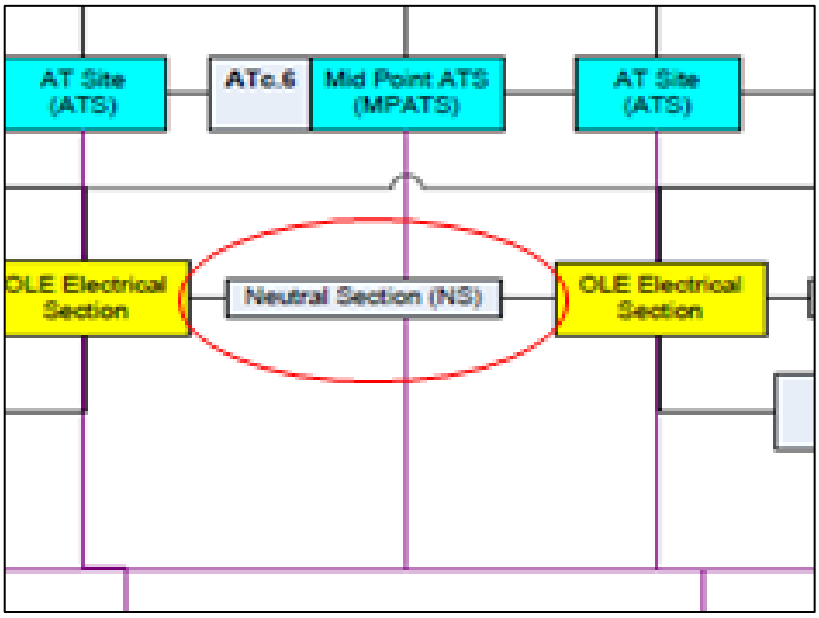

Figure 3.26 Extract from neutral section Functional Block Diagram source (Network Rail, 2013a)

The performance requirement from a physical/mechanical (i.e. non-electrical) point of view is given in brief form in BS EN 50119 (British Standards Institution, 2009) as:

> *"The sectioning device shall be designed such that no permanent or temporary deformation shall appear at 1,33 times the working tensile load. When traversed by a pantograph at the operational speed as defined in 5.2.5, the contact forces shall comply with 5.2.5.2. In addition, the sectioning device shall not damage the pantograph collector strip".*

Although the reference to 'temporary deformation' is unhelpful as it clearly cannot refer to elastic strain.

Clause 5.2.5.2 of EN 50119 requires that the peak force is less than 350N.

The Energy TSI (EU, 2014a) defines a "Neutral section insulator" as:

> *"An assembly inserted in a continuous run of contact line for isolating two electrical sections from each other that maintains continuous current collection during pantograph passage."*

However, this is an error, as the reference to 'continuous current collection' is erroneous. It is thought that this should say 'continuous pantograph contact' (NB this definition is correct for a 'section insulator'). It is understood that this error will be corrected in the next version of the TSI, expected around 2020/21 (RSSB, 2018b).

In the body of the TSI text, the general requirements for a phase separation section are given in 4.2.15 as:

> *"(1) The design of phase separation sections shall ensure that trains can move from one section to an adjacent one without bridging the two phases. Power consumption of the train (traction, auxiliaries and no-load current of the transformer) shall be brought to zero before entering the phase separation section. Adequate means (except for the short separation section) shall be provided to allow a train that is stopped within the phase separation section to be restarted.*
>
> *(2) The overall length D of neutral sections is defined in EN 50367:2012, clause 4. For the calculation of D clearances in accordance to*

EN 50119:2009, clause 5.1.3 and an uplift of S_0 shall be taken into account."

The specific requirements for a short neutral section, which is prescribed for speeds lower than 250 km/h, are given as:

"The design of separation sections shall normally adopt solutions as described in EN 50367:2012, Annex A.1. Where an alternative solution is proposed, it shall be demonstrated that the alternative is at least as reliable."

The above requirements can be seen to map onto what is described above as primary functionality and shown in Figure 3.23. What I have called secondary functionality is provided by those parts of the neutral section that are there to support or facilitate the primary functionality.

3.9 Developing a neutral section performance specification

The somewhat brief details given in 3.8 above are all that is available in the published standards, and many networks, including Network Rail, believe more detail and prescription is required to fully define the type of neutral section they require.

Equally for the purpose this research, more specific detail is required to provide an assessable benchmark against which both existing and any proposed neutral section design can be tested.

Consequently a fuller specification for neutral section performance and functionality is developed here.

The Network Rail company standard for maintenance and inspection standards for overhead line equipment, NR/L2/ELP/21088 (Network Rail, 2006), in item 12.3, indicates pantograph longitudinal acceleration limits, in normal operation, for neutral sections of 15g. Accelerations found in the range 5g – 15g are to be 'monitored'. Item 12.1 gives a limit for peak contact forces of 250N. However, in Appendix D of NR/L2/ELP/21087 (Network Rail, 2015d) values of 8g and 15g (for pantograph longitudinal acceleration) are given as triggers for investigative and/or remedial action to be taken.

As of August 2015, Network Rail have produced a draft version of a proposed neutral section procurement specification (Network Rail, 2015e) which contains a number of performance requirements, (as well as compatibility, commercial, etc).

The performance requirements stated include the following items:

- References to BS EN 50367 and BS EN 50119 (as above)
- References to 'smooth transitions' and not damaging or chipping pantograph carbons
- a peak force of less than 350N under single and multiple pantograph passages at speeds up to 125 m/hr (200 km/h)
- withstand a longitudinal pantograph acceleration of 10g
- cater for static, dynamic and aerodynamic uplift displacements up to 250mm.

Additionally the specification seems to suggest a single neutral section design or type to be provided which will accommodate all of the OCL designs currently in usage on Network Rail. This implies a range of conductor tensions and sizes to be accommodated.

The author has fed comments on this draft back to Network Rail, including the following suggestions, based on the work done here so far:

- clarification of how compromises associated with attempting to accommodate OCL types of differing conductor tensions and sizes in a single neutral section type are to be addressed;
- clarification of pantograph head types and dimensions to be accommodated;
- clarification that the spatial relationship of all the parts should remain unaffected (e.g. arcing horns etc) by high forces and uplifts during pantograph passage.

In assessing the performance of any neutral section in later parts of this research, the two criteria that will be examined are peak forces, and uplift (vertical displacement). Values of peak force of both 250N and 350N will be considered as upper thresholds. As it is extremely unlikely that a vertical displacement of anything close to 250mm is encountered, uplift will be assessed on a relative basis to a baseline model.

3.10 Conclusions

This chapter has identified the need for short neutral sections, and the early and more recent development of the design and construction features of widely used types.

It has been shown how the performance has always been below expectations, and pointed out the difficulty to intuitively optimise the design, and the overall need to achieve a blend of competing compromises. Although current and recent performance data for Network Rail in the UK is poorly detailed, the high level picture is of a cause for concern.

The use of short neutral sections at main line running speeds in UK, if not unique, is at an extreme compared to wider European practice. I have defined a generic model of a neutral section, identified some performance criteria from experience, standards and users specifications that might be used as criteria in the analysis of the design. This has satisfactorily answered an initial research question and created the context for the remainder of this research.

Chapter 4 Developments in Analysing the Pantograph and Overhead Line Interaction

4.1 Summary

This chapter describes the theory and practice of analysing the physical, mechanical and dynamic interaction between the pantograph and an overhead contact line (OCL). Different approaches to modelling and analysing are described and assessed. The relevance of any of these methods to the application of neutral section performance is discussed, with a view to adapting this approach to analysis of the neutral section problem.

4.2 Background

The economics of railway electrification require that the infrastructure provided to supply electricity to the trains is as cost efficient as possible. As described in section 2.7 the advent of ac electrification, with higher voltages and lower currents, allowed a more economic contact line, with lightweight overhead line equipment, to be utilised. This in place of the heavier and more expensive type OCL required for higher currents found in the previous dc electrification. The lighter weight permitted an increased spacing between supports, and hence fewer supports. However these longer spans introduced the potential of problems with current collection quality, as a greater variation in OCL system elasticity (defined a vertical displacement per pantograph uplift force, expressed usually in mm/N) at the supports relative to the middle of the span occurs, leading to dynamic movement of pantograph head, and resulting in variations in contact forces. In current European standards for OCL, elasticity variation (within a span) is a defined criterion (British Standards Institution, 2009), and is recommended to be minimised.

Clearly the reliable performance of a vulnerable piece of roof mounted train equipment – the pantograph – is important to the robust operation of the railway. An adequate contact between the pantograph and the CW of the OCL allows for uninterrupted transfer of electric current, and contributes to the overall operational performance.

It is the purpose of the study of the pantograph/OCL interaction to identify a behaviour that delivers a satisfactory contact (and hence collection of current) between the pantograph head and the contact wire of the OCL. The objective is to achieve an

optimisation where the applied forces are sufficiently high to achieve this contact continuously, without interruption, while at the same time not so great as to introduce excessive energy into the system, causing unacceptable wear to the components, and leading to poor reliability and early failures (Dahlberg, 2006).

More recently, the pantograph/OCL interface has also been defined as an assessable criterion of the energy subsystem in the Technical Specifications for Interoperability (TSIs) (EU, 2014a) supporting the EU Interoperability Directive (EU, 2008); see later in this chapter, and also in Appendix A for general description of Interoperability.

4.3 Early work on pantograph/OCL interaction analysis

The relevant early history of the analysis of pantograph/OCL interaction dates from the early 1960s, with the increasing wider application of ac electrification and the availability of (relatively) ready access to computing power, in Europe and the US.

The early work of Morris (Morris, 1965) was geared towards solutions using analogue computers to understand the interaction and optimise the parameters of the OCL and pantograph, and although not contributing to a numerical solution, made a good start on the discussion of the concept of 'quality of current collection'.

Abbott (Abbott, 1968), in 1968 looked at the particular case of a "trolley wire" type of OCL (being a single wire without a supporting messenger) and adopted the finite difference method for the solution of the partial differential equations that are used to describe the motion of the wires, at the discrete time steps considered.

Levy, Blain & Leclerc (Levy *et al.*, 1968) in the U.S. described the dynamics in terms of Lagrangian equations of motion (of each wire) and used these to create modal matrices, solved by an eigenvalue programme to give mode shapes and frequencies.

All of these early studies used a simple lumped parameter (mass – spring – damper) model of the pantograph (example shown in Figure 4.1) that has been perpetuated in most studies since, although in earlier work generally incorporating only two masses, as suggested by the less sophisticated pantograph types of the time.

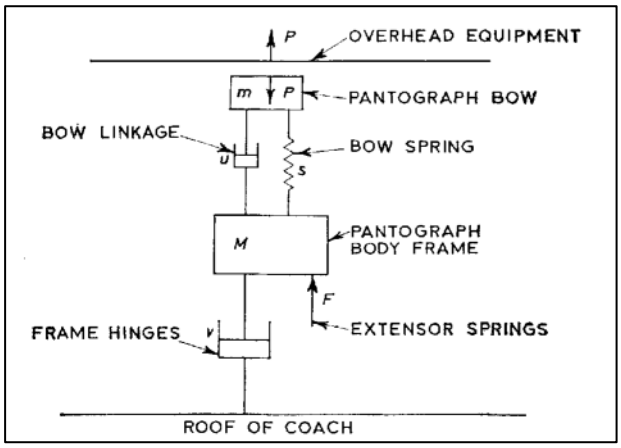

Figure 4.1 A simple pantograph model of the type used in early studies source (Abbott, 1968)

Ockenden and Tayler (Ockendon and Tayler, 1971), alternatively, proposed a system which only required the solution of linear ordinary differential equations.

Work from British Rail (BR) research in 1976 (Elkins, 1976) did a comprehensive and critical review of much of the earlier work, including those mentioned above, and formulated a development of the normal modes method of Levy (Levy *et al.*, 1968). This also allowed a theoretical prediction of mode shape and frequencies to be compared with measured values, and thus achieving validation.

This work, via a better understanding of pantograph dynamics, led directly to the development of the so-called BR/Brecknell Willis pantograph, which is in use to this day, and allowed improved current collection on the lighter UK type of OCL, (Gostling and Hobbs, 1981) and (Gostling and Hobbs, 1983), and indirectly contributed to the low cost of electrification obtained in the UK railways at the time.

4.4 Recent development work supporting spread of high speed rail

In recent years the worldwide (but particularly in Europe) development of high speed railway applications has initiated a wider interest in the theoretical approach to pantograph/OCL interaction, modelled via a variety of techniques. This has created a significant amount of academic material, and documented research on the subject. The key contributors are Politechnico Milano (POLIMI), IST Lisbon, Universidad Pontificia Comillas Madrid, and Japanese Railway Technical Research Institute (RTRI), together with German Railways (DB) and French Railways (SNCF), amongst others.

In more recent years, the performance of the pantograph/OCL interface has been defined as an 'interoperable' requirement in the context of the EU Interoperability

Directive, (EU, 2008) (and described more fully in Appendix A), and articulated in the various Technical Specifications for Interoperability (TSIs) where the subsystems of the railway are defined technically to allow independent and separate assessment of each component, to allow pan-European technical interoperability to be achieved (Harassek, 2015). This has been made more difficult as the pantograph is defined as a component in the locomotive and passenger rolling stock (known by acronym LOC&PAS) TSI and the OCL as a component in the Energy (ENE) TSI; this notwithstanding the traditional and widely held view that the pantograph and OCL are a 'couple' (Bobillot *et al.*, 2008) and should be treated as such.

The push from high speed rail development in this field of research has been supported by a number of EU funded programmes. Two in particular are relevant: EUROPAC and PantoTRAIN.

EUROPAC (European Optimised Pantograph Catenary Interface) is a project funded by EU FP6[18] (project no. 012440), which took place from 1 January 2005 to 31 December 2007, and gathered major European railway stakeholders around a research project on vehicle-infrastructure interaction through the pantograph/OCL contact. It resulted in three major outcomes: a joint simulation software, a track-side monitoring station and an on-board monitoring system (EUROPAC Consortium, 2008).

PantoTRAIN is one of a group of three projects, together called TrioTRAIN, (Hanley *et al.*, 2014), (from the acronym for Total Regulatory Acceptance for the Interoperable Network[19]) and aimed *"…to propose an innovative methodology that would ease rail vehicle certification process in Europe"* (UNIFE, 2011).

It involved a number of rail and academic partners throughout Europe, ran from 2009 to 2013 (RSSB, 2012a), and was funded by EU FP7[20] (project no. 234015).

---

[18] FP6 is the short name for the EU Sixth Framework Programme for Research, Technological Development and Demonstration. This was the EU's main instrument for funding research in Europe from 2002-2006. EU (2015) *Research and Innovation: Sixth Framework Programme*. Available at: https://ec.europa.eu/research/fp6/index_en.cfm (Accessed: 03 Nov. 2016).

[19] http://www.triotrain.eu

[20] FP7 is the short name for the EU Seventh Framework Programme for Research and Technological Development. This was the EU's main instrument for funding research in Europe from 2007-2013. EU (2016) *Research and Innovation: FP7*. Available at: https://ec.europa.eu/research/fp7/index_en.cfm (Accessed: 03 Nov. 2016).

The three main aims of PantoTRAIN were:

- To increase pantograph interoperability, by virtual assessment of the interaction of the same pantograph with different types of overhead line equipment;
- To reduce the number of line tests required for certification, the overall certification time, the associated costs, and the influence of uncontrolled conditions; and
- To explore the synergies between the (virtual) certification with the design stage of the pantograph and of the OCL subsystems, to reduce substantially the time-to-market of new concepts.

The work was divided amongst the participants and into six workstreams (work packages, WP):

WP 1: Criteria to build and validate pantograph/OCL numerical simulation tools;

WP 2: Hardware-in-the-Loop testing of pantographs;

WP 3: Virtual homologation for interoperability;

WP 4: Virtual extension of homologation for a pantograph with minor changes;

WP 5: New innovative pantograph designs with control functionalities;

WP 6: Assessment of virtual homologation procedures and Regulatory Acceptance.

Output from these workstreams that is of particular interest here is included in the following deliverables (D):

- D1.1 Key parameters for pantograph/catenary numerical models (Ambrósio *et al.*, 2011).
- D1.2 Pantograph Models based on laboratory tests (Bruni *et al.*, 2011a).
- D1.3 Validation requirements for pantograph/catenary simulation tools (Leouatini *et al.*, 2011).
- D3.1 Collection of pantographs and catenary data base at European level (Cau *et al.*, 2011).

In particular D1.2 includes useful information on the development of pantograph lumped parameter models (and multi body models) including specific data from the particular pantograph types included in the study (the Faiveley type CX and the Contact type ATR-95). D3.1 includes a collection of OCL and pantograph data from participating

European countries (including UK), that has been validated, and can provide an important source both of raw data, and validation material for this neutral section study.

Very little of the detailed outputs from the above is in the public domain, (but is summarised in a RSSB brief (RSSB, 2012a)) although many of the contributing authors and institutions have presented work from their individual contributions at conferences, and these have been subsequently included in a special issue of the Journal of Vehicle Systems Dynamics (Facchinetti and Bruni, 2015), see below.

Other work was undertaken by the PACIFIC consortium (Rachid *et al.*, 2011), delivering a software platform called SIMPAC, consisting of modelling and simulation tools, reported at a conference in Amiens in 2011 (Brown, 2012), although the subsequent promised presentations did not materialise.

Complementing the EU funded research described above, the rapid expansion of high speed rail in Europe and world-wide has generated academic interest represented at conferences and in journal papers. Most of these papers report on the computing and mathematical issues surrounding the development of models for the overhead contact line (ranging from simple beam representation to full FE models) and models for the pantograph (ranging from simple one-dimensional 'lumped parameter' mass-spring-damper models to full multi-body formulations), and models for the contact (penalty method or LaGrange), and solving of the equations of motion. The computing methodology utilised frequently involved co-simulation of the combined models solving equations of motion at discrete time steps, (or in some cases in real time, where a 'hardware in the loop' facility is employed, (Bruni *et al.*, 2011b) and (Resta *et al.*, 2008)). Many papers deal extensively with the laboratory testing necessary to obtain the physical characteristics of (mostly) the pantograph components and construction, to create a valid multi-body model.

In relation to this being in the context of High Speed Rail development, and the prediction of good quality current collection, on average, over a distance of many hundreds of kilometres, the criterion being used (quite reasonably it seems) to judge the simulation output (and the 'real' OCL performance it represents) is the statistical mean contact force F_m and its standard deviation, σ (notwithstanding that such forces are not displaying a normal or Gaussian distribution) (Thelisson, 2012). This is based upon the current de facto standard for good quality current collection being absence of 'loss of

contact', and a zero contact force being used as a proxy for loss of contact. This criterion was established by British Rail in the early 1980s and articulated as a target of F_m - 3σ being positive (Hetzel and Smith, 1978), and has been adopted in the current European standards and TSIs on the subject of overhead contact lines: BS EN 50119 (British Standards Institution, 2009), BS EN 50317 (British Standards Institution, 2012a), BS EN 50318 (British Standards Institution, 2018) BS EN 50367 (British Standards Institution, 2012b) and the ENE TSI (EU, 2014a). The early work by BR Research on the development of the BR/BW pantograph correlated this measure to the actual percentage loss of contact, which is the real criterion (Gostling and Hobbs, 1983).

Although the validity and usefulness of the F_m - 3σ method was subsequently questioned in further BR research (Holmes, 1982), mainly due to the distribution not being Normal or Gaussian, the convenience of such a characteristic for quick analysis of both simulated and measured results has contributed to its continued use. This has since been perpetuated into the TSI requirement and has embedded its adoption.

However as the evaluation of this characteristic requires to calculate out the forces over a large quantum of data (minimum of 650m of OCL, at 200 km/h, with time-steps of up to 1 ms) and generates a large amount of data, the applicability of which to the neutral section problem will be considered in Chapter 5.

As noted above, more recently, and particularly following the introduction of the EU High Speed Directive (see Appendix A) in 2002, a significant amount of work has been published on the numerical methods of simulation of pantograph/OCL interaction. A good proportion of this has come from a small number of authors associated with POLIMI (Collina and Bruni, 2002), (Bruni *et al.*, 2011b), (Resta *et al.*, 2008), IST Lisbon (Ambrósio *et al.*, 2008), (Ambrósio *et al.*, 2012a), (Ambrósio *et al.*, 2012b) and French railways, SNCF, (Bobillot *et al.*, 2011), (Bobillot *et al.*, 2006), (Bobillot *et al.*, 2008). All of these bodies were involved in the PantoTRAIN project (see above) (RSSB, 2012a).

In addition, although the general pantograph/OCL interface issue may not be completely solved, it appears sufficient progress has been made to allow attention to divert to more specialised or niche aspects of the interface in recent years (of which this research may be an example), concentrating on reliability and maintenance issues, such as tension variation within spans (Capitaine *et al.*, 2019), behaviour on curves and canted tracks

(Antunes *et al.*, 2020) and variability introduced by irregularities during installation (Gregori *et al.*, 2019).

Equally, in the same time frame, one of the underlying European standards supporting the ENE TSI, BS EN 50318 (British Standards Institution, 2002) is being re-drafted, and the drafting group (WG07 of Cenelec TC9X subcommittee C[21]) has been assembled to include many members of the bodies involved in PantoTRAIN. Included within the scope of this re-write is dealing with such issues as a methodology for validation of pantograph models, introducing more representative benchmark data for 'desktop' validation of OCL-pantograph simulations, presenting data for different types of OCL (ac simple and stitched, heavy dc, etc.), and allowance for hybrid 'hardware in the loop' simulations, etc. (British Standards Institution, 2016). This draft has now been published as the 2018 version (British Standards Institution, 2018).

The two underlying principles of both the original 2002 version, and this re-drafted BS EN 50318 is that a pantograph/OCL simulation method can be initially assessed by comparison with 'benchmark' reference data aggregated from multiple other simulations, which have themselves previously been validated against real line test data. This allows for simulation method assessment without the logistical and cost difficulties of undertaking line tests on real electrified railway lines, and meets one of the basic objectives of PantoTRAIN. This assessment is not mandatory in the standard, but is provided to allow the initial filtering out of unsuitable methods by a desktop approach (anecdotally however, many assessment bodies require to see this step undertaken). The mandatory step for validation is assessment against target values from actual line test data, for which accuracy limits are given.

Validation is required so the simulation method can be used in assessing the pantograph and OCL compliance with the TSIs for verification under the EU Interoperability Directive, and allowing formal 'authorisation to place into service' of the railway sub

[21] CENELEC is the European Committee for Electrotechnical Standardization and is responsible for standardization in the electrotechnical engineering field. Designated as a European Standards Organization by the European Commission, it is responsible, under a mandate from EU, for creating technical standards to support specific Directives. CENELEC (2016) *Cenelec: who we are*. Available at: https://www.cenelec.eu/aboutcenelec/whoweare/index.html (Accessed: 03 Nov. 2016). Cenelec committee TC9X is responsible for railway electrotechnical applications.

system (for more detail of the EU railway legislation and its impact on the industry, see Appendix A).

It is the author's view that use of the initial benchmark assessment is a legitimate methodology for assessing the behaviour of a dynamic simulation method whist in its development phase, and, furthermore, as will be made clear later in sections 5.3 and 5.4, the use of progressively more complex models (from the 2002 and 2018 benchmarks) prior to the full line test data comparison is an extremely valuable tool for incrementally developing greater functionality into a simulation method.

Although the working papers of this drafting group are not in the public domain, many of the contributing members of the WG07 (and indeed the PantoTRAIN consortium members) are represented as authors of papers in a special issue (Vol. 53 issue 3) of Vehicle System Dynamics (Facchinetti and Bruni, 2015), 'The pantograph-catenary interaction benchmark' (referred to subsequently as VSD 53-3). In this issue ten (mainly European) research and railway institutions describe their own approach to the pantograph/OCL simulation, and in a concluding chapter, comparisons of the output of each of the ten simulation methods when analysing the same 'benchmark' situation (Bruni *et al.*, 2015) are made. The benchmark analysed is a defined set of OCL and pantograph data, for a given analysis section, and the simulation results are expressed in terms of mean contact force (F_m), standard deviation of contact force (σ) and contact point vertical displacement (S_0), as per the requirements of the Energy TSI (EU, 2014a) and the underlying European standard BS EN 50367 (British Standards Institution, 2012b). Additionally a comparison of the major features of each of the ten approaches is presented. The actual benchmark used is very similar to that introduced into the revised 2018 version of EN 50318.

This work is an extremely timely and useful contribution to this study, and some of the significant and relevant points are:

- Only one (Finner *et al.*, 2015) of the ten approaches uses the finite difference rather than finite element method;
- The penalty method is the most frequently used to represent the sliding contact;
- Seven out of the ten approaches use a 3D representation, but only four of those use a multi body model of the pantograph for this, others using instead a 3D enhancement of the lumped parameter model, see Figure 4.4;

- Most use a Matlab environment, but some use Visual C++ (Zhou *et al.*, 2015) or Ansys (Jönsson *et al.*, 2015).
- The majority of the approaches model the OCL wires elements as Euler Bernoulli beams.

All ten methods showed a good agreement when analysing the benchmark case.

In another work (Antunes, 2012) finds pantographs can be modelled as either lumped parameter (mass-spring–damper) or as true multi body (MB) formulation. An example of a lumped parameter formulation is shown in Figure 4.3. There are a number of advantages and disadvantages associated with each method discussed, but, in summary, Antunes finds a multi body formulation of the pantograph (see examples in Figure 4.6) can be developed from the manufacturers technical drawings and data, where such information can be made available (and part of the commercial confidentiality of the PantoTRAIN output is in the disclosure of this type of information) as the specific details of joints, components and mechanisms are different in each manufacturer and specific type of pantograph, whereas a lumped parameter model must be inferred from laboratory tests on an actual pantograph. These tests must be re-visited for each minor adjustment to the pantograph's construction and characteristics. Although a lumped parameter pantograph model can be solved using the same FE code as the OCL model, a separate code must be employed to solve the true multi body model of the pantograph, and many papers (Ambrósio *et al.*, 2008), (Laurent *et al.*, 2013) describe a complex computational procedure (referred to as 'co-simulation') where data is passed between the FE and MB codes in Matlab (for example) and Fortran in real time. Significantly, Antunes demonstrates that the quality of the simulated output is equivalent for the lumped parameter and full MB pantograph formulations, and it is lumped parameter pantograph models that will be used in this research.

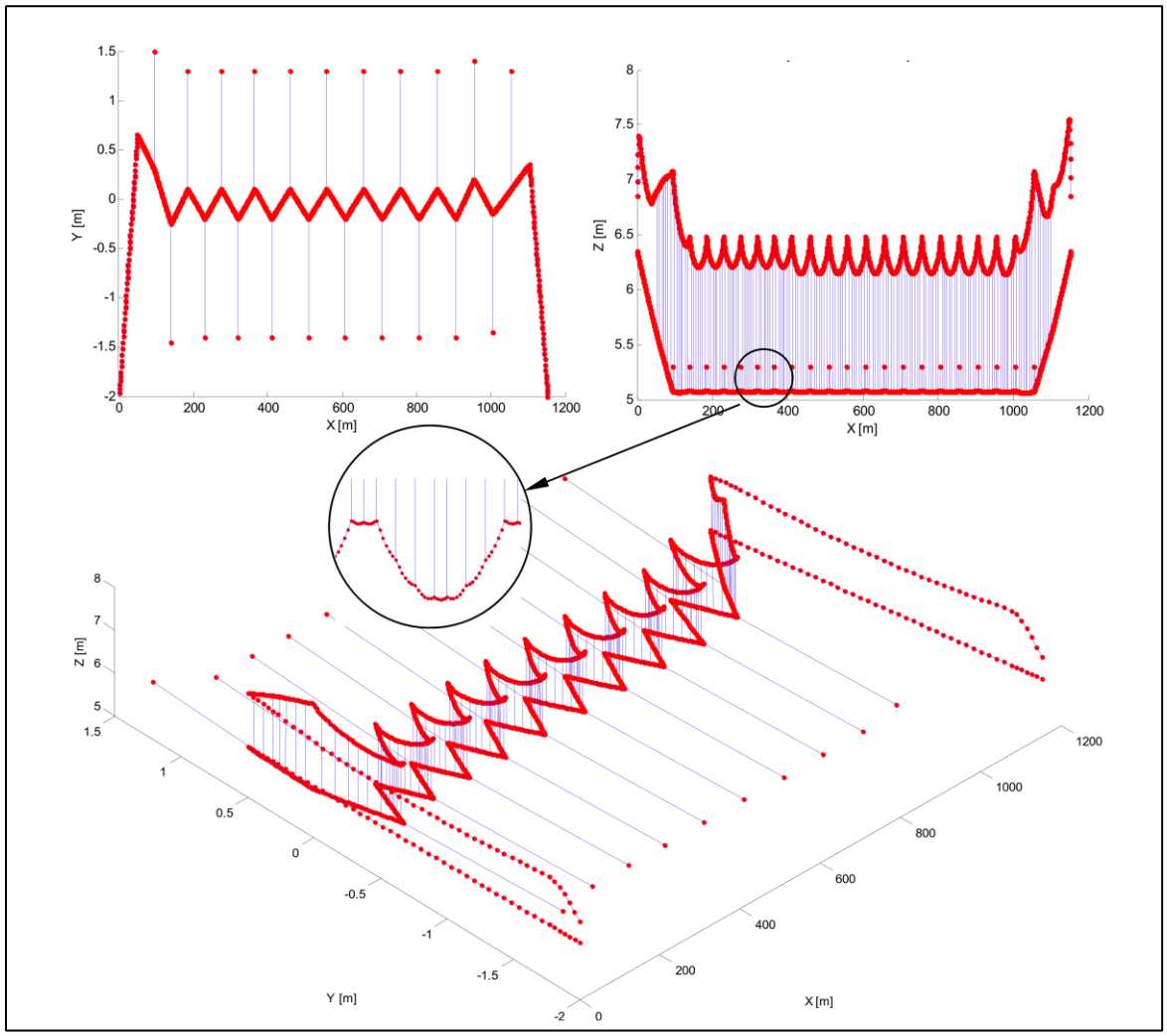

Figure 4.2 Typical 3D OCL finite element model showing 20 spans of contact and catenary wires, and the zig zag of the stagger, source (Antunes, 2012)

Again as noted above, all these methods are seeking to solve the equations of motion for the time history of the contact force between the pantograph head and the contact wire, and the displacements of the contact point at the supports and registrations, as prescribed by the TSI and EN requirements for 'acceptance' within the European interoperability framework (Thelisson, 2012). See also Appendix A.

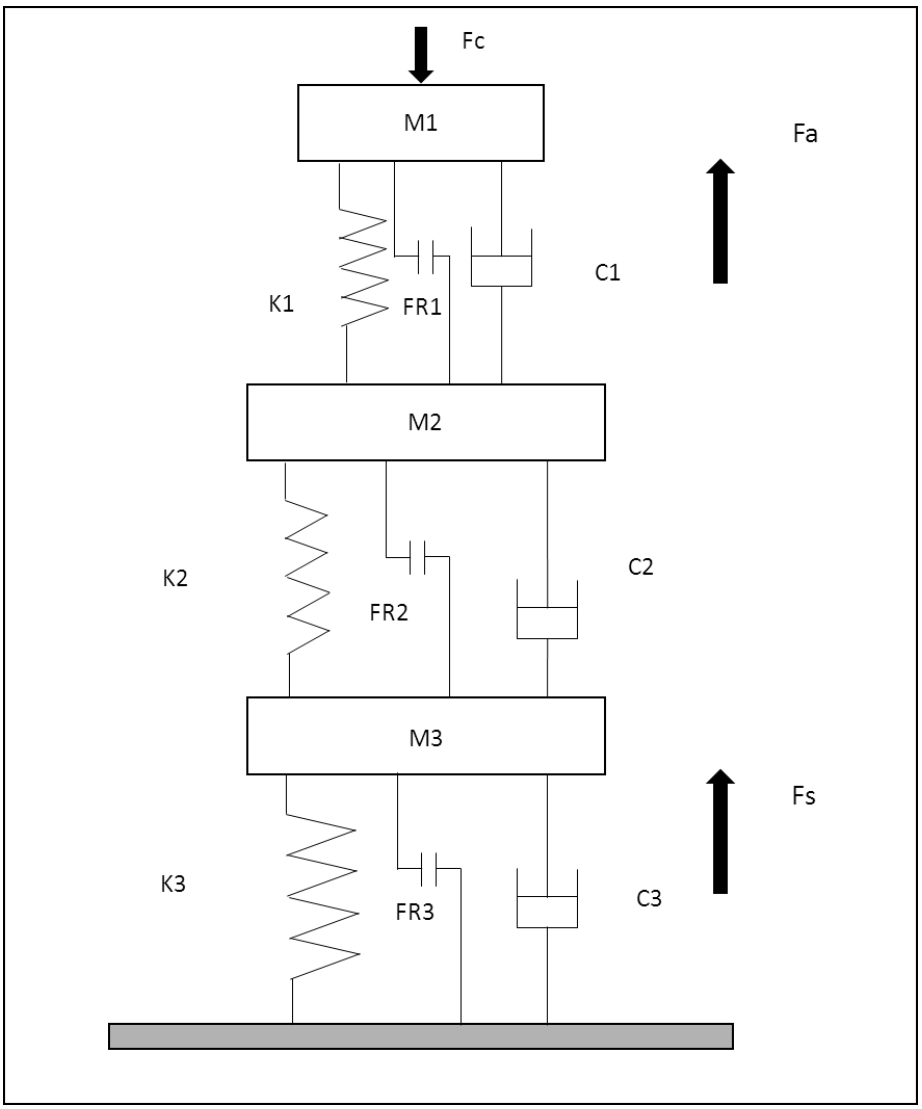

Figure 4.3 Typical arrangement of a one dimensional lumped parameter pantograph model amalgamated from variety of published works (for example RSSB, 2009; Network Rail, 2010b; Collina and Zuin, 2014; RSSB, 2016)

Noting the typical generic one dimensional lumped parameter pantograph model shown in Figure 4.3 in this case for a three mass model, showing the stiffness (K), damping (C), friction (F_R) and mass (M) parameters, as well as the forces. The contact force (Fc) is usually specified in its static value for a pantograph type (British Standards Institution, 2010), and its dynamic value is the subject of the pantograph/OCL interaction studies. The uplift force (Fs) is often confused with the static contact force, but clearly is in excess of the static uplift force (contact force) by the aggregate values of the masses M1 to M3 which also need to be raised (in most – but not all – common pantograph types, this is effected by the initial extension of the pantograph springs). The aerodynamic force Fa is usually a coefficient quoted as a function of speed squared.

It can be noted especially in the work presented in (Facchinetti and Bruni, 2015), that the conventionally used one dimensional lumped parameter model for the pantograph

has been extended into 2 and 3 dimensions (see Figure 4.4), without recourse to a full multi body model. An example of some of the data for a full multi body model of a typical pantograph is shown in Figure 4.6.

Pantograph lumped mass models as described above can be seen to have the characteristics as shown in Table 4.1.

Table 4.1 Pantograph lumped parameter model characteristics in common usage

Pantograph model	Characteristics
1D model	vertical axis only, parameters usually assumed linear with extension (Figure 4.3)
2D model	vertical and across track axis on pantograph head only, stiffness and damping vary with contact wire stagger (see Figure 4.4 left)
2D model	vertical and along track axis on pantograph head only, stiffness and damping vary with collector head strip (see Figure 4.4 centre)
3D model	vertical, across track and along track to allow for two separate collector head strips, and stagger (see Figure 4.4 right)

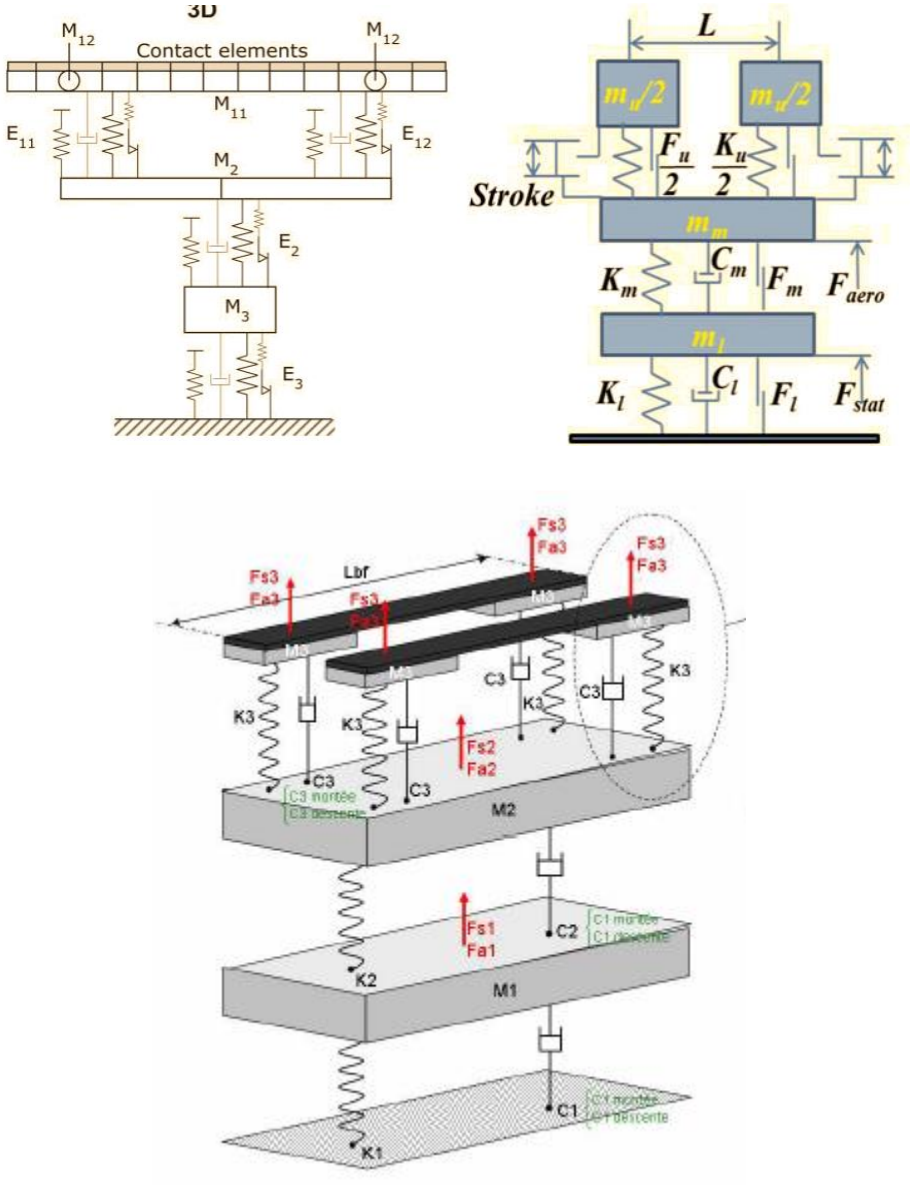

Figure 4.4 Multi-dimension lumped mass pantograph models showing: (top left) two dimensional with the second dimension taken across the length of the collector head (Jönsson *et al.*, 2015); (top right) two dimensional with the second dimension taken across the two collector strips (Cho, 2015); and (bottom) three dimensional (Massat *et al.*, 2015). All from VSD 53-3 (Facchinetti and Bruni, 2015)

A characteristic of the lumped parameter models (vice the full multi-body formulation), as usually implemented by the researchers quoted, is that the parameters are assumed linear, and the model is only able to deal with linear parameters, and not able to deal with non-linear or bi-linear parameters. This is probably a feature of the coding, as using a proprietary software (e.g. Ansys), such non linearities can be accommodated (assuming the data is known).

It is clear, that for a conventionally constructed, asymmetrical, pantograph (as per Figure 2.10) that the stiffness vertically is a function of the knuckle stiffness, and it can be expected that this knuckle stiffness will be broadly linear with the knuckle angle θ,

see Figure 4.5. This angle however, will then be non-linear with pantograph head extension (height) y.

All three assume parameters are linear, which would appear reasonable, except for the extension (height) which is assumed to be linear over the small variations in height of a conventional high speed pantograph, used on a high speed line (i.e. where contact wire height is controlled at a constant height). (This feature betrays the origin of these studies being used in assessing against the High Speed Interoperability Directive, see Appendix A.) Note this is not the case for conventional lines, at conventional speeds where contact wire height is variable for low bridges and high over level crossings. This is particularly the case in the UK. For the purposes of validating pantograph and OCL models for simulation, it is explicitly assumed in the later revision of EN 50318:2018 (the previous revision being silent) that the pantograph main frame stiffness is effectively linear over the 20-80% of working height range. It is worth noting that, in UK, the working height of a pantograph is from around 4.2m to 6.1m, making this linear range 4.58m to 5.72m (RSSB, 2014a). Both the upper and lower non-linear ranges are infringed at most bridges and level crossings, where usually no speed restriction is imposed. Thus UK pantographs can be operating at 200 km/h in these non-linear ranges. Anecdotally, the performance of UK pantographs at higher wire heights is found particularly poor. For the purposes of this research, the line test data used in the final validation incorporates CW heights within the above quoted linear range, and so the use of the essentially linear pantograph model data is not an issue. However, more generally, although the inclusion of the explicit reference to the limits of the linear height range in the latest version of EN 50318 is a welcome acknowledgement of the variabilities in practice that can exist across Europe's railway networks, it is regrettable that a document specifically prepared by RSSB (RSSB, 2016) to provide usable models for UK pantographs did not address this aspect.

Allowing for CW stagger is clearly useful, in general terms of OCL-pantograph interaction, as it allows the effect of the CW offset across the collector head and its being affected by (multiple) head suspension mountings to be assessed, but as it is the practice to align a neutral section on the centre line of the track, with no (appreciable) stagger, nor for that matter, radial load, it would seem a 3D OCL model would not be necessary in this case. However, the effects of the stagger in the OCL model, (i.e. the radial force, the registration arm mass and inertia, and the effective arm vertical stiffness) can be

modelled and the contribution to CW behaviour included. This is addressed specifically in Chapter 5.

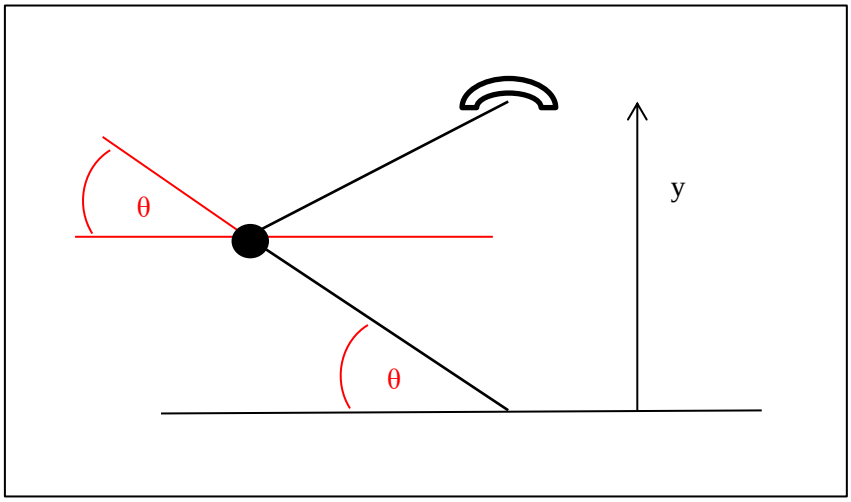

Figure 4.5 Pantograph non-linear frame stiffness showing knuckle angle θ relative to height extension, y.

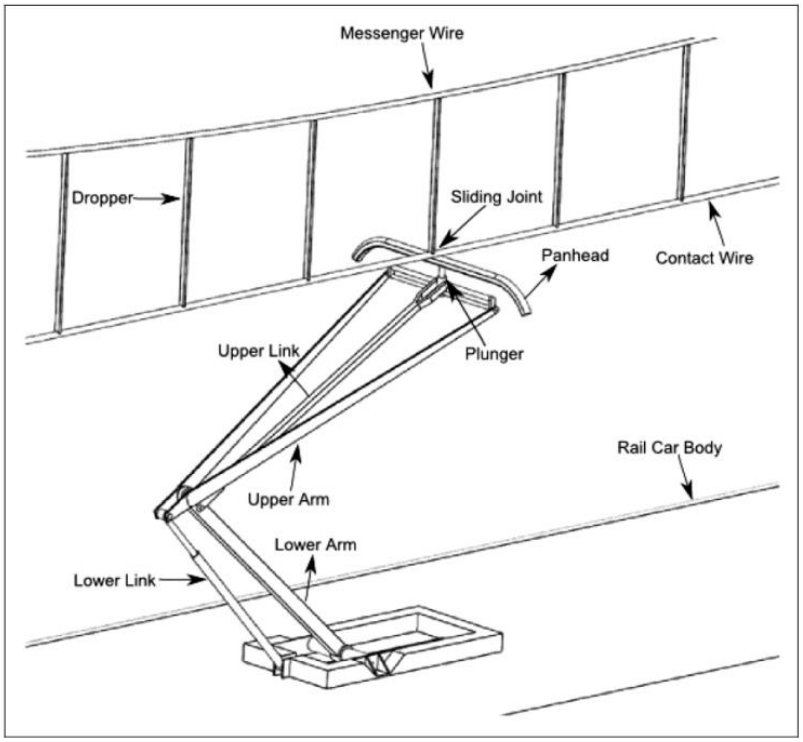

Figure 1. Pantograph and catenary system.

Table 1. Pantograph body data.

Body	Mass (kg)	Initial position (m) (x^i_0, y^i_0, z^i_0)	Initial orientation (φ, θ, ψ)	Inertia (kg·m^2) (I_{xxi}, I_{yyi}, I_{zzi})
[illegible] arm	32.18	11.26924156, 0, 3.84511275	$\pi/2$, 0.5528807212, $-\pi/2$	0.31, 10.43, 10.65
Upper arm	15.60	11.45796454, 0, 4.52440451	$-\pi/2$, 0.2896816713, $\pi/2$	0.15, 7.76, 7.86
Lower link	3.10	10.96436876, 0, 3.81940451	$\pi/2$, 0.6234559506, $-\pi/2$	0.05, 0.46, 0.46
Upper link	1.15	11.58587608, 0, 4.49940451	$-\pi/2$, 0.3028168645, $\pi/2$	0.05, 0.48, 0.48
Plunger	1.51	12.5, 0, 4.835	0, 0, 0	0.07, 0.05, 0.07
Pan-head	9.50	12.5, 0, 4.945	0, 0, 0	1.59, 0.21, 1.78

Figure 4.6 Typical pantograph multi-body model (Faiveley CX) source (Pappalardo *et al.*, 2015)

4.5 Numeric formulation

The underlying numeric formulation of pantograph/OCL interaction, at least insofar as the majority of the current state of art approaches is concerned, is the methodology for establishment of the time variant displacements, velocities, accelerations and forces, under the consideration of inertia and damping. The global equation of motion to be solved is,

$$M\ddot{z} + C\dot{z} + Kz = F(t)$$

where M, K and C are the mass, stiffness and damping matrices.

These and other numeric interpretations are, in most cases, coded explicitly into the chosen engineering software (e.g. Matlab or Mathematica). In the chosen proprietary

system for this research, Ansys, these are intrinsically incorporated into the proprietary software, and are invoked when choosing a transient dynamic analysis.

4.6 Application to the neutral section problem

All the material discussed so far, and indeed generally available in the public domain, has been in relation to the OCL as the subject of interest. There are some papers dealing with the 'discrete features' of the OCL, and are generally (but not exclusively) in relation to the use of rigid overhead conductor beams (vice the normal OCL system of tensioned wires). In particular, the transition between the conductor beam and the tensioned OCL is a specific discrete feature, which, on face value, might have some characteristics and challenges in common with the short neutral section, as it represents a discontinuity in the normal tensioned conductor and the difference in mass and stiffness to the adjacent contact wire causes peak forces and accelerations, affecting the pantograph trajectory, and potentially initiating damage to components.

Some Japanese authors, like many reporting from the RTRI, produced published work which concentrates heavily on experimental results and testing, rather than extensive analysis (Kobayashi *et al.*, 2008a) (Kobayashi *et al.*, 2008b). The consequential effect of the poor transitions between tensioned contact wire and conductor beam is in this case fatigue of the contact wire, although high contact forces can also cause problems. The paper describes the development of a 'transition structure' as a 'stress relaxation mechanism', see Figure 4.8. It is interesting to note that contact wire fatigue at insulator/contact wire splices is now being seen as a recurring problem by Network Rail with the AF single rod neutral section, see section 3.4 above. In the 1980s, in relation to a proposed installation of rigid conductor beam across a swing bridge at Norwich Trowse, BR R&DD undertook similar testing and development of a contact wire to rigid conductor beam transitions. The author was involved in that work, and became aware of the issues surrounding the characteristics of such transitions. Subsequently a similar transition structure to that described in the Japanese papers was developed, and can still be seen, installed in the OCL at that location in Norwich, see Figure 4.7.

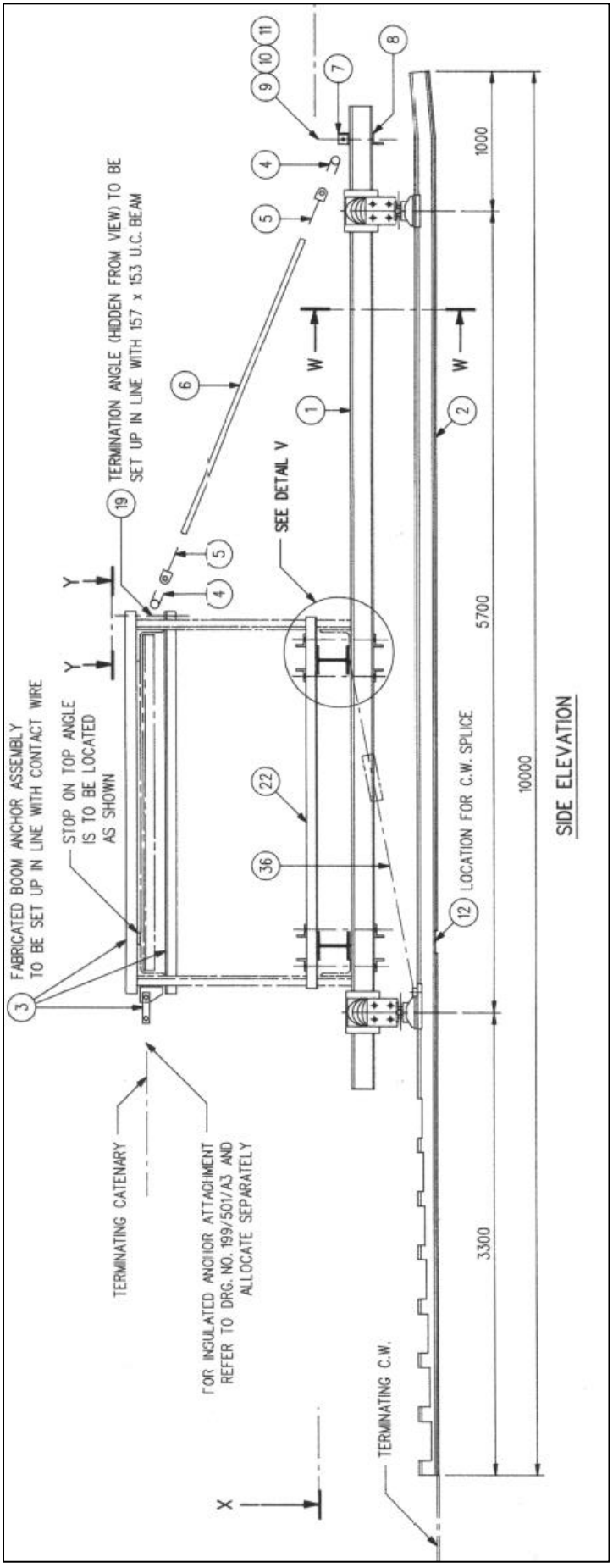

Figure 4.7 Trowse bridge transition structure: showing transition structure (notched beam) at left hand end (extract from OLEMI drawing 1/113/801/A1)

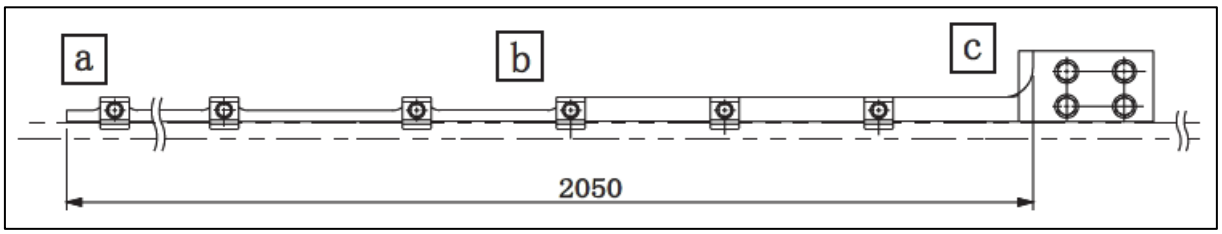

Figure 4.8 Arrangement of a Japanese conductor beam transition structure from (Kobayashi *et al.*, 2008b)

One other example of a discrete feature is a section insulator, on which there is a single paper. In dealing with the effect of section insulators, the Swedish authors (Harell *et al.*, 2005) (who may also be speaking of neutral sections but the terminology used is ambiguous) refer to an analysis method and modelling of the catenary, and the section insulator, as beams. However as the model applies the section insulator at mid-span rather than the more common (if not universal) placing of a neutral section at the support point, it may be of limited value. Not all the referenced material here is in the public domain.

Engineers at Balfour Beatty (Seddon and Lester, 1992) indicated that they had developed a special version of their OCL dynamics programme to deal with the special situations of neutral section and section insulators, which involved very short time-steps, and consideration of higher frequencies of wires and pantographs, although no further technical details were given.

In addition, a later BR research report (Cook, 1996) looked at the performance of a special kind of BICC ceramic bead neutral section, which included three sets of insulator rods (and in some ways emulated the 5 section, 4 overlap type of carrier wire neutral sections, see section 3.2) to be used at ac/dc interfaces on the North London line. It only includes a limited amount of neutral section simulated performance data, forces and uplift displacements, for a limited set of scenarios, and at speeds much below the higher speeds of interest here, but could be used to support validation.

The experience of maintaining and repairing neutral sections (Network Rail, 2015c) indicates that the behaviour of a neutral section is governed by a number of factors, being:

- The characteristics of the OCL tension length in which it is situated, in particular those on the approach to the neutral section;

- The characteristics of the insulator component(s) inserted into the OCL at the neutral section;
- The characteristics of the joints between the insulator component(s) and the contact wire of the OCL.
- The characteristics of any supporting attachments to the neutral section insulators (e.g. anti-torsion elements)
- The number, location (within the train), orientation and characteristics of the pantographs.

All these would need to be adequately modelled to achieve an effective simulation, and proposals are described in Chapter 5.

This form of modelling can be used for a number of purposes:

1. Developing a new optimised pantograph/OCL couple in a 'clean sheet' situation to fulfil a new requirement (e.g. developing for a 400 km/h new railway);
2. Seeking improvements to an existing OCL for use when a new pantograph type is to be introduced (e.g. modifications to series 1 OCL to accommodate the BW HSX 250 pantograph);
3. Seeking improvements to a pantograph to allow improved performance on an existing OCL (e.g. the original development of the BR BW pantograph in early BR days);
4. Validation or demonstration of performance (or an initial step in such a process) for the purposes of regulatory acceptance, or homologation (e.g. as required by ENE TSI).

Whether the object of the interest is the pantograph or the OCL might govern the level of detail and form of modelling undertaken for each. In example 2, the pantograph might be modelled as lumped masses, whereas in example 3, to explore in greater detail the performance of the pantograph, a full multi-body representation would be preferred, even to the extent of mixing flexible and rigid body elements in a single hybrid model, for greater realism in replicating all the nuances of the pantograph performance, and in particular, to allow the effect of fine tuning of the pantograph components and construction to be assessed.

This current research can be seen as a sub set of example 2, where the OCL, with the neutral section included, is the object of interest and is modelled with greater attention to detail. In particular the neutral section is included in the OCL as a hybrid of flexible and rigid body elements, each chosen specifically to best represent the real world behaviour, and, crucially, to allow the effect of fine tuning of the neutral section components and construction to be assessed.

4.7 Conclusions

It has been seen in preceding sections how from the wide spread and convenient availability of quick and powerful computers a number of approaches to the problem of a pantograph running on an OCL were formed. The first problem to be addressed once the equations of motion of the wire(s) had been established, was the choice of normal modes, finite difference or finite element method for solving the partial differential equations, which has been settled, in most (but not all) modern studies on the finite element method, no doubt influenced by the wide availability of proprietary software.

The parallel development of Multi Body Systems (MBS) techniques and software has led a number of researchers to develop Multi-Body models of the various pantographs, and this has particularly been useful in contributing to making pantograph developments. However it can be noted that, for convenience, lumped parameter models of the pantograph are still used for the task of assessing pantograph/OCL performance, although it would seem that these are used in quasi-MBS format, and the opportunity has been taken to extend this type of model by the extension into 2D and 3D formats (for pantograph head only). The issue of dealing with non-linear parameters for this type of model still exists. This often requires a co-simulation method, as MBS deals with rigid bodies, and will not deal with the flexible bodies of the OCL model.

The F_m-3σ > 0 criterion for quality of current collection was developed, and then partly abandoned, by BR in the early 1980s. However it has been perpetuated in the TSI for acceptance, at a European level, of the quality of pantograph/OCL interaction, and so endures, with the added attraction of its simplicity. It is however of little interest to the research here, although as will be described later, is still of use when validating the pantograph/OCL dynamic simulation method (DSM) to be developed here against industry standards. The criteria to be investigated are those which are developed from the standards and experience of neutral section failures, which are the peak forces and physical (vertical) displacement of the components of the neutral section assembly during pantograph passage. Both these however are considered in the form of analysis used to determine F_m-3σ, and so the same techniques can be adapted.

Chapter 5 The Core Pantograph/OCL Modelling Approach

5.1 Summary

This chapter describes the work to generate (and validate) a core OCL and pantograph modelling scheme, and the simulation of their dynamic interaction (the 'dynamic simulation method', DSM). This is a necessary precedent to allow the eventual full simulation of the neutral section's interaction behaviour with the pantograph, which is to be incorporated as a specific feature within the regular OCL.

5.2 Chapter structure

This chapter is structured as follows. The initial concepts for the approach to the modelling are described within 5.3, along with the initial plan for validation. A revised plan for the modelling, derived after initial investigations into the modelling feasibility, is then described. 5.4 and 5.5 then describe the creation and validation of this chosen model/DSM against, initially, benchmarks from the relevant European standards and then against real line test data from actual pantograph/OCL measurements, including all the work undertaken to model 'real' OCL and pantograph characteristics. (Comprehensive detail is given for the initial model, subsequent models concern only with the additional features, and do not repeat the fundamentals.) Further improvements to the model/DSM, post the validation, to facilitate easier use of the DSM going forward, are described in 5.6. Overall conclusions are summarised in 5.7.

In these descriptions, the term 'model' is used to refer to the particular details of the representation of the pantograph and OCL, and the term 'dynamic simulation method', abbreviated DSM, is used to refer to the combination of the models with simulation characteristics and parameters to achieve the satisfactory output of the required data. The European standards refer to validating a particular 'dynamic simulation method'.

5.3 Modelling and validation philosophy

5.3.1 General approach

The work by others described in Chapter 4 indicates that the following elements need to be modelled for the study of the pantograph-neutral section interaction problem:

- The multi (rigid) body pantograph
- The flexible body OCL

- The contact
- The flexible body neutral section (eventually)

This work, and other reference material, summarised in Chapter 4 indicates a preference amongst the researchers for the following approaches:

The multi (rigid) body pantograph	1D, 2D or 3D lumped parameter
The flexible OCL	2D or 3D Linear finite elements, Euler Bernoulli beam
The contact	the penalty method
The flexible neutral section	not considered in the literature

The conclusion to be drawn from the work is that a lumped parameter model of a pantograph, in one dimension, and a two dimensional model of the OCL (within which will ultimately be incorporated a neutral section) should be adequate to represent the physical interaction of pantograph with OCL and neutral section, to identify the behaviour in terms of statistical vertical forces and vertical displacement. This contention is tested in the remainder of this chapter.

A necessary precedent for this approach is the initial development of a 'plain'[22] (i.e. the simplest OCL arrangement without any specific features) pantograph/OCL dynamic simulation method, into which the neutral section discrete feature can be inserted subsequently. In addition, for robustness, this method should be capable of being validated to provide confidence.

In order to be applied to a realistic neutral section performance problem, in the context of UK electrification, a representative example of both OCL type and pantograph type should be modelled. The objective is to realistically simulate the behaviour of a current neutral section type in its interaction with the pantograph, in the context as part of an OCL system, and then to perform various analyses, to understand the effect of each individual component or element, in providing, or detracting from, that behaviour. A further stage would then perform parametric analysis, and investigate amendments to

[22] Sometimes referred to as 'open route' meaning simplest OCL without any specific features (other than construction overlaps)

the parameters of the components and elements, to investigate how the performance might be improved. This is covered in Chapter 6 and Chapter 7.

A progressive validation scheme has been chosen, so that confidence can be gained as the process is built up from simple to more complex analyses. Prior to constructing and validating the OCL model with the neutral section included, a simple model of pantograph/OCL interaction will be constructed and validated, to prove the concept of the simulation method chosen. After this validation, the neutral section model will be included in the OCL model, and further validated.

The European standard, EN 50318, whose title is "Railway applications - Current collection systems - Validation of simulation of the dynamic interaction between pantograph and overhead contact line", is directly relevant having the scope:

> *"Simulation techniques are used to assess the dynamic interaction between overhead contact lines and pantographs, as part of the prediction of current collection quality. This document specifies functional requirements for the validation of such simulation methods to ensure confidence in, and mutual acceptance of the results of the simulations."*

The 2002 version was current at the time of starting this research, but since 2013 a revision was in progress in Working Group WG07 of Cenelec SC9XC. The author has been a member of this working group throughout. In particular, the 2016 (publicly available) working group draft of the next revision of this standard (British Standards Institution, 2016) includes additional validation data, and more sophisticated 'benchmark' tests. This revised version has now been published, in late 2018, as BS EN 50318:2018 (British Standards Institution, 2018).

The philosophy of BS EN 50318:2002 is that an initial validation is done using 'benchmark data', which is fictitious, but realistic (although idealised, and of low complexity) OCL and pantograph data for which typical output results are given (the 'low complexity element is that it is ten equal identical spans of OCL without pre-sag or dropper mass, a 2DOF pantograph model, and a single pantograph). Then, having filtered out inaccurate methods, to validate an actual OCL and pantograph model against real line test data. In the requirements of the standard this is presented as a mechanism

to perform an initial filter without the financial and logistics costs of full line tests (and so also meets some of the PantoTRAIN objectives).

Once this benchmark is completed, validation against line test data is performed. This requires the actual OCL and pantograph (for which the line test data is available) to be modelled, and simulation output to be compared to statistical values of actual measured data, and validation to be achieved when the two results are within the tolerances specified.

Ability to access line test data is then a consideration.

A specific range of UK OCL and pantograph type combinations is shown in Table 5.1 below, where X indicates an operational combination. (More details on the pantograph and OCL types referenced have been given in sections 2.6 and 2.7.5.) In particular, the availability of suitable line test data for the particular combination will prove crucial, and is also indicated by shading.

Table 5.1 Combinations of UK OCL and pantograph types and availability of line test data (indicated by shading)

	UK OCL types			
	Mk3b	Mk3d	UK1	Series 1
Pantographs				
BR/BW	X[1]	X[1]	X	
BW HSX 250	X	X		X[3]
Faiveley CX				X[2]
BW HSP MkII	X[2]		X[2]	X[2]

Note – availability of test data – shaded cells

1. Data from ECML two pantograph tests (RSSB, 2009)
2. Data from 2015 Old Dalby tests (Bryan, 2016),
3. Data from 2016 Old Dalby tests (Bryan, 2016), see Appendix C

Although primarily for the purpose of validating software used by assessment bodies to verify the electrification sub-system in accordance with the Energy TSI, and for the purposes of the EU Interoperability Directive (see Appendix A), the latest version of European Standard BS EN 50318 additionally includes extracts from actual line test

measurement data (of German Railways origin), to allow validation to be made even where access to line test data is not possible.

Additional benchmark data is also available in the unpublished working material of the drafting group, to which access has been made available.

In addition the BR research report (Cook, 1996) referred to in section 4.6 includes a limited amount of neutral section simulated behaviour data, forces and uplift displacements, for a limited set of scenarios, which, if possible to replicate, could support validation.

Additionally there exists data from East Coast Main Line two pantograph line tests (RSSB, 2009) which were undertaken to allow validation of modelling by SNCF for Network Rail, and data from 2015 Old Dalby tests (Bryan, 2016), for Series 1 OCL tests using a modified and unrepresentative train/pantograph combination.

Finally, there have been more recent (2016) line tests undertaken by Furrer + Frey at Network Rail's Melton Mowbray (formerly Old Dalby) test track, which have included instrumented pantograph tests at speeds above 160 km/h on Series 1 OCL, which included an AF neutral section. This data was available for this research. Access to the raw data of these tests can also be used for comparison to validate the model and methodology. Further details of the test installation and the collection of this data are given in Appendix C.

It is these latter tests at Old Dalby which offer the most promising basis for full validation against line test data. This is because:

- The test uses recent modern UK OCL and pantograph types;
- The installed OCL data and coordinates are well known;
- There is an AF single rod neutral section installed in one of the test sections;
- Full time history data of pantograph instrumentation is available, 'raw' and unfiltered;
- The tests are in accordance with the relevant standards BS EN 50317 (British Standards Institution, 2012a);
- The circumstances of all the tests are known.

BS EN 50318 additionally contains methodologies and limits for comparing data and statistical output. In particular, for validation against line test data the criteria as shown in Table 5.2 are given.

Table 5.2 Validation criteria for simulation results vs line test data from BS EN 50318:2018

	Required accuracy
Mean contact force, F_m	± 2.5 N
Standard deviation of the contact force, σ	± 20%
Range of vertical position of the point of contact	± 20mm
Maximum uplift at the support, S_0	- 10mm, + 20mm

5.3.2 The proprietary software platform

The previous work described in Chapter 4, and particularly in VSD 53-3 (Facchinetti and Bruni, 2015) and PantoTRAIN (Ambrósio *et al.*, 2011) describes the separate coding for the FEM model of the elastic OCL, and the MB model of the pantograph. It is the intention of this study to use proprietary software as far as possible, for all the modelling. This should allow less attention to be paid to coding and programming, and more to be paid to the exact details of the OCL, pantograph and neutral section. This research is about neutral sections, not about coding. There are a number of proprietary FEM/MB software combinations available for this.

The choice made was to use Ansys Mechanical[23] for the elastic OCL model and Universal Mechanism[24] (UM) for the multi body pantograph model. UM has a feature which allows elastic sub systems to be modelled in a FEM software (including Ansys) and these then to be imported into a MB model, creating a hybrid model for simulations. Additionally UM has a very convenient graphical user interface which allows bodies, joints/force elements and other components of the model, to have parameters attached and easily amended via dialogue boxes. Parameters can be numerical values, expressions, functions, tabular data, etc. Animated graphical output can be easily presented. UM is also a modern piece of software, with no 'legacy' issues, and, importantly it was thought, direct access to the programme developers in Russia was available due to good relations

[23] Developed and marketed by ANSYS, Inc., Canonsburg, PA, USA http://www.ansys.com
[24] Developed and marketed by Laboratory of Computational Mechanics, Bryansk State Technical University, Russia www.umlab.ru

between Newcastle University and CML[25]. (Although also a vehicle dynamics analysis tool, there was no intention to use this facility to underlay a consideration of vehicle roof movement to the pantograph model.)

Using this facility in UM, the initial proposal of this research was that the neutral section be modelled as a FE/MB hybrid with the some of the neutral section components modelled as elastic elements and others as joint/forces. This will in particular avoid the need to create the exact detail of the neutral section components, some of which have complex internal mechanisms (e.g. the 'clicker' mechanism by which the PTFE rod is rotated to allow even wear around its surface) in Ansys, requiring access to detailed manufacturers engineering drawings, and replace this with only the mass, inertia and joint/force characteristics. It is anticipated though that many of these characteristics will need to be extracted from laboratory tests on actual samples of the components. This approach can be seen as an analogy to the choice of lumped parameter models rather than a full multi body representation, for the pantograph in much of the literature (e.g. PantoTRAIN and VSD 53-3). The basic OCL would however be predominantly modelled as elastic elements in Ansys. All the simulations would be undertaken in the UM environment.

The initial proposal as described above was to use Ansys FEM for the elastic elements and Universal Mechanism (UM) for the rigid bodies and joint/force elements, and to perform the dynamic simulation in UM. A significant number of advantages to this approach had been identified (Morris *et al.*, 2017).

Although not well documented, in common with a number of similar rigid body analysis programmes, the import of elastic element data from FEM software is undertaken using the Component Mode Synthesis technique (Computational Mechanics Limited, 2017b), sometime referred to as 'Craig Bampton'. This technique (Bampton and Craig Jr, 1968), was developed for large FEM models with many nodes, elements and DoFs, to reduce the complexity and to expedite the computation by aggregating nodes and elements into a fewer number of larger 'super elements'(my phrase). A brief overview is given by Scott Gordon (Gordon, 1999). However the Craig Bampton technique is only applicable for linear models, and it appears that the non-linear elements used to model the OCL are

[25] CML, (Computational Mechanics Limited) are the producers of the Universal Mechanism software

unsuited to this approach, notwithstanding the possibility described later, of using linear Ansys 'legacy' elements. Although some work has been done on a non-linear implementation (Apiwattanalunggarn *et al.*, 2005) this is not used in Universal Mechanism. The one example of using UM to model overhead contact lines uses short linked rigid bodies to represent the contact wire, rather than flexible elements (Kolpakhchyan P.G. *et al.*, 2006). The import of non-linear flexible bodies is not well implemented currently in UM, and the UM authors CML have a solution in development, but the anticipated updates to rectify this are not yet available, after over a year (Computational Mechanics Limited, 2017a), and their arrival could not be guaranteed. Consequently an alternative approach was subsequently adopted.

In this amended approach models in Ansys only, which is capable of modelling the rigid bodies, forces and kinematic constraints, contacts associated with rigid body analysis (Thieffry *et al.*, 2007), are developed and validated comparatively for the pantograph/OCL interaction and for subsequent neutral section modelling. In particular, the original ambition of modelling the neutral section components as rigid bodies is achievable. The use of Ansys in this fashion is not widely documented in the literature, but a number can be identified.

- In the studies associated with investigating the current collection from a rigid overhead conductor beam (Vera *et al.*, 2006), Ansys is used for the rigid beam, but not for the modelling (where they use Simpack); the beam modelling is not complex, and is linear flexible element.

- ABAQUS, which is a very similar product to Ansys, was used by (Haugland, 2015) in a study to determine numerically the natural frequencies of an OCL, and compare with measurements on a full size, but small extent (i.e. 15m long spans) laboratory model. The work however made some assumptions in eliminating gravity (i.e. the model had mass but not weight).

- One of the papers in Vehicle System Dynamic 'Special Edition on the Catenary Benchmark', VSD 53-3 (Jönsson *et al.*, 2015) uses Ansys for the OCL model, although little technical detail is given, the results are validated against the benchmark tests;

- Work at Sheffield university, which had some support from Network Rail (Beagles *et al.*, 2016), describes the use of Ansys in a very similar manner to

adopted here in this research, purely for the purposes of demonstrating that it could be done, and validation achieved.

Of these Beagles *et al* and Jönsson *et al* are the most directly relevant to the work here, although Jönsson gives too little detail to be truly helpful. Beagles was published in September 2016, but not brought to this authors attention until 2017. It was not instrumental in the decision to use Ansys, but certainly gave comfort. Many of the major decisions were already made by the time the paper was seen, and some were gratifyingly similar. There are some differences however, including the use by Beagles of multiple force constraints to apply the tension to the main messenger and CW wires, which, due to minor movements in dropper nodes, causes components of force to be directed into the droppers, and thus tension is lost throughout the span. This can be corrected by re-meshing, but the method chosen here is to apply an initial stress.

The revised approach, using only Ansys, and incorporating the multi stage incremental progressive validation scheme is shown in Figure 5.1. The essence of this validation as applied to this case in question, is the use of low complexity 'benchmark' data in BS EN 50318:2002 to perform an initial assessment (steps 1 to 3). Opportunity is taken of the more complex benchmark test in EN 50318:2018 to develop techniques further, in steps 4 to 6. Then the OCL and pantograph models, for the types of OCL and pantographs for which line test data is available, are modelled, and compared with line test results to assess validation (steps 7 to 9). The test of accuracy is described in clause 10 of BS EN 50318:2018, and shown in Table 5.2 above. Ultimately the neutral section model will be inserted into this OCL model and the neutral section/pantograph simulation validated against line test data as described in Chapter 6. Where validation in any step is not achieved, then an improvement to the model(s) or simulation parameters must be effected before continuing.

Ultimately five models are developed and tested, as shown in Table 5.3. For internal reference purposes, certain data, tables and graphs in this thesis may be annotated with the model version, i.e. 003-v2a, etc.

Table 5.3 Ansys model summary

Model	Purpose	Pantograph	OCL
001	EN 50318:2002 benchmark validation	Single pantograph, two speeds, 250 and 300 km/h	2 spans OCL analysis section
002	EN 50318:2018 benchmark validation	Two pantographs, single speed 275 km/h	10 spans OCL analysis section
003	ODTT line test (exc. Neutral section) data validation	Trailing pantograph of two, 200 km/h	7 spans OCL analysis section
004	ODTT neutral section portion validation	Trailing pantograph of two, 200 km/h	2 spans OCL analysis section
005	Generic neutral section baseline, and options	Single pantograph, 200 km/h	2 spans OCL analysis section

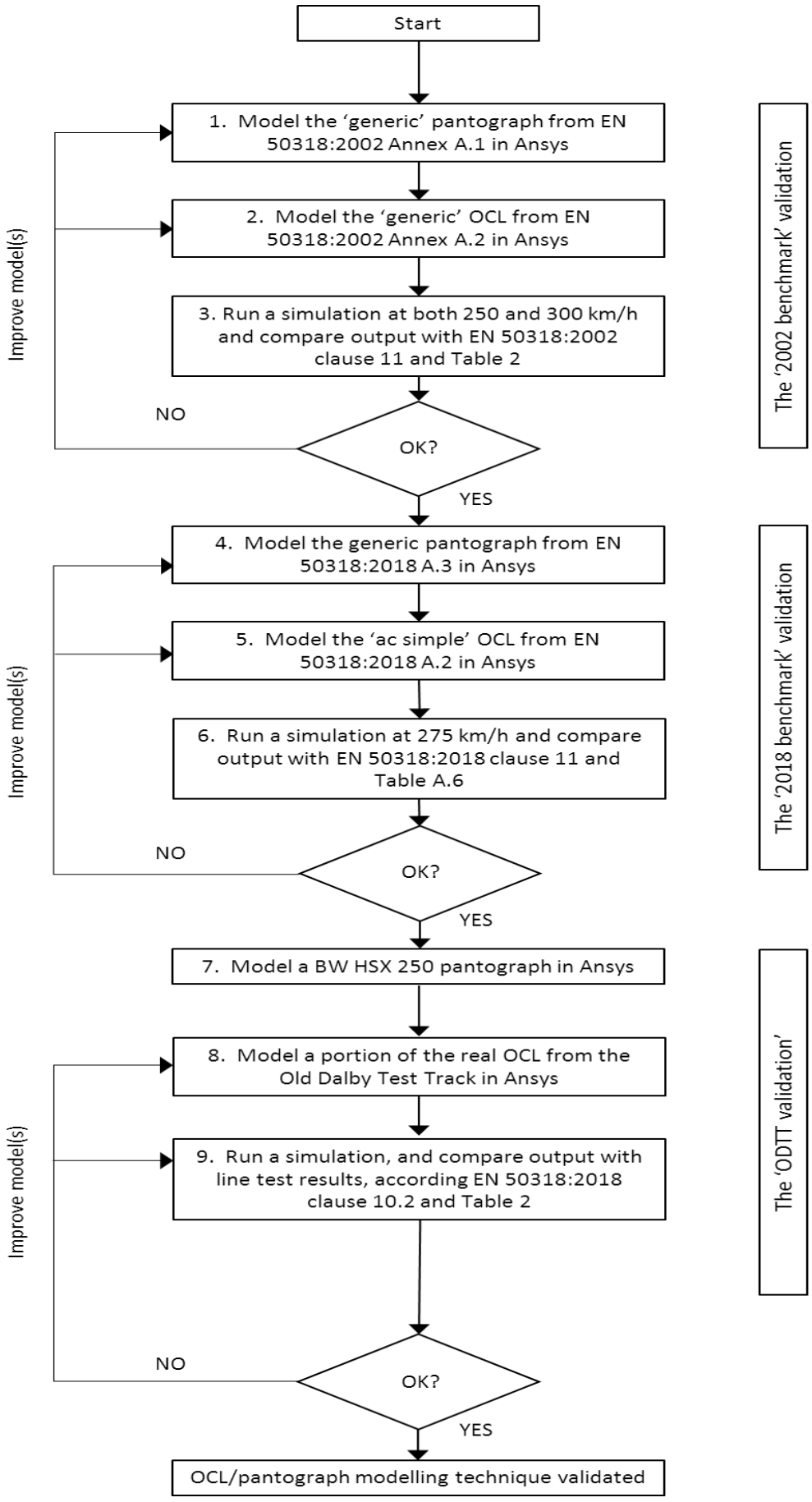

Figure 5.1 Flow chart of validation scheme for Pantograph/OCL simulation

5.4 Pantograph/OCL model validation against EN 50318 benchmarks

5.4.1 Fundamentals

The version of Ansys used for the development of these methods is Ansys Mechanical APDL 15.0, although version 18.1 is used for some of the validation runs. The models were created by the 'direct generation' method, rather than 'solid modelling' so as to maintain control over node placement and numbering. The code was created in the Ansys APDL scripting language, and run as a batch process

The models are created under the conventional Ansys coordinate system as shown below: X axis is along the track/OCL, Y axis is vertical, and Z axis (where used) is across track.

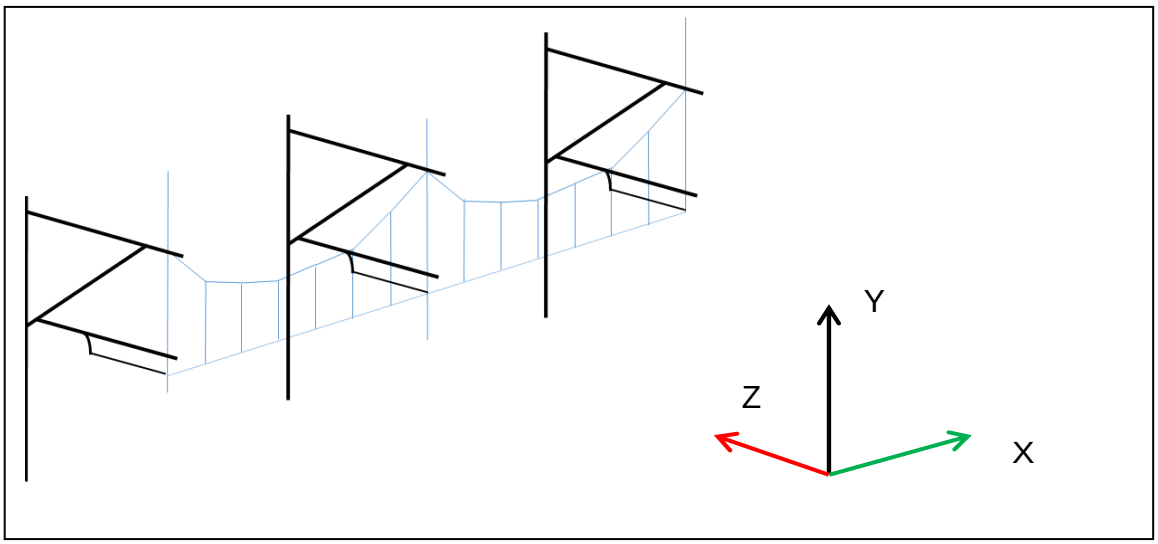

Figure 5.2 Coordinate naming system for the Ansys models

5.4.2 The EN 50318:2002 benchmark

The EN 50318:2002 benchmark consists of a defined OCL with certain given characteristics, a defined pantograph with certain given characteristics, and certain parameters of simulation. Target values are provided for the statistical values of key simulation outputs for two pantograph speeds, and a validation is achieved when the candidate dynamic simulation method (DSM) replicates the output within the target value range for both speeds. These target values are shown in Table 5.4. According to the standard these values are a composite of the values achieved by a number of already

validated simulation methods in use in Europe. As such they represented (at the time) the 'state of art'.

Table 5.4 Range of target results from 2002 reference model (actual table from EN 50318:2002)

	Range of results	
Speed [km/h]	250	300
F_m [N]	110 to 120	110 to 120
σ [N]	26 to 31	32 to 40
Statistical maximum of contact force [N]	190 to 210	210 to 230
Statistical minimum of contact force [N]	20 to 40	- 5 to 20
Actual maximum of contact force [N]	175 to 210	190 to 225
Actual minimum of contact force [N]	50 to 75	30 to 55
Maximum uplift at support [mm]	48 to 55	55 to 65
Percentage of loss of contact [%]	0	0
NOTE The values in the table are based on results from five independent simulation methods. These methods have been checked with results from line tests.		

Note that the target values include statistical maxima and minima. These are the values of $F_m \pm 3\sigma$, and are less significant than the actual maximum and minimum forces. The statistical maxima and minima represent the range within which 99.73% of the population will fall. The actual target maximum and minimum forces do not fall below zero.

In this research and when undertaking model development, and comparison to target values, a metric based on the error expression defined in a related European standard for line test measurements, EN 50317:2012 (British Standards Institution, 2012a) is used, where error E is defined:

$$E = |(Xsim - Xmeas)/Xmeas|$$

And is modified for each target range to create a 'conformance score'.

If Xmin<Xsim<Xmax (i.e. X within the target range) Score = 0.0

Otherwise Score = |(Xsim – Xmean)/Xmean|, where Xmean is the mean of the target range.

Total score for a simulation run = Score 1 + Score 2 +…+Score n +1.00. Consequently a fully conforming score is 1.00.

The Ansys representation of the benchmark pantograph is constructed as shown below using Ansys rigid body and kinematic constraint elements, with the data as given in the standard. Initially the base is fully constrained, all other elements are free only in Y.

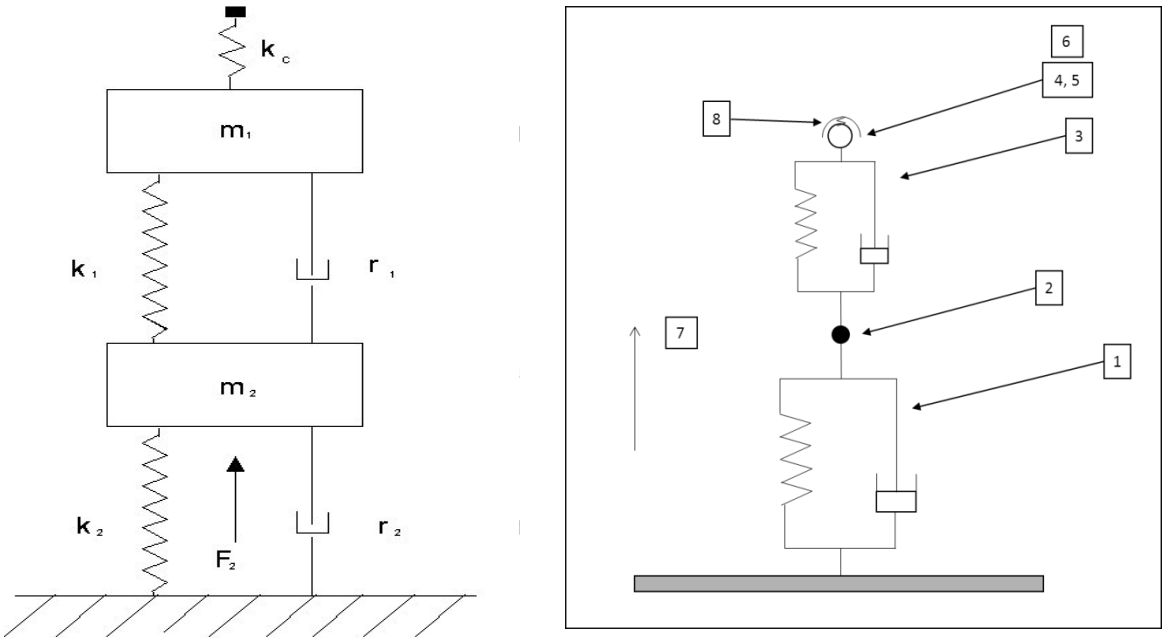

	Effective dynamic mass kg	**Stiffness** N/m	**Damping** Ns/m
Contact spring	-	k_c = 50 000	-
Collector head	m_1 = 7,2	k_1 = 4 200	r_1 = 10
Articulation frame	m_2 = 15	k_2 = 50	r_2 = 90

Figure 5.3 Ansys pantograph model construction. Left EN 50318:2002 Figure A.1; right the Ansys pantograph model implementation (see Table 5.5 for key to elements).

Table 5.5 Ansys pantograph model elements Relate to Figure 5.3

Item	**Component**	**50318 Figure A.1/Table A.1 item**	**Ansys element**	**Note**
1	Frame suspension	K_2, R_2	COMBIN14	1D spring/damper – Y-axis
2	Frame mass	M_2	MASS21	Point mass
3	Head suspension	K_1, R_1	COMBIN14	1D spring/damper – Y-axis
4	Pantograph head	M_1	BEAM188 – cylinder	Mass by density and volume parameters

Item	Component	50318 Figure A.1/Table A.1 item	Ansys element	Note
5	Contact surfaces		TARGE170 – crossing beams	Contact surface on pantograph head
6	Contact surfaces		CONTA176 – crossing beams	Contact surface on CW
7	Uplift force	F_2	FY	FY = ΣM.g + 120 + 'k'
8	Contact stiffness	K_c	CONTA176 parameter	See text for values

The pantograph head was modelled as a single cylinder with a nominal length of 200mm (in the Z coordinate dimension), as this was a 2D model implemented with 3D elements. The form of contact chosen was the 'penalty' method using crossing beams, see Figure 5.4. For convenience the dimensions of the pantograph head beam were chosen as identical to those of the contact wire. The beam density was manipulated to provide the effect of the specified pantograph head mass. Ansys differentiates the surfaces as 'target' and 'contact' (known elsewhere as e.g. 'master' and 'salve'). The choice is made on relative elasticity, the stiffer surface should always be the 'target' (Kim, 2015), which in this case is the pantograph head. However, contact pressure (which in Ansys can either be force or force/area) can only be output for the 'contact' surface, which in this case is made of not one, but several hundred elements (one for each CW element). Each output for each element is a 'variable' in Ansys system, and, as Ansys has a limit of 200 variables being stored, then a routine had to be devised which takes the first 200 variables, stores them to output, then redefines the 200 variables with the next 200 values and so on. This is done within the script by do-loops, and is a limitation of using the Ansys software in this manner.

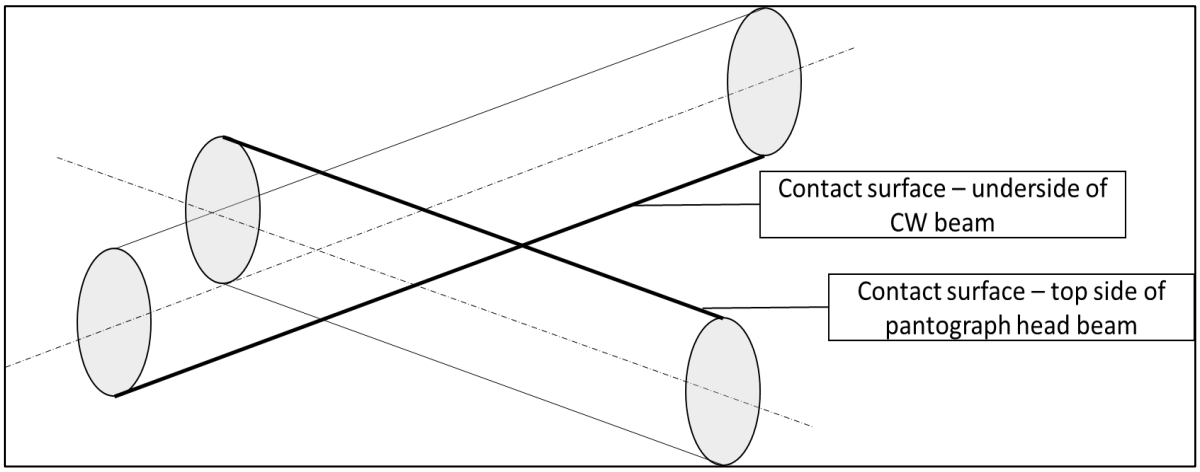

Figure 5.4 Arrangement of crossing beams representation of pantograph head contact with the contact wire for EN 50318:2002 benchmark.

The data for the 'benchmark' OCL is given in BS EN 50318:2002 Annex A. The OCL for the benchmark is formed of ten identical spans of 60m long, each with 9 droppers. There is no CW pre-sag, the CW is level. The analysis section is defined as the centre two spans.

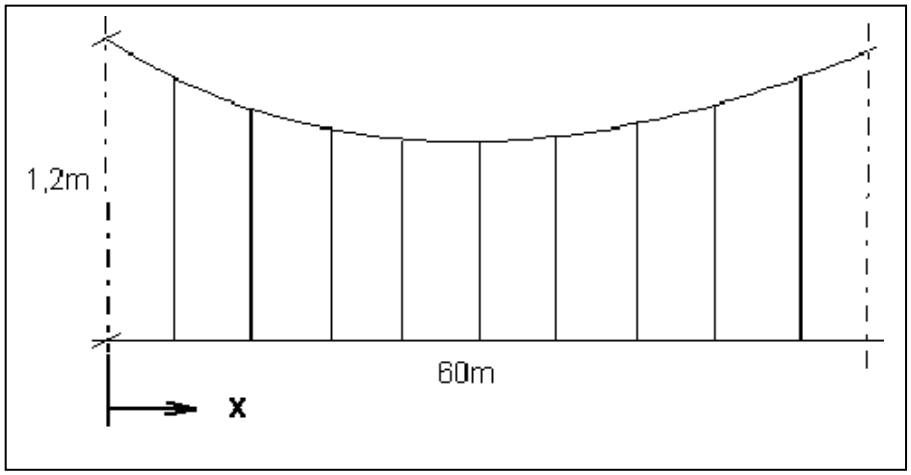

Figure 5.5 Arrangement of a single span of OCL from EN 50318:2002 benchmark. Parameters are shown in Table 5.6

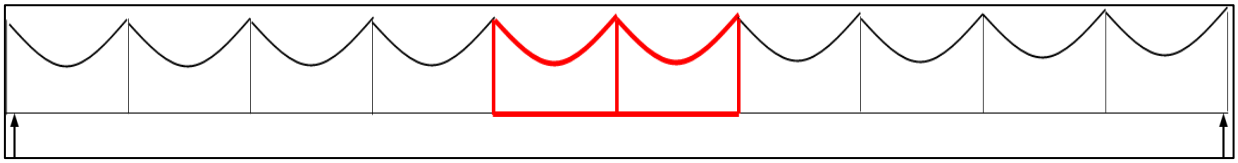

Figure 5.6 EN 50318:2002 benchmark full OCL model showing analysis section in red, and pantograph start and end positions (arrows)

As only tension and mass/length data is given for the messenger and contact wires, some obvious inferences have been made to determine values for the other

characteristics needed for the analysis, e.g. Young's modulus, E, and section modulus, I. This has been based on standard conductors used in the railway electrification industry, and the current European standards, matching the linear mass with a range of manufacturer's published technical data (e.g. Liljedahl Bare Wire, 2014). For the registration arm, most data is given to allow the 2D effects to be determined, but a feature of registration arms is the uplift force produced by the moment about the fixed end pivot created by the 'heel setting' see Figure 5.7. No heel setting is given, but a typical value for high speed OCL of 250-300 km/h capability would be 250mm, based on current European designs (Cau *et al.*, 2011). The full derivation is shown in Appendix B, and summarised in Table 5.6 below.

Table 5.6 Specified and inferred parameters for 'benchmark' OCL from BS EN 50318:2002. Inferred values shown in shaded box, given values in clear box

	Linear mass kg/m	**Tension N**	**Conductor material and construction**	**Young's modulus, E kN/mm²**	**section modulus, I mm⁴**	**Cross section mm²**
Messenger	1.07	16,000	Bz II, 19/2.8	117.21	1216.17	117.00
Contact wire	1.35	20,000	Cu, 150 mm²	120.00	1766.36	150.00
	Linear mass kg/m	**Length m**	**Heel setting mm**			
Registration arm	1.00	1.00	250			

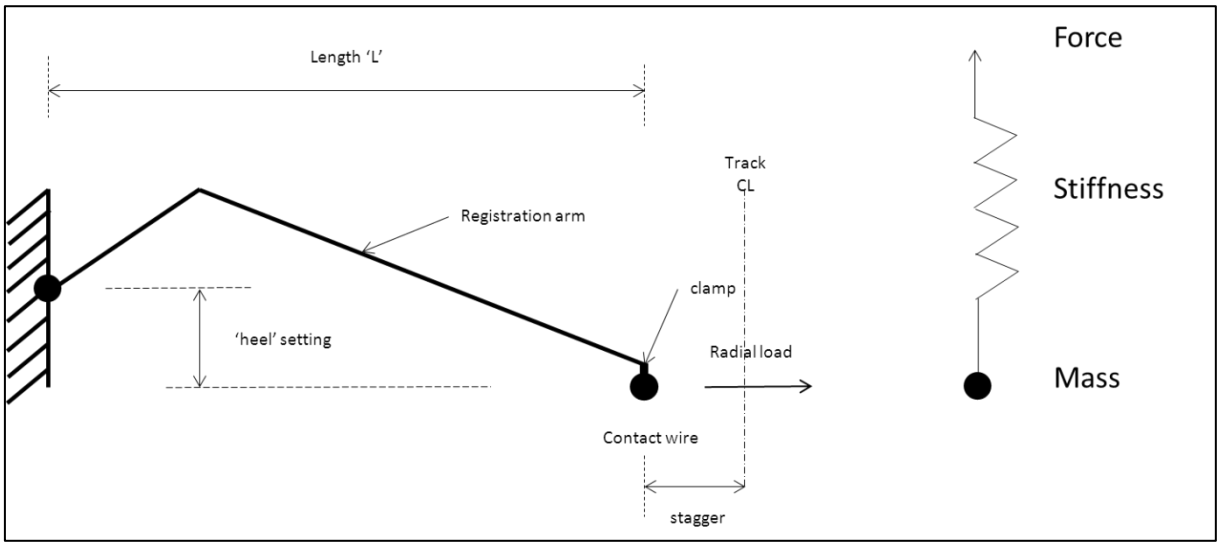

Figure 5.7 Registration arm representation showing conventional geometry (left) and 2D implementation in Ansys model (right)

The model of the elastic OCL has been constructed in Ansys, according to the scheme in Figure 5.8. The OCL model was constructed using Ansys mechanical elements. The elements have been chosen as shown in Table 5.7.

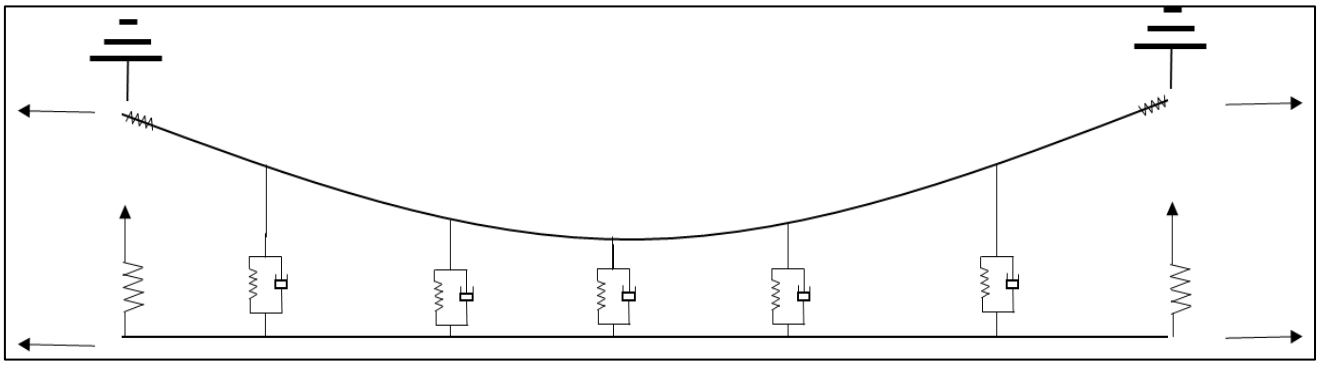
Figure 5.8 OCL model for Ansys implementation of EN 50318:2002 benchmark

Table 5.7 Ansys OCL model elements. Relate to Figure 5.8.

Figure 5.8 **item**	**Component**	**Ansys element**	**Note**
1	Contact wire	BEAM189 – cylinder	3-node 3D beam
2	Messenger wire	BEAM189 – cylinder	3-node 3D beam
3	Droppers	COMBIN39	1D spring/damper – Y-axis, no compression
4	Dropper clamp mass	MASS21	Not implemented in 2002 benchmark
5	Registration arm mass	MASS21	Point mass
6	Registration arm effects	COMBIN14	Stiffness and force

Figure 5.8 **item**	**Component**	**Ansys element**	**Note**
7	Tensions		Tension created by initial stress

The contact wire and messenger wires were modelled using BEAM188 and BEAM189 elements. BEAM189 is a 3D three node Timoshenko beam element. The 3 node formulation is an aid to reducing the numbers of elements, where this may be a consideration in not exceeding Ansys system limits (not an issue for this application). Virtually all the simulations currently reported in this field use a linear Euler-Bernoulli beam representation for the contact wire, and the majority also for the messenger wire, although not exclusively (Bruni *et al.*, 2015).

The Timoshenko beam is a development of the Euler Bernoulli beam theory, but with additionally the consideration of shear deformation, in which case the cross section remains plane, but not normal to the neutral axis. (Although not documented, current versions of Ansys can still employ the legacy element type BEAM4, which is a Euler-Bernoulli beam, and may be used if difficulties arise. So far this has not been necessary.) For the static case with slender beams (which is the case here, with slenderness ratios for contact and messenger wires of the order of 10^6) this has been shown to make little difference, however for the dynamic cases, the rotational inertia considered does improve the results (Goerguelue, 2011; ResearchGate, 2014) and hence it is appropriately used here.

(It can be noted that most of the current simulation practices, particularly those reported in (Bruni *et al.*, 2015), use linear Euler-Bernoulli beams theory: the rationale in the literature in often pragmatic, i.e. that the linear FE approach produces results which correlate well with line test results. Although this appears to produce respectable results, the problem is clearly a non-linear one. It is also noted that producing non-linear code in Matlab - their platform of choice - is considerably more difficult.)

The Ansys script invokes the NLGEOM command to account for the large geometrical displacements in the OCL and the geometrical non linearity this produces. In fact the model would not converge without it. Material property non linearities are not significant here.

The wires were modelled as cylinders. The material and section properties of the two wires have been established, as shown in Table 5.6, and for the purpose of modelling as cylinders an 'equivalent' radius has been established which delivers the same section property. Linear mass has been set using a value of density, which too has been modified to take account of the equivalent radius of the cylinder. These details are explained fully in Appendix B, and summarised in Table 5.8 below.

Table 5.8 Ansys OCL wires elements 'equivalent' characteristics as circular cross sections. Full derivation given in Appendix B

	Conductor material and construction	Cross section mm^2	Section modulus, I mm^4	'Equivalent' cylindrical radius mm	'Equivalent' cross section mm^2	'Equivalent' density kg/m^3
Messenger	Bz II, 19/2.8	117.00	1216.17	6.273	123.62	8574.38
Contact wire	Cu, 150 mm^2	150.00	1766.36	6.886	148.98	9061.27

The droppers are modelled as COMBIN39 spring damper elements. The spring stiffness has been set as the value given in the EN 50318 benchmark data (which, can be noted, is an order of magnitude different to realistic values). The tension only option is set, the dropper having no resistance in compression. No clamp or dropper mass is included in this model, as required, but the facility is included in the code, in anticipation of 'real' OCL models.

In a full 3D representation of the OLE, the registration arm (Figure 5.7) can be modelled with greater accuracy, often as a link, connected to ground and the contact wire with spherical joints. Mass is usually around 1kg, and length around 1.1m. Heel settings vary, but for high speed lines, around 200-300mm is the norm (Cau *et al.*, 2011). Some researchers include also the bending stiffness of the arm, and its contribution to loads on the contact wire, e.g. (Tur *et al.*, 2015), but this is not a consideration here, as arm geometry is not known with certainty, and the resultant relaxation of stagger, and hence radial load, is trivial in this context (it is also not certain that this effect actually exists in reality, or whether installation practices compensate for it).

For a simpler model (2D OLE and 1 or 2D pantograph) the influence of the registration needs to be taken into account as a set of 'effects' at the CW registration point. These are the equivalent stiffness (representing the pendulum stiffness of the arm), the equivalent

mass (representing the moment of inertia) and an upward force from the radial load and heel setting. Most researchers using 2D perform such a translation e.g. (Cho, 2015; Jönsson *et al.*, 2015). For the 2002 and 2018 models, the 2D equivalent effects as shown on the right hand side of the diagram in Figure 5.7 have been applied, where

Force = (Radial load x Heel)/Arm length, and

Stiffness = Radial load/Arm length

Tension is applied to the two wires by setting an initial stress. Applying tension by means of a force was found to be cumbersome, as the minor adjustments in node position caused droppers to be not completely normal to the messenger and contact wires, and a component of tension was transmitted into the droppers at each dropper node, causing tension to be lost from the CW and messenger. Once again the value of the stress is adjusted to take account of the 'equivalent' cylindrical cross section employed. This adjustment is undertaken within the code.

Degree of freedom (DoF) constraints were applied. All nodes were fixed in Z, ROTX and ROTY. Additionally the extreme ends of the messenger and CW were fixed in X and Y. The remote ends of the registration arm (equivalent, i.e. the registration arm springs) were fixed in X and Y. The messenger supports were fixed in X, but remained free in Y, to allow tension to be transferred between spans.

In developing the approach for establishing the OCL equilibrium geometry, an obvious initial approach to adopt is to attempt to emulate the process as it occurs in the real world situation.

This real world process for erecting the OCL involves (inter alia) the following significant relevant steps:

- Messenger and CW temporarily (but loosely) connected together ('temporary droppers');
- Both wires run out and supported in pulleys (i.e. not fixed at the supports);
- Both wires run out at a specific erection tension (a fixed tension calculated to emulate the final automatic tension that would obtain ultimately, and based on erection temperature and span lengths);

- Along track positions set. Pulleys replaced by fixed supports and auto tension implemented;
- Temporary droppers replaced by final calculated length droppers.

To replicate this process in the Ansys model requires the following issues to be addressed

1. All along track movement of the messenger and CW (for tension, temperature and geometry) takes place before the dropper, supports, and registrations are attached.
2. In the Ansys direct generation method, all connections (messenger-dropper, messenger-support, CW-dropper, CW-registration) have to be made at node positions.

Consequently, in order to create nodes at the necessary final positions, the locations of the unloaded nodes need to be calculated, as they are before the application of tension and geometry. So adjustments, within each span, as shown in Figure 5.9 (top) for a simplified 4 dropper span, are required.

Two actions are required:

1. The unloaded nodes of the dropper connections to the CW are required;
2. A mechanism within Ansys to pay out or absorb the adjusted length of the messenger and CW.

The unloaded geometry is shown in Figure 5.9 (bottom), and the application of tension and mass loads results in the adjustments shown.

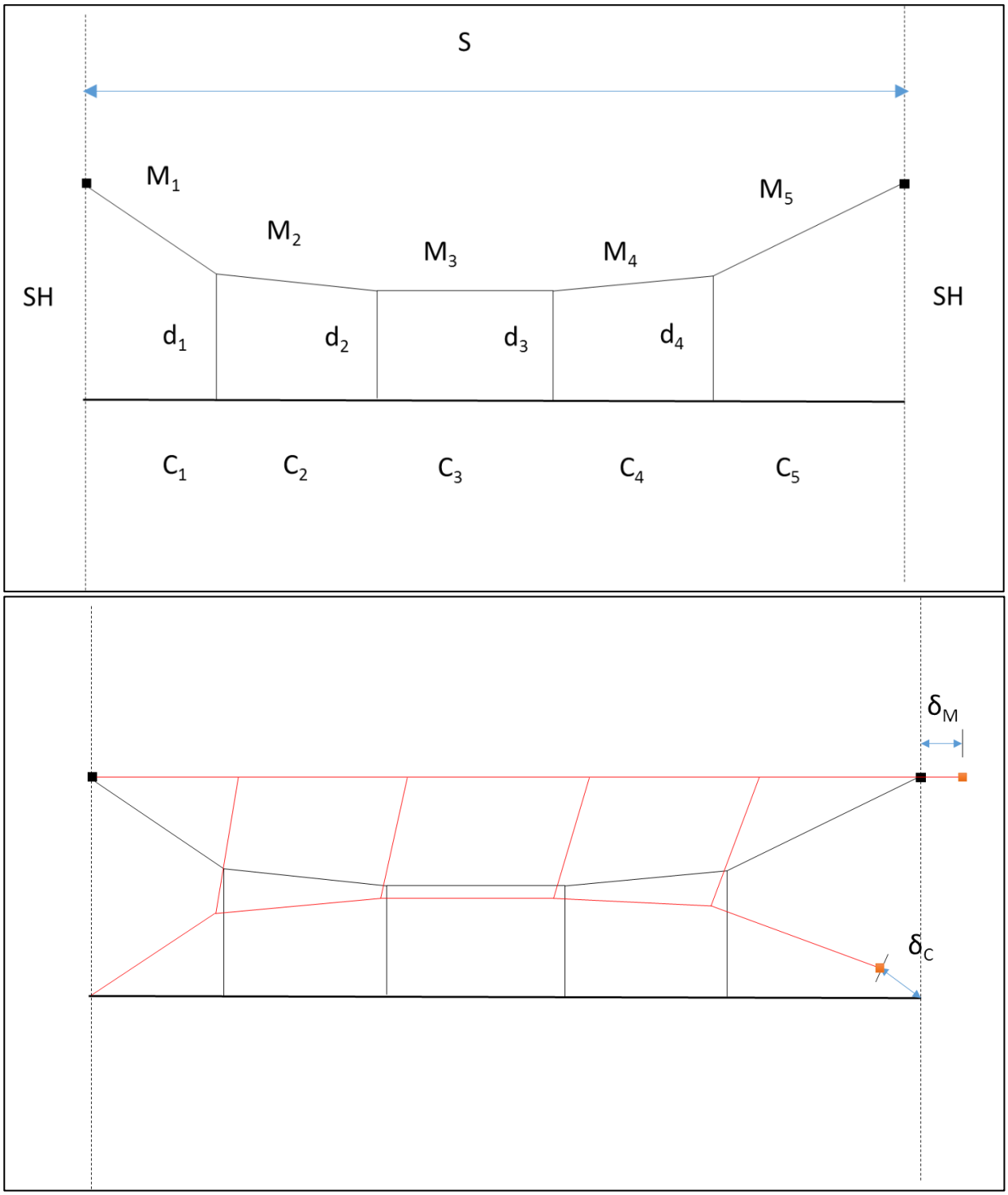

Figure 5.9 Unloaded OCL geometry development showing (top) final loaded geometry (black) and (bottom) related unloaded geometry (red)

The magnitudes of the adjustments are calculated as

$$\delta_M = \sum_{1}^{n=5} M_n \; - S$$

$$\delta_C = \sum_{1}^{n=5} C_n \; - S$$

Where the segment lengths M_n and C_n, dropper lengths d_n, and system height SH are calculated from the general method for calculation of the static geometry, as described in full in Appendix B.

Also note that the messenger adjustment is positive, in that an additional messenger length needs to be fed in to accommodate the developed length of the sagged messenger wire, whereas the CW adjustment is negative, as the level CW length is shorter than the developed length of the unloaded CW.

The adjustments for each messenger span can be made within that span, using the messenger springs at each end of the span, where the messenger spring stiffness is set to

$$K_m = \delta_m / T_m$$

And the additional messenger length is provide by the extension of the spring, under the messenger tension.

However the CW adjustment cannot be accommodated in this way, as the CW needs to remain integral, without springs, to allow the contact elements to be created to be used with the matching pantograph head contact elements. In this case, the CW adjustments are aggregated over all the spans in the model, and one single adjustment made at one end of the model, as

This can be seen as an emulation of the action of the balance weight anchor or equivalent tensioning device in real OCL practice (see section 2.7.2).

The unloaded OCL geometry is calculated by inverting the calculation for the dropper lengths, as explained in detail in Appendix B, and then applying the adjustments at each dropper connection point.

The coordinates of all the dropper and other connection nodes, in their initial unloaded position can be calculated as follows, for each dropper panel.

Each dropper panel is formed of a quadrilateral, whose four sides lengths are known from the static geometry calculation, being for the first panel at the left hand end (fixed end), the system height SH, the messenger panel length M_1, the CW panel length C_1 and the dropper length d_1, see Figure 5.10.

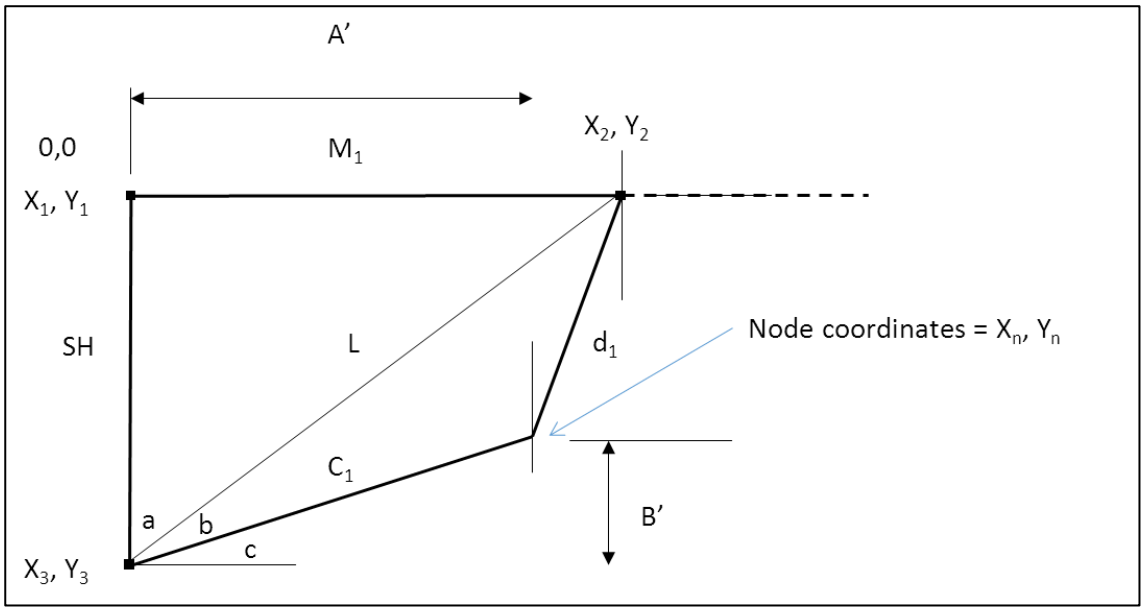

Figure 5.10 Calculation of unloaded OCL geometry nodes typical arrangement for first (LH end) panel

The construction line *L* is calculated by Pythagoras, and the angles a and b by conventional trigonometry, so that the dropper-CW connection node coordinates are

$$X_n = X_1 + A' = X_1 + C_1 \sin (a+b)$$

$$Y_n = Y_3 - B' = Y_3 - C_1 \cos (a+b)$$

These coordinates then are used to inform the calculation of the nodes coordinates in the next panel to the right, and so on.

The calculation of the aggregated adjustment to the CW nodes positions becomes more complex as the individual adjustments in each panel and in each span are accumulative, and the minor inaccuracies in the original static geometry (see B.6 in Appendix B) together with any inaccuracies in the trigonometrical functions become compounded, and the accuracy of the CW level nodes is lost.

Consequently, the adoption of this reverse unloaded OCL geometry approach is not perpetuated.

The approach adopted is to use the loaded OCL geometry as the starting point. The equilibrium of the OCL geometry is a product of the masses and tensions, and it can be seen that, if any two of the mass, tension or geometry are defined, the third is then fixed. Consequently, creating the final loaded OCL geometry, by the methods described in

Appendix B, will provide sufficient accuracy for the initial equilibrium position, and this is demonstrated in later sections.

Consequently the coordinates of the nodes have been developed using the calculated sag of the loaded messenger wire, and the profile of the contact wire to derive node locations at support and dropper connection points. Node locations within dropper panels have been interpolated linearly. As this was chosen as a 2-D model, the contact wire stagger is ignored, and all Z coordinates are taken as zero. All nodes are constrained in the Z direction. The calculated geometry for the initial position of the CW and messenger wires is developed according to the methods known as the 'separated model' method, and is fully described in Appendix B.

The simplified method (the 'separated model' method) for calculating the OCL geometry, described in Appendix B, is a simplified static calculation based on wires acting as strings without consideration of bending stiffness, a non-linearity associated with large deflections. There are also some other assumptions made, e.g. very stiff droppers, which are described more fully in B.6 in Appendix B..

The initial step of finding the OCL equilibrium, applying the non-linearities, naturally adjust the OCL from the initial (although reasonably accurate) starting geometry, and these minor adjustments introduce additional tension in the messenger wire due to the elastic strain.

This is addressed by the introduction of small springs (~0.01m) in the messenger span, at each end, adjacent the support points. These messenger springs are initially set to messenger stiffness (K = EA/L) and then adjusted to compensate for the additional elastic strain. A compromise value is found to deliver best accuracy for tension and geometry.

The number of nodes has been set at 12 per dropper panel (equates to roughly less than one per metre) in accordance with findings of PantoTRAIN work, as being optimised (Ambrósio *et al.*, 2011). BEAM189 is a three node element and hence there is one element per sets of 3 nodes, i.e. 60 elements per 60m span. In this case the 'inter-nodal' distance, rather than element length (nominally 1:2 ratio, although the middle node of the three is not forced to be at the centre) is the criterion to be compared with 'element length' in other published work. In this model maximum 'inter-nodal' distance is 0.5m. (Not all nodes/elements are same length, as it is necessary to place nodes at dropper

points, which are not equally positioned within a span.) This was chosen after experiments with regular, fine and super fine mesh, with parameters as shown in Table 5.9, and where this is related also to choice of time interval frequency sampling rate.

Table 5.9 Regular, fine and super-fine model mesh showing range of inter-nodal lengths, for coordination with ITS length

	element length (m)		inter-nodal length (m)	
	max	min	max	min
regular	2.167	1.663	1.083	0.832
fine	1.083	0.832	0.542	0.416
super-fine	0.542	0.416	0.271	0.208

Even for the largest intermodal length, in the regular mesh model, the first frequency of the CW is 56.2 Hz, which is well above the frequency range of interest for this study, so the single finite element can be considered to display a quasi-static behaviour (Collina *et al.*, 2015). This frequency is dependent upon tension (T), linear mass (ρ) and nodal distance (l), and is given in Hz by (Ren *et al.*, 2005) as:

$$Fq = \frac{\sqrt{\frac{T}{\rho}}}{2\,l}$$

and is shown in Figure 5.11 for values of nodal distance in the ranges in Table 5.9 for the parameters of the benchmark OCL.

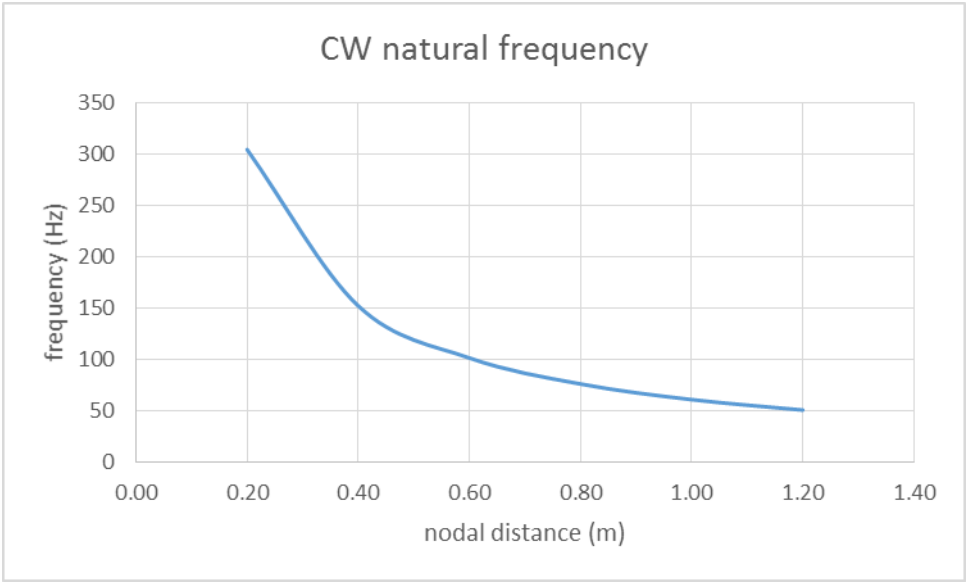

Figure 5.11 CW natural frequency plotted against inter-nodal distance, for 2002 benchmark OCL, where T=20,000 N and ρ = 1.35 kg/m

The 2002 benchmark results to be compared against are shown as low pass filtered at 20 Hz. To study frequencies up to 20 Hz requires, by Nyquist principle (Meddins, 2000) a sampling frequency of minimum of 2 x 20 Hz, i.e. 40 Hz.

In Ansys technical literature 20 points per highest looked for frequency cycle are recommended (*ANSYS Mechanical User's Guide*, 2013), i.e. for 20 Hz it gives 400 Hz, or an integration time step (ITS) of 0.0025 sec. PantoTRAIN (Ambrósio *et al.*, 2011) furthermore suggests a sampling frequency of 200 Hz. The intention is to find the frequency that gives acceptable balance between accuracy of output, and computation cost. Exercises were undertaken to establish to maximum integration time step, between 0.025 and 0.0025, consistent with accurate results, and computational efficiency. This was paired with parallel work on assessing the relative accuracy of models or progressively reducing size. The smallest possible model size, paired with the largest accurate time step, was chosen to give the most efficient method, combined with accuracy.

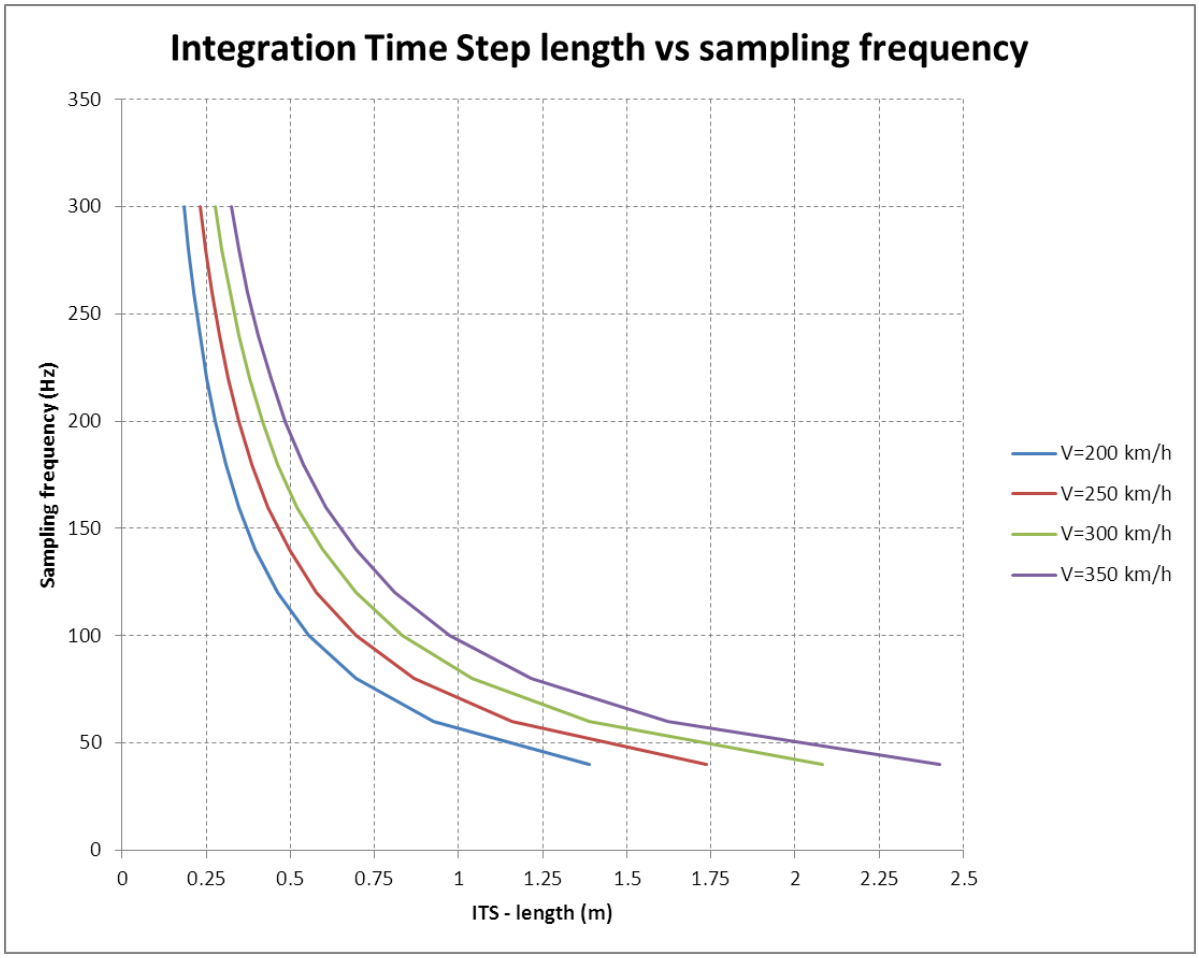

Figure 5.12 Integration time step length plotted against sampling frequency, for different simulation speeds

The EN 50318:2002 benchmark model specifies no damping in the OCL. However it seems a certain amount of damping is required to achieve convergence during the iterations/integrations. In Ansys, both numerical and structural damping is available.

For these models, experiments were undertaken with both forms. Structural damping represents the physical characterises of the physical elements. In real world OCL, only a small amount of damping is present, from such as friction on joints and air resistance. Although no structural damping is initially specified in the OCL for the 2002 benchmark, as springs have been introduced into the model, a moderate amount of structural damping is considered. In Ansys this is specified either explicitly as Nm/s values with the spring characteristics, or as proportional damping (Rayleigh) alpha and beta coefficients of the mass and stiffness matrices respectively in the CW material properties (*ANSYS Mechanical APDL Structural Analysis Guide*, 2013). Values are described below.

Numerical damping is introduced into the integrations to facilitate convergence (and is not in any way related to 'real world' physical damping). The integration method chosen was from the family of Newmark time integration methods (which Ansys offers as option to the HHT method) in which velocity and displacement (and then acceleration) at the end of a time increment are solved using the average acceleration method. This involves the use of the Newmark 2nd order transient integration parameters, conventionally identified as beta and gamma, with values typically (but not exclusively) of 0.25 and 0.5 respectively. (Note that the terminology used in the Ansys technical manuals, and the command input descriptions, uses the identifiers alpha and delta, and are defaulted to 0.02525 and 0.505.) These can be specified directly in the relevant Ansys command for time integration parameters. However an option exists for the specification of numerical damping in the form of an amplitude decay factor, unhelpfully called gamma in Ansys, and this has been set to a value of moderately high value of 0.2 in the initial transient 'settling down' load step, and a slightly lower value of 0.01 in the dynamic load step, in place of the Ansys 0.005 defaults. In the case of user specified amplitude decay factor, Ansys generates internally the relevant values of alpha and delta (*ANSYS Mechanical APDL Multibody Analysis Guide*, 2013), in this case alpha=0.3025 and delta=0.600.

Comparison of the effects of these damping regimes was undertaken by evaluating the statistical values of the contact force for different scenarios: with and without structural

damping, with and without numerical damping, and with both combined. The scenarios are:

1. No damping
2. With global damping
3. With 'custom' structural damping
4. With numerical damping
5. With both structural and numerical damping

The comparison of the accuracy of a selected number of these scenarios is shown in Table 5.10. The 'score' is a metric of conformance with the target values, and is determined as described above at the start of this section.

The application of global damping produces a model which fails by breaking and failing to remake contact during the run. It is most likely that this is due to the 'global' damping, being applied uniformly to the global mass and stiffness matrices, causing the pantograph (which requires specific values of damping to be accurate) to be essentially over damped. Other users of Ansys in this application have seen similar effects (Beagles and Hayes, 2018). Various combinations of discrete damping applied to specific elements of the model were investigated. The data shows a slight improvement created by the structural damping over no damping, and a significant improvement from the numerical damping. There is little actual noticeable difference between the two numerical damping scenarios with and without structural damping, however subsequent analyses are using the combined damping as per scenario 5.

Development versions of 2002 benchmark model - 250 km/h

			L2		P		R		V2		W4		Y	
targets														
110	120	Fm=	115.684	0.000	116.301	0.000	115.668	0.000	110.863	0.000	114.017	0.000	113.310	0.000
26	31	sigma=	29.107	0.000	33.371	0.083	35.220	0.148	31.698	0.025	32.833	0.064	27.403	0.000
175	210	max=	183.372	0.000	195.615	0.000	196.267	0.000	181.586	0.000	186.939	0.000	188.094	0.000
50	75	min=	42.512	0.800	31.529	0.296	29.915	0.321	39.250	0.172	44.905	0.082	52.087	0.000
190	210	max=	203.005	0.000	216.415	0.032	221.328	0.057	205.958	0.000	212.515	0.013	195.519	0.000
20	40	min=	28.364	0.000	16.186	0.127	10.007	0.333	15.768	0.141	15.518	0.149	31.101	0.000
		Score		1.8000		1.5379		1.8592		1.3376		1.3078		1.0000

version features

L2	full registration arm effects included, force, stiffness and damping
P	CW spring added at LH end
R	damping added to CW spring, and increased CW material damping
V2	CW spring damping removed, adjustment to implementation of CW spring
W4	registration arm stiffness reduced (by heel setting)
Y	registration arm stiffness reinstated, static nodes adjusted, run in and run out spans removed

Table 5.10 Development of Ansys models for 2002 benchmark

The ‘custom’ structural damping employed is described against the elements in Table 5.11.

Table 5.11 ‘Custom’ damping for 2002 benchmark validation model

Element	‘Custom’ damping value	Note
Contact wire end spring	10 Nm/s	One only
Catenary (Messenger) springs	1.0 Nm/s	In each span
Droppers	--	
Registration arm spring	1.0 Nm/s	
Catenary (Messenger) material	$\alpha = 0.0125$, $\beta = 1.0E\text{-}04$	Proportional Rayleigh damping
Contact wire material	$\alpha = 0.0125$, $\beta = 1.0E\text{-}04$	proportional Rayleigh damping
Global	--	

Much of the literature on the subject emphasises the importance of the initial conditions, to the successful delivery of the simulation, particularly authors contributing to the Vehicle System Dynamics special issue (Massat *et al.*, 2014; Ambrósio *et al.*, 2015; Collina *et al.*, 2015; Finner *et al.*, 2015). Here this takes the components:

1. OCL initial ‘static’ geometry
2. OCL equilibrium geometry
3. The OCL pantograph contact interface
4. The prelude to the actual dynamic load step(s)

For item 1, the static geometry is calculated according to the ‘separated model’ method, and is described fully in Appendix B.

For item 2, this is achieved within Ansys in a static analysis, using 5 sub steps. Due to the non linearities of the OCL treated as a beam (which isn’t considered in the static calculation) this will result in some adjustment to the geometry. These differences are only minor and are tabulated below, see Table 5.12. These can be compared to the static accuracy check described in the 2018 revision of EN 50318 where accuracies of 10mm in dropper length were considered acceptable.

Table 5.12 Initial adjustment to static geometry in Ansys equilibrium step, showing very small values of adjustment, showing accuracy of the initial static calculation method

Dropper	**1**	**2**	**3**	**4**	**5**	**6**	**7**	**8**	**9**
X (m)	5.50	10.50	17.00	23.50	30.00	36.50	43.00	49.50	55.00
Adjustment (mm)	4.354	4.391	4.256	4.074	3.758	3.371	2.850	2.282	1.602

For item 3, the critical aspect here is that, for Ansys, the contact should be made between the contacting pairs, the pantograph head and the CW surface, and should not be broken during the precedent steps to the full dynamic simulation, as this will result in the contact's not being re-made, and the dynamic simulation will fail.

This is achieved by a careful initial positioning of the pantograph head height. See Figure 5.13, showing the mechanism for the making of the contact during the first two load steps.

The initial value of this setting – of the 'gap' so that the pantograph head can make contact with the CW – in fact the other way round – and then remain in contact whilst equilibrium is achieved in the first load step – is quite crucial to the integrity of the contact in the subsequent load steps. Due to the vagaries of Ansys, contact lost in this load step will not be re-made (as the pantograph head travels upwards under the action of the static uplift force, 'through' the CW).

The gap between the pantograph head and the underside of the CW, is set such that when the CW reaches equilibrium, and sags a little from its original position, this sag is just sufficient to lower the CW onto the pantograph head, which at this time is constrained in the Y direction. This downwards movement is a deliberate consequence of the CW nodes positioning on a straight line between dropper points, and not following the 'catenary' curve. When the Y direction constraint is released, in the next load step, the upwards force maintains this contact.

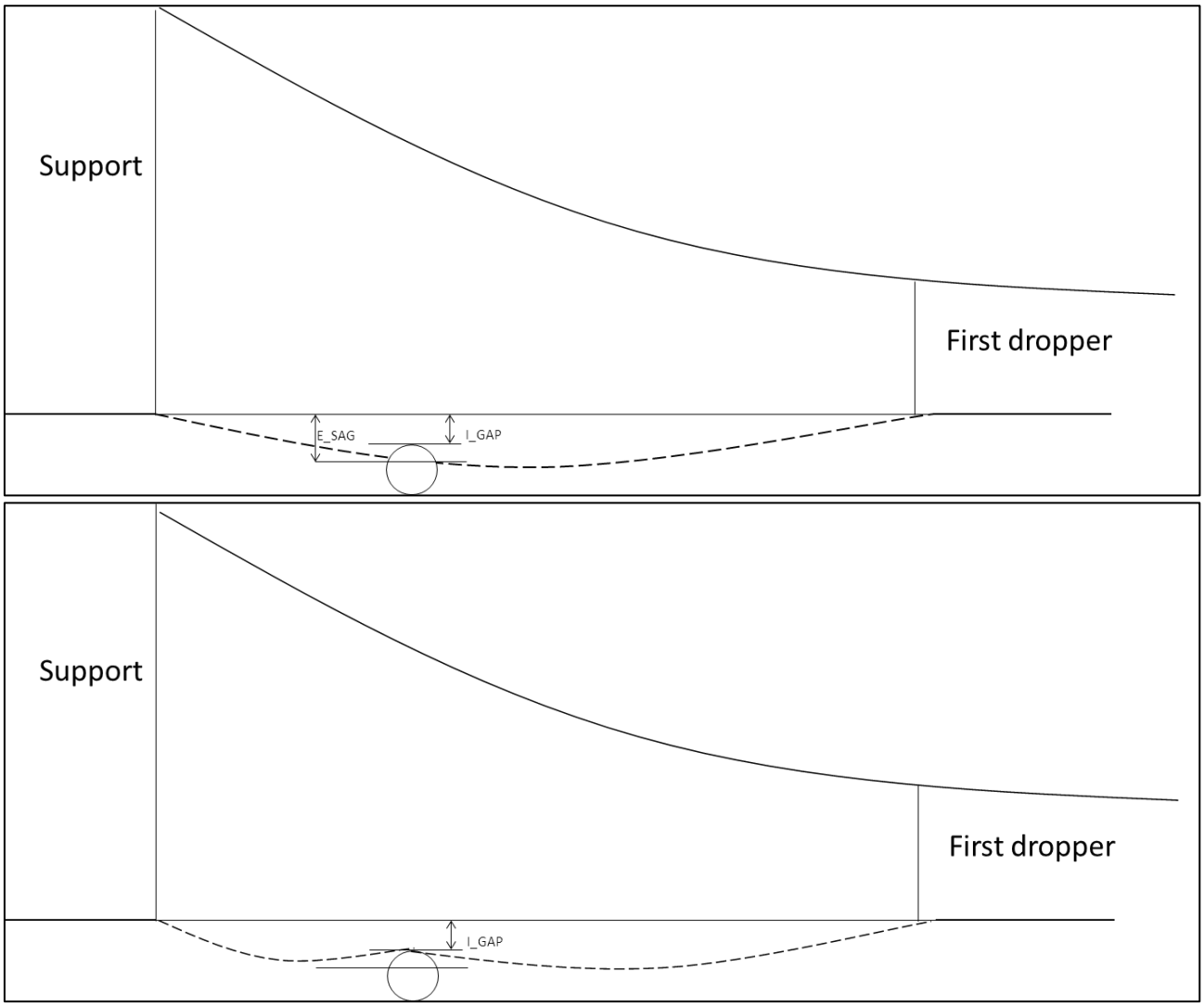

Figure 5.13 Initial pantograph head position, showing initial CW coordinates (full line), initial CW equilibrium sagged position (dotted line) and sag (E_SAG) and gap between pantograph head and initial CW (I_GAP)

This initial setting is further complicated due to the actual (UY) deflection of the CW occurring during the initial OCL equilibrium seeking load step is highly sensitive to the parameters of the model constriction, e.g. presence of catenary springs, damping and stiffness, presence or otherwise of registration arm affects (pendulum stiffness and radial load uplift) and their values. Consequently for any given simulation exercise, a new set of PAN-START (X-coordinate) and I-GAP (Y-coordinate) values must be established to maintain the integrity of the contact, in accordance with the regime described above.

In practice, this is achieved by running the simulation for load step 1 only, and extracting the CW equilibrium positions from the DoF solution for the first span (or wherever the pantograph start position is located) from which the most favourable PAN-START and I-

GAP values can be chosen. The action of the pantograph in seeking and achieving equilibrium in contact with the CW is shown in Figure 5.14.

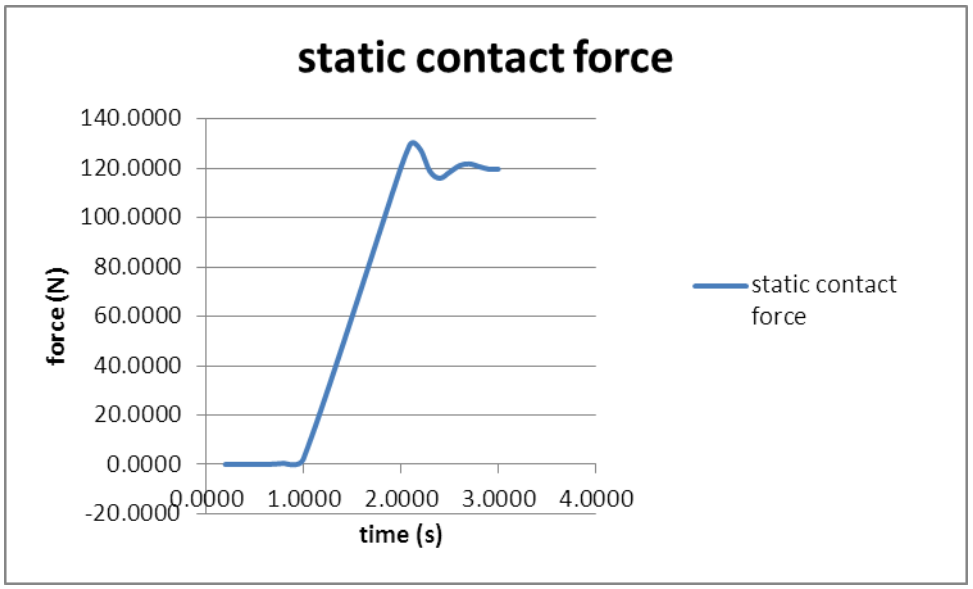

Figure 5.14 Initial pantograph static uplift force achieving equilibrium in the first three load steps, 2002 benchmark

For item 4, a 1 second, 10 sub step dynamic load step without pantograph x direction movement is included, to allow the initial displacements, velocities and accelerations of the nodes to be defined for the start of the true dynamic (moving pantograph) load steps. The full sequence of load steps is shown in Table 5.13 below.

Table 5.13 Ansys simulation steps showing preparatory steps before the dynamic simulation step

Step	Analysis	Actions
1	Static	Pantograph DoFs constrained in all directions 5 sub-steps with OCL mass and tension loads applied as 'ramped'
2	Static	Pantograph DoFs un-constrained in Y direction Single sub-step with pantograph mass and forces applied as 'ramped'
3	Transient	'Settle down' load step, 10 sub steps, to 'seed' accelerations and displacements Numerical damping applied

Step	Analysis	Actions
4	Transient	Pantograph DoFs un-constrained in X direction Integration Time Step set to required value, X velocity set to required value Numerical damping applied
NOTE: Steps 1 and 2 are also transient dynamic load steps, but with time integration OFF (Ansys cannot change analysis type mid run).		

The results of the dynamic simulation are shown in Table 5.14. The simulation was performed twice, using the same model and parameters, with only the speed of the pantograph adjusted for the two values required, 250 and 300 km/h. The output data, in the form of contact forces at each time step, was then filtered to 20 Hz (as required) using a Fast Fourier Transform (FFT) within an Excel file (Kerr, 2009), and the filtered output analysed and plotted. See Figure 5.15.

Table 5.14 Comparison of results from Ansys model against EN 50318:2002 'benchmark', showing acceptable validation in all categories for both speeds (model 001-v1y)

	Range of results			
Speed [km/h]	250		300	
	EN 50318: 2002 benchmark	Ansys model	EN 50318:2002 benchmark	Ansys model
Mean contact force, F_m [N]	110 to 120	113.31	110 to 120	111.20
Standard deviation, σ [N]	26 to 31	27.40	32 to 40	37.53
Statistical maximum of contact force [N]	190 to 210	195.52	210 to 230	223.81
Statistical minimum of contact force [N]	20 to 40	31.10	- 5 to 20	-1.39
Actual maximum of contact force [N]	175 to 210	188.09	190 to 225	205.86
Actual minimum of contact force [N]	50 to 75	52.09	30 to 55	35.23
Maximum uplift at support [mm]	48 to 55	54.4	55 to 65	61.5
Percentage of loss of contact [%]	0	0	0	0

Data for all spans (1 - 10) was collected. As expected spans 1 and 10 show extreme values due to boundary conditions and end effects. However spans 2 – 9 are remarkably consistent. The designated analysis section, the two model spans 5 and 6 (240 – 360 m)

produce results which are within the nominated range, and hence meet the validation criteria. Not all spans (individually) meet the criterion. However, as the data from a single span may be thought of as 'unrepresentative', due to its not fully including the effects from the pantograph transiting the registration point, a two-span section may be considered more useful indicator, data was aggregated for successive overlapping two span pairs, and plotted, see Figure 5.18.

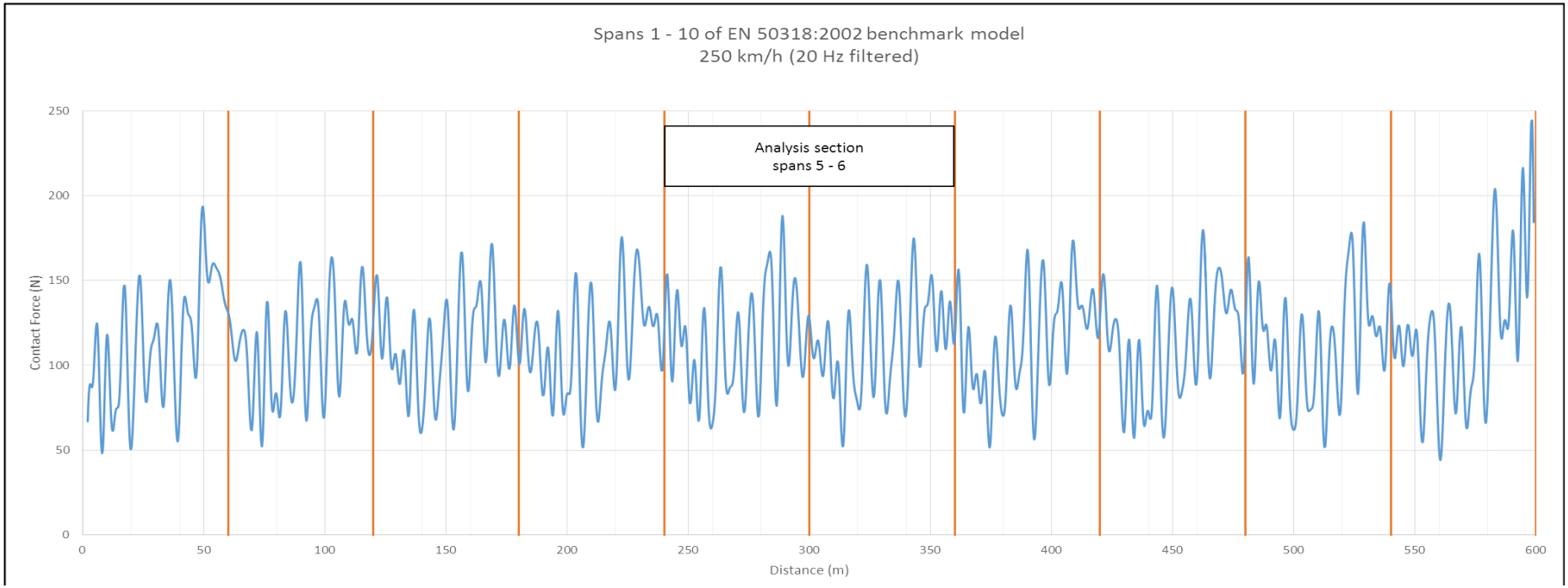

Figure 5.15 Simulated contact force for 2002 benchmark

showing model section and analysis section (250 km/h

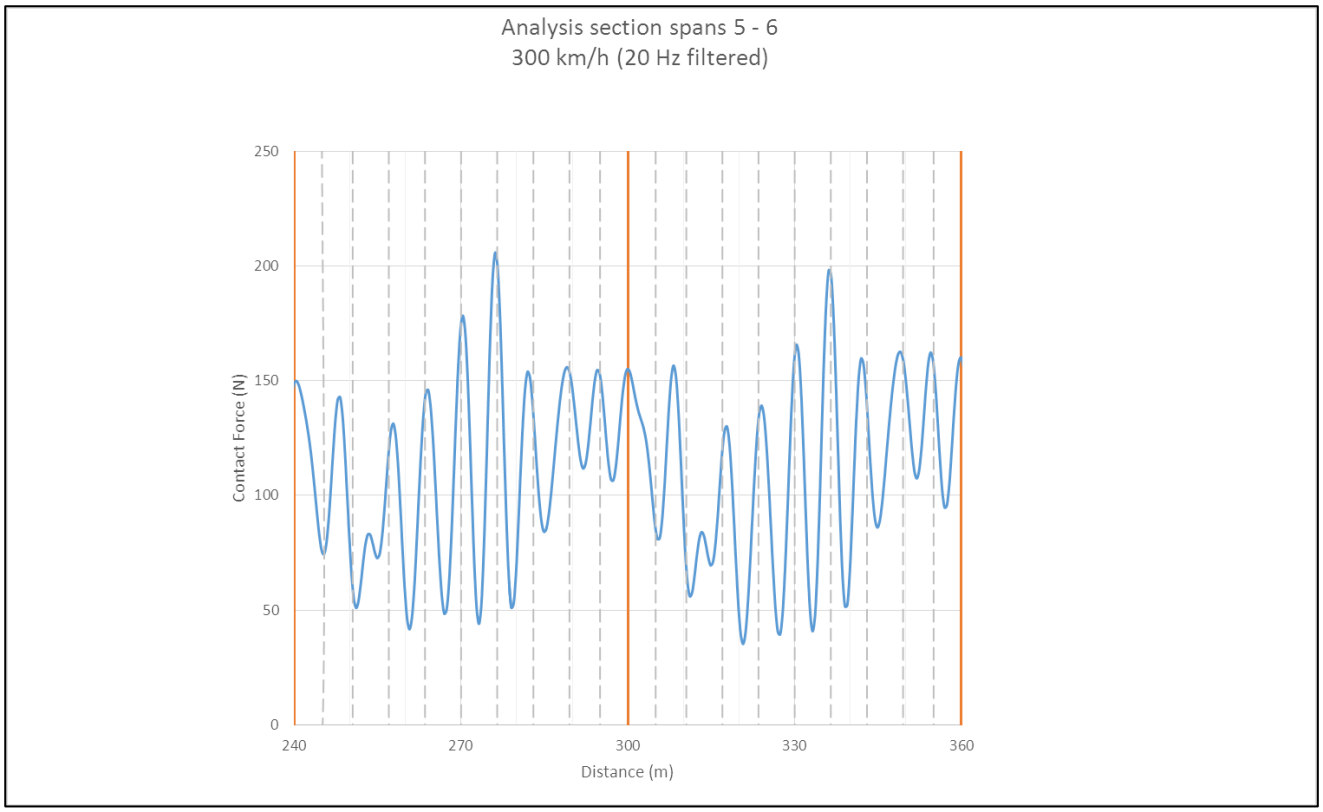

Figure 5.16 Detail of contact force in 2002 benchmark analysis section, showing dropper positions

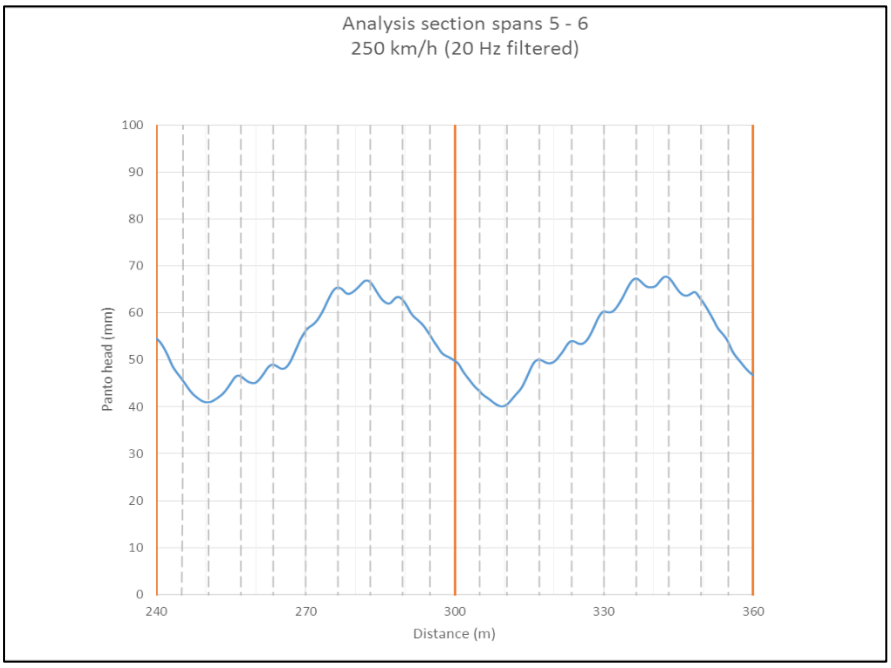

Figure 5.17 Detail of pantograph head trajectory in 2002 benchmark analysis section, showing dropper positions

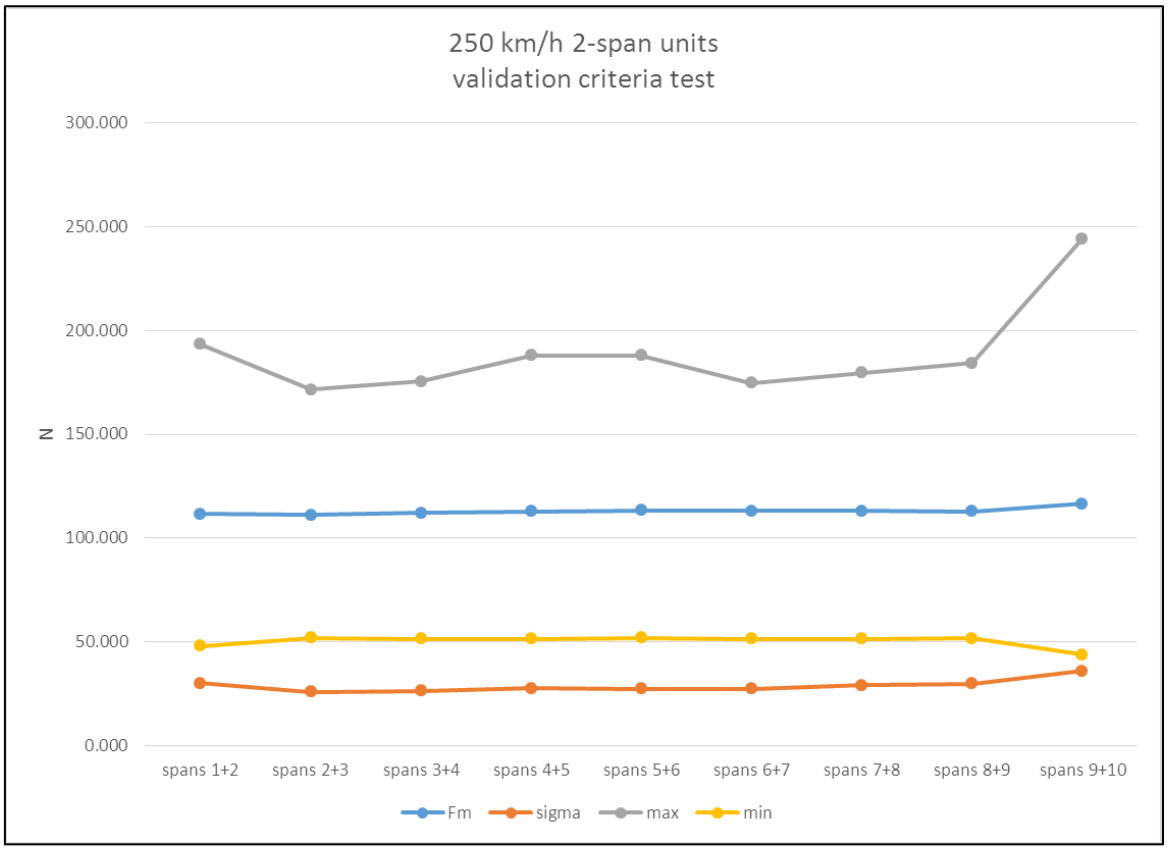

Figure 5.18 Validation criteria for 2002 benchmark in two span pairs, showing consistency even outside analysis section

The worst performing span are spans 7 and 8, whilst 4-5 and 5-6 meet all the criteria. As can be seen, the spans 2 – 9 are remarkably consistent, and all bar one pair equally meet the validation criteria. This gives comfort to the reliability of the model, and gives useful insight into how much 'lead in' section is required between the limits of the model, and the start of an analysis section for which reliable and representative output can be obtained. In this case it seems a minimum of 2 spans is required for 'lead in'.

Looking at the analysis section graph, Figure 5.16, the response of the contact force in relation to the dropper positions can be clearly seen, being aligned through most of the span with a force peak excepting for a blip between the 1st and 3rd dropper. This also indicated the effect of the registration arm (at the support points).

The value of the registration point uplift, also one of the validation criteria, was taken at the three registration points within the analysis section. Data for the whole time integration was available, and the uplift was evaluated as the extreme displacement of the registration point away from the initial equilibrium position (Table 5.15). In all

three cases the maximum uplift occurred at the point of pantograph passing, as might be expected.

Table 5.15 Comparison of support point uplift from Ansys model against EN 50318:2002 'benchmark', for spans 5-6, showing acceptable validation for both speeds

	250 km/h		300 km/h	
Location (m)	Support point uplift (mm)	Maximum 'target' (mm)	Support point uplift (mm)	Maximum 'target' (mm)
240	54.4	48 to 55	57.3	55 to 65
300	49.7		58.4	
360	46.6		61.5	

Outside of the validation criteria, the trajectory of the pantograph head through the analysis section was also plotted. This is shown in Figure 5.17. It can clearly be corroborated with the force plot and the dropper points. What can also be seen is the maximum pantograph head displacement occurs not at the registration points, but around the 2/3 point of the span. (This maximum is 67.7mm where at the registration point it is 49.7mm. The overall range of the pantograph head displacement throughout the analysis section is 27.65mm.) This indicates both the uplift at supports (i.e. registrations) and range of displacement of the pantograph head are both important criteria in assessing OCL performance, and both are included as validation criteria in the later 2018 version of EN 50318.

The full catalogue of all the key features of the Ansys DSM that met the requirements of the 2002 validation benchmark are shown in Table 5.16.

Table 5.16 Significant features of the Ansys DSM that satisfies the EN 50318:2002 benchmark (model 001-v1y)

Significant features of the Ansys DSM that meets the EN 50318:2002 benchmark
1. 2D only (no Z, except for pantograph head) 2. Exactly 10 spans, all spans identical, no start or end spans 3. Springs in each catenary span (K=EA/L) 4. 1 x LH end spring in CW 5. Tension applied by initial stress 6. Registration arm pendulum stiffness and uplift force 7. Custom cocktail of damping

8. Settle down load step before dynamic load steps
9. Use of components and OUTRES to select output data
10. Fine mesh, 1m max 3 node element (0.5 max intermodal distance)
11. Use of specific pan-start position and I-GAP to create (and maintain) initial contact
12. +3N pantograph force augment
13. NLGEOM on (large deflections)
14. CNVTOL specific convergence tolerance settings for displacements, force, rotations, moments
15. AUTO CLOSE off
16. Newmark integration, numerical damping TINTP of 0.1 and 0.2
17. Integration Time Step at 200 Hz
18. Penalty contact with CW as 'contact' and pantograph head as 'target' surfaces
19. Penalty Contact stiffness of 50k
20. Catenary & CW as circular cross sections with 'equivalent' properties
21. Convergence tolerance values for U, F, ROT, M set slightly higher than default
22. Multiple looping around variables to output more than 200 variables
23. Pan head same section and properties material as CW

5.4.3 EN 50318:2018 benchmark

As has been remarked, the additional availability during the course of this research of the revised version of the EN 50318:2002 (2018 version) introduces a more complex benchmark model (whilst retaining the same requirement for an ultimate mandatory comparison against line test measurements). The 2018 benchmark contains additional elements of complexity in pantograph and OCL which will be required for the chosen (ODTT) line test comparison, and it is valuable to use, additionally, the 2018 benchmark as a test bench for these features.

The 2018 benchmark includes the following amended features, beyond the 2002 benchmark:

1. A 10 span OCL model analysis section;
2. A three stage pantograph, without specification of static uplift force, or contact stiffness;

3. Two pantographs in running, with output assessed for both pantographs;
4. A choice of one of three ac OCL formulations, based on that which nearest resembles the one to be used subsequently for the line test measurement validation, at either 275 km/h or 320 km/h;
5. Stiffness and damping specified for the OCL mast (messenger wire support);
6. Full messenger, CW, dropper and registration details provided.

Referring item 4, the benchmark chosen for this validation was the ac 'simple' OCL at 275 km/h, as it most resembled, in geometry and speed, the ODTT series 1 OCL. The targets for the statistical values of contact force and uplift are given in Table A.6 of the standard.

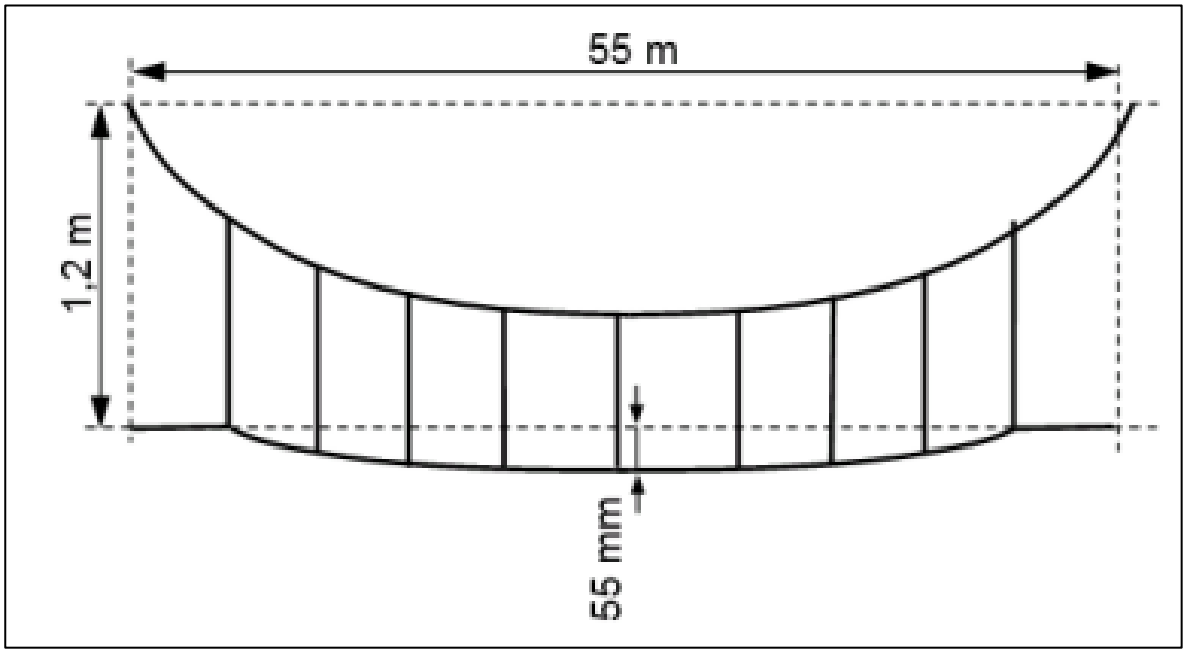

Figure 5.19 OCL model 'ac simple' for 2018 benchmark from EN 50318:2018 Figure A.1

The more onerous requirements in EN 50318:2018 for validation against real line test data require that the simulation copies the real pantograph configuration. In the Old Dalby line test, this means a two pantograph run, i.e. a train with two pantographs raised, with both in contact with the OCL. Data for both pantographs should be analysed, and both should meet the validation criteria. In practice it is usually found that the trailing pantograph is the critical performer. Further to the single pantograph situation of the benchmark validation, in 5.4.2 above, this requires a two pantograph capability to be introduced into the DSM.

In the real world, the pantographs are separated by a fixed distance, dependent on the train configuration, usually of the order of 200 metres. However, to implement this in the Ansys model as a physical representation would require an additional model length of 200m at each end, representing an increase in model and simulation size of around 55 -75%, thus increasing the data preparation workload, and computational cost. This full distance separated scheme is illustrated in Figure 5.20

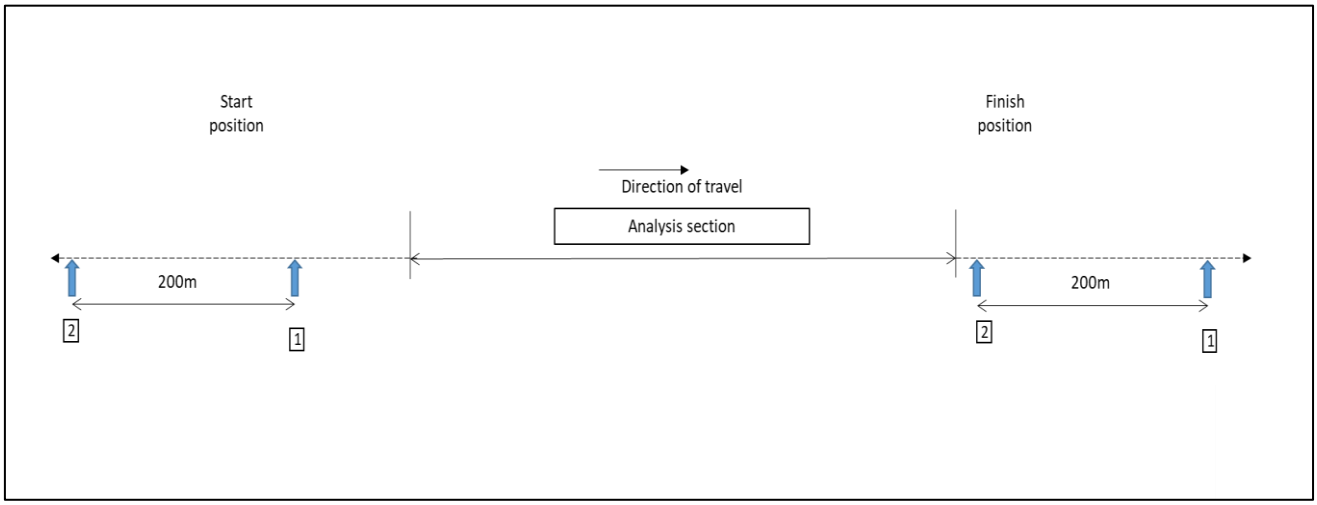

Figure 5.20 Full distance separation scheme for two pantograph modelling

So, in this case, the 'spatial' separation of the two pantographs is proposed to be replaced by time based separation. The two pantographs are initially located in approximately the same point in the run-in span (close, but not coincident, to avoid contact forming problems). At speed V_p (m/s) and for an initial separation S_0, with a pantograph separation distance of S_p, the second pantograph is initially stationary, and only starts when the first pantograph reaches the S_p separation, i.e. after time = $(S_p - S_0)/V_p$ seconds. The ending time for both the pantographs is adjusted in a similar manner, leading to a dynamic transient analysis being completed in three load steps with the full simulation being as shown in Table 5.17.

Table 5.17 Ansys simulation steps – 2 pan time separation mode showing preparatory steps before the dynamic simulation step

Step	Analysis	Actions
1	Static	Pantograph DoFs constrained in all directions 5 sub-steps with OCL mass and tension loads applied as 'ramped'
2	Static	Pantograph DoFs un-constrained in Y direction Single sub-step with Pantograph mass and forces applied as 'ramped'

Step	Analysis	Actions
3	Transient	'Settle down' load step of 1.0 seconds, 10 sub steps, to 'seed' accelerations and displacements Numerical damping applied
4a	Transient	Pantograph #1 DoFs un-constrained in X direction Pantograph #2 remains constrained Integration Time Step set to required value, pantograph #1 X velocity set to required value Numerical damping applied
4b	Transient	(Pantograph #1 is 200m ahead of pantograph #2) Pantograph #2 DoFs un-constrained in X direction Pantograph #2 X velocity set to required value Integration Time Step set to required value
4c	Transient	Pantograph #1 constrained in X direction (stopped) Pantograph #2 continues to its end point
NOTE: Steps 1 and 2 are also transient dynamic load steps, but with time integration OFF (Ansys cannot change analysis type mid run).		

The time durations for each load step are developed accordingly based on speed and position, see also Figure 5.19 (top).

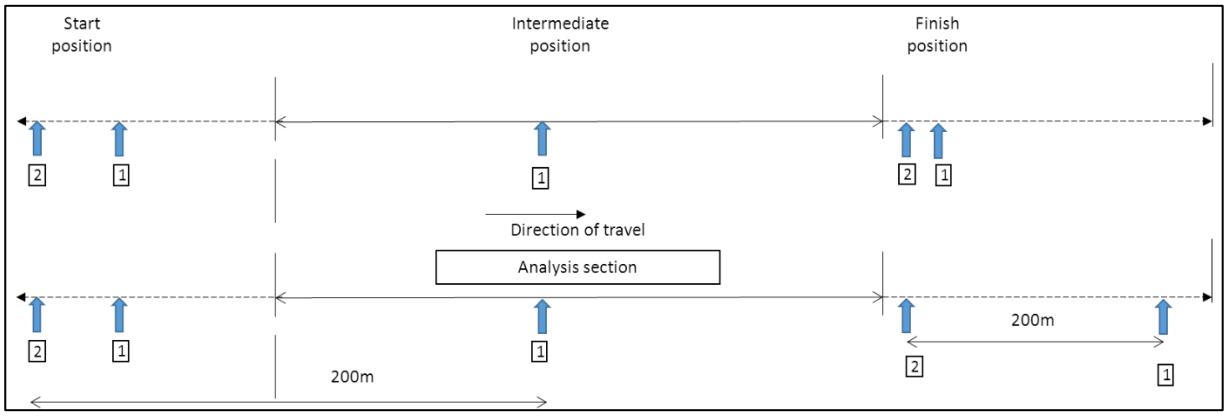

Figure 5.21 Separation schemes for two pantograph runs, showing (top) time separation scheme, and (bottom) hybrid time/distance separation scheme (not to scale)

Although the full time separation method involves the best efficiency in terms of computational cost (elapsed run time) there are potential areas of underperformance. The determining feature of a two pantograph test is the performance of the 2nd (trailing) pantograph running in the disturbed OCL caused by the passage of the 1st

(leading) pantograph, and as moderated by the system damping and pantograph separation. The leading pantograph is also affected by the travelling wave propagated from the trailing pantograph. Both these issues need to be considered before this approach is accepted.

The dynamic behaviour of the pantograph OCL interface is subject to and influenced by the travelling waves in the OCL. These waves are initiated by the pantograph-OCL contact, and are reflected at (at least) the boundaries.

The propagation velocity V_w of a transversal wave in the OCL is given by

$$V_w = \sqrt{\frac{\sum T}{\sum \rho}}$$

where T is conductor tension and ρ is linear mass (Kiessling *et al.*, 2016). For the OCL parameters in this benchmark case, V_w = 125.05 m/s. This is the OCL critical speed, and standards require that train speeds be restricted to no more than 70% of this speed (British Standards Institution, 2009) and European practical experience suggests 66% to 71% (Kiessling *et al.*, 2016).

For this test the train/pantograph speed V_p is 275 km/h, i.e. 76.4 m/s, and so is at 60% of the critical speed.

However the situation of two pantographs (relatively) close together is a particular case. In this case one can be imagine the leading pantograph being caught by the wave propagated/initiated by the trailing pantograph, at a rate of V_w - V_p

In the real world, wave propagation can be initiated by a number of types of events: pantograph raising, train starting movement, pantograph passing from one tension length to another at an overlap, etc. In the Ansys model in particular with the sequence of load steps employed, as identified in Table 5.17, wave initiation can be identified at the point the pantograph(s) DoF is released in the Y- direction, and contact with the CW is made. Note that this means that wave propagation starts before either pantograph is moving.

Referring then to Table 5.17, the initiation point of the wave is at step 2, when both the pantographs are released in the Y direction and contact with the CW is made. Thus the feature of the time separation approach at the start, in this context, is that the trailing

pantograph wave is already initiated 1.0 seconds (the duration of load step 3) before the leading pantograph starts moving, and in fact will catch the leading pantograph sooner than it would in the distance separation approach, due to the lower initial separation (55 m vice 200 m). This is shown graphically in the time distance plots in Figure 5.22 for distance separation and Figure 5.23 for the time separation. (Note in these graphs the origin of the distance axis is the location of the trailing pantograph.)

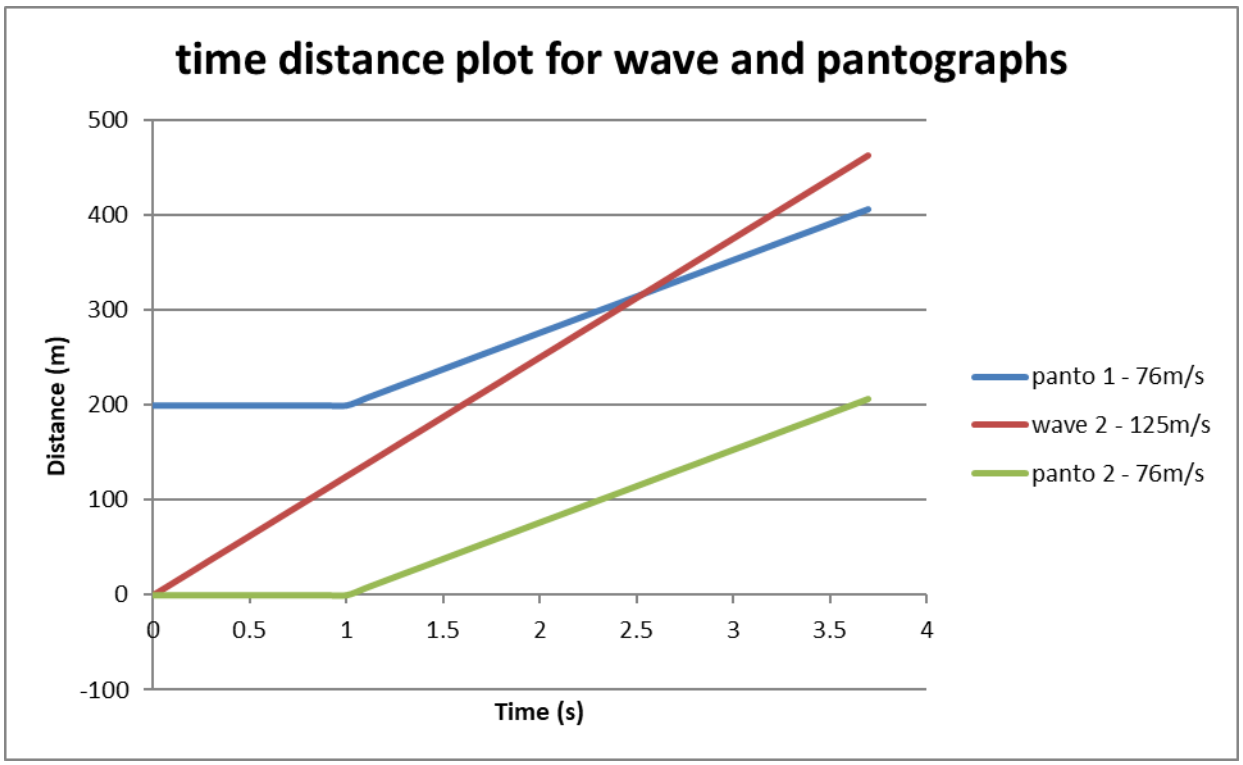

Figure 5.22 Time distance plot for waves and pantographs for two pantograph runs, showing distance separation scheme

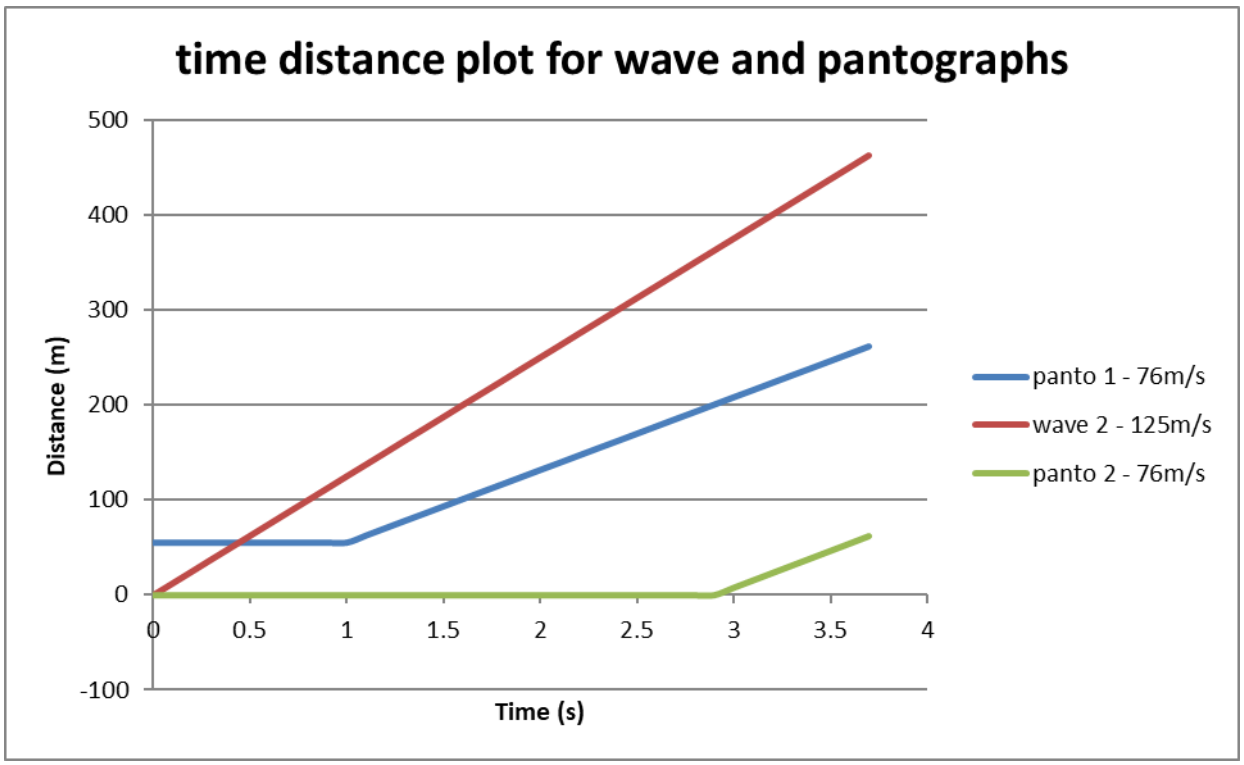

Figure 5.23 Time distance plot for waves and pantographs for two pantograph runs, showing hybrid time/distance separation scheme

In fact the wave will catch the leading pantograph *before* it starts to move, as the 55m separation is covered in less than 1 second. Thus the leading pantograph will always be disturbed by the wave propagated by the trailing pantograph.

In this case then for the distance separation case, the wave will interfere with the leading pantograph after

$$T = 1.0 + \left(\frac{S_p - V_w \,.\, 1.0}{(V_w - V_p)}\right)$$

seconds after the leading pantograph starts moving, where S_p is 200m, i.e. at a point 116 m from pantograph 1 starting point, which is in span 4, the 1st span of the analysis section.

For the time separation case, the wave will meet the leading pantograph after

$$T = \left(\frac{S_p}{V_w}\right)$$

Where S_p is 55m, i.e. at point 55 m, which is in span 2, which is outside of the analysis section. See Figure 5.23. (The term 1.0 in the above expression is for the 1.0 second settle down load step 3.)

Consequently, it can be seen that for the time separation case, the leading pantograph is in fact under the influence of the wave (whatever that might be, as we are neglecting for this instant any decay factor) for a longer time duration than the distance separation case. This is a worse case, and for the purposes of assessing whether the time separation approach is unacceptable because it 'masks' any feature of the real behaviour, we can conclude that quite the opposite occurs. Therefore, as long as the output produced by adopting this approach meets the criteria, we can be confident it is representative.

Considering the issue of the trailing pantograph experiencing the disturbance of the leading, for the distance separation method this is not a problem as both pantographs are in motion at the same time. For the time separation method the leading pantograph stops as soon as it exits the analysis section, and so the trailing pantograph runs for the last 200m (say, the typical separation distance) on an OCL which is not disturbed by the movement of the lead pantograph, but is only displaying the decay by damping of the previous disturbance.

As this is likely to produce inconsistent results compared to the full distance separation method and more importantly the real line tests results, a hybrid method was adopted. The hybrid method involves the application of time separation at the start of the dynamic run but distance separation at the end, see the diagram in Figure 5.21 (bottom). So the three dynamic load steps (4a – 4c in Table 5.17) are reduced to two, as seen in Table 5.18.

Table 5.18 Ansys simulation steps – 2 pan hybrid separation mode showing preparatory steps before the dynamic simulation step

Step	Analysis	Actions
1	Static	Pantograph DoFs constrained in all directions 5 sub-steps with OCL mass and tension loads applied as 'ramped'
2	Static	Pantograph DoFs un-constrained in Y direction Single sub-step with Pantograph mass and forces applied as 'ramped'

Step	Analysis	Actions
3	Transient	'Settle down' load step of 1.0 seconds, 10 sub steps, to 'seed' accelerations and displacements Numerical damping applied
4a	Transient	Pantograph DoFs un-constrained in X direction Integration Time Step set to required value, X velocity set to required value Numerical damping applied
4b	Transient	(Pantograph #1 is 200m ahead of pantograph #2) Pantograph #2 DoFs un-constrained in X direction Pantograph #2 X velocity set to required value Integration Time Step set to required value
NOTE: Steps 1 and 2 are also transient dynamic load steps, but with time integration OFF (Ansys cannot change analysis type mid run).		

The advantage of this is that the best results for the least computational cost are achieved. Additionally the time separation at the start allows the starting positions of the two pantographs to be chosen freely, which allows positioning within the span where it is best able to achieve and maintain the contact during initial equilibrium finding load steps, as described above.

The full model was created as a 3 + 10 + 5 span, where the first 3 span are a run in section, the next 10 spans are the analysis section, and the final 5 spans are the run out section. The 3 span run in section allows pantograph 1 to be started 2 spans from the start of the analysis section, as has been established in the 2002 validation as a suitable allowance for end affects. This is shown in Figure 5.24.

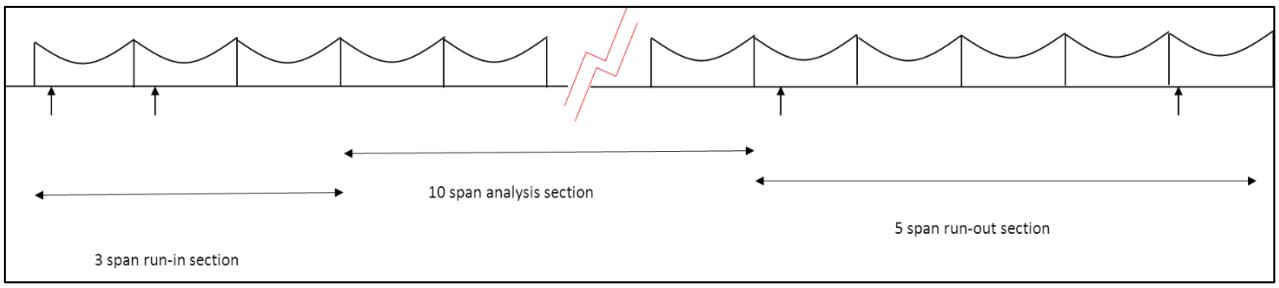

Figure 5.24 3 + 10 + 5 model for two pantograph runs for 2018 validation. Showing 3 span run in and 5 span run out sections, either side of the 10 span analysis section

The 2018 pantograph model does not include any indication of the contact stiffness, required by the 'penalty method' (the 2002 benchmark specified a value of 50,000 N/m). The modelling of the contact between the pantograph head and the CW by the penalty method requires a defined stiffness (or penalty parameter) which resists the contact force correcting the (very small) penetration (Kim, 2015). Ansys allows either a proportional or explicit stiffness parameter, where proportional stiffness is a % of the elastic modulus.

PantoTRAIN work (Ambrósio *et al.*, 2011) recommends that the penalty contact stiffness K_c is chosen such that the pantograph head natural frequency is much higher than the study frequency of interest, where natural frequency is given by:

$$Fq = \frac{\sqrt{\frac{M_3}{K_c}}}{2\pi}$$

and the requirement is that $F_q >> F_{study}$

Comparative results from differing values of K_c are shown in Table 5.19. For a study maximum frequency range of 20 Hz and it is taken that a K_c = 250,000 N/m will provide sufficient distinction for a pantograph head mass M_3 of 7.5kg, and is used here, see graph Figure 5.25. For subsequent simulations (e.g. ODTT and the neutral sections) a choice is made based on the pantograph head mass and the frequency range of interest at that time.

Table 5.19 Penalty contact stiffness for 7.5kg head mass showing resulting ratio over study frequency

pan head mass	**contact stiffness K_c**	**natural freq**	**natural freq**	**study freq**	**ratio**
kg	N/m	Rad/sec	Hz	Hz	
7.5	150,000	141.4214	22.50791	20	113%
7.5	200,000	163.2993	25.98989	20	130%
7.5	250,000	182.5742	29.05758	20	145%

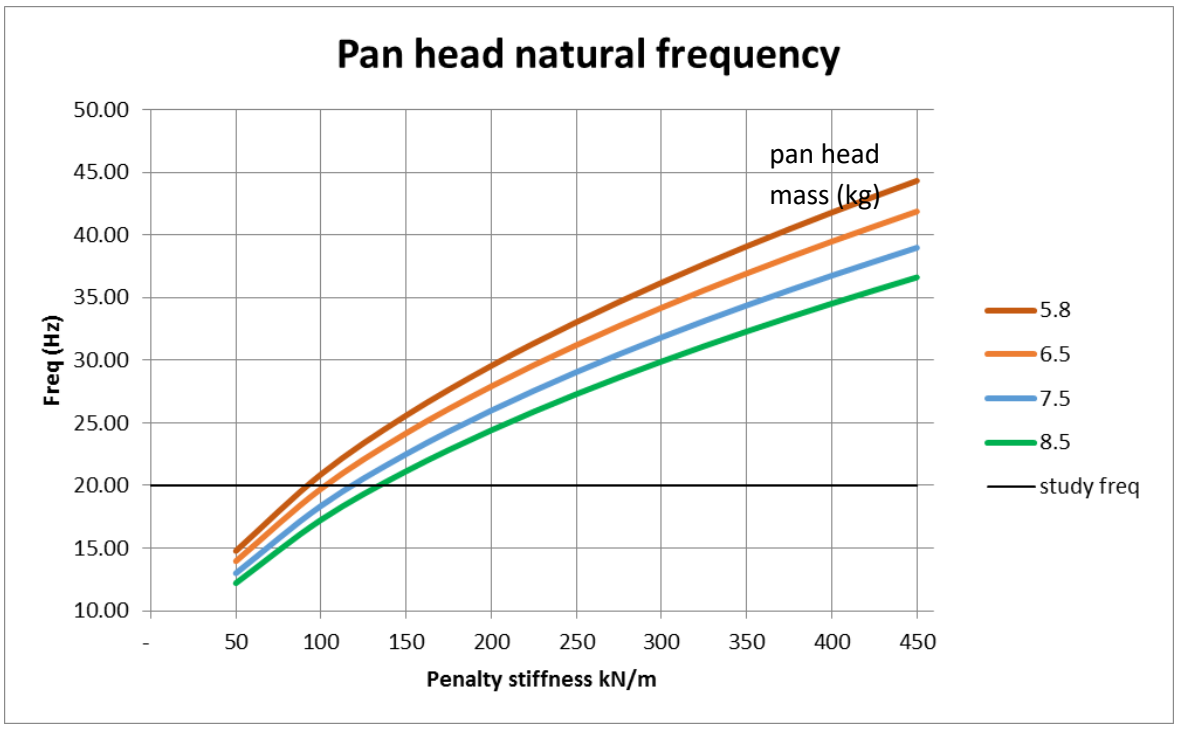

Figure 5.25 Pantograph head natural frequency vs penalty contact stiffness for a variety of pantograph head masses

Unlike the 2002 benchmark, the 2018 benchmark pantograph data gives no value for the static uplift force or contact forces. The only values provided are those of the dynamic mean contact force, Fm (for both pantographs, leading and trailing) as target values for validation.

As has been described before, the uplift force is required to raise the mass of the pantograph frame and head, before it applies a force on the CW. In most pantograph designs this is achieved by an initial extension of the pantograph main spring. As in this benchmark model no detail of any springs are provided, the implementation is an aggregate static uplift force F_S which represents this value, plus the contact force F_C, plus an additional constant (or 'augment') K, i.e.

$$F_S = \Sigma M.g + F_C + K$$

where K is the augment to overcome the particular features of the CW geometry at the start of the model, where the pantograph start position is located. In this case it was found that a contact force of 150.5N, achieved by using an augment of 10.5N, delivered the target values for mean force. This contact force is established during the second load step of the simulation, as shown in Figure 5.26. (Note that this is significantly higher

than seen in UK pantographs, but for this benchmark test, based largely around European practice, the OCL parameters are also much heavier than UK equivalents.)

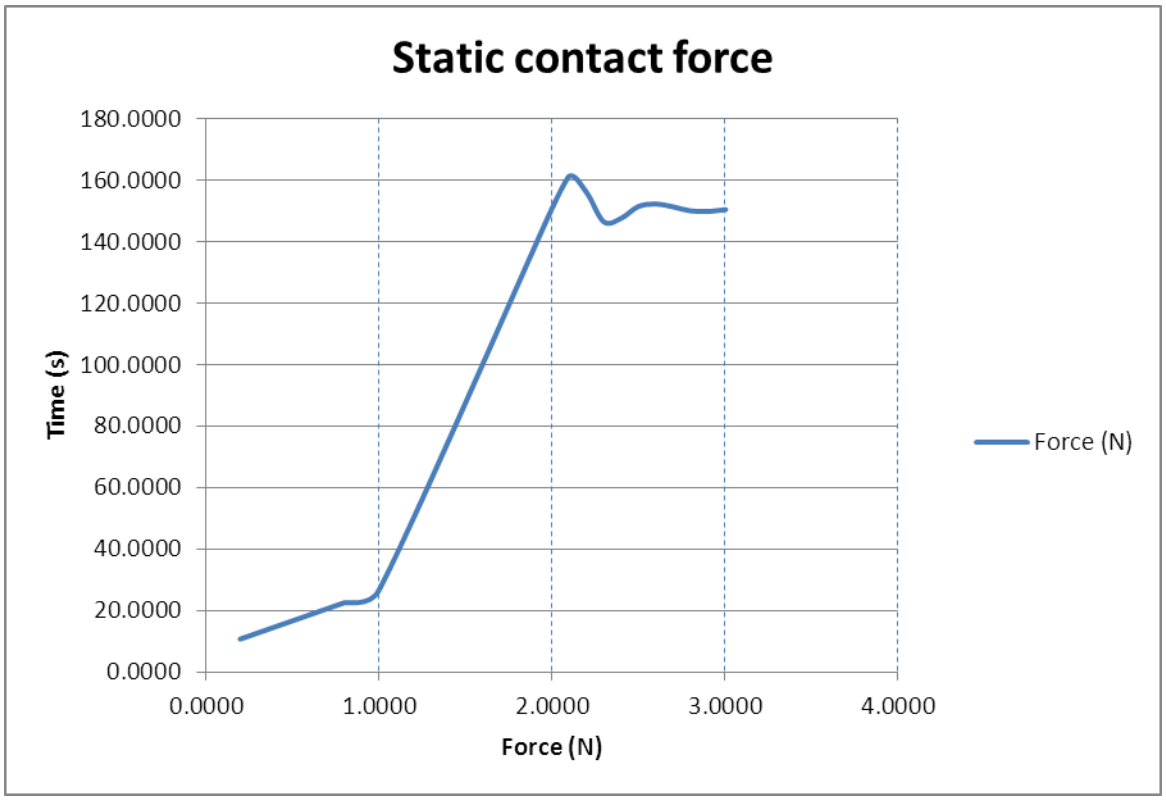

Figure 5.26 Initial pantograph static uplift force achieving equilibrium in the first three load steps, 2018 benchmark

In this case, forces are seen in the first load step, this is caused by the CW settling onto the pantograph head, as shown in Figure 5.13.

Greater detail of droppers is given in the 2018 benchmark than the 2002. The specific lengths for all 5 droppers in the standard span are given, along with their individual stiffnesses. As a comparison, the exact dropper lengths were calculated directly by the same separated model method as described for the 2002 benchmark. These calculated lengths are shown against the specified ones in Table 5.20. As can be seen the accuracy (bottom row of table) is more than acceptable, being always less than 1.6mm, well within the ±10mm required by clause 7.3 ('Static check of overhead contact line model') of the standard. From the dropper length and stiffness, based on K=EA/L, the elastic modulus is deduced for the dropper wire, and is shown also in the Table. For this the value of cross section area of the dropper was deduced from the given linear mass of 0.117 kg/m, which corresponds to the standard European flexible bronze wires of 12 mm^2. This value of EA is used as a parameter in the Ansys script.

Table 5.20 2018 benchmark dropper accuracy comparison BS EN 50318 requirements (top, shaded), calculated values (below), showing high accuracy of static OCL geometry.

X co-ord	m	4.50	10.25	16.00	21.75	27.50	33.25	39.00	44.75	50.50
presag	mm	0	24	41	52	55	52	41	24	0
dropper stiffness for tension	kN/m	197	223	247	264	269	264	247	223	197
dropper length	m	1.023	0.902	0.815	0.764	0.747	0.764	0.815	0.902	1.023
EA (calc) (=K*L)	kN	201.531	201.146	201.305	201.696	200.943	201.696	201.305	201.146	201.531
messenger node Y co-ord	m	1.016	0.871	0.768	0.706	0.685	0.706	0.768	0.871	1.016
CW node Y co-ord	m	0.000	-0.024	-0.041	-0.052	-0.055	-0.052	-0.041	-0.024	0.000
CW radius	m	0.007	0.007	0.007	0.007	0.007	0.007	0.007	0.007	0.007
dropper length	m	1.024	0.903	0.817	0.765	0.748	0.765	0.817	0.903	1.024
difference	mm	0.578	0.770	1.514	0.774	0.530	0.774	1.514	0.770	0.578

As for the 2002 model, global damping was not implemented, but rather a specific combination of individual damping values applied to various parts of the model, as can be seen in Table 5.22. Only minor differences to the 2002 model are used, being the lack of damping in the initial CW spring. Damping and stiffness of the mast support is specified in the standard, but is not a feature of the 2002 model, nonetheless a variation in this was experimented, with no apparent effect on the outputs from the damping, and only a very slight worsening by removing the stiffness.

Of greater significance, it was apparent, was the actual registration arm, and its 2D implementation (as described for the 2002 model). In finessing the model to achieve the target values, although mean force was satisfactory, variation of force, and standard deviation initially remained out of range for pantograph #2. (Pantograph #1 was easily found to meet the targets.). As all OCL geometry and parameters were given, the representation of the registration arm in 2D was considered a likely source as this was mainly inferred' from the scant details provided, and a variety of interpretations were tested. As all registration arm effects are functions of the arm geometry (see Figure 5.7) both stiffness and uplift force contribute to pantograph force at the registration point. The uplift force is calculated from radial load, which is calculated from CW tension and stagger as 320N (see B.5 in Appendix B), and in this case is:

$$F_{reg} = \text{radial load x heel/arm length} = 320 \times 0.2/1.2 = 53.34 \text{ N}$$

The adjustment of heel setting therefore influences uplift force, but not stiffness, but was found to also disturb the OCL geometry (which is based on inclusion of uplift force). A heel setting of 200mm was found suitable (and is supported by being a common value in use in Europe). Normal uplift stiffness ('pendulum stiffness') is also based also on radial load, and in this case is:

$$K_{reg\ uplift} = \text{radial load/arm length} = 320/1.2 = 266 \text{ N/m}$$

Consequently a variety of explicit uplift stiffness values were tried, in combination with values of heel setting controlling the uplift force, giving results expressed as accuracy scores as shown in Table 5.21.

Table 5.21 Tested values of registration arm uplift stiffness showing achievement of satisfactory score

Registration arm uplift stiffness (N/m)	Heel setting (mm)	Uplift force (N)	Accuracy 'score'	How achieved
266	0	0	1.00	Explicit input
266	200	53.34	1.0895	Normal expression
798	200	53.34	1.00	Normal expression and multiplier (3)
1000	200	53.34	1.01	Explicit input
2660	200	53.34	1.90	Normal expression and multiplier (10)

Additionally, a particular approach to the registration arm mass was taken. The linear mass was applied to the 'developed' length of the arm (i.e. the sum of the straight elements of the arm geometry, rather than the 'taut string' length from end to end), based on typical arm geometry, using the arm in the VSD 53-3 benchmark as a guide (Bruni *et al.*, 2015). A typical mass of a clamp was also added at the CW end (0.165kg based on standard OCL components).

It can be seen from Table 5.21 that the value of 3 x calculated stiffness (798N) with a 200mm heel setting, and the regular uplift force with a zero heel setting, both provided the most satisfactory values. However, the zero heel setting is not a realistic assumption, as the geometry check of the given dropper lengths against a specific calculation requires a heel setting of 200mm (and its consequent uplift force) to deliver the equivalent dropper lengths (thus confirming indirectly that heel = 200mm is a valid

assumption). Therefore the effect of the enhanced registration arm stiffness was included, on the basis it successfully delivers the results of the benchmark best. There is no basis for this, other than the 2D representation, *as implemented in this Ansys model*, requires this adjustment in order to meet the target values achieved by other methods, the details of which are not known. However, the values chosen are all reasonably found values associated with registration arms in common use, and can be compared to the registration arm presented for simulation in the benchmark associated with VSD 53-3 (Appendix to Bruni *et al.*, 2015).

Furthermore, it is required only in this particular benchmark, and the full validation against actual line test data (presented later in section 5.5) performs well and achieves compliance using the exact registration arm data. It has been remarked that meeting benchmark results requires a 'second guessing' of the approach taken by a number of researchers in aggregate, and this appears to be a further manifestation of that

Table 5.22 'Custom' damping for 2018 benchmark validation model Note only minor differences to that for 2002 model

Element	'Custom' damping value	Note
Contact wire end spring	--	
Catenary (Messenger) springs	1.0 Nm/s	In each span
Droppers	--	
Registration arm spring	1.0 Nm/s	
Catenary (Messenger) material	$\alpha = 0.0125$, $\beta = 1.0E\text{-}04$	Proportional Rayleigh damping
Contact wire material	$\alpha = 0.0125$, $\beta = 1.0E\text{-}04$	Proportional Rayleigh damping
Messenger support (mast)	1,000 Nm/s	Specified
Global	--	

The force and uplift outputs were processed as described for the 2002 model, with the addition of a frequency band analysis being required for the standard deviation of the contact force, which was effected using the FFT as before. See the results tabulated against the specified target values (ranges) in Table 5.23, where the conformance is seen against every category for both pantographs and hence the model is considered validated.

Table 5.23 Comparison of results from Ansys model against EN 50318:2018 'benchmark', 'ac simple' 275 km/h, showing acceptable validation (model 002-v3g-6b)

	2018 benchmark	Ansys model	2018 benchmark	Ansys model
Pantograph	1		2	
Pantograph distance [m]	200		200	
Mean contact force F_m [N]	141.5 to 146.5	142.64	141.5 to 146.5	144.96
Standard deviation σ [N]	31.9 to 34.8	33.94	50.0 to 54.5	50.74
σ (0 Hz to 5 Hz) [N]	26.4 to 28.9	28.30	41.2 to 45.4	43.82
σ (5 Hz to 20 Hz) [N]	16.2 to 22.4	19.21	25.2 to 34.7	26.07
Actual maximum of contact force [N]	219 to 244	239.52	241 to 290	259.27
Actual minimum of contact force [N]	71 to 86	73.85	14 to 50	16.43
Range of vertical position of the point of contact [mm]	38 to 49	45.7	53 to 70	69.0
Maximum uplift at support [mm]	39 to 48	46.7	45 to 54	50.3
Percentage of loss of contact [%]	0	0	0	0
NOTE: Pantograph 1 is leading, 2 is trailing				

The contact force for both pantographs is shown in Figure 5.30. It can be clearly observed that the pattern of forces for both pantographs is periodic with the spans. The expected difference in the behaviour of the two pantographs is seen. The second, trailing pantograph, is displaying 'worse' behaviour in that there is a slightly higher mean contact force, the maximum and minimum forces show a wider spread, standard deviation is much higher at 50.74 vice 33.94, and the pantograph head range of vertical displacement is higher. CW registration point (support point) maximum uplift is slightly higher at 50.3 mm against 46.7 mm for the leading pantograph (Figure 5.27).

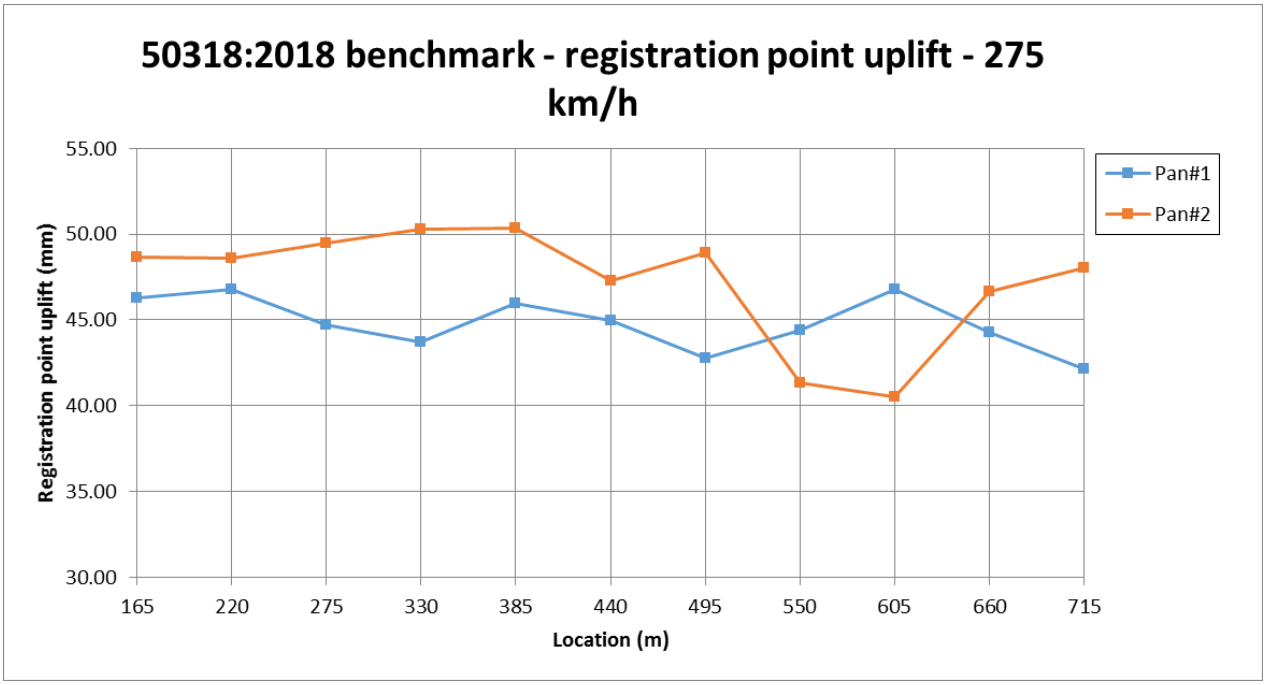

Figure 5.27 2018 benchmark registration point uplift at 275 km/h for the analysis section (10 x 55m spans)

Some variation between the behaviour in the different spans is noted. As spans are identical, this required investigation and explanation. The force plots for both pantographs appear reasonably consistent, across all the 10 spans of the analysis section, but the registration point uplift (Figure 5.27) less so. In particular the trailing pantograph uplift for spans 7/8 and 8/9 is seen as lower than that for the leading pantograph, which is inconsistent with the generally expected behaviour of the trailing pantograph as being 'worse' than the leading. A possible explanation as a source of variation in the spans is the influence of travelling waves, and their reflections.

The initiation of the waves has already been dealt with previously, in discussing the 2 pantograph hybrid regime (previously in this section on pages 149-152) and Figure 5.23 refers. Additionally reflected waves shall be considered, initially from the boundaries (and also, and only if required, from other mass points in the OCL, although by necessity this latter results in a much more complex analysis).

An additional consideration is the initiation of secondary waves, triggered by the original wave meeting the pantograph. The objective is to look for 'zones of interference' where waves and pantographs meet, and examine if any such zone could account for the uplift anomaly seen in the simulation output in spans 7-8-9.

As shown previously the velocity Vw of the waves and Vp of the pantograph for the parameters used in this OCL, is Vw=125.0 and Vp=76.4 m/s.

Using Figure 5.23 as a base, this figure is now re-presented with the pantograph 1 wave included, and the x-axis modified to align with the simulation coordinates, as seen in Figure 5.28. As noted, the model length is 3 + 10 + 5 spans of 55m each, i.e. the x coordinate extends from 0 to 990m. The 10 span analysis section is from 165m to 715m. The pantograph start positions are at P1 = 57m and P2 = 2m. Pantograph 1 terminates at 917m and pantograph 2 at 717m.

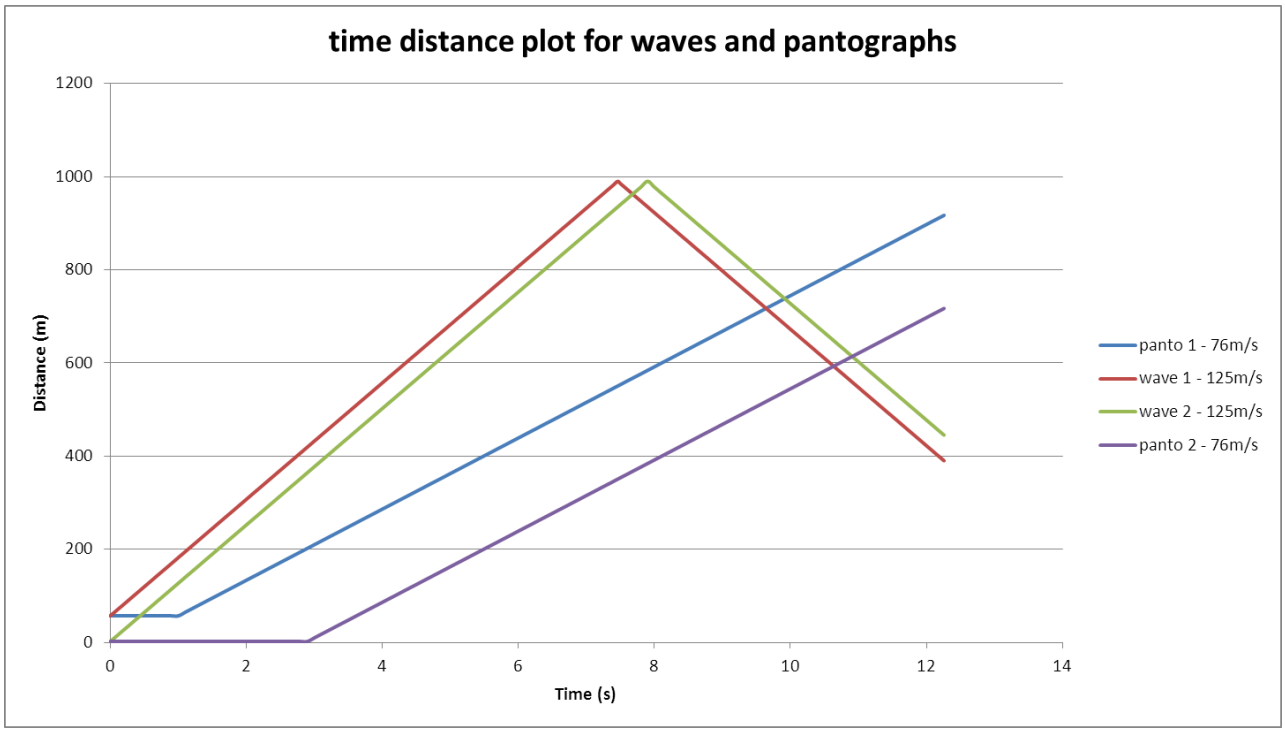

Figure 5.28 Time-distance plot for pantographs and waves, showing waves reflecting from end boundary of the model, and the likely zone of interference where they meet the pantograph

As can be seen graphically, the two pantograph waves, initiated at time = 0, as previously described (when the pantograph uplift force is applied to the CW) run ahead of the pantographs, meet the boundary where they are reflected and they return to cross the path of pantographs. In this case, the waves meet the pantograph 2 at around 595 and 613m points.

In reverse, if the waves were to meet the pantograph 2 in the vicinity of the two anomalies, i.e. between 550m and 605m, then a higher wave velocity is required. If in determining the wave velocity from the expression quoted above the CW parameters only are taken (previously the pantograph wave has been calculated on the sum of the

messenger and CW tensions and linear mass), and an additional allowance of +2% made for the possible variations in actual tension in the segments of the CW (which is realistic due to the equilibrium finding process), this provides a Vw = 130 m/s. In this case, as seen in Figure 5.29 the waves meet the boundary at time 7.16 and 7.58 respectively, and, assuming they are reflected, return to cross the path of pantograph 2 at 10.4 and 10.6 seconds. In this zone (circled) the pantograph is between the 575m and 590m points, i.e. in the zone where the uplift anomalies are noticed (550-605m). This provides one feasible explanation for the uplift anomaly.

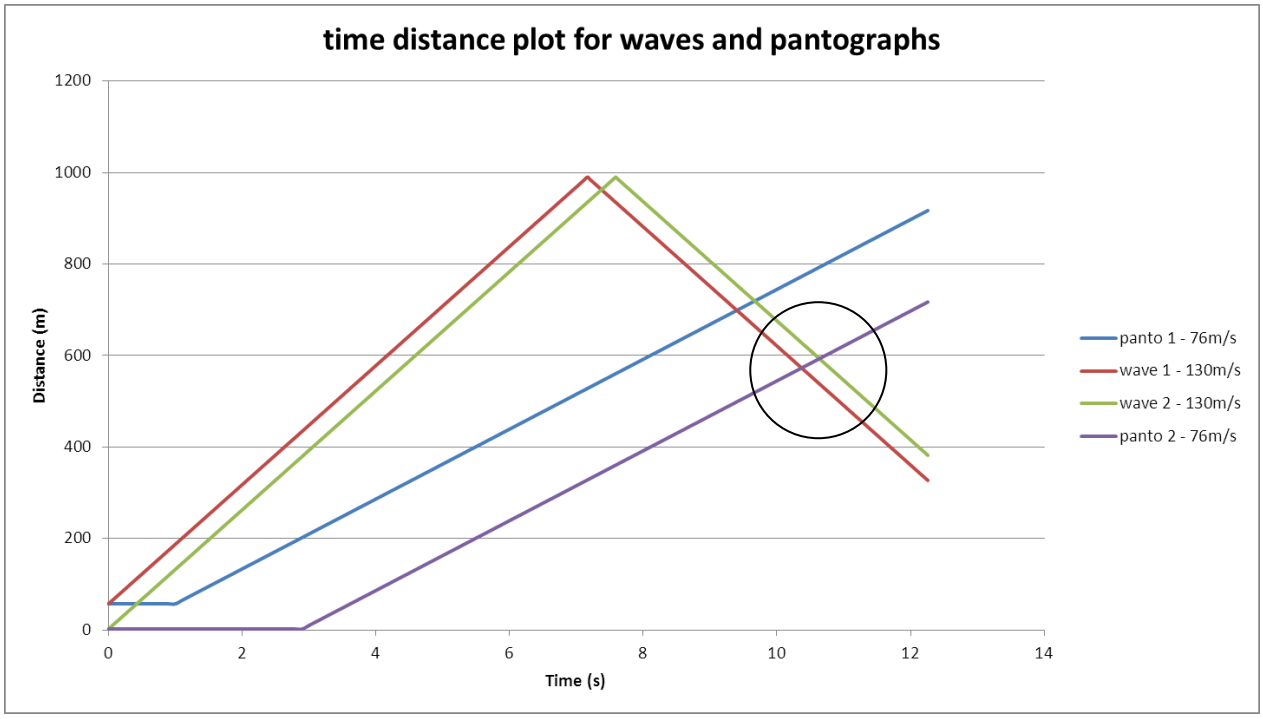

Figure 5.29 Time-distance plot for pantographs and waves, showing waves reflecting from end boundary of the model, and the likely zone of interference where they meet the pantograph (modified wave velocity)

The significant additional features (above the 2002 benchmark model) of the Ansys DSM that met the requirements of the 2018 validation benchmark are shown in Table 5.24.

Table 5.24 Significant additional features of the Ansys DSM that satisfies the EN 50318:2018 benchmark (beyond the 2002 benchmark model) (model 002-v3g-6b)

Significant additional features (above the 2002 benchmark model) of the Ansys DSM that meets the EN 50318:2018 benchmark
1. 3 + 10 + 5 spans model 2. Two pantographs 3. Pantograph separated by time and distance in hybrid scheme 4. 2 x dynamic load steps for pantograph separation 5. Dropper stiffness and mass included 6. 10.5 N pantograph force augment gives 160.5 static uplift gives 150.55 static contact 7. Contact penalty stiffness = 250k based on pantograph head natural frequency 8. Bespoke cocktail of damping, but different to 2002 model 9. Mast support stiffness and damping included 10. 2 sets of 'contact' elements on the CW, one for each pantograph 11. Registration arm pendulum stiffness enhanced by factor 3

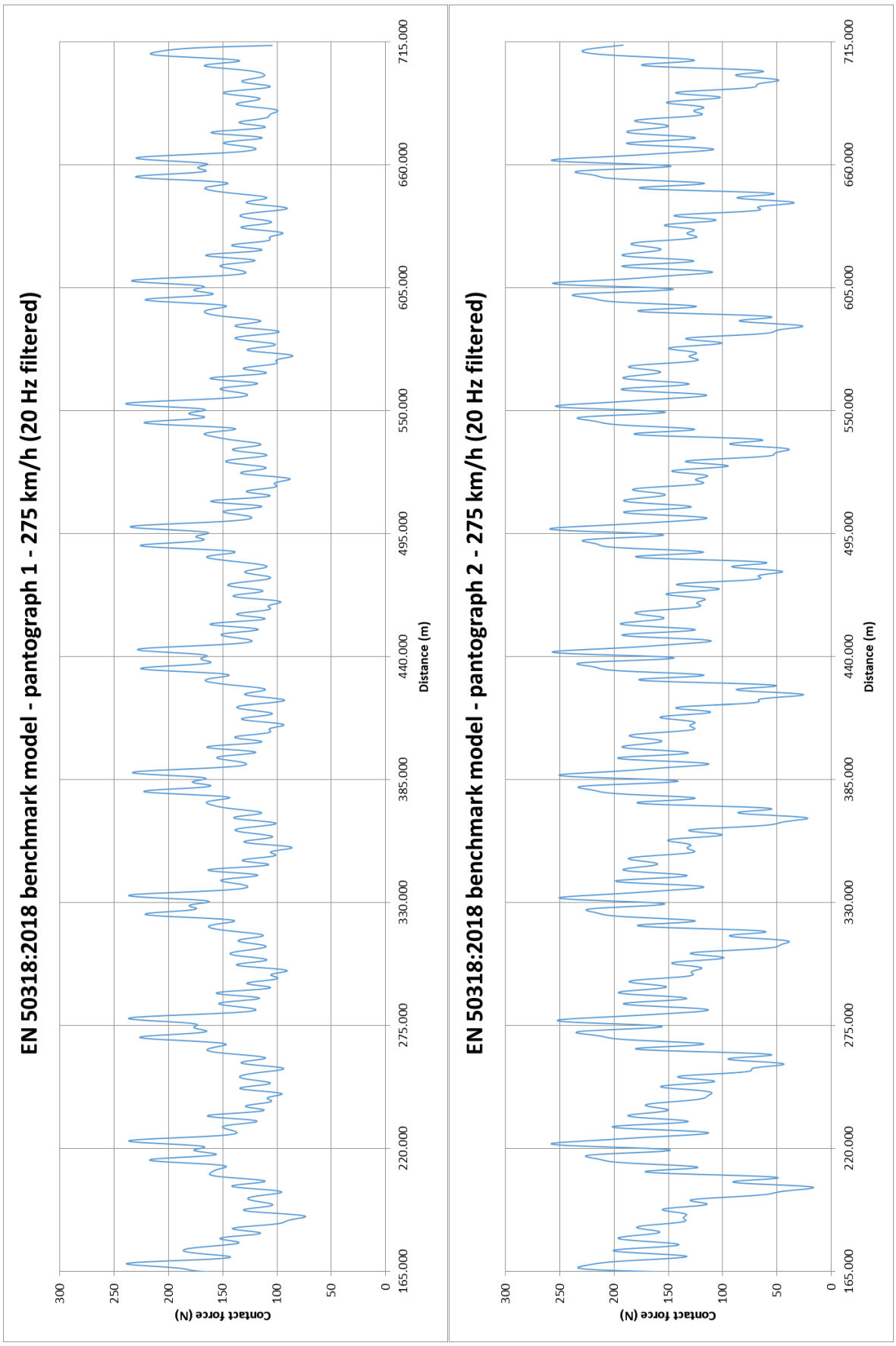

Figure 5.30 EN 50318:2018 benchmark model contact force at 275 km/h (20 Hz filtered) for the leading pantograph (1) and trailing pantograph (2)

5.5 Pantograph/OCL model validation against line test data

5.5.1 Line test data and validation criteria

The third and final validation is against real line test data, in accordance with clause 10 of the standard EN 50318:2018, and the chosen validation scheme in Figure 5.1.

The benefit and value of all the initial development work being undertaken against the relatively simple 'benchmark' OCL and pantograph model from both 2002 and 2018 versions of EN 50318 can be understood when the validation of the DSM is attempted against real data from an actual line test.

Whereas the benchmark test OCL and pantograph use realistic values, but are idealised and simplistic, the circumstances of the real line test includes more complex features and situations:

- varying and irregular OCL span lengths, system heights, staggers, dropper spacing and CW heights;
- the inclusion of dropper clamp masses, variable dropper stiffness and 'real' support stiffness;
- the effect of 'real' registration arms and varying radial load;
- 3 stage pantograph with non-linear head suspension stiffness, additional friction component, plus aerodynamic enhancements; and
- multiple pantographs on the train, each with differing static uplift forces.

In addition, whilst the 'benchmark' validation was done by comparing one set of simulation results with those from other simulations, which used the same input data, and only that data, for the real data validation test the comparison is against measured test results which are influenced not only by the given pantograph and OCL characteristics, but the actual (and possibly different) values of those data at the point of the test, including temperature and wind related effects, the actual state of the pantograph and the inputs from track irregularities and vehicle body dynamics, for which no input data is known.

Furthermore, the output data is in a 'raw' format and needs to be interpreted. In particular, the Old Dalby Test Track (ODTT) data is under distance interval sampling, rather than time interval, which needs to be adjusted for speed to give an equivalent time interval. Fortunately the speed is consistent throughout the analysis section.

As the DSM employed here is based upon the work done in developing against the 'benchmark' model described in 5.4 above, the following description will just concentrate on the differences and enhancements to that model, for the ODTT validation. The fundamentals discussed previously which still apply are not repeated.

In accordance with the scheme previously set out, this method is to be validated in accordance with clause 10 of the standard EN 50318:2018. For a formal validation in strict accordance to that standard, the requirement for the model is that it should include at least ten spans of OCL, for which panto/OCL simulation data is available, collected in accordance with EN 50317. The full requirements for the model for a formal assessment, are shown below:

- At least 10 spans of OCL;
- Minimum model length of 3 x pantograph spacing;
- Contains two half tension lengths and one overlap;
- Includes any specific 'items of interest'; and
- Analysis section is determined on basis of issue to be analysed.

The details of the available Old Dalby Test Track (ODTT) measured data are described in Appendix C. The limitations of this data in relation to its ability to provide a basis for a formal validation in accordance with EN 50318:2018 are described. In particular the following shortcomings were identified:

- No continuous 10 span section available;
- Anomalous behaviour displayed in a number of spans, possibly related to a track fault (described in full in C.6.2 in Appendix C);
- Issue surrounding the filtering regime of the data, effectively having been post filtered at 35 Hz (described in full in C.6.3 in Appendix C);
- Inconsistencies in the odometer indexing of the data; and
- No absolute CW uplift values provided.

However, as the data was the only available data within which an Arthur Flury neutral section was included (being the overriding value of this data to this research), a modified sub set of validation data was established. This allowed a validation to be performed solely for the purposes of supporting this research. The OCL spans chosen for the full model section were a 13 span section from ODTT chainage 1196.000 (structure location TT/11/18A) to 1937.000 (structure location TT/12/08A), a full

length of 741m. Beyond this section the ODTT OCL consist of a variety of multi span overlaps and bridges, some naturally occurring, some specifically introduced in order to observe and test the behaviour of those features.

The evaluation criteria are expressed in terms of the mean contact force, its standard deviation and pantograph head and CW contact point uplift (displacement). There are differences in validation criteria in EN 50318 between the 2002 and 2018 versions. This is indicated in Table 5.25 below. No filtering frequency is specified, the only stipulation being that the simulation data is filtered in the same way as the measured data. For the sake of completeness, as this study straddles the validity dates of both versions of the standard, comparison against both shall be included. In practice this only requires the vertical displacement of the point of contact to be assessed against two criteria.

Table 5.25 Comparison of validation requirements between previous (2002) and new (2018) versions of EN 50318. Note: mean contact force assessment was not specified in the 2002 version.

	EN 50318:2002	**prEN 50318:2018**
Parameter	**Required accuracy**	**Required accuracy**
Mean contact force F_m	--	± 2.5 N
Standard deviation of the contact force σ	± 20 %	± 20 %
Maximum uplift at the support	± 20 %	-10 mm; +20 mm
Range of vertical displacement of the point of contact	± 20 %	± 20 mm

The full force data filtered at 20 Hz is shown in Figure 5.31 For the reasons outlined in C.6.2 in Appendix C the data in span 3 is 'suspect', due to the occurrence of an anomalous force peak, associated with a pantograph head height sudden movement, itself associated with a vehicle body sudden acceleration (assumed to be a track fault) and therefore has been omitted from the derivation of the statistical results, together with that for spans 8 and 9 as this is the neutral section zone, which is not modelled in this open route validation. Consequently the validation criteria for this assessment were extracted from spans 01-02, 04-07, 10-11, and are as shown in Table 5.26. Maximum uplift at the supports (from trackside measurement) was not measured as part of the tests from which this data is extracted.

Table 5.26 Derivation of validation criteria from ODTT measured values based on EN 50318:2018 requirements. No data is available from the test for support point uplift.

Parameter	Measured values	Required accuracy	Validation min. value	Validation max. value
Mean contact force, Fm (N)	109.61	± 2.5 N	107.11	112.11
Standard deviation of the contact force, σ	30.57	±20 %	24.46	36.69
Maximum uplift at the support (mm)	*Not included*			
Range of vertical position of the point of contact (mm)	64.00	±20 mm	44.00	84.00

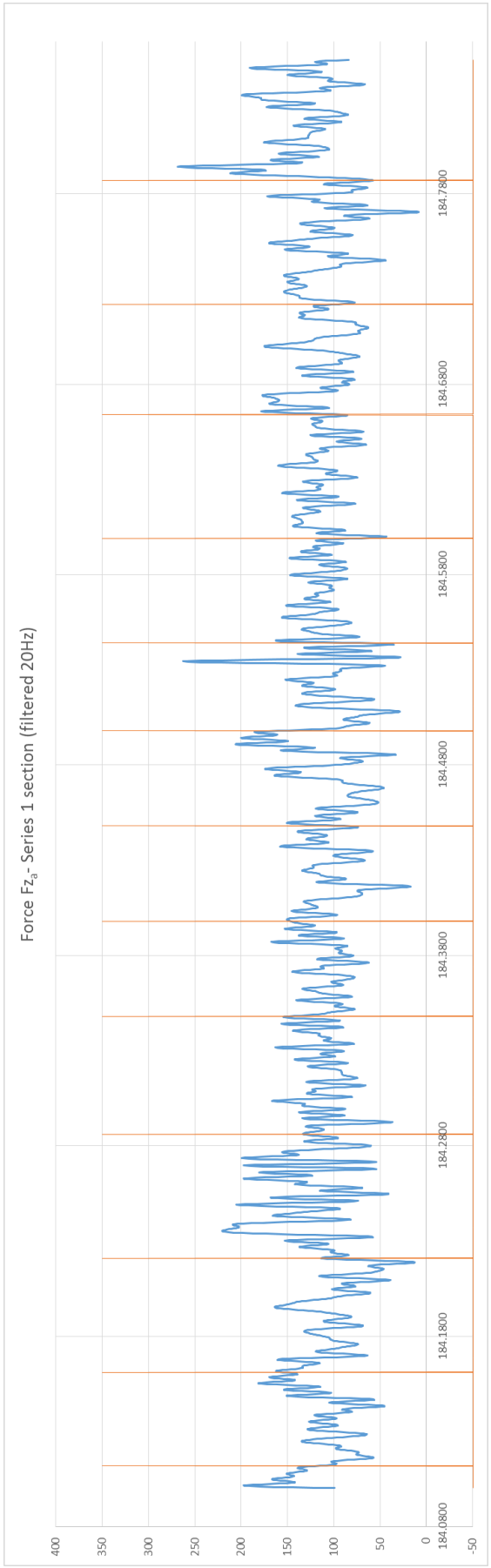

Figure 5.31 Measured contact force from Old Dalby test filtered at 20 Hz, for spans 1-13

5.5.2 Ansys model construction

As outlined above, the requirements of the 'real world' pantograph and OCL which obtain for the ODTT line test measurements require further development of the techniques already validated using the 2002 and 2018 benchmarks.

The IEP train's pantograph is a Brecknell Willis type HSX 250. For the purpose of engaging with OCL system suppliers, to allow them to comply with the requirements of the Energy TSI (EU, 2014a), Network Rail includes lumped parameter models of the commonly used UK pantographs in their system specifications. Additionally an exercise has recently been undertaken by RSSB to update (and validate) all the lumped parameter models for UK pantographs in current use, and the results are presented in a research report T1105 (RSSB, 2016), and the model included therein for the BW HSX 250 pantograph is shown in Figure 5.32. (This report uses the DBST testing rig in Munich, as described in PantoTRAIN report D1.2 (Bruni *et al.*, 2011a).)

This data in RSSB T1105 is difficult to interpret, and a full derivation of its meaning, in terms of the pantograph head stiffness and other parameters, which might be ambiguous at first reading, is given in Appendix D, based on further communication from the authors.

Of particular interest is the non-linear stiffness of the pantograph head. As well as the vertical non linearity of the value of C3, and the bump stops, an additional consideration is the variation of stiffness related to the point of contact position across the pantograph head. This particularly requires attention due to the 2D model used here, which does not have an across track (Z direction in our scheme) component.

The method to address the non-linear stiffness and bump stop (which is just a further manifestation of the non-linearity) is to use a different Ansys element type, COMBIN39 in the pantograph model, as shown in Figure 5.33. COMBIN14 is retained to apply the damping values (which COMBIN39 does not have) and a tabular data of the stiffness is included as force/deflection values, hence implementing the non-linearity. The bump stops are represented by very large stiffnesses in the tabular data, expressed as force/deflection (around 1E+12 to keep within the limits of Ansys), but it is noted that they only come into play at contact forces which are far higher than are seen in these studies.

The static contact forces were set at 70N for the leading pantograph, and 90N for the trailing, as is the practice for the Hitachi IEP train.

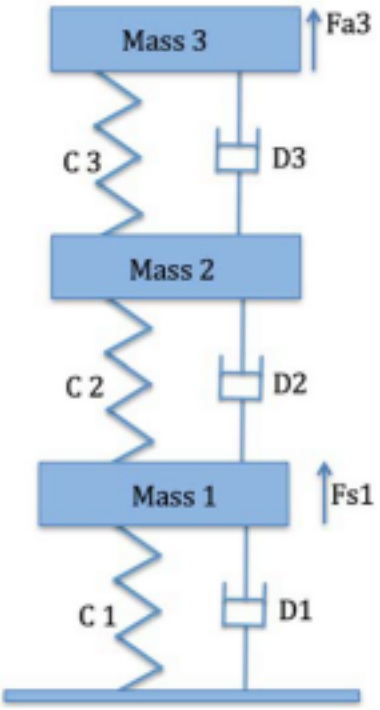

Parameter	Value
Masses	
M1	3.53 kg
M2	7.50 kg
M3	5.30 kg
Damping	
D1	32.6 Ns/m
D2	0 Ns/m
D3	70.0 Ns/m
Springs	
C1	0 N/m
C2	5000 N/m
C3	See manufacturers data below
Externally Applied Forces	
Fs1	70 to 120N
Fa3	0.006 Ns^2/m^2 (Variable if required)

Manufacturers data for secondary suspension	
Preload (vertical force required before suspension displacement)	Approximately 20N
Spring rate	Effective rate at head centre-line increases with displacement approximately as per $0.07(x^2+50x)$ N/mm (reducing to 50 % of this value at the suspension assembly)
Total available displacement	Approximately 60mm

Figure 5.32 Lumped parameter data of BW HSX 250 pantograph from RSSB T1105 (RSSB, 2016)

As the OCL geometry on ODTT is mostly on straight track, and displays the conventional side to side stagger, the value of 'offset' of the contact force was chosen as the centre line, and the stiffness characteristic developed accordingly, as described fully in Appendix D, and shown in Figure 5.34.

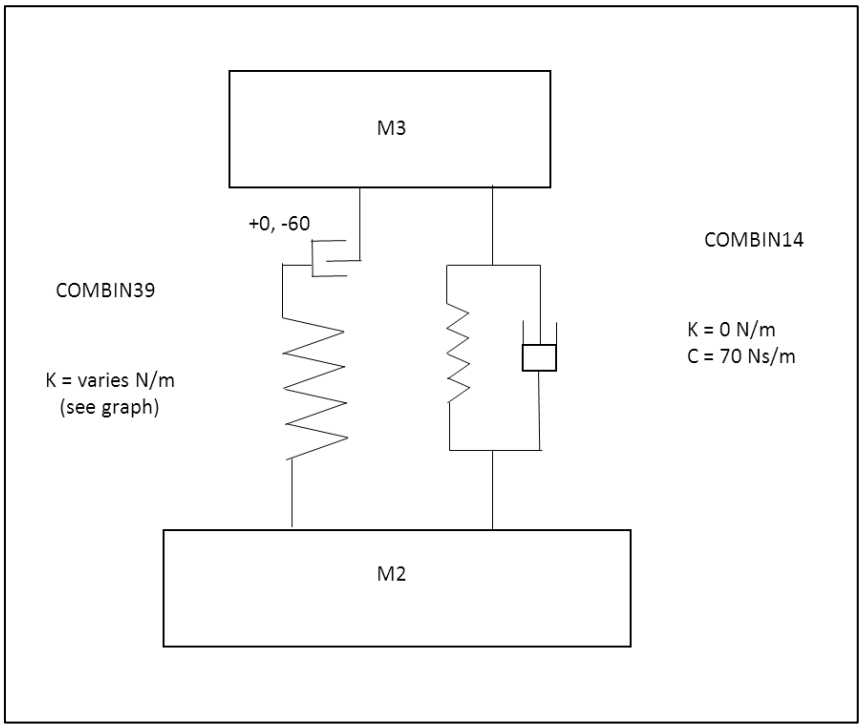

Figure 5.33 Implementation of non-linear BW HSX 250 pantograph in Ansys model (top part of pantograph only shown)

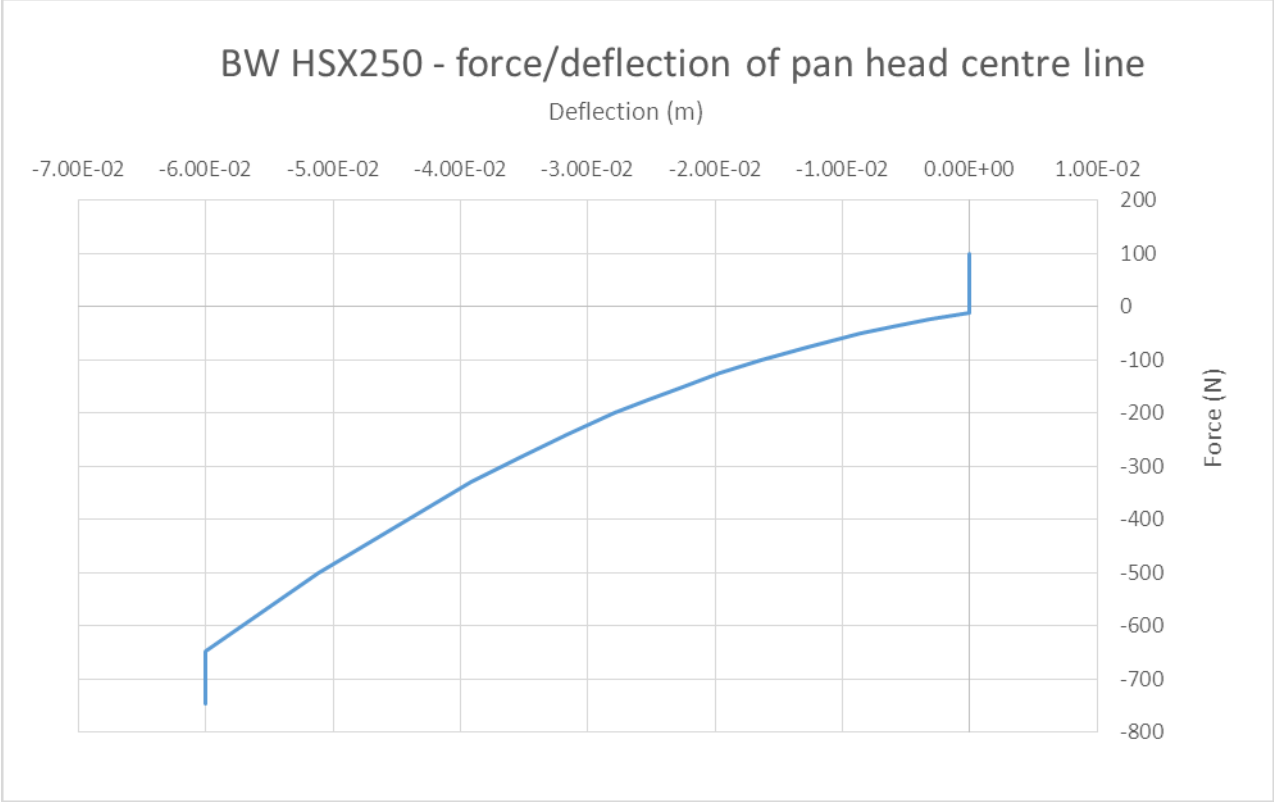

Figure 5.34 Characteristic of non-linear BW HSX 250 pantograph also showing implementation of the bump stops

The OCL model is created in a very similar manner to the 2018 validation model. Nodes data is created from the supplied ODTT surveyed OCL geometry, which is given for support and dropper points only, so requires an interpolation to be made for intermediate node positions, in an Excel spreadsheet. The data is generated for a full 13 spans, plus 'lead in' and 'run out' spans at both ends. The genuine OCL data for these spans is not used as it is highly atypical, and includes multiple overlaps and bridge arrangements. The 'lead in' and 'run out spans are copies of the first and last spans in the analysis section respectively. The model was created for the full 13 spans, although only a sub set of this is used for the open route validation. The full model will be required for the eventual neutral section validation. The full model scheme is shown in Figure 5.35.

The regular repetitive dropper spacing scheme of the benchmark models is of course now replaced with real, highly varied data. The quick and easy identification in the Ansys script of dropper and registration points in the previous models, based only a repeating pattern of node and element number, can no longer be applied. In this case the script requires additional input data in the form of three arrays (actually Fortran format text files, which are read in as arrays) for dropper, support and registration data. The script reads these arrays and, performs the following routines.

For droppers, the top and bottom node definitions are used to extract the dropper length, which is then used to calculate dropper mass and dropper stiffness, the latter from the expression K = EA/L. Dropper clamp masses are added at the top and bottom dropper nodes.

For support points, an additional node and element pattern is created 1.0m above, and a spring damper element introduced, to provide the mast stiffness and damping characteristic, which in the first instance was set at the same value as used for 2018 benchmark, i.e. K = 500,000 N/m and C = 1,000 Nm/s.

For the registrations individual data on registration arm length, radial load and heel setting were provided in the array. The script uses these values to generate the 2D equivalent of the registration arm as described for the 2018 benchmark.

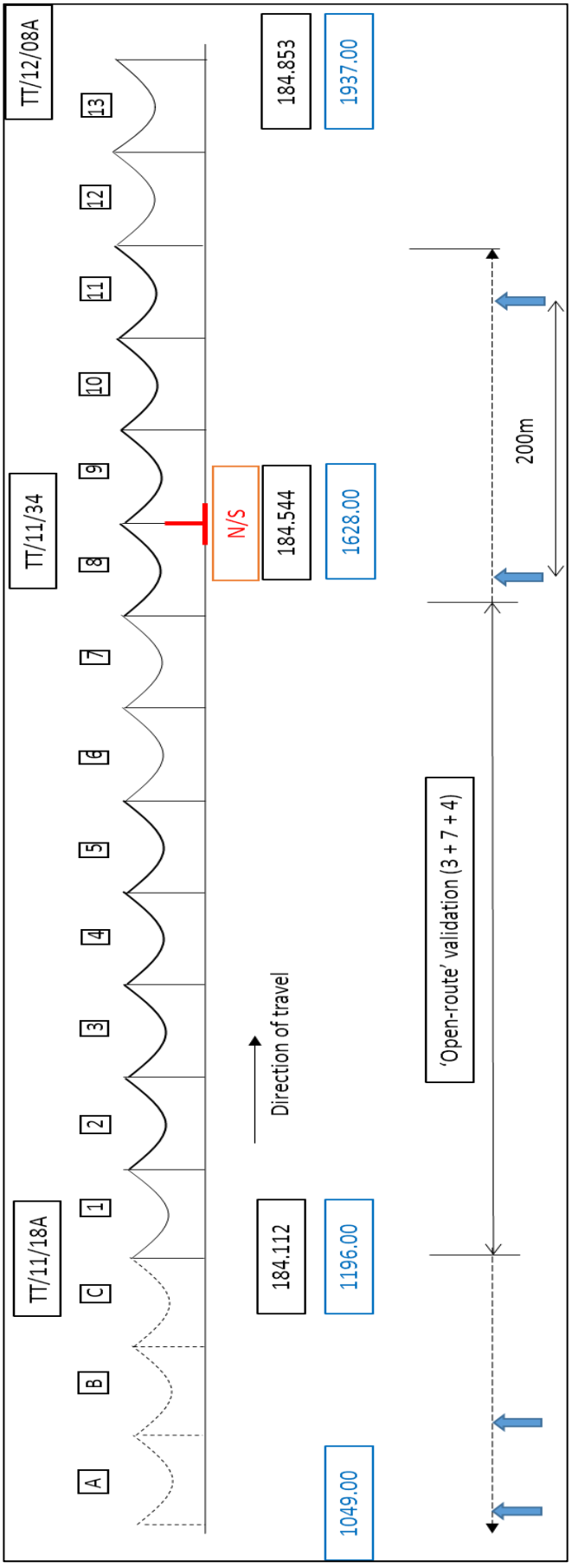

Figure 5.35 ODTT simulation model scheme showing the full 13 spans and initial 7 span analysis section, with lead in spans A-C (not shown are run out spans D-G at right hand end)

The data of the 13 spans is summarised in Table 5.27. The full data is given in Appendix C.

Table 5.27 ODTT simulation model section data showing key values

Structure No.	INDEX	span north	CW ht	Catenary ht	system ht	stagger	rad load (N)	Arm length (mm)	Arm mass (kg)	Heel setting (mm)
Dummy (C)		*49*				*-0.230*				
TT/11/18A	1196	49	4.711	5.995	1.284	0.290	341.8	1000	2.203	80
TT 11/20A	1245	61	4.700	5.999	1.299	-0.225	271.8	1000	2.203	80
TT 11/22	1305	65	4.706	6.012	1.306	0.230	277.5	1000	2.203	80
TT 11/25A	1370	63	4.709	5.998	1.289	-0.235	234.7	1000	2.203	80
TT 11/26	1432	50	4.715	5.985	1.270	0.230	268.3	1000	2.203	80
TT 11/28	1482	51	4.699	6.007	1.308	-0.230	297.4	1000	2.203	80
TT 11/30	1532	50	4.703	6.003	1.300	0.220	294.1	1000	2.203	80
TT 11/32	1582	46	4.697	6.002	1.305	-0.230	231.0	1000	2.203	80
TT 11/34	1628	55	4.695	5.990	1.295	0.000	150.0	1000	2.203	80
TT 12/01	1683	65	4.704	5.992	1.288	-0.225	129.4	1000	2.203	80
TT 12/03	1748	60	4.702	6.010	1.308	0.220	234.4	1000	2.203	80
TT 12/04	1806	65	4.658	5.954	1.296	-0.225	317.4	1000	2.203	80
TT 12/06	1871	64	4.617	5.934	1.317	0.220	115.4	1000	2.203	80
TT 12/08A	1937	64	4.434	6.077	1.643	-0.222	158.2	1000	2.203	80
Dummy (D)						*0.230*				

Full details of the messenger and contact wires, and other technical data necessary to construct the model was taken from Furrer + Frey technical manuals(Furrer + Frey, 2016a). Radial loads were calculated as give in Appendix B. The principal characteristics of the F+F series 1 equipment are shown in Table 5.28.

Table 5.28 Series 1 OCL principal technical data

Wire	**Material**	**Cross section (mm^2)**	**Tension (kN)**	**Linear mass (kg/m)**
Messenger	Bz II	65	13.00	0.596
CW	Cu	120	16.50	1.067

5.5.3 The simulation results

Although a two pantograph model was created, and both pantographs were active in the simulation, as the validation data that is available is only for pantograph 2 (the trailing pantograph), then only those data are output and analysed. The same two pantograph scheme was implemented as for the previous models. The speed through the majority of the analysis section was averaged at 201.75 km/h, and this was used in the simulation.

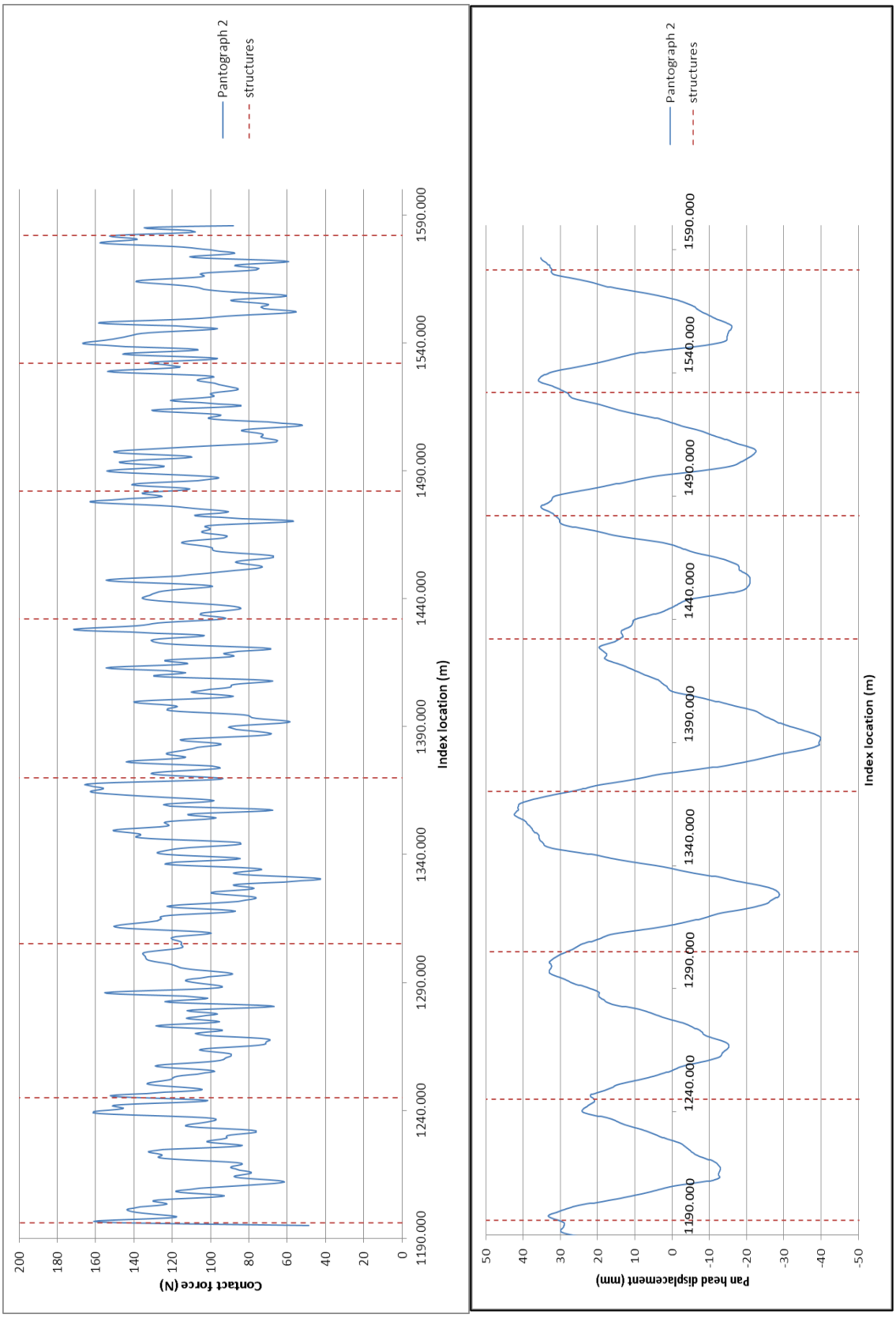

Figure 5.36 ODTT simulation output showing left, the contact force, filtered at 20 Hz, and right, the pantograph head vertical movement. Correlations between the force and movement can be seen.

The results of the simulation are shown in the plots of contact force (filtered at 20 Hz) and the pantograph head trajectory for the analysis section spans 1 – 7, in Figure 5.36. Correlations between the force and pantograph movement can be seen. The greatest vertical movement occurs in the longest spans, as would be expected. Additionally the peak of vertical movement is found in the lead up to a support point, again as would be expected, and has been seen in the 2018 benchmark validations.

The statistical values are shown in Table 5.29. The statistical values show an acceptable accuracy for the contact force and the standard deviation of force. The displacement of the pantograph head, i.e. the vertical movement of the contact point is also within the acceptable range, although at the top end, but it doesn't meet the earlier 2002 accuracy requirement of ±20%, which makes the acceptance range narrower at 51 to 77. It can be noted that the standard deviation of the contact force is at the very low end of the acceptable range.

It is also interesting to note that this UK Series 1 OCL exhibits a 'low force/high uplift' characteristic, typical of UK systems, and comparing to typical European systems, exemplified by the 2018 benchmark (see 2018 benchmark results in Table 5.23) which show, relatively, a higher mean force, for a lower uplift range. The higher system elasticity of typical UK OCL systems is identified in Table 4 of PantoTrain report D.3.1 (Cau *et al.*, 2011).

Table 5.29 Comparison of ODTT simulation output to validation criteria showing acceptable results (model 003-v1e)

Parameter	**Required accuracy**	**min value**	**max value**	**Simulation value**	**Achieved accuracy**
Mean contact force Fm	± 2,5 N	107.11	112.11	108.5812	100%
Standard deviation of the contact force σ	±20 %	24.46	36.69	25.14993	100%
Maximum uplift at the support	−10 ; +20 mm			*Not measured*	
Range of vertical position of the point of contact	±20 mm	44.00	84.00	82.2	100%

The application of the non-linear pantograph head stiffness, described above, did not produce the quality of output required, and a better output was achieved by replacing with a single value of K_3 stiffness, one based on the slope of the force deflection curve over a range of 50 – 250 N, as shown in Figure 5.37. The value used was 7500 N/m. It is noted that other published work using this same pantograph has also used a single linear value of the same order, with successful results (Collina and Zuin, 2014). (The non-linear aspect of the script was not removed, however, merely suppressed and can be reintroduced for a later study, should it seem meaningful.) A possible explanation is the pantograph state of maintenance affecting the behaviour of the suspension. At the same time, the pantograph head mass was increased from the specified 5.3 kg to a value which allowed for the inclusion of some mass of the instrumentation, realistic in the circumstances, and in this case taken as an additional 0.5 kg.

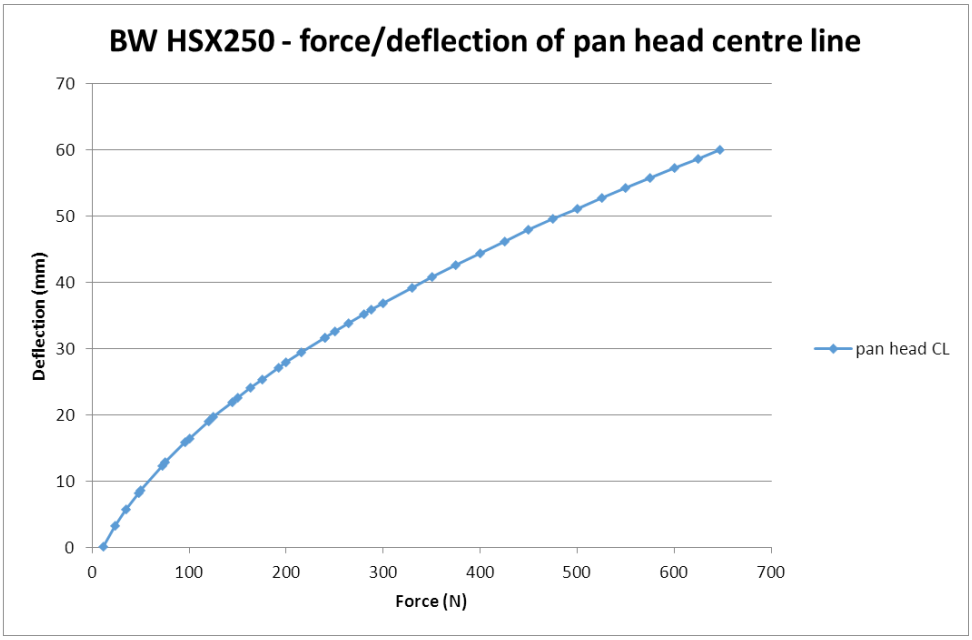

Figure 5.37 Extract of HSX 250 pantograph head stiffness curve showing the approximately linear zone between 50 and 250N, used for the fixed value of K_3.

In summary, the statistical values of force and displacement are acceptable, and given the variable quality of the measured data (less so than had been hoped or expected), the results are encouraging. The additional features beyond those employed in the 2002 and 2018 benchmark models are listed in Table 5.30.

Table 5.30 Key additional features of the Ansys DSM that satisfies the EN 50318:2018 line test data validation criteria (beyond the 2002 and 2018 benchmark models) (model 003-v1e)

Key additional features (above the 2002 and 2018 benchmark models) of the Ansys DSM that meets the EN 50318:2018 line test data validation criteria
1. 3 + 7 + 4 spans model 2. Stiffness and damping of mast support included 3. Specific location by location registration and dropper data included 4. Pan head mass allows for mass of some instrumentation 5. Pantograph head non-linear stiffness and bump stop allowed for, but in this case suppressed and replaced by a single figure, equivalent to the slope of the force deflection curve for a centre point load, in the range 50 – 250 N 6. Dropper stiffness is based on K = EA/L, specifically for each dropper, and dropper elastic modulus is taken as 50 kN/mm^2 7. A pantograph static force augment of 3.5N was included.

5.6 Creating a 'universal' version of the model

Having established the effectiveness of the model and DSM, further work was then undertaken to improve the flexibility and functionality of the Ansys script etc. to facilitate the modifications and adaptability that would be required for the subsequent later studies. This addressed both convenience and ease of data entry (as the reference model had totally unrealistic consistent and repetitive geometry) and optimisation of model size for computational efficiency.

The data entry convenience was achieved by an increased parametrisation of the input variables within the Ansys script, with a greater amount of use of expressions to calculate explicit values. All initial variables were set to default values in the script, and a text file (parameter file in Ansys terminology) was read in by the script to override the defaults, before internal expression calculated the explicit data for the simulation.

The high level flow of the process, involving the Ansys programme and its peripheral input and output processing mechanisms is shown in Figure 5.38. Fuller detail of the Ansys process as incorporated in the script is given in Appendix E.

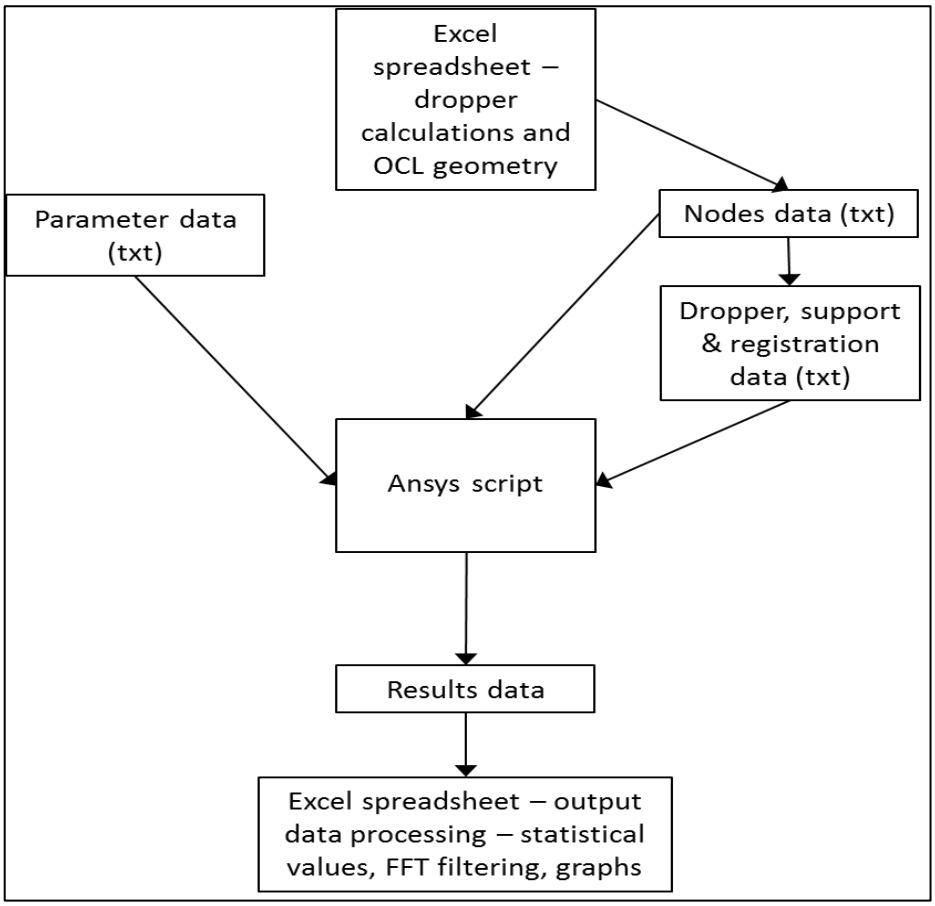

Figure 5.38 Flow chart of final Ansys DSM implementation. The principles of the Ansys script are given in further detail in Appendix E

5.7 Summary of findings

The use of proprietary tool Ansys to perform the panto/OCL dynamic simulation was found to be satisfactory. The simulation output was compared to two sets of benchmark results given in European standards (2002 and 2018 versions), and was found to be within the tolerances, and thus was validated. Finally the simulation of a real length of OCL at the Old Dalby test track was validated against measured data from the same OCL. Some anomalies in the data (representing anomalies in the OCL installation) were found, but having allowed for these, the DSM was found to be validated for the variety of circumstances shown in Figure 5.1 in accordance with BS EN 50318:2018.

These results are summarised in Table 5.31, showing the successful model version number, and linked to the significant features of its construction.

Table 5.31 Ansys model summary of successful validation models

Model	Purpose	Pantograph	OCL	Successful version	Significant features
001	EN 50318:2002 benchmark validation	Single pantograph, two speeds, 250 and 300 km/h	2 spans OCL analysis section	V1y	Table 5.16
002	EN 50318:2018 benchmark validation	Two pantographs, single speed 275 km/h	10 spans OCL analysis section	V3g-6b	Table 5.24
003	ODTT line test (exc. Neutral section) data validation	Trailing pantograph of two, 200 km/h	7 spans OCL analysis section	V1e	Table 5.30

In addition to the key aspects of a good model, identified by other researchers in the field, and identified at the start of this chapter, in developing the DSM the following aspects were also identified as being fundamental to accurate results:

- Registration arm modelling, especially 'pendulum stiffness' and uplift force (from radial load);
- Dropper bi-linear stiffness, especially as influenced by (apparent) elastic modulus (and value of that modulus);
- Messenger and CW tensions and linear mass;
- Specific values of damping in various components of the OCL.

By comparison, the messenger and CW material and section properties were found to be less significant, the model was less sensitive to them.

A number of issues were identified. The use of a 2D model, although convenient and supported by some of the literature, is restricted in its ability to fully represent the behaviour and contribution of the registration arm to the pantograph/OCL interface. This is especially interesting given the significance of the registration to an accurate simulation.

The three validations can be thought of as incremental, and the 'key features (shown in Table 5.16, Table 5.24 and Table 5.30) are shown incrementally. However the first two validations have a characteristic different to the third. Whereas the first two are based

on an attempt to replicate the results of other researchers methods, and in some ways require not only accurate modelling of physical characteristics, but also a level of 'second guessing' the assumptions and approaches of the researchers, the final validation, against the ODTT data, however, replaces this particular area of uncertainty with one associated with the quality of the data, insofar as it is influenced the quality of the real world installation, with its unknowns in terms of geometrical accuracy, temperature affects, state of maintenance, etc. In particular, the additional effort in the 2018 validation required to effectively model the registration arm effect, was not replicated in the ODTT validation. It seems possible that this is a feature in the 2018 benchmark that is directly related to how the various researchers (in aggregate) addressed this problem, and is now locked into the standard, albeit in the 'optional' benchmark test rather than the mandatory line test comparison..

In some ways these validations are more than just technical exercises. However, the subjective judgments that need to be made can be supported by reason, and are so here.

However, the ODTT validation also required some interpretation of the line test data, insofar as some seemed anomalous, and was possibly caused by track, vehicle or OCL 'anomalies' which were not known or could be modelled. The model and analysis length of the target data was manipulated to exclude these sections. In this respect this validation of the simulation method against the line test data is qualified, but there is sufficient confidence to justify its use for the neutral section investigation.

Finally, Ansys is also extremely slow, even across a range of computing options, from CAD spec PC to remote servers, and this is clearly an area where a custom code in language such as Matlab or Mathematica will be superior.

5.8 Conclusions

After investigating various approaches, as described, a methodology for simulating the interaction of pantograph and OCL has been established, based on the Ansys proprietary software, and emulating the current state of the art. This is the 'dynamic simulation method' (DSM).

The method involves the use of Ansys FE software, modelling the flexible OCL as finite elements, and the pantograph with lumped parameters of mass, stiffness and damping. The contact between the pantograph head and the underside of the contact wire is modelled using the penalty method. Multiple pantographs are modelled and results for

each are obtained. Statistical values of contact force, filtered in a frequency range of interest are obtained, along with pantograph head and registration point vertical displacements.

Using this tool a section of actual OCL installed at the Old Dalby test track has been modelled and pantograph interaction simulated, delivering a close correlation with the actual measured test results from the line, and meeting the validation requirements for statistical values of force and contact point displacement in the relevant European standards (the target values for registration point vertical displacement were not available, and so could not be validated). The optimum size for a model containing the specific analysis section has been determined, to reduce manual input, human errors and computational cost. This contributes significantly to answering the research questions posed.

This will be the basis for the method for the modelling and subsequent pantograph/OCL interaction simulation of a neutral section inserted into the contact wire.

Chapter 6 Neutral Section Model Development

6.1 Summary

This chapter describes the development of a neutral section model for inclusion in the pantograph/OCL dynamic simulation method described in the previous chapters, and its validation against line test data.

6.2 Examining the construction of the neutral section

The full detail of the AF single rod neutral section is shown in the manufacturers drawing at Figure 3.17. The actual neutral section installed on the Old Dalby test track is shown in Figure 6.1.

Figure 6.1 Neutral section installed at Old Dalby from DBST trackside video. Note the 'lever arm' at the nearer end.

The neutral section is an assembly of components installed into otherwise regular OCL. Diagrammatically the neutral section installed in a two span section of OCL is shown in Figure 6.2, and a detail of just the neutral section is shown in Figure 6.4. Note that this is the slightly earlier version of the neutral section, where the spring dropper rods are attached to the messenger insulators, where a later model has a shorter messenger

insulator, and the spring dropper rod is connected directly to the messenger wire (Arthur Flury (UK), 2018), see the two in comparison in drawing extracts in Figure 6.3. The version installed at ODTT is the earlier version, as can be seen from the photograph.

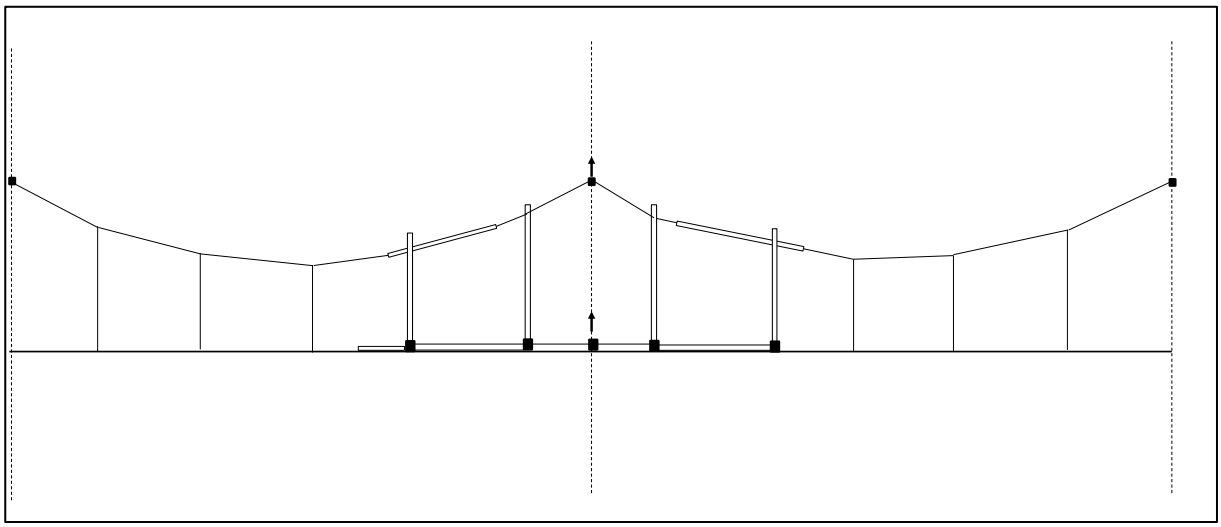

Figure 6.2 General arrangement of a neutral section within two spans of OCL (exaggerated vertical scale). See Figure 6.4 for identification of parts

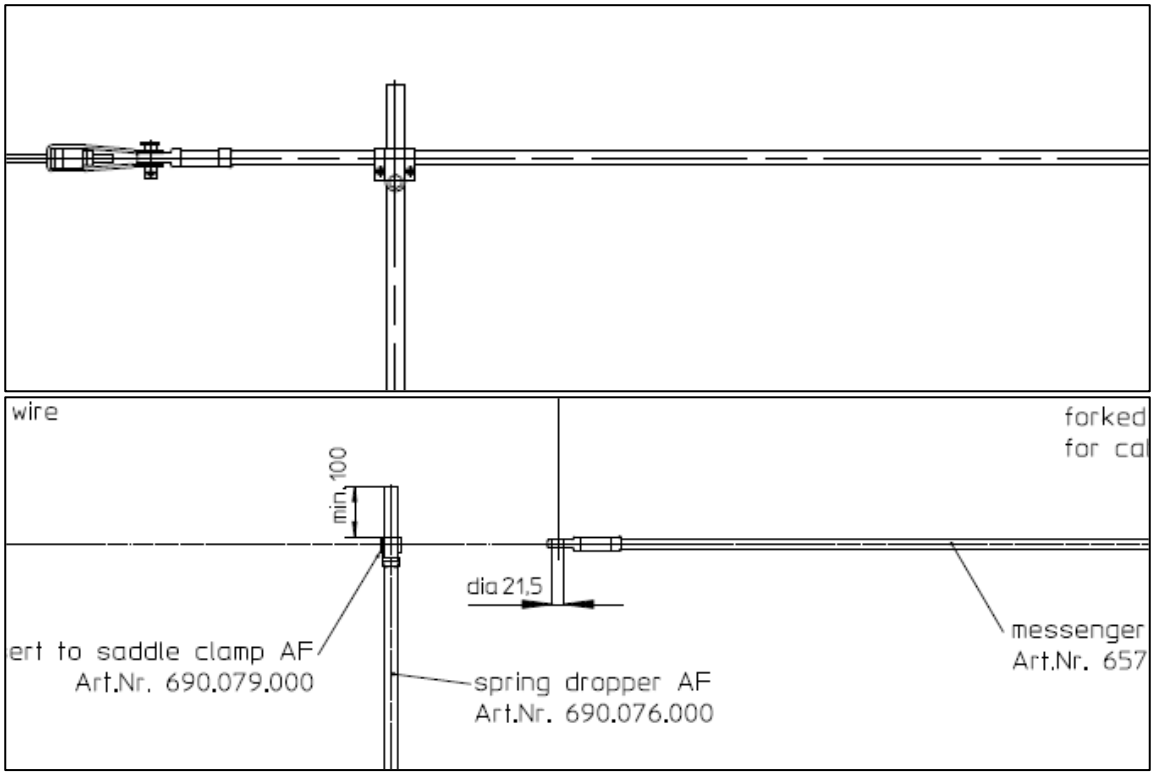

Figure 6.3 Connection of spring dropper to messenger, direct to insulator, old style (top) and direct to messenger wire, new style (bottom). Source Arthur Flury drawings (Arthur Flury, 2019).

The following description is taken from the sources cited, and an inspection of a collection of neutral section parts (removed from the line by Network Rail) in the lab at

Newcastle University. The following Arthur Flury drawings and data sheets were consulted for data of the neutral section, together with supplementary data from the Arthur Flury product catalogue (Arthur Flury, 2019).

- 655.936.504 neutral section assembly 120mm^2 CW
- 657.017.728 messenger insulator
- 690.076.000 spring dropper
- 655.900.002 neutral section insulator 120mm^2 CW
- NSR25 neutral section parts list (Arthur Flury (UK), 2016; Arthur Flury (UK), 2018)

In addition reference was made to the manufacturer's installation instructions MA_NSR_ENG_00_2017_03 (Arthur Flury, 2017).

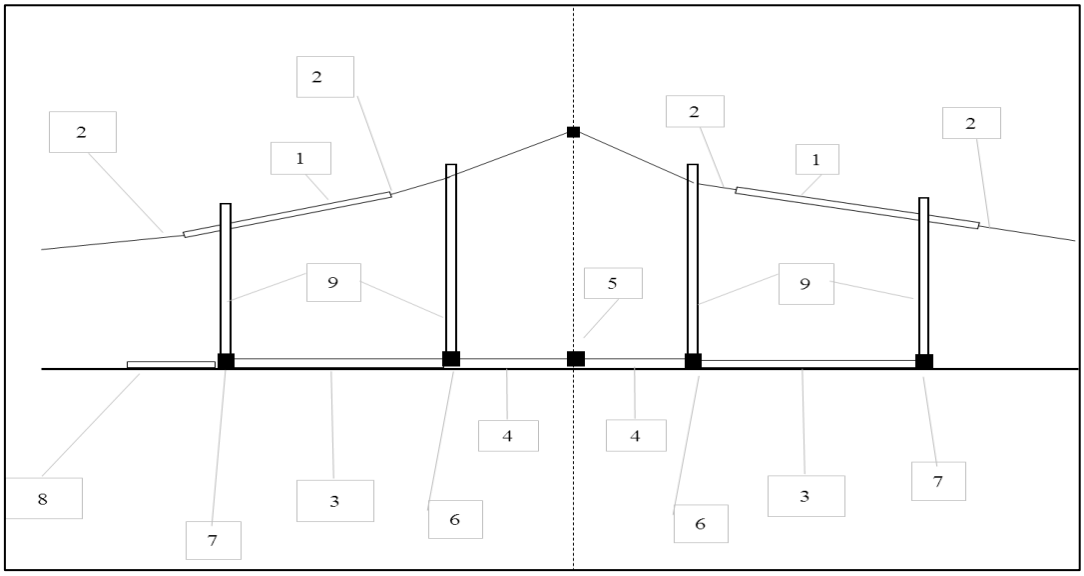

Figure 6.4 Neutral section major components

Referring to Figure 6.4, the messenger insulator [1] is a PTFE coated GRP rod, of outer diameter 21mm, with 14mm GRP core. It is 2750mm long and weighs 3.2kg. It is attached to the messenger wire by a 'forked collar' end fitting [2] at each end (Figure 6.5). The connection is a pin as can be seen.

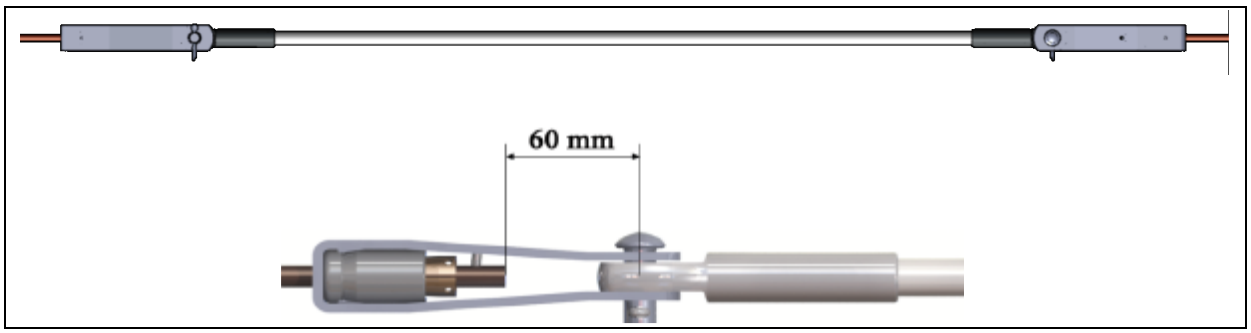

Figure 6.5 Messenger wire insulator showing detail of forked collar termination of messenger wire (Arthur Flury, 2019)

The CW insulator [3], [4] is similar to the messenger insulator, but with an external diameter of 24mm, but the same core of 14 mm (Figure 6.6). Each insulator PTFE/GRP rod is terminated in a stainless steel end fitting, the GRP portion of the composite rod appears to be bonded into the end fitting (or the part of the fitting that mates with the internal 'clicker' mechanism). All end fittings include an internal 'clicker' mechanism to rotate the insulator rod within the end fitting, by four indexed positions, at 90° apart (used under maintenance to spread the wear evenly around the rod, before replacement is required). All fittings have a slightly chamfered end, and a threaded socket. Two types of fitting are used, with respectively LH and RH threaded sockets. This allows the double ended bi-threaded stud to be used to connect the insulators together, incorporating one of the intermediate fittings, as described below.

There are two CW insulator forms, the long and the short. They differ only in the length of the composite rod sections. The long insulators provide the primary insulation at each end of the neutral section, the shorter rods act as continuity pieces in the centre section, and are, at least at the stainless steel end fittings, earthed. The rods are connected to each other by stainless steel studs, which are used to mate the end fittings of each insulator via a threaded socket in the end (Figure 6.7). In each case, the stud holds another fitting captive, and there are three such.

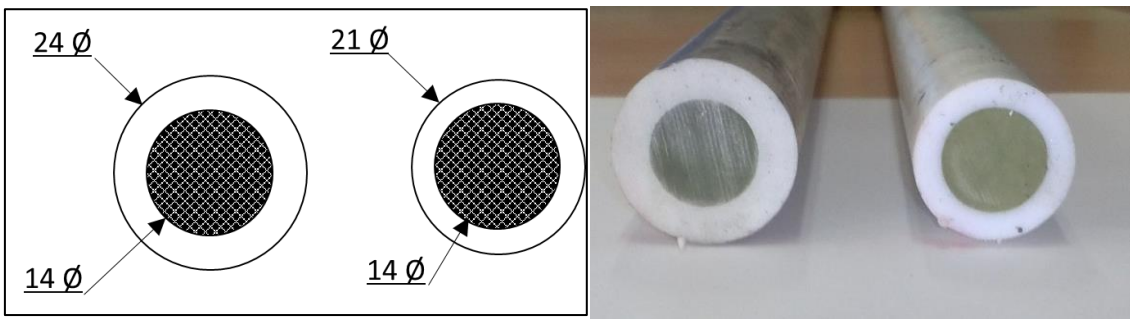

Figure 6.6 Insulator rods cross sections and dimensions CW left, messenger right (in each figure) showing GRP core and PTFE coating

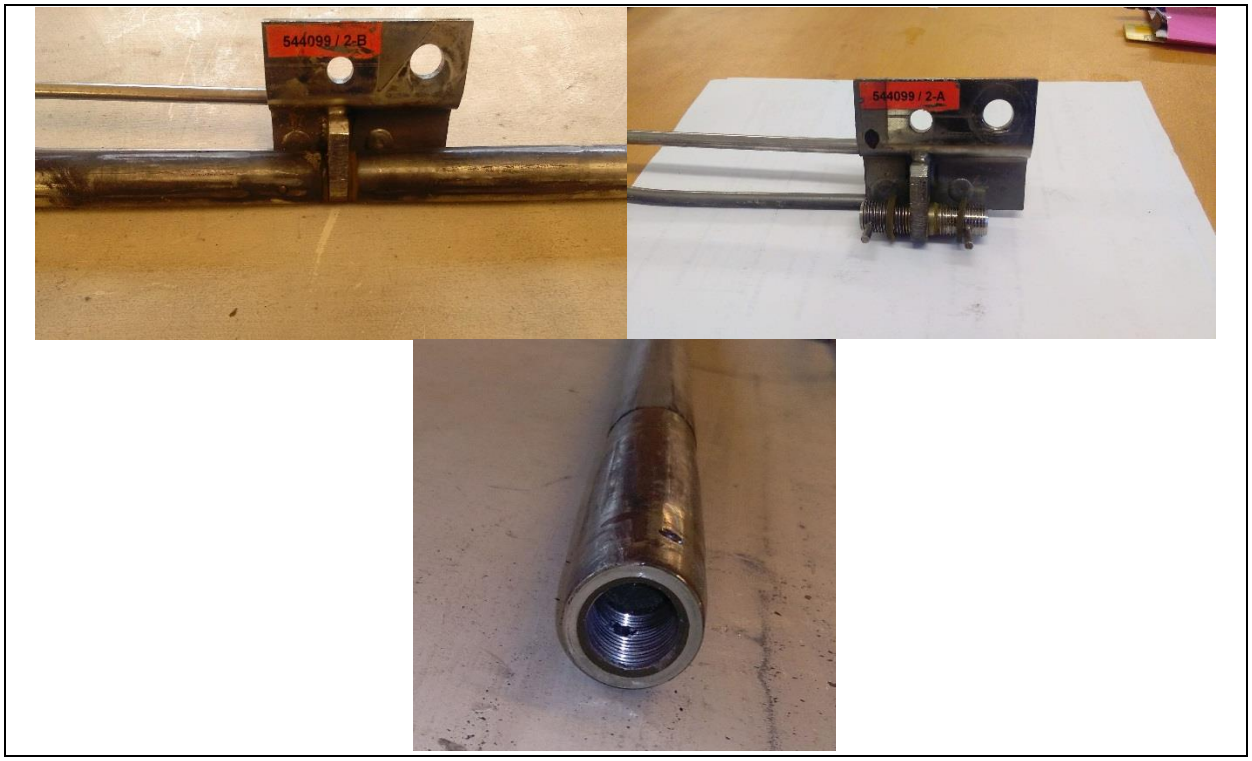

Figure 6.7 Connection between CW insulators showing top left, fully assembled, top right, threaded stud and below threaded end of insulator end fitting

Item [5] is the centre connector, and carries a fitting that mimics the CW profile, to allow a registration arm to be attached (Figure 6.8).

Figure 6.8 Centre connection between CW insulators showing registration arm attachment

Items [6] are the inner connectors, which carry a small arcing horn and allow the lower end of the spring dropper tube to be attached (Figure 6.9). All these fittings appear to made of stainless steel.

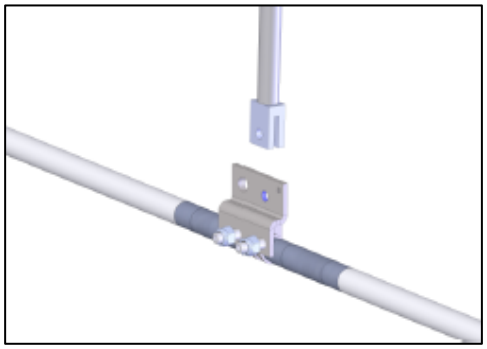

Figure 6.9 CW insulators inner connector showing threaded stud and short arc horns, and connection for spring dropper tube (Arthur Flury, 2017)

At the outer ends, different arrangements obtain for the entry and exit ends.

At both ends the connection to the regular CW is made by a composite cylindrical ferrule which is formed into a vertical plate at the outer end [7], with holes aligned to take one half of a contact wire splice. (Figure 6.10). At the entry end, in addition, there is a 'lever arm' device [8] which consist of a 25mm diameter stainless steel tube, approx. 910 mm long, fitted from the CW splice outwards, and mounted above the CW (Figure 6.11).

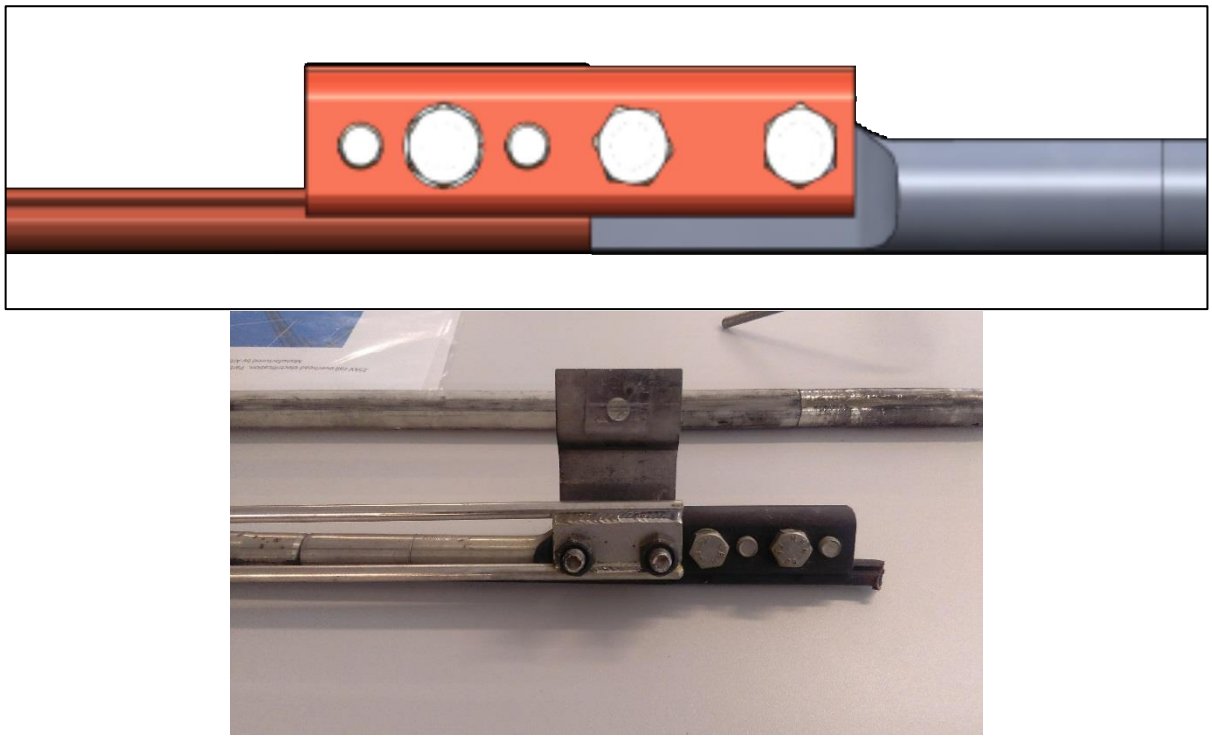

Figure 6.10 CW insulator terminated into a CW splice note the differing number of bolts in the drawing to the photograph, indicating the different splice designs caused by one of the failure causes (see 3.4)

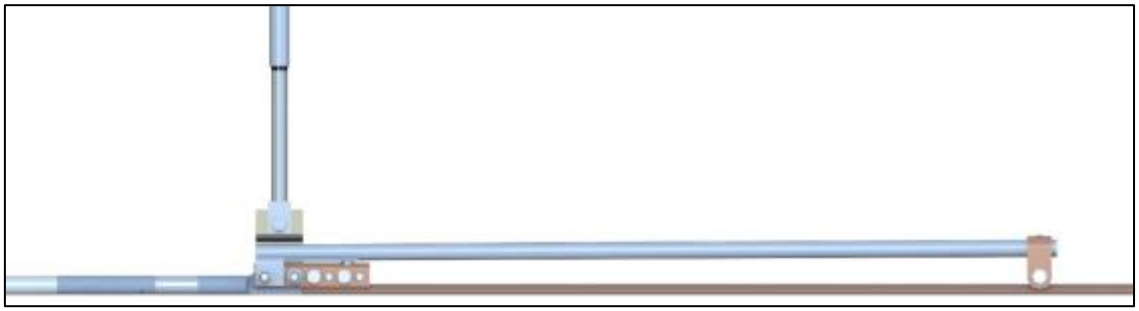

Figure 6.11 Lever arm fitting at entry end of CW insulator termination (Arthur Flury, 2017)

The spring dropper tubes [9] are stainless steel tubes, with an internal spring connected to a forked end rod at the bottom. They are connected at the top to the messenger insulators (at least in this variant) directly. At the lower end, the forked end fitting of the sprung rod connects to the inner connector pieces (Figure 6.12, left and right). According to the manufacturer's installation instructions, the spring is installed in tension, by extending from its rest position until a black mark is shown. This amounts to around 170 mm of spring extension, and provides an uplift vertical force on the CW insulators when installed.

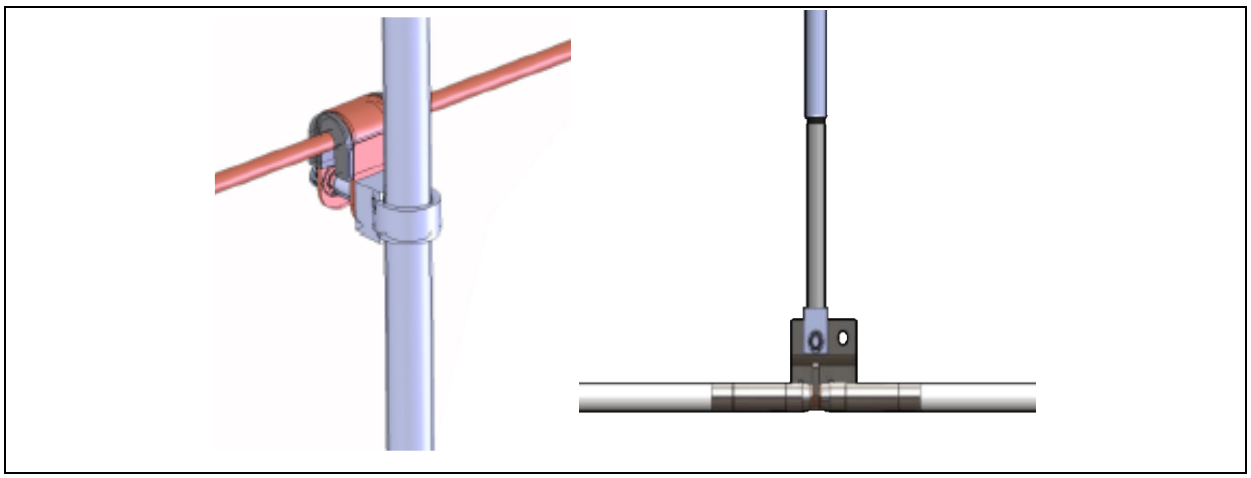

Figure 6.12 Spring dropper tubes showing connection to messenger (left) and to CW insulator connector, (right). (Arthur Flury, 2017)

Masses and dimensions of all the components were established from manufacturer's drawings or by inspection and measurement in the lab. The manufacturer's literature confirmed the material of the metallic parts to be either stainless steel 316L, or the copper alloy CuNi1Si (European Copper Institute, 2012). There is no information available for the grade of the PTFE or GRP.

Material properties, such as density, elastic modulus, etc for most of the components are obtained from published sources (e.g. *Materials Data Book*, 2003). The only property then not available is the elastic modulus of the PTFE/GRP rods. This was established in lab tests.

Three point bending tests were undertaken on samples of both the messenger and CW insulator rods. The samples were approximately 1 m long. The instrument used was an 'Instron 2580'.

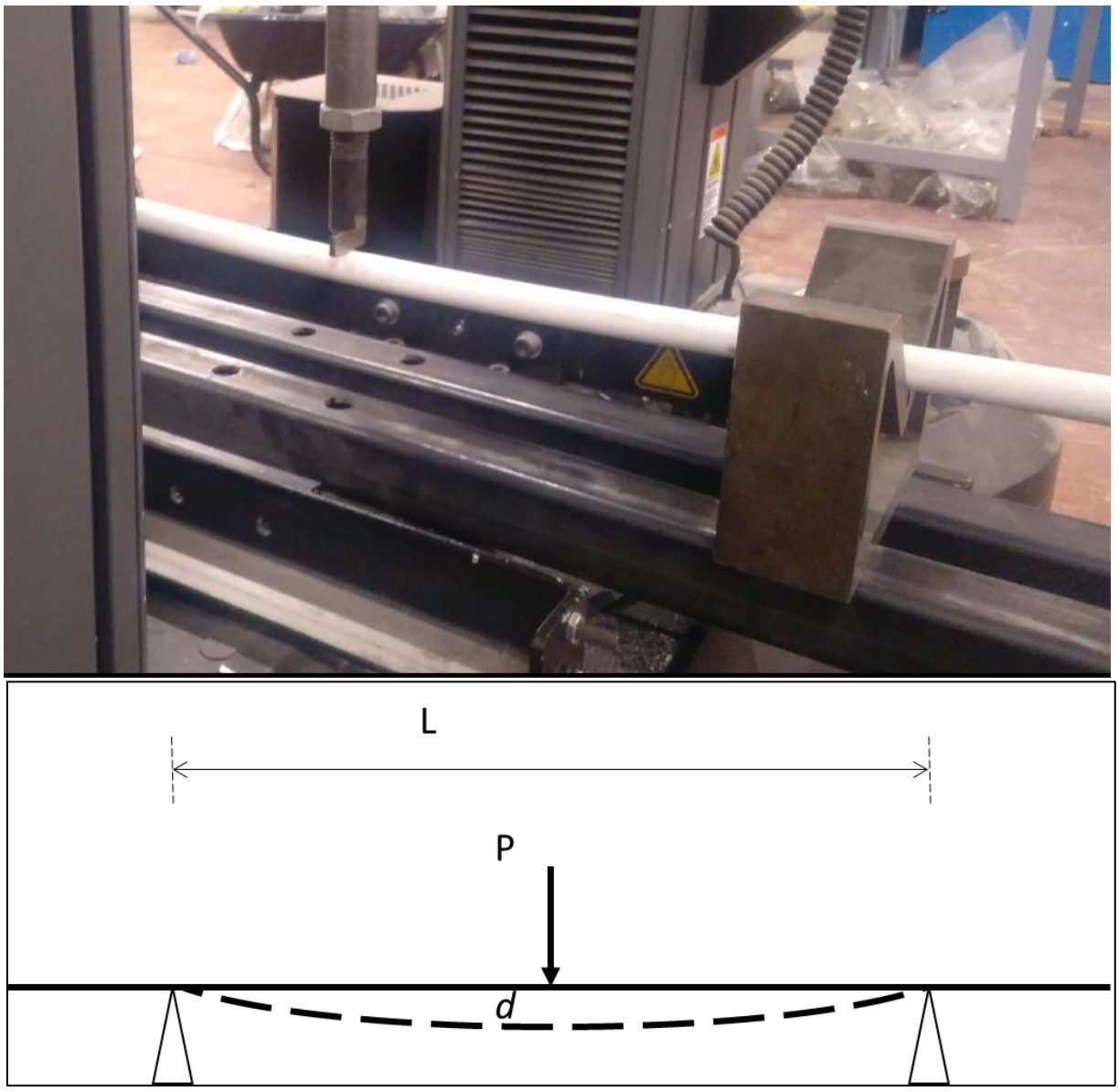

Figure 6.13 Insulator rods three point bending test arrangements showing test arrangement

The test arrangement was a shown in Figure 6.13. A load was applied centrally to the test piece. Readings of deflection against load were taken. The results are shown in Figure 6.14. As can be seen, over the range considered, the deflection/load curve is essentially linear.

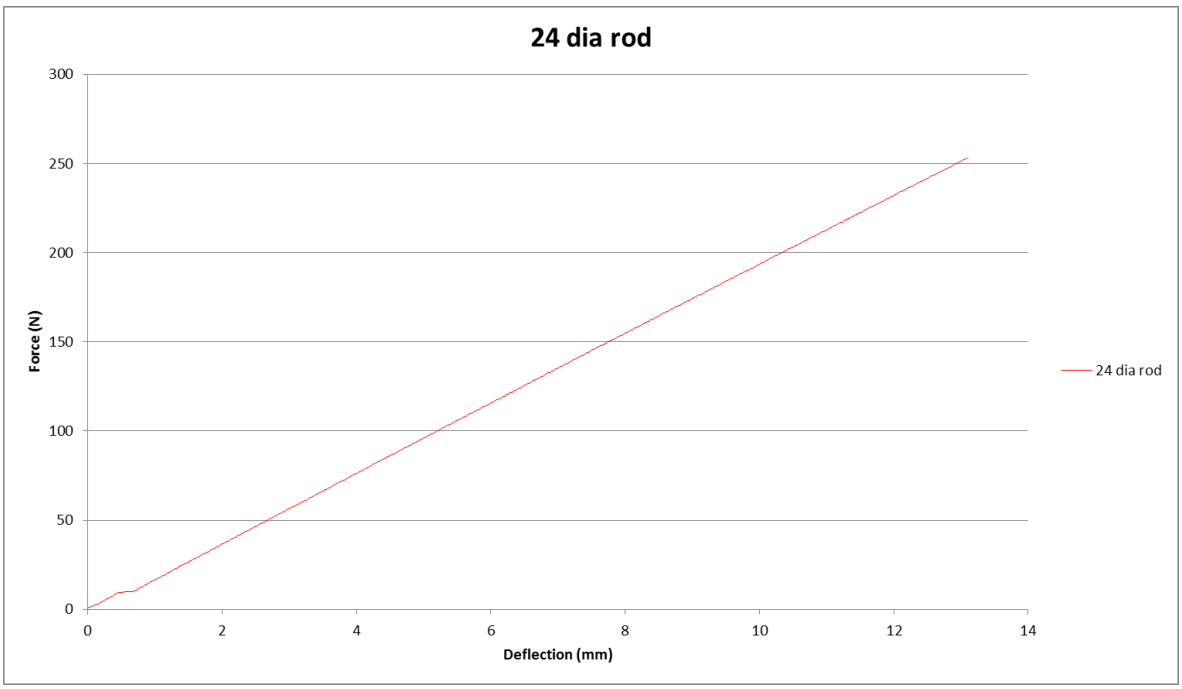

Figure 6.14 Insulator rods three point bending test results for 24 dia CW insulator rod (similar obtained for 21 dia rod)

By application of the expression for deflection *d* of a simply supported beam, span *l*, subject to a central point load *P*:

$$d = Pl^3/48\ \mathrm{EI}$$

and so

$$\mathrm{EI} = P/d\ .\ l^3/48$$

Where the *P/d* term is the slope of the deflection/load curve over a linear section.

The section is circular of known diameter, and so the second moment of area I, is calculable, delivering a value for E, being the effective elastic modulus of the composite section.

The relevant values of the component parameters so determined are shown in Table 6.1.

Table 6.1 Insulator rods material properties extracted from bending test

Component	**EI (from test) N mm²**	**I (calculated mm⁴**	**E (deduced) MPa**
CW insulator rod (24 dia)	62.94	16,286.0	3,864
Messenger insulator rod (21 dia)	66.53	9,546.6	6,968

These can be compared to a basic calculation for a composite rod, based on general material properties for PTFE and GRP (which may well be quite different to those employed here). Based on (*Materials Data Book*, 2003) and a methodology for the aggregate elastic modulus of a composite bean, based on 'equivalent area' (Hajianmaleki and Qatu, 2011), the following values were derived, as shown in Table 6.2. Both insulator's values are in a similar ballpark with this quick 'sense check', which provides a degree of correlation.

Table 6.2 Insulator rods calculated properties from published data

Rod	Overall dia/core dia (mm)	E of PTFE range (MPa)	E of GRP range (MPa)	Composite rod E range (MPa)
CW insulator	24/14	400 – 600	6000 – 7500	2310 – 3120
Messenger insulator	21/14	400 - 600	6000 - 7500	2890 - 3890

All the parameters for the neutral section assembly, collected either from direct measurement or deduction from manufacturers literature, are shown in Table 6.3.

Table 6.3 Neutral section parameters used in the model. Item numbers relate to Figure 6.4

Item No.	Component	Parameters
1	Messenger insulator – composite rod part	Linear mass = 0.770 kg/m Dia 21mm
1	Messenger insulator – end ferrule part	Mass = 0.480 kg
2	Messenger wire – forked collar end fitting	Mass = 0.900 kg
3 & 4	CW insulator – composite rod part	Linear mass = 0.997 kg/m Dia 24mm
3 & 4	CW insulator – end ferrule part	Mass = 0.293 kg
5	Registration – centre connector	Mass = 0.150 kg
6	Inner connector plus arc horn and spring dropper attachment piece	Mass = 0.856 kg
7	Outer connector plus arc horn and spring dropper attachment piece, plus CW splices	Mass = 1.54 kg
8	Lever arm – entry end	Tube 22mm OD, 15.5mm ID 930mm long Mass = 1.424 kg
9	Spring dropper – tube	1280 mm long Mass = 0.955 kg
9	Spring dropper – spring part plus connector forked fitting	Mass = 0.420 kg Stiffness = 405 N/m Initial extension, from black strip = 170 mm

Item No.	Component	Parameters
9	Spring dropper – connection to messenger insulator	Mass = 0.180 kg

6.3 Modelling and validation philosophy

Following on from the work in Chapter 5, where a validated pantograph/OCL dynamic simulation method was developed and validated, for open route situations, this method has been extended to incorporate a neutral section into the OCL.

The modelling approach, as described earlier, is that the elements representing the neutral section components are inserted into the Ansys OCL model, alongside, or instead of, the 'plain' OCL model elements, as described in the description of the validation of the DSM against the ODTT and 'benchmark' models in the previous chapter.

The experience gained from the work in Ansys has indicated that the neutral section itself can be modelled using the rigid body and joint/force elements available in Ansys. The characteristics of the elements and joints etc. have been extracted from the technical data of the neutral section, and, where necessary, from laboratory tests.

The elements chosen for the neutral section representation are chosen from the regular Ansys finite element types, for the flexible components, and Ansys 'multi-point constraints' for the multi-body representation of the joints and lumped masses. This approach was chosen over the option of creating detailed finite element models of all the discrete neutral section components for a number of reasons. These are parallel to the reasoning for the other researchers (in Chapter 4) choosing to use the lumped parameter model of pantographs against the full multi-body formulation. The exact construction details of the item cannot be fully known depending on the availability of manufacturing drawings from the manufacturer, their accuracy (against the actual model used in line tests) and the ability of the modeller to accurately represent these in the model. In the case of the AF neutral section, there was an issue of disclosure with the manufacturers which could not be overcome. The use of lumped parameters for the neutral section components (and assembly) allows the model to be constructed using the data extracted from lab tests, more conveniently. The derivation of the physical characteristics of the assembly of the neutral section and its components, used to define these elements, is as described above.

The accuracy of the simulation by the model and the performance of the method can be established by comparison with the line test data from the Old Dalby tests (described in Appendix C), if suitable validation criteria can be identified. In this case the validation criteria chosen are those used previously and as defined in European Standard EN 50318, i.e. statistical values of contact forces and vertical movement of the point of contact. Note that these map closely onto the parameters defined in the (draft) Network Rail specification for such neutral sections. (See section 3.9 in Chapter 3.)

Anecdotally, work undertaken elsewhere but not in the public domain, has indicated that frequencies of up to 100 Hz can be seen within the neutral section in a modal analysis (Network Rail, 2014d). This will require a sampling rate frequency of at least 200 Hz to capture.

6.4 The measurement data from the Old Dalby neutral section

The neutral section behaviour data was derived from the ODTT line test data as an extension of the method described in 5.5 in the previous chapter, using essentially a 'cut down' version of the OCL model, where the analysis section is just the two spans (spans 8 and 9) containing the neutral section, as shown in the upper part of Figure 6.15.

As described in Appendix C, the line test measured data, as collected by DBST, is essentially filtered at 35Hz (the force FFT in the frequency domain shows virtually no amplitude above 35 Hz). It is expected, based on the close spacing and short length of many of the features of the neutral section construction, in particular in how they will be presented in the Ansys model, that a higher frequency range of interest might be more informative, and representative. Consequently, the ODTT data is presented as 20, 30 and 35 Hz low pass filtered in the first instance.

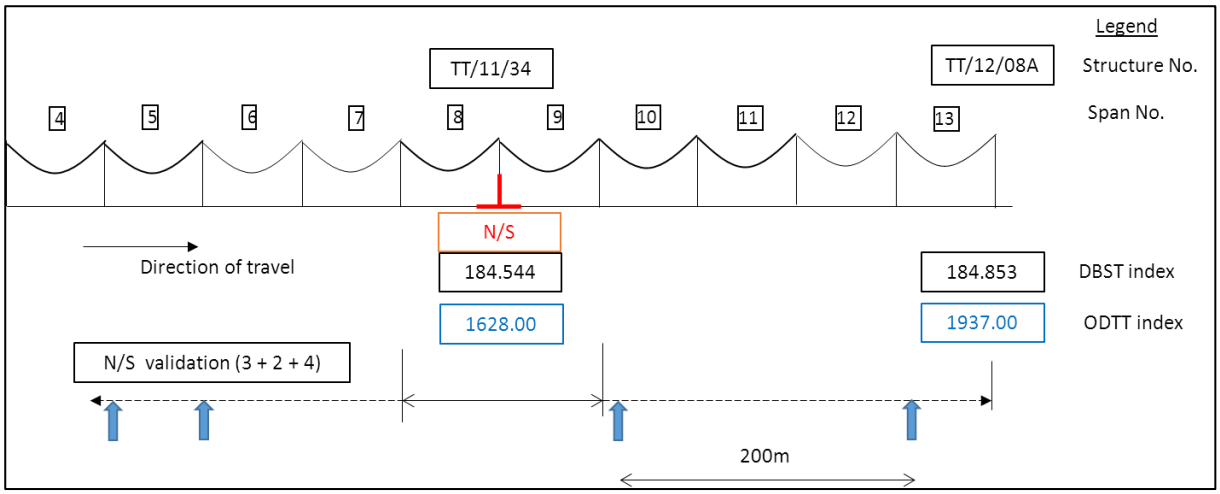

Figure 6.15 The sub set of the Old Dalby OCL model used for neutral section validation tests showing the 3 + 2 + 4 span arrangement, around a 2 span analysis section (spans 8 & 9), accommodating the start and end positions of both pantographs. ODTT index in blue boxes, equivalent DBST index in black boxes.

The three force plots for the two spans in the analysis section are shown below in Figure 6.16. The X-coordinate index shown is the DBST index. This will be converted to the same index as the OCL for the comparison. The main features of the neutral section are indicated by vertical lines A - F; namely the centre line (support and registration), the four spring droppers (two either side) and the start of the lever arm at the entry end (left hand in the figure). The legend for these features (A – F) is the same as shown in Table 6.4 and Figure 6.19.

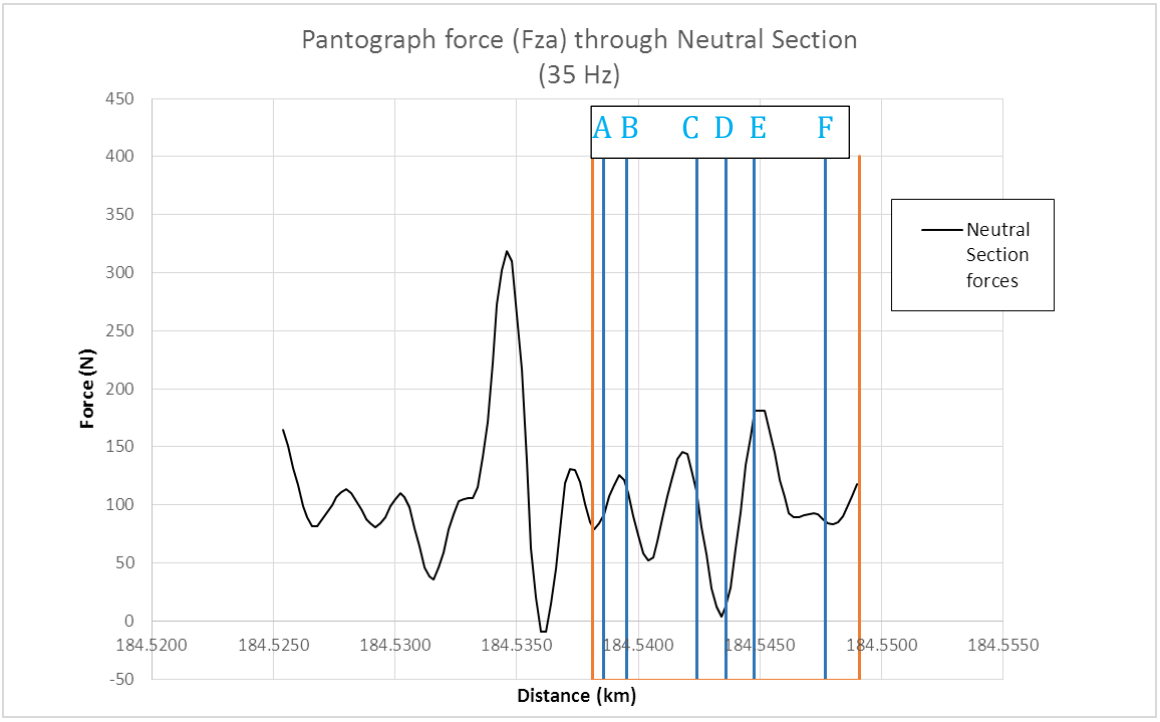

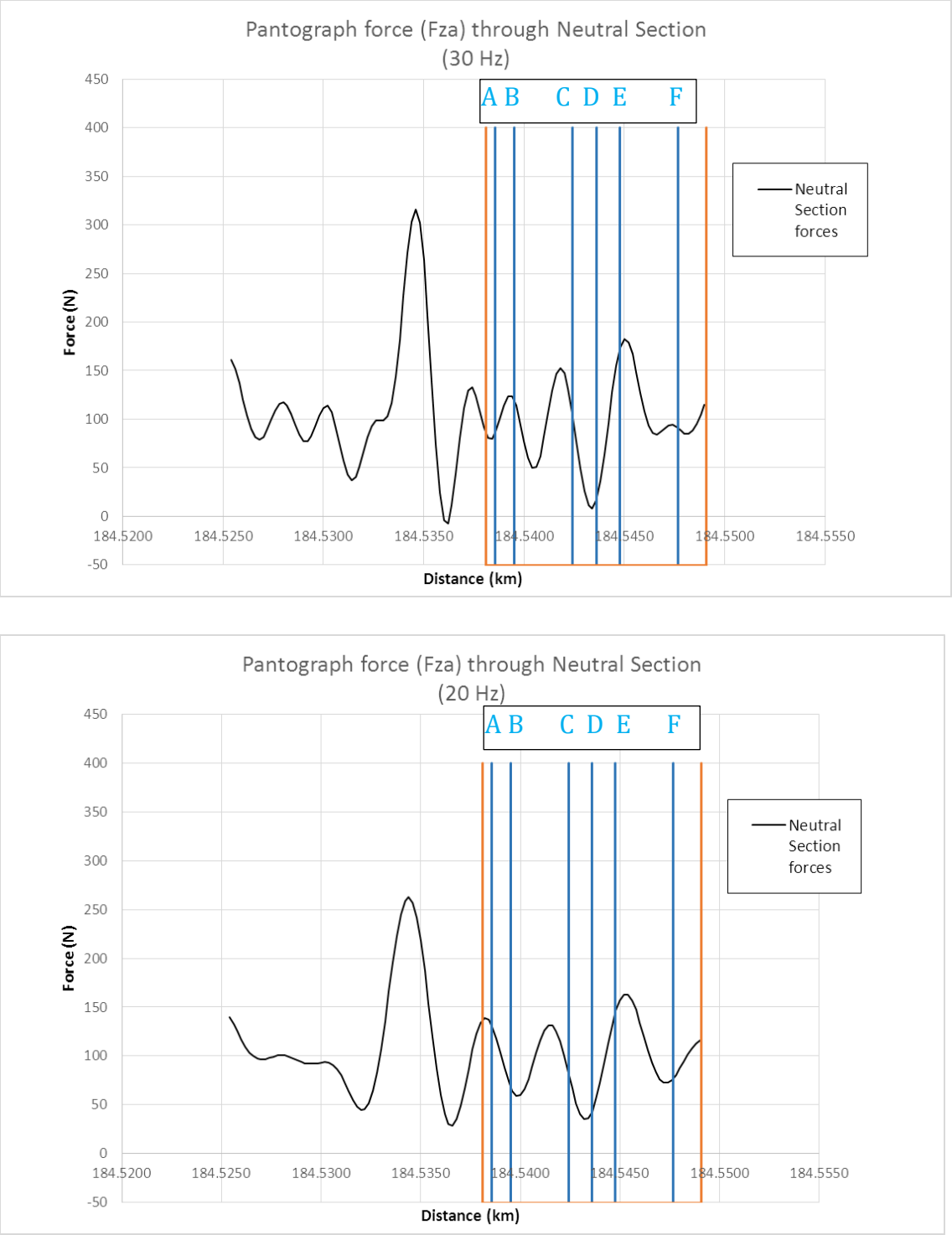

Figure 6.16 Measured contact forces through ODTT neutral section filtered at 35 Hz (top), 30 Hz (centre) and 20 Hz (bottom), showing main neutral section features (blue lines) and immediate adjacent droppers (orange lines). The legend for the neutral section features (A – F) is the same as shown in Table 6.4 and Figure 6.19.

Two aspects are apparent. At all frequencies, a spike in the contact force is observed around the 184.5346 point, 319N in the 35Hz plot. This is in advance of the neutral section and is also in advance of the last dropper in the span. The accuracy of the DBST index (184.nnn km) has been synchronised with the OCL features by aligning with the

staggers, as described in Appendix C, and an accuracy of ~1m is accepted. This still places this force spike outside the actual neutral section.

To further inform this assessment, the pantograph head vertical position (the 'point of contact') has been plotted in Figure 6.17 and no significant anomaly is apparent, at this point, or in its vicinity. Equally, on inspection of the train roof vertical acceleration data, (shown in the plot in Figure C.12 in Appendix C) there is no anomalous acceleration event at this point, which would have pointed to a vehicle or track anomaly as the source. Note that the DBST measurement data for pantograph head height is not an absolute measure, as it accounts for pantograph frame extension only, and vehicle body movement is not accounted, so can only be relied upon as a relative measure from an initial (approximate) datum.

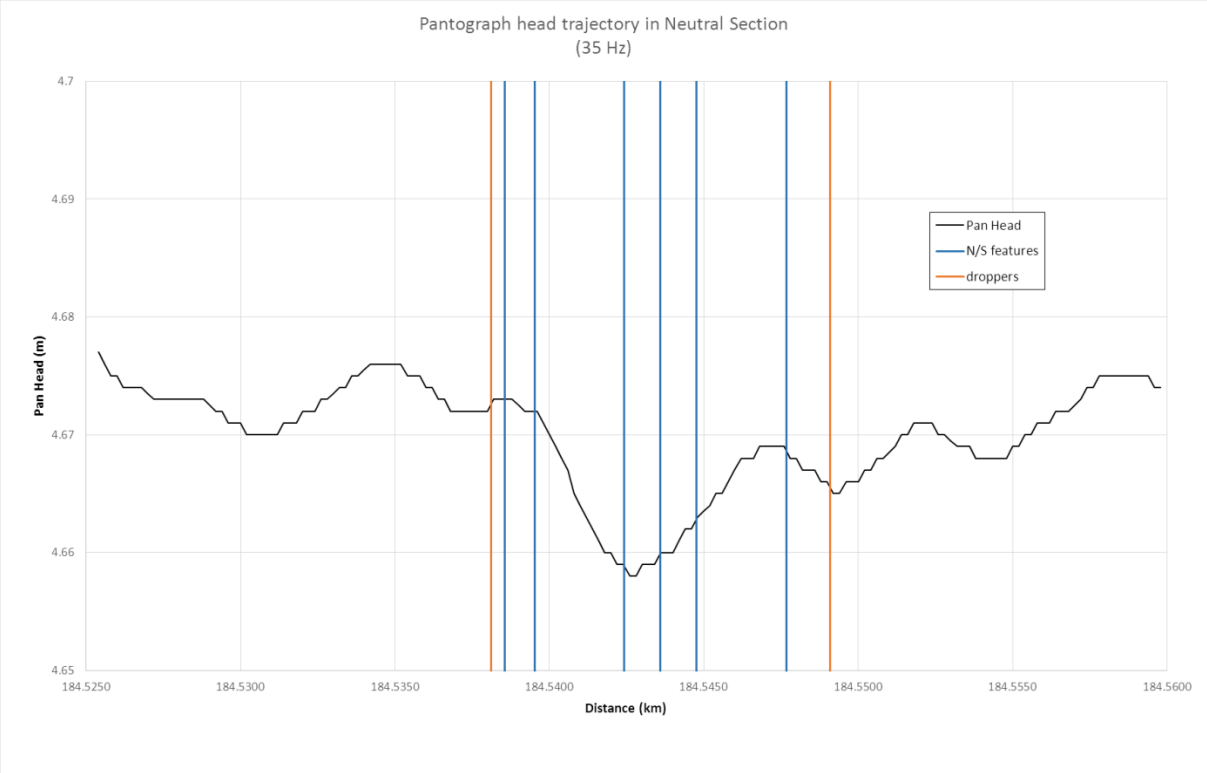

Figure 6.17 Point of contact through ODTT neutral section , showing main neutral section features (blue lines) and immediate adjacent droppers (orange lines)

In the absence of other information, it seems possible that this spike is caused by an OCL feature, not associated directly with the neutral section itself. It is known that the neutral section was installed retrospectively, and not at the time of original OCL installation, and it may be that an anomaly was introduced at this time, associated with dropper lengths, tensions or other adjustment to the OCL geometry made to accommodate the insertion of the neutral section.

Another potentially valid reason for the force peak in the approach to the neutral section may be the interference between the pantograph and a wave reflected at a feature (mass point) within the neutral section itself. This was investigated.

As noted previously, the propagation velocity Vw of a travelling wave is given by

$$V_w = \sqrt{\frac{\Sigma T}{\Sigma \rho}}$$

where T is conductor tension and ρ is linear mass (Kiessling *et al.*, 2016).

For the Series 1 OCL at Old Dalby, using the data in Table 5.28, Vw = 124.35 m/s. The pantograph speed is 201.75 km/h, i.e. Vp = 56.04 m/s.

The relationship between the location of the force peak and the significant features of the neutral section i.e. mass points which may reflect the wave, is shown in Figure 6.18. The distance Xp from the force peak to an initiating point at the pantograph, for a given reflection point, is given by

$$X_p = \frac{2\,X_f}{(V' - 1)}$$

Where $V' = \frac{V_w}{V_p} = 2.219$.

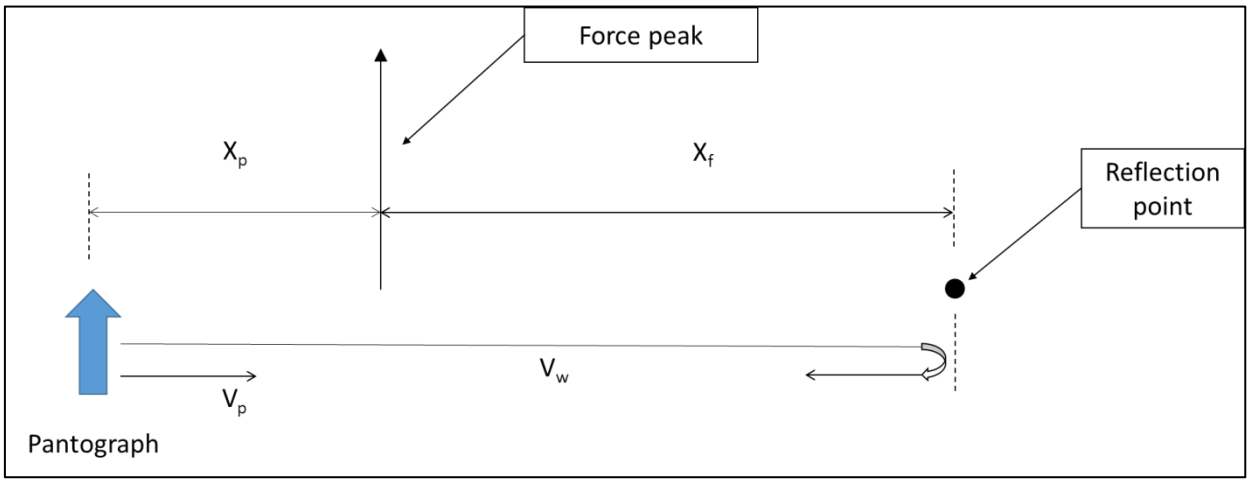

Figure 6.18 Notation scheme for a wave initiated by the pantograph reflected from a point within the neutral section, meeting the moving pantograph and creating a force peak

The location of the features (lettered A to F) and their relative distance from the force peak and the position of the initiation of a wave that would, when reflected, meet the pantograph at the location of the force peak is shown in Table 6.4.

Based on this and the expression above, the locations of the potential points of initiation for each of the six reflective points is also shown in Table 6.4, identified as points 1 to 7 (right hand columns).

Table 6.4 Locations of potential wave initiating points for reflective points within the neutral section. Relate to Figure 6.18 and Figure 6.19

ID	Feature (reflective point)	Feature location	Force peak location	X_f	V'	X_p	ID	Initiating point location
	support	1582.000	1619.000					
	dropper 1 span 8	1587.500	1619.000					
	dropper 2 span 8	1599.170	1619.000					
	dropper 3 span 8	1610.840	1619.000					
	last dropper span 8	1622.510	1619.000					
A	lever arm start	1622.953	1619.000	3.953	2.219	6.486	1	1612.514
B	1st spring dropper	1623.928	1619.000	4.928	2.219	8.086	2	1610.914
C	2nd spring dropper	1626.826	1619.000	7.826	2.219	12.841	3	1606.159
D	registration (CL)	1628.000	1619.000	9.000	2.219	14.767	4	1604.233
E	3rd spring dropper	1629.174	1619.000	10.174	2.219	16.693	5	1602.307
F	4th spring dropper	1632.072	1619.000	13.072	2.219	21.448	6	1597.552
	first dropper span 9	1633.500	1619.000	14.500	2.219	23.791	7	1595.209

All these points are shown graphically on the OCL geometry in Figure 6.19. It can be seen that one of the locations (point '2') coincides closely with a dropper position, dropper 3 of 4 at ODTT index 1610.840.

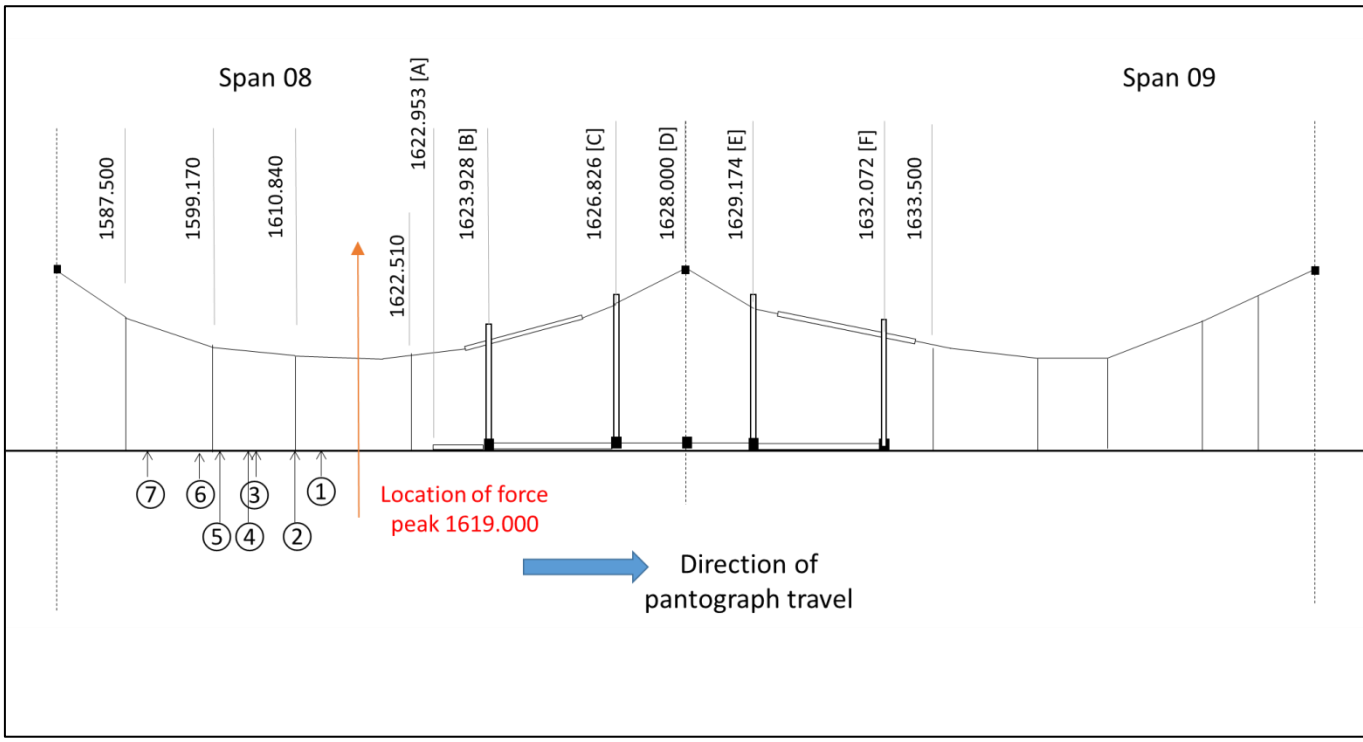

Figure 6.19 Schematic representation of locations of potential wave initiating points (1-7) reflected from points within the neutral section (A–F). See also Table 6.4

It is possible, although by no means certain, that a wave initiated by the pantograph at dropper 3 in span 8 (point '2'), for whatever reason, will be reflected from the mass point at the first spring dropper (point 'B') and meet the pantograph at the point of the measured force peak. The pantograph may meet reflected waves at many points, and not all will be detrimental. Waves can be in-phase, or out of phase by (up to) 180° with the pantograph, and thus can be either benign or detrimental (Kalsbeek *et al.*, 2013), and it may be that this wave/pantograph interference is of the in-phase/detrimental category. This cannot be known for sure without a more sophisticated analysis of the neutral section, using a much more detailed model than provided here.

In either case, this theory supposes an OCL anomaly at either dropper 3, to create the wave, or at the force peak location itself. The anomaly at dropper 3 seems more plausible than one in a location remote from any OCL feature, however, at this distance in time it cannot be known, or explained, let alone modelled.

The other item to note is that the higher frequency filtered data shows forces of less than zero in a couple of instances, possibly implying losses of contact, but more probably the transition point from positive upwards forces to negative downwards forces. In this Ansys analysis, a loss of contact is indicated by an absence of an output value.

Taking account of the unexplained high force peak, three zones of analysis were identified. The three analysis zones are all within the two spans either side of the neutral section. Zone 1 is the full extent of these two spans (spans 8 and 9); zone 2 is the two half-spans either side of the neutral section (i.e. span mid-point to span mid-point) and zone 3 is the neutral section only, between the two droppers immediately enclosing it. The zones are shown in Figure 6.20. The 'neutral section only' zone 3 excludes the point of the force spike identified above, and is between the last and first dropper.

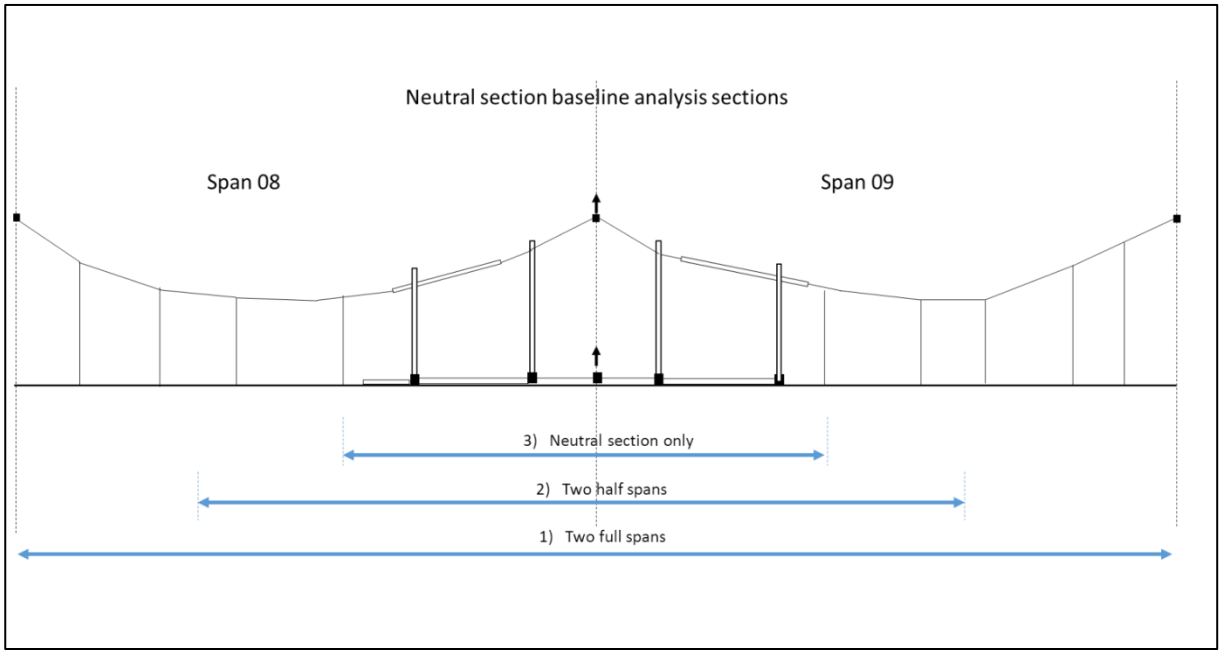

Figure 6.20 ODTT neutral section 'analysis zones', showing the three zones for which statistical values comparison will be made

It should be noted that the analysis zones are fixed zones into which the pantograph moves. Other researchers (e.g. Sánchez-Rebollo *et al.*, 2015) have used a moving analysis zone, where a fine local mesh is used either side of the pantograph head contact point, and moving with the pantograph, with a coarser mesh elsewhere in the model. This requires a continual re-meshing, but allows a point to point (node to node) contact to be made. This, however, is not associated with analysis of a feature such as a neutral section, but just with general mean contact force and uplift evaluation. In our case, as the regular CW is replaced by the specific neutral section elements as will be described in section 6.5 later, with the finer mesh implicit in the use of the smaller element lengths, no such finer re-meshing is considered necessary.

Statistical data has been extracted for these three zones, and these will be used as the target values for comparison with the simulations, tabulated in Table 6.5, Table 6.6 and Table 6.7.

Table 6.5 Target force statistical data for neutral section analysis zone 1

N/S section - spans 08-09 analysis zone 1			
	35Hz filtered	30Hz filtered	20Hz filtered
Fm (N)	107.7332	107.7365	107.8051
σ	37.1277	37.0036	32.1944
F max (N)	319.0000	315.6254	262.9901
F min (N)	-9.0000	-7.0279	28.1036

Table 6.6 Target force statistical data for neutral section analysis zone 2

N/S section - half spans either side analysis zone 2			
	35Hz filtered	30Hz filtered	20Hz filtered
Fm (N)	113.1457	113.1267	113.5340
σ	43.8979	43.7192	36.5872
F max (N)	319.0000	315.6254	262.9901
F min (N)	-9.0000	-7.0279	28.1036

Table 6.7 Target force statistical data for neutral section analysis zone 3

N/S only - dropper-dropper analysis zone 3			
	35Hz filtered	30Hz filtered	20Hz filtered
Fm (N)	98.6404	98.3883	99.5483
σ	39.7309	39.8473	33.2493
F max (N)	181.0000	182.3034	162.5897
F min (N)	4.0000	8.2235	35.3000

Graphically the mean force and standard deviation for the two span zone is shown in Figure 6.21.

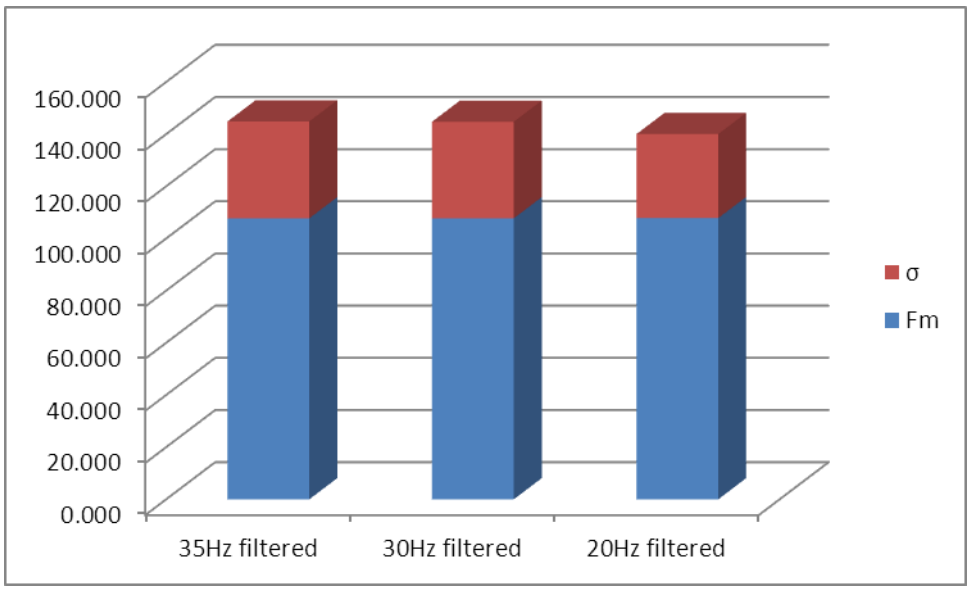

Figure 6.21 Target force statistical data for neutral section analysis zone 1

The pantograph head vertical height and range of movement data is shown in Table 6.8. Caution should be applied to the mean height value, for the reasons given above, but the standard deviation is valid if expressed as a ratio to the range, as is the range, for comparison with simulated values.

Table 6.8 ODTT neutral section measured contact point vertical height and range of movement

ODTT neutral section contact point vertical height and range of movement	
	spans 08 -09 (zone 1)
Mean (m)	4.6724
SD	0.0115
SD % of range	17.42%
Max (m)	4.709
Min (m)	4.643
Range (m)	0.066

6.5 The neutral section model construction

The plain open route OCL used in the preceding validations is characterised by its having homogenous properties of the contact surface and that the dynamic behaviour of the OCL are governed mainly by the main conductor tensions and their geometry.

For the situation after the inclusion of the neutral section components into the OCL, this changes, and now the contact surface is not homogenous, indeed is characterised by a series of different materials and forms, with interceding irregularities (and discontinuities) and the vertical dynamic characteristics are created by the specific properties of the components, rather than the geometry, as is the case with plain OCL.

As an illustration (only) the bending stiffness parameter (EI) of the contact surface components of the neutral section is shown as a function of length (x-coordinates) through the neutral section, where zero is the start of the entry lever arm, in graphical form in Figure 6.22. Note the logarithmic vertical axis, as the bending stiffness of the entry lever arm is significantly higher than the other components.

A point of interest to note from Figure 6.22 is the 'brutal' introduction of the very high stiffness of the lever arm – a component which is intended apparently to smooth the entry into the stiffness of the neutral section. This can be compared – in functionality at least – to the transition beam employed to perform the same function on entry to a rigid overhead conductor beam, as has been illustrated in Chapter 4 (see Figure 4.7 and Figure 4.8). Here the high bending stiffness of the conductor beam is introduced over a 3.3m long stiffness gradient, at a rate of 8.75E+07 $kNmm^2/m$. Compare this to the abrupt and immediate change of stiffness at the introduction of the lever arm from around to around 1.5E+05 to around 1.5E+07 $kNmm^2$.

The modelling approach, as described earlier, is that the elements representing the neutral section components are inserted into the Ansys OCL model, alongside, or instead of, the 'plain' OCL model elements, as described in the description of the validation of the DSM against the ODTT and 'benchmark' models in the previous chapter. The initial approach was to model as many as these components as possible as 'rigid' bodies.

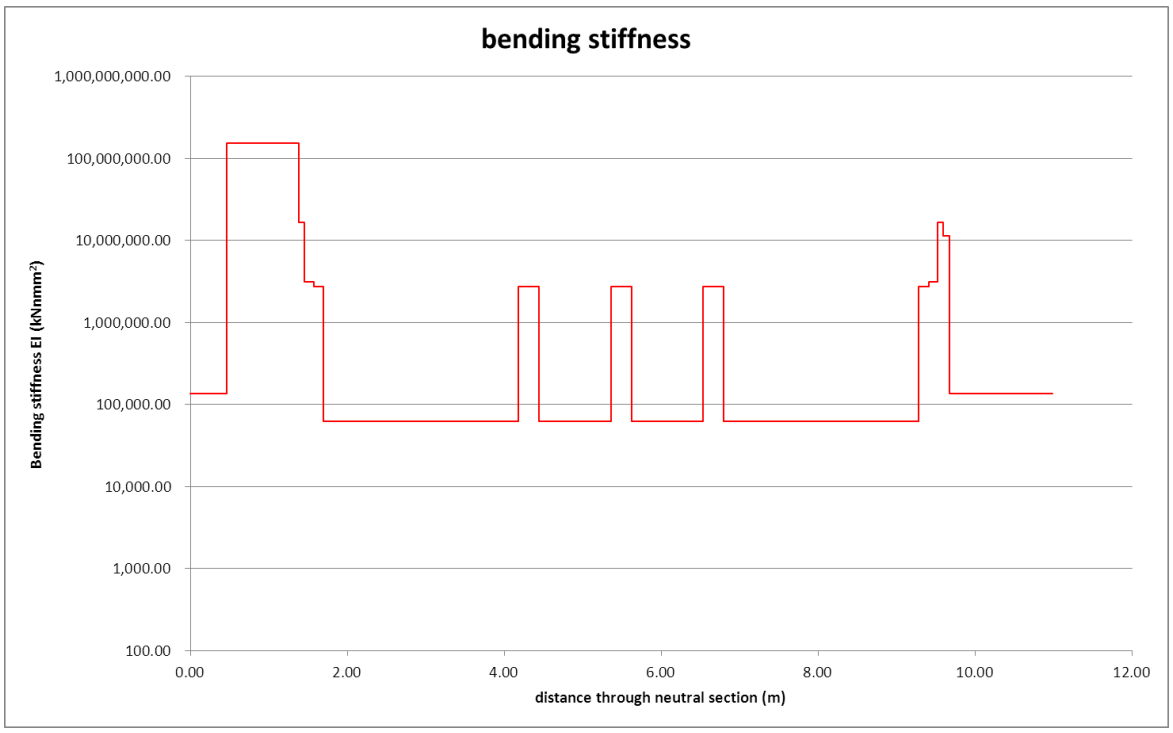

Figure 6.22 AF neutral section bending stiffness profile, showing the variation through the extent of the neutral section (NOTE logarithmic vertical scale)

A separate particular approach is also taken to the modelling of the physical properties of the connection pieces (as opposed to their function as a 'joint') as can be seen they are made up of various forms of manufactured items, of irregular shape and form. In order to simplify the Ansys modelling and to maintain the spirit of the 'lumped parameter' approach that has been adopted, the following approach was applied.

Each discrete element was replaced/modelled by a cylindrical element, either solid or hollow section, with the properties chosen and manipulated so as to mimic the properties of the real element's behaviour. The choice of elements and their form is shown in Table 6.9 below, with reference to the diagrammatic representation in Figure 6.4. All cylinders are Ansys beam elements (BEAM188 or 189) on the same basis as the messenger and contact wires.

Table 6.9 Ansys representation of neutral section components, related to item numbers on Figure 6.4

Item no.	Item	Representation	Properties
01a	Messenger insulators composite rods	Solid cylinder	21 dia
01b	Messenger insulators – end ferrules	Hollow cylinder	28 OD 14 ID

Item no.	Item	Representation	Properties
02	Messenger forked collar end fitting	Solid cylinder	28 dia
03a	Long CW insulators - composite rods	Solid cylinder	24 dia
03b	Long CW insulators – end ferrules	Hollow cylinder	24 OD 14 ID
04a	Short CW insulators - composite rods	Solid cylinder	24 dia
04b	Short CW insulators – end ferrules	Hollow cylinder	24 OD 14 ID
05	Registration/centre connector	Hollow cylinder	24 OD 14 ID
06	Inner connector	Hollow cylinder	24 OD 14 ID
07	Outer connector/CW splice	Solid cylinder	36.5 dia
08	Entry lever arm	Hollow cylinder	79 OD 69 ID
09	Spring dropper tubes	Various (see text)	Stiffness K N/m

For all elements not being modelled as 'rigid' bodies, elastic modulus, Poisson's ratio and density were specified, according to the material.

Cylindrical hollow sections were chosen where possible, as this allows the section property to be adjusted by wall thickness without affecting external diameter and neutral axis, as this would interfere with the lower surface acting as the contact surface. Similar density was chosen to generate an accurate equivalent linear mass. The primary criterion was the second moment of area, I, of the section, which was translated to a cylindrical (hollow or solid) section of the same value. All such section are initially centred along their neutral axis, and so an offset is applied so that the under surface of the sections of differing diameters is aligned, for the continuity of the contact surface with the pantograph. The offset of the neutral axes also mimics the effect in reality.

Joints/elements/connections described by this method include:

- Entry end lever arm
- Outer CW splice/insulator end fitting
- Inner insulator end fitting/spring dropper connection.

An example of how such a section is treated is shown below in the example for the lever arm. Referring to Figure 6.23, the second moment of area, I, of the lever arm tube, with reference to the underside of the CW is established by the parallel axis theorem. This is then translated to a hollow cylinder with the same section property. This is naturally centred on the CW centre line axis, and so must be offset by the difference between the CW radius and hollow cylinder radius, to achieve a continuous contact surface to the passage of the pantograph. Note that this section is in addition to the CW which exists in the same space.

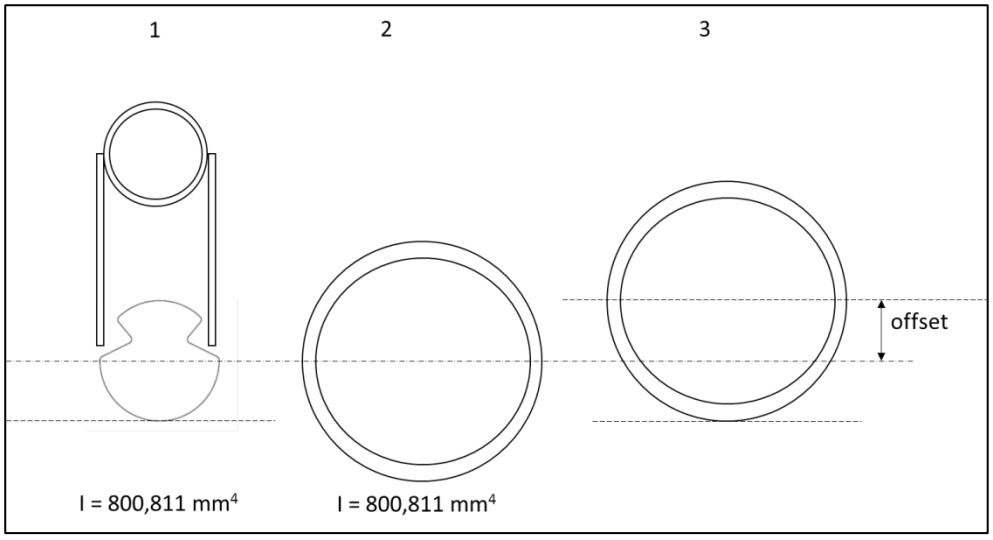

Figure 6.23 Development of an 'equivalent' circular section' for the lever arm, showing the original section (1), translated to a hollow cylinder of same section property (2), which is then offset to the CW axis (3) to allow underside to be present a continuous contact surface. (Not to scale)

A similar approach was taken to this for the CW end splice connectors. All the cylindrical section equivalents of the elements in the CW level of the neutral section are indicated in Table 6.9.

A particular approach was taken to model the joints and connections featuring in the CW level of the neutral section, and especially those at the CW level. Three approaches were developed, applied to the joints/connections, as considered appropriate, based upon their characteristics as displayed in the laboratory tests, and by inspection:

1. As a continuous 'built-in' connection of a continuous beam, where the adjacent elements share end nodes (i.e. same displacement, rotation, velocity and acceleration);

2. As a joint where the adjacent elements have separate but coincident end nodes, an Ansys 'joint' being applied to these two coincident nodes;

3. As a 'pseudo-joint', created by using a short element of a more flexible material (i.e. lower value of EI).

Approach 2 was the initial model to be built, only for the reason that it was more complex and had more nodes, which could be removed/suppressed for the other two approaches, more easily than adding nodes/elements to a simpler model. Approach 2 also allows the applying of a very high stiffness to the joints. Approach 1 was the most basic, and was not expected to provide a realistic simulation of the real behaviour. Approach 3 was developed as a result of difficulties encountered in early experiments with approach 2.

For approach 2, a combination of revolute and translational joints was employed, at various points in the model, which can be seen schematically in the sketch at Figure 6.24.

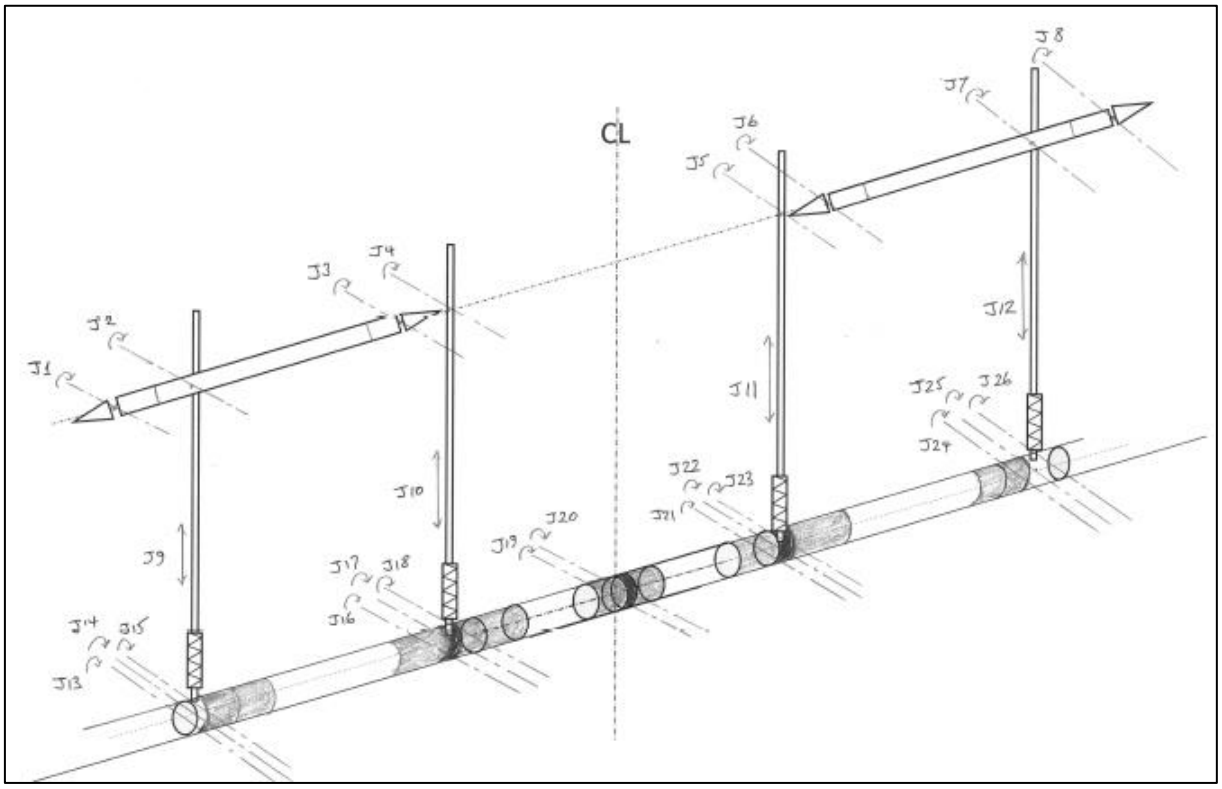

Figure 6.24 Sketch of the neutral section model with joints implemented, showing revolute joints in the messenger and CW levels, and translational joints in the spring droppers

All the joints in the CW (and messenger) levels were defined as revolute joints, with one DoF in the Z axis, essentially a hinge. Four were defined as joints for the connection of the spring dropper tubes, and the rest were representing the effect of the connections between components, and their behaviour in reality (i.e. not as good 'solid' connections).

The spring droppers were modelled as rigid beams with a translational joint with stiffness and uplift force (representing the initial extension in the real life spring) applied. See Figure 6.25 for the options tested, with the two right hand versions, with the translational joint, applied in approach 2. All the joints were Ansys multi point constraint (MPC) elements.

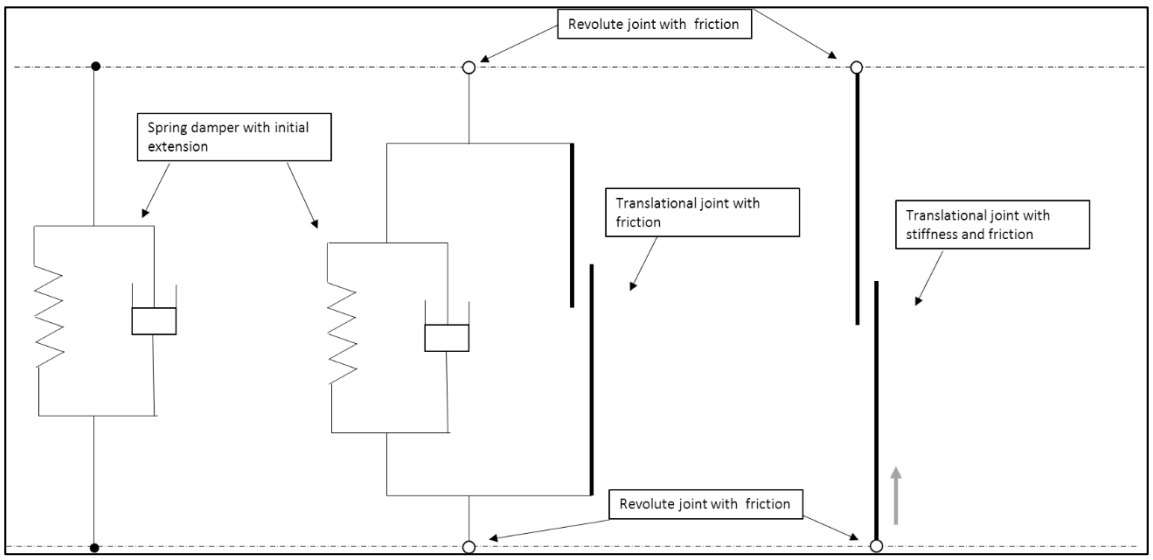

Figure 6.25 Options for the representation of the spring droppers, showing (left to right) a spring damper element only, a translational joint, with the stiffness and friction applied via a parallel spring damper element, and a translational joint only with stiffness and friction applied in the joint

In every case, the resultant Ansys model was found to be 'ill-conditioned' and failed to converge. There are a number of highly restrictive constraints applied when creating and using joints and rigid bodies in Ansys, which hindered the development of a well-conditioned model, namely:

- Rigid bodies must be connected to at least one flexible body;
- Joints must have a Local CSys (co-ordinate system) defined;
- Inability to mix elements employing direct elimination with those employing Lagrangian multiplier;
- Multiple joints can lead to an un-constrained or under-constrained model.

For the purposes of comparison against simulated data, the 35 Hz data would not corroborate with simulated data at a 200 Hz sampling frequency. For this a 300 Hz sampling frequency, at least, should be employed. As this increased computation time

by possibly 50%, this step was undertaken cautiously (but was implemented), and the 30 Hz value, along with the conventional 20 Hz, used to create data for comparison with the targets.

In addition, as has been seen before in the 2018 benchmark validation (Chapter 5) the penalty stiffness should be tuned to the frequency range of interest, such that the pantograph head natural frequency is well above the frequency of study. For a 35 Hz study frequency, and with a pantograph head mass of 5.8kg, a penalty stiffness of around 450k is required. Experiments with a variety of stiffness values in the Ansys model of the neutral section indicated a failure to converge above 300/350k values of penalty stiffness. Consequently, for both above reasons, the frequency range of the study of the ODTT neutral section was restricted to 20 and 30 Hz.

The model and analysis section arrangement and pantograph start and end positions (of the two pantographs) is shown in Figure 6.26.

The options developed and tested are shown in Table 6.10 below. All the options with the multi point constraint joints failed to converge or failed in other ways, indicating a very ill-conditioned model, which was not easily rectifiable, at least not within the spirt of the objective to create a model largely independent of a detailed engineering drawing based model construction.

Table 6.10 Development of the neutral section simulations

Test	Joint features	Results
1	All revolute (messenger and CW line) and translational joints (spring dropper) included	Fails to converge, 'ill-conditioned model'
2	Translational joints replaced by linear spring with stiffness and initial extension	Fails to converge, 'ill-conditioned model'
3	All revolute joints on messenger and CW replaced by 'built-in' connections	Ok
4	CW line short connector pieces (S/S) replaced with a more elastic material property (centre section)	Slightly better than 3
5	CW line short connector pieces (S/S) replaced with a more elastic material property (centre section and inner connectors)	Slightly better than 4

Test	Joint features	Results
6	Penalty contact stiffness increased incrementally from 350k to 500k	Fails to converge

Approach 2, including the use of 'rigid' bodies for certain components of the neutral section, was thus abandoned, and approach 1 was soon superseded by approach 3. In approach 3, the locations of the joints in the CW line, essentially at the centre and inner and outer connectors, are replaced by small elements of a different material, with more flexible properties (in this case a much lower value of elastic modulus, for the sake of convenience, equal to that of the insulator composite rod). Thus a 24mm dia. element of stainless steel, with stainless steel properties, is replaced by a 24mm dia. element with a much lower value of elastic modulus, effectively creating a 'joint' with some, small degree of flexibility.

It could have been expected that the use of rigid bodies (rather than 'solid' bodies) would improve computational efficiency, as described in the Ansys manual, but as the arrangement could not be made to converge successfully, this was not tested. In any case, as the neutral section elements were only a small part of the active model in these tests, the improvement would have been expected to be relatively minor.

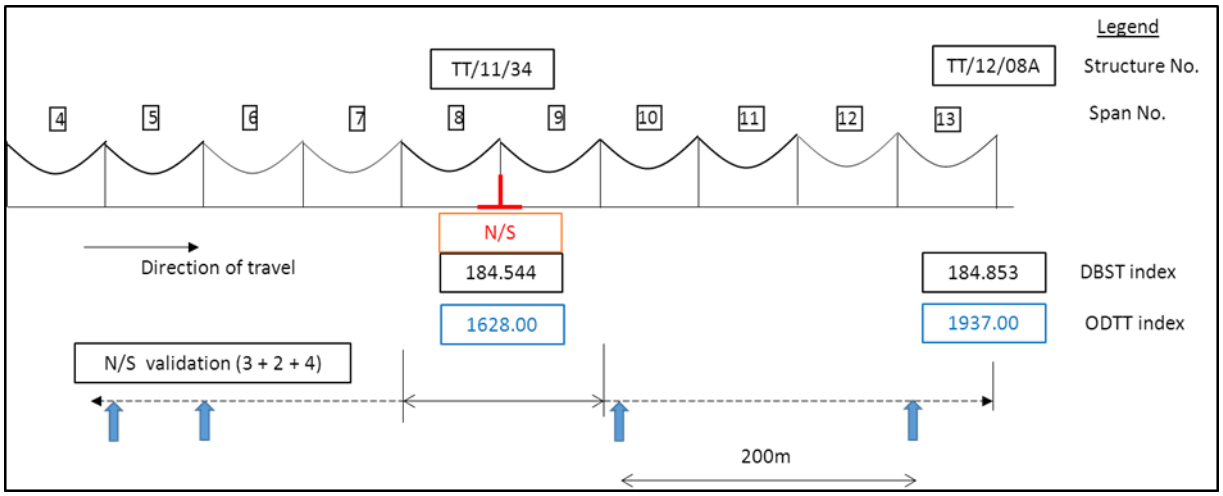

Figure 6.26 The sub set of the Old Dalby OCL model used for neutral section validation tests showing the 3 + 2 + 4 span arrangement, around a 2 span analysis section (spans 8 & 9), accommodating the start and end positions of both pantographs.

6.6 Dynamic simulation results and validation

The output of the neutral section simulations is presented against the target data for the three analysis zones previously described (Figure 6.20 and Table 6.5, Table 6.6 and Table 6.7) for the filtering frequencies of 20 and 30 Hz. The simulation was undertaken

at a sampling frequency of 300 Hz (i.e. Integration Time Step of 0.00333 sec). The data is shown in Table 6.11 for 20 and 30 Hz filtering, and is discussed below.

Table 6.11 Neutral section simulation statistical results for all three analysis zones, at 20 and 30 Hz filtering frequency. Red shaded cells are outside 20% of target values

	spans 8/9 – zone 1			2 x half spans – zone 2			N/S only – zone 3		
	Target	Value	Diff.	Target	Value	Diff.	Target	Value	Diff.
20 Hz									
Fm	107.805	106.5764	6.13%	113.53	104.8395	7.66%	99.55	110.9584	11.46%
σ	32.194	29.57356	19.17%	36.59	30.61138	16.33%	33.25	36.52183	9.84%
F max	262.990	181.1647	31.11%	262.99	181.1647	31.11%	162.59	181.1647	11.42%
F min	28.104	36.96093	31.52%	28.10	36.96093	31.52%	35.30	36.96093	4.71%
30 Hz									
Fm	107.737	106.5661	5.80%	113.13	104.8224	7.34%	98.39	110.2634	12.07%
σ	37.004	32.14296	26.48%	43.72	35.24082	19.39%	39.85	50.51625	26.77%
F max	315.625	199.3607	36.84%	315.63	199.3607	36.84%	182.30	199.3607	9.36%
F min	-7.028	-23.5121	234.56%	-7.03	-23.5121	234.56%	8.22	-23.5121	385.91%

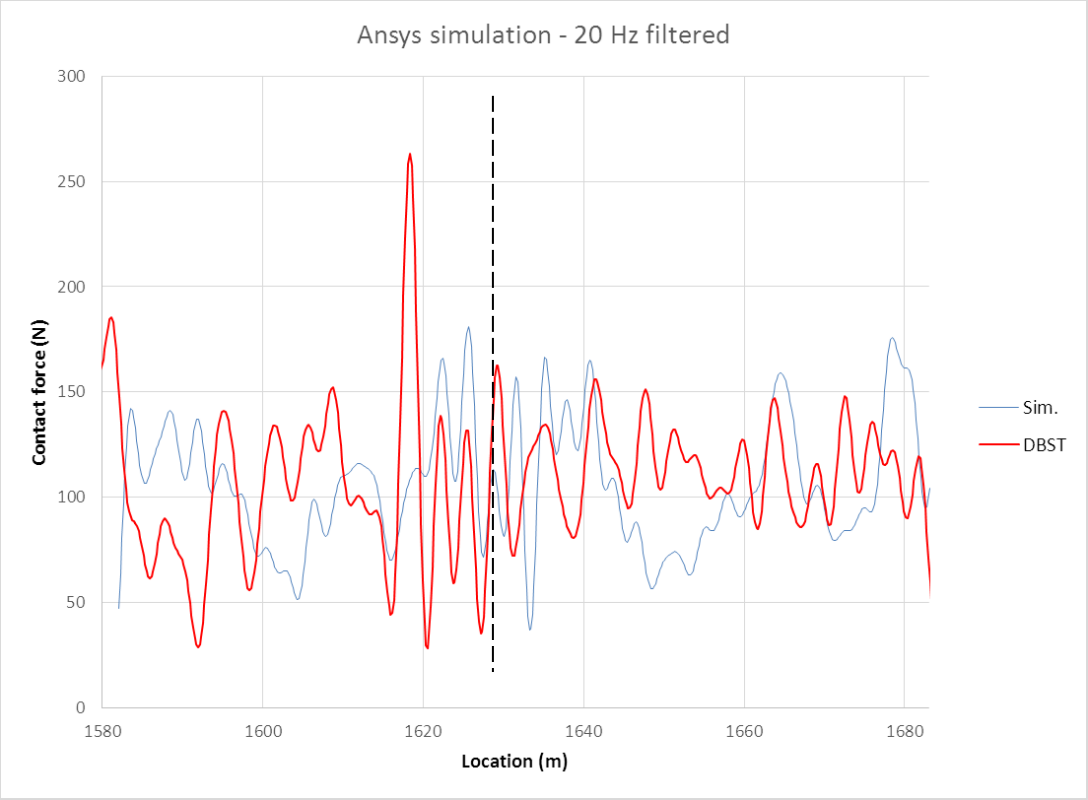

Figure 6.27 Simulated contact force through the neutral section showing analysis zone 1. DBST measured values shown in red. Neutral section centre line shown dotted.

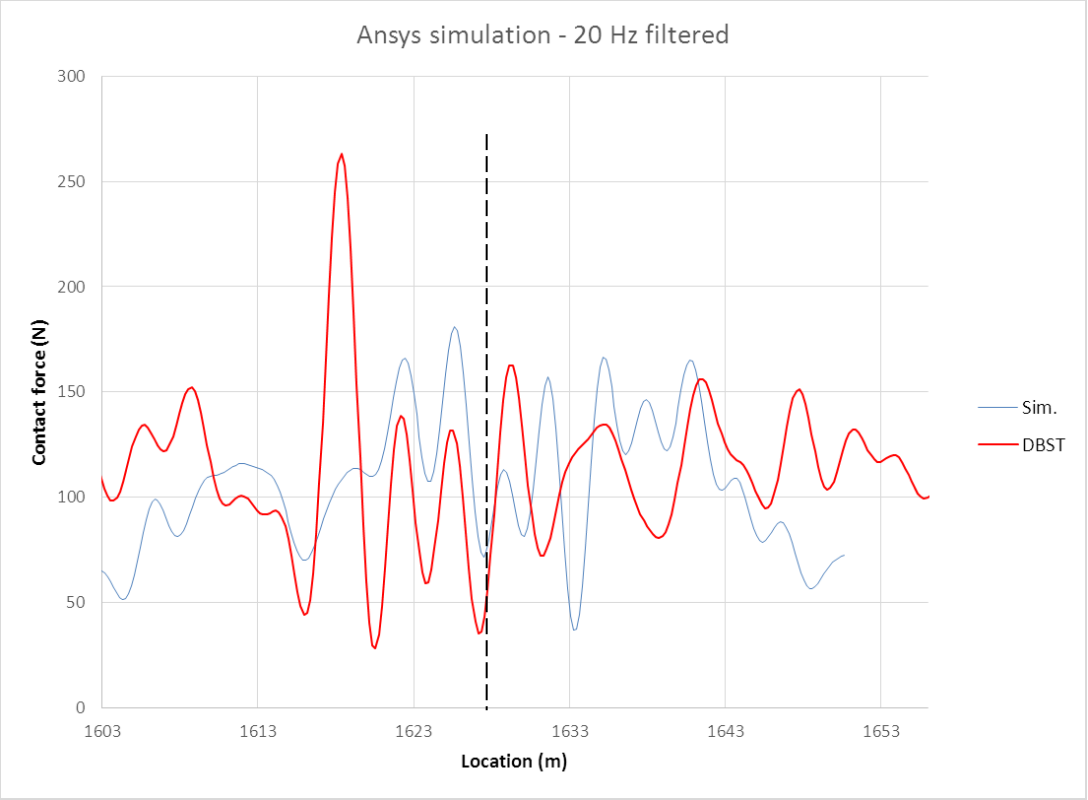

Figure 6.28 Simulated contact force through the neutral section showing analysis zone 2. DBST measured values shown in red. Neutral section centre line shown dotted.

The statistical values in Table 6.11 show a good correlation at 20 Hz in the neutral section only zone, analysis zone 3. (Due to the anomalous 'peak' the other zones can be expected to be less representative.) All statistical values are within ±20% of the measured values ('target' values), as required by EN 50318:2002 (the earlier standard, see Table 5.25). The simulated mean force and maximum force is higher than measured by about 11%.

The 30 Hz filtered results are less representative. The simulated standard deviation is significantly higher at 50N against 39N, and the minimum force is well below zero, at -23N, when the measured minimum forced is positive at 8N. As has been described earlier, the pantograph head natural frequency, based on the pantograph head mass and penalty contact stiffness influences the valid frequency range of interest, and in this case it seems probable that the there is insufficient 'headroom' when using the 5.8kg pantograph head mass (as described in the ODTT validation in section 5.5 of Chapter 5) to accommodate a 30 Hz frequency range of interest (refer to Figure 5.25).

Consequently, insofar as comparisons between measured and simulated data for validation purposes, it seems the 30 Hz filtered results are less reliable, and the 20 Hz filtered range will be the only results considered.

The contact force is plotted in Figure 6.27 and Figure 6.28 for both analysis zones 1 and 2, in conjunction with the DBST measured forces (in red), for a 20 Hz frequency range of interest. As can be seen ignoring the anomalous force peak at 1619m (ODTT index) in advance of the neutral section zone itself, the simulated force follows the peaks and troughs of the measured data quite well, in the first half or three quarters of the neutral section. The amplitude of the force, both peaks and troughs, appears about 20N higher generally. At the exit of the neutral section, from around 1630/1631m (the location being around 2/3 along the exit long CW insulator) the two plots start to diverge. The simulation continues to show a 'cleaner' pattern, whilst the measured results show a less regular pattern, with the peaks and troughs out of step with the simulation. As the neutral section is essentially (apart from the lever arm) symmetrical, it seems possible that this represents (again) an anomaly with the installation of the ODTT neutral section, although there is no parallel anomalous vertical movement of the contact point, as seen in Figure 6.17.

The simulated vertical height and range of displacement of the pantograph CW contact point is shown in Figure 6.29. The statistical values associated with this plot are shown in Table 6.13, where Y is the vertical height.

Looking at this data (essentially the uplift of the neutral section as the pantograph passes), a minor 'dip' occurs at about the location of the first dropper after the exit of the neutral section. (This cannot be compared to the measured height in Figure 6.17 because, as discussed, the DBST height data is only relative to an approximate datum, and is not absolute.)

Based on the simulated profile, it would seem that, although the pattern of peaks and troughs is not repeated in the exit portion of the neutral section, there is a feature associated with the exit of the neutral section that causes a particular characteristic in the response. For the ODTT neutral section this may be exaggerated by combination with an anomaly in the installation.

A similar potential causation for this exit end anomaly is postulated as for the entry end force peak, based on reflected waves from features within the neutral section as has

been described above, and illustrated in Figure 6.18. Thus reworking Table 6.4 for an anomaly location at 1630m, and including only those features beyond it, see Table 6.12, it can be seen that there is a single reflecting point within the neutral section that would create an interference at that location, and that is at the location of the second spring dropper (point C in the figure), which reflects a wave from the fourth spring dropper (point F).

Table 6.12 Locations of potential wave initiating points (exit end anomaly) for reflective points within the neutral section. Relate to Figure 6.18

ID	Feature (reflective point)	feature location	force peak location	X_f	V'	X_p	initiating point location
A	lever arm start	1622.953	1630.000				
B	1st spring dropper	1623.928	1630.000				
C	2nd spring dropper	1626.826	1630.000				
D	registration (CL)	1628.000	1630.000				
E	3rd spring dropper	1629.174	1630.000				
F	4th spring dropper	1632.072	1630.000	2.072	2.218951	3.400	1626.600
	first dropper/9	1633.500	1630.000	3.500	2.218951	5.743	1624.257

Once again, as described in 6.4 above when discussing the force peak in advance of the neutral section, it cannot be known from the data available if the anomaly observed exists at the observed location, or is at some other location (e.g. the second spring dropper) and is triggering a wave which reflects back from a neutral section feature (e.g. the fourth spring dropper) and interferes with the pantograph at the location of the observed anomaly.

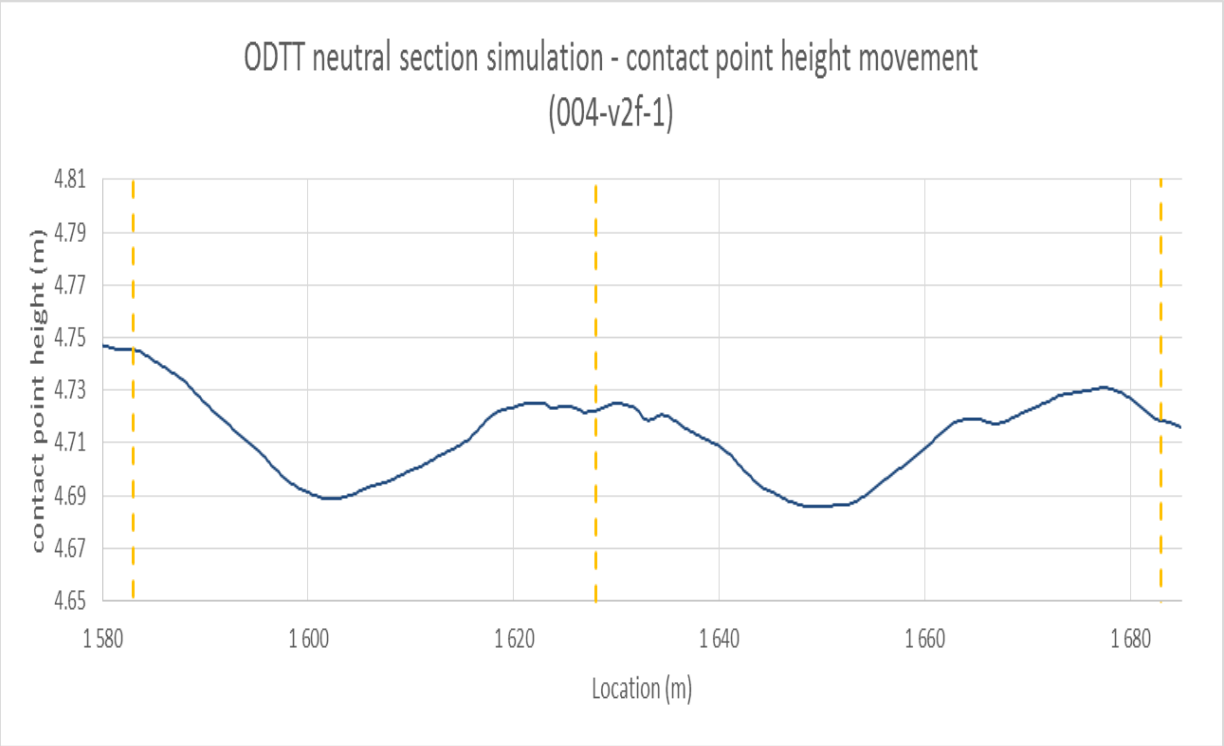

Figure 6.29 Simulated contact point vertical height through the neutral section showing analysis zone 1

Table 6.13 Contact point vertical height and range of movement through the neutral section: statistical results (see statistical data in Table 6.13)

	Zone 1	**Zone 2**	**Zone 3**
	span 8/9	half spans	N/S only
Ymean (m)	4.712	4.707	4.723
sigma (m)	0.015	0.014	0.002
SD % range	25.58%	35.81%	26.52%
Ymax (m)	4.745	4.725	4.725
Ymin (m)	4.686	4.686	4.719
Y range (m)	0.060	0.040	0.007

6.7 Conclusions

An Arthur Flury single rod neutral section has been modelled and inserted into the previously validated model for the simulation of plain open route OCL, and simulations carried out. The output from the DSM filtered at 20 and 30 Hz has been compared against the line test results from a similar installation at Old Dalby, and the 20 Hz results were found to agree, within the tolerances given in European and International

standards. The results filtered at 30 Hz did not show such a good correlation, and this is probably due to the 30 Hz range being insufficiently distinct from the pantograph head natural frequency. Some anomalies have been found in the ODTT data, which may be due to installation issues, and cannot be modelled. This would appear to be a feature of the requirement in EN 50318 (all versions) that ultimately simulations must be validated against line test data. There is therefore an inherent danger that the simulation methodology actually is manipulated to generate results that are themselves atypical of a 'perfect' OCL installation, and bend too far in the direction of accommodating the imperfections in the installation, which cannot be known. This may be the case here.

In this case here, this validated neutral section DSM can be used with a reasonable degree of confidence, with the qualification mentioned above, for the subsequent analyses, described in the next chapter.

The method of modelling the discrete features in the OCL, using a 'hybrid' of rigid multibody and flexible elements, modelling the neutral section parts with rigid bodies, joints and force element, was only partially successful, and the implementation of Ansys multi point constraint joint elements was substituted with regular solid elements using a 'softer' material specification to mimic the joints.

Analysis of a neutral section, or other 'discrete feature' in the OCL, in this manner is thought to be previously untried, and this successful development can be seen to be beyond the state of the art. This has successfully answered one of the most significant research questions.

Chapter 7 Parametric Analysis and Concept Proposals

7.1 Summary

This chapter describes the use of the model developed previously to assess the effect of individual characteristics of the neutral section's construction on its performance and behaviour, with a view to optimisation, and to propose potential improvements. This is a limited assessment, in order to demonstrate the model's feasibility, and confirm the usefulness of this approach developed in previous chapters.

7.2 Philosophy

The approach to the parametric analysis is as follows. Based on the work described in the earlier chapters, a single neutral section model is created and a simulation carried out for a single pantograph. For the sake of convenience and continuity this included many of the characteristics of the ODTT based model. The neutral section model replicated the standard AF single rod neutral section used in previous studies (in Chapter 6). This will become the baseline against which the effect of the adjustments to various parameters of the neutral section construction will be compared. The comparison will be based upon the criteria of force and vertical displacement. This is on the basis of these being the characteristics whose simulation has been validated in the preceding work, and is also the basis of the (draft) neutral section performance specification produced by Network Rail (Network Rail, 2015e).

7.3 Parametric analysis

The following items of the neutral section construction shown in Table 7.1 have been identified for parametric analysis. This is based on the knowledge built up in the development of the ODTT neutral section validation model described previously, engineering judgement and the feedback of experience from Network Rail engineers.

Table 7.1 Elements for neutral section parametric analysis

Neutral section component/characteristic	Note
Insulator length	Affects whole neutral section length
Insulator mass	
Insulator stiffness	Governed by material E and diameter (for constant length)
Overall length (earthed section length)	
Earthed section mass and stiffness	Governed by material E and diameter (for constant length)
Entry lever arm characteristic	Enhancement or removal
Catenary insulator – short version	As per current design
Anti-torsion dropper stiffness	Including any asymmetry
Joint 'characteristics'	

From these a short list is chosen which represents a limited range of achievable options, the object being to demonstrate, by a practical application, the validity and utility of the approach developed in the previous chapters. *Inter alia* it will confirm the legitimacy of the work carried out. In the first instance a set of options is chosen which can be effected using the existing node and elements spacing, without the need for a wholesale reconstruction of the entire neutral section model, with the attendant risk that changes to the model will be introduced which are not entirely due to the option being tested, thus masking their impact.

7.4 The neutral section baseline

The approach of this analysis is to study the relative performance of a number of specific design amendments, compared to a baseline of the conventional Arthur Flury single rod insulator, as seen at Old Dalby, and described in the previous chapter. As the results sought will be relative, the detail of the baseline is less significant, and so a number of modifications to the model developed in previous chapter have been made, to facilitate the amendments being introduced, and to improve computational efficiency. The basic data is in spans 8 and 9 of the ODTT OCL model, as used for the neutral section validation, with some changes, namely:

- Single pantograph, basically the BW HSX 250 used in the ODTT validation, but with the removal of the unnecessary non-linear pantograph head stiffness, and a reduced head mass of 5.2 kg, to allow a higher penalty stiffness, for a better 30 Hz filtered output;

- Reduced model length (6 spans), see Figure 7.1 with a 2 span analysis section, a 3 span lead in, and 1 span run out section (exploiting the single pantograph);
- Speed of 200 km/h, integration time step sampling rate of 300 Hz
- Some normalisation of the particular ODTT geometry.

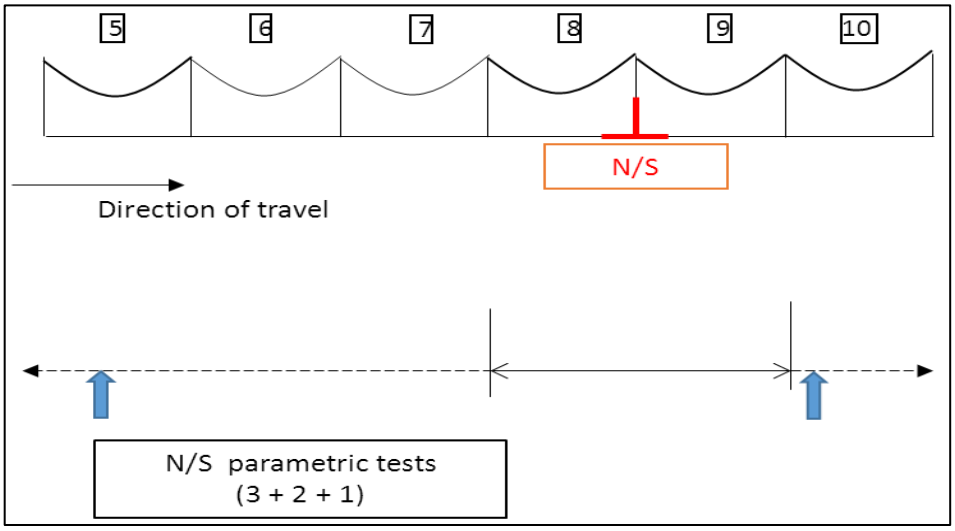

Figure 7.1 Model and analysis section for parametric analysis baseline, showing single pantograph start and end positions, in a 3+2+1 span arrangement

The shorter model length shown prompts potential issue with interference from reflected waves, due to the end boundary being that much closer to the analysis section and pantograph passages. Although the shorter model length shown in Figure 7.1 does show a slightly worse behaviour than that of the analysis section in a full length (18 span as per Figure 5.35) model length, as this model is used purely as a baseline for comparison with the parametric testing outputs, its absolute behaviour is not germane, and as the shorter model offers better computational efficiency, it was adopted.

Otherwise all other features were as described in Chapter 6. The simulation was conducted at 200 km/h and output force data filtered at 20 and 30 Hz. The analysis length was two spans. Notwithstanding the much shorter model length, the ODTT index (X coordinates) was retained. The baseline output is shown in Figure 7.3, and summarised in Table 7.2. The extent of the OCL for which the comparison is made (i.e. the 'analysis section') is essentially the same as for the initial ODTT neutral section validation in Chapter 6, i.e. three 'zones':

1. The entire two spans which include the neutral section;

2. The two half spans from the mid-point of the first span to the mid-point of the second;
3. The neutral section only, in practice from the last dropper of the first span to the first dropper of the second span.

These are shown in Figure 7.2.

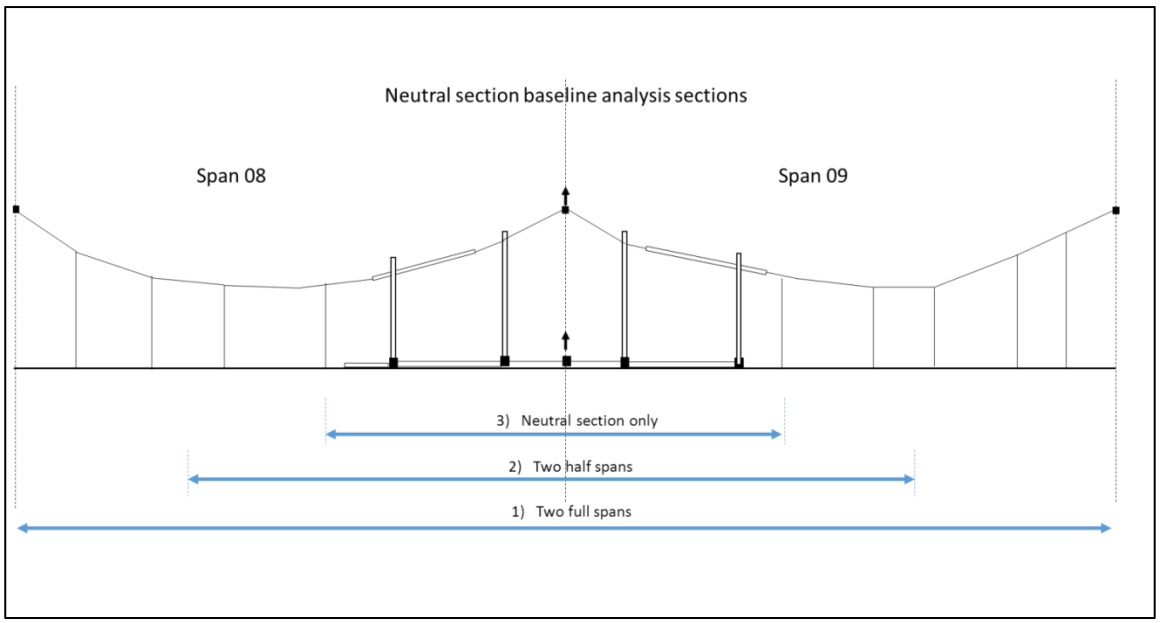

Figure 7.2 Baseline neutral section 'analysis zones', for parametric analysis tests, showing the three zones for which statistical values comparison will be made

The plots of the contact force through the analysis section for both the 20 and 30 Hz filtered cases are shown in Figure 7.3. Both indicate a significantly low force at a point beyond the exit of the neutral section, which in the 30 Hz filtered data is in fact negative, after which reasonably normal forces obtain. This is probably a feature of the original ODTT data, which includes a change in CW gradient at the point of the neutral section, the CW rises away from the support point. See orange line in Figure 7.4. However as this is a baseline, the feature will be the same for all options considered, and does not impair its usefulness as a comparator.

The statistical values for the contact force, for both the 20 and 30 Hz filtered cases are shown in Table 7.2.

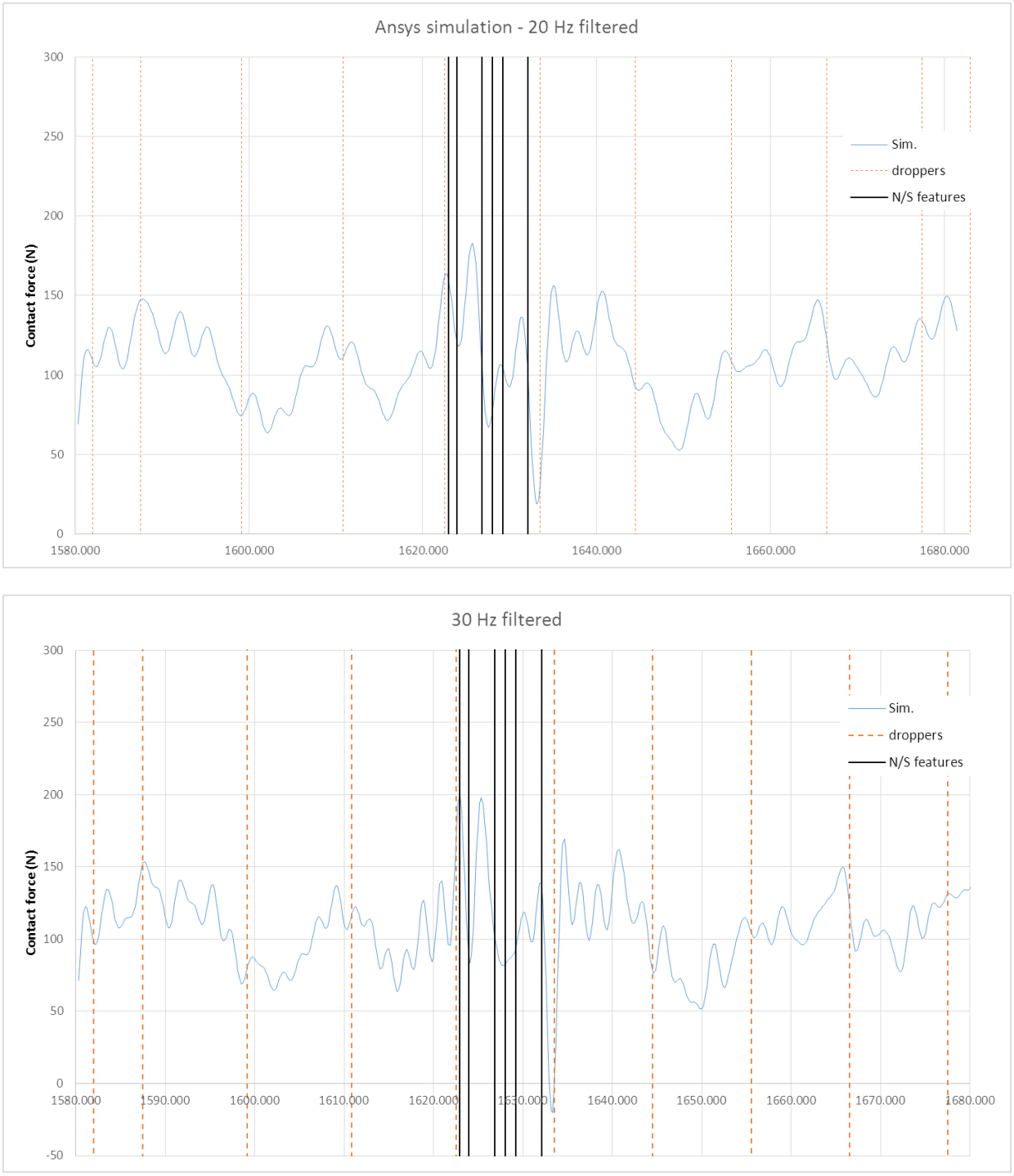

Figure 7.3 Baseline neutral section contact force, for the two span analysis section. 20 Hz (above) and 30 Hz (below). Location of neutral section features shown in black

The height and range of vertical movement of the point of contact is shown in Figure 7.4 and statistical values in Table 7.3.

Table 7.2 Baseline neutral section contact force statistical values, for the three analysis zones, at 20 and 30 Hz filtered.

	spans 8-9 (analysis zone 1)	half spans (analysis zone 2)	neutral section only (analysis zone 3)
20 Hz			
Fm (N)	108.179	103.894	116.964
sigma (N)	25.033	28.869	36.681
Fmax (N)	182.966	182.966	182.966
Fmin (N)	18.778	18.778	23.210
30 Hz			
Fm (N)	108.176	103.874	118.971
sigma (N)	27.588	32.662	41.274
Fmax (N)	199.608	199.608	199.608
Fmin (N)	-20.034	-20.034	0.462

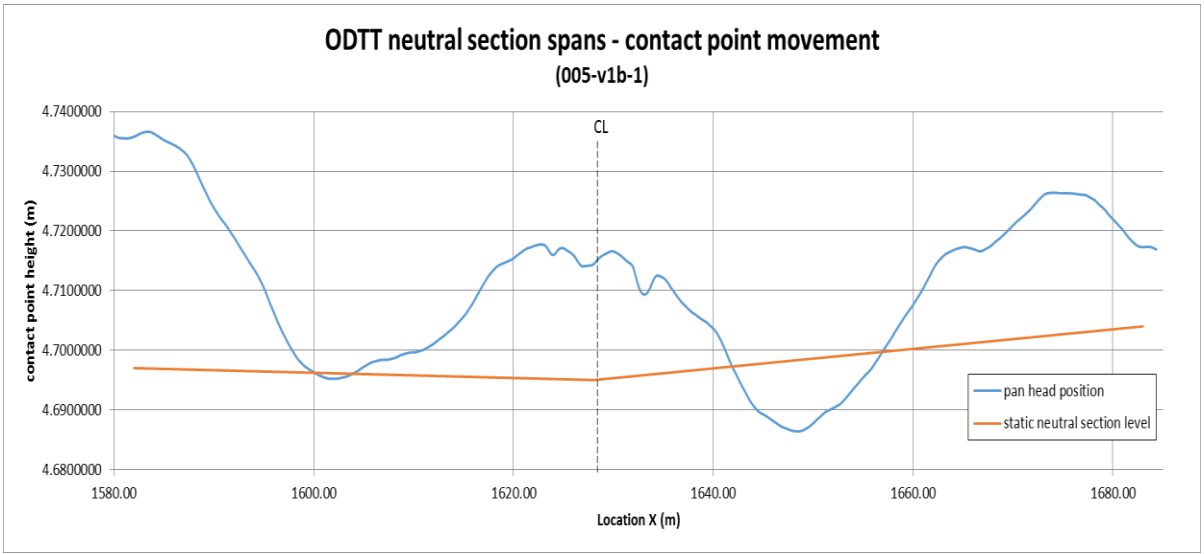

Figure 7.4 Baseline neutral section model: vertical height and range of movement of the point of contact, for the 2 spans, showing neutral section centre line

Table 7.3 Baseline neutral section model: statistical values of contact point height and range of vertical movement, for the three analysis zones.

Baseline neutral section model: vertical height and range of movement of the point of contact			
	spans 8-9 (analysis zone 1)	half spans (analysis zone 2)	N/S only (analysis zone 3)
Y mean (m)	4.711	4.704	4.716
Sigma (m)	0.013	0.010	0.001
Y max (m)	4.737	4.718	4.718
Y min (m)	4.686	4.686	4.713
Y range (m)	0.050	0.031	0.005

The CW height profile through the neutral section is not constant at this point, as the baseline model is built upon the real ODTT neutral section, where there are changes of gradient (albeit minor) at this point. So the relative movement of the point of contact to the static CW height through the neutral section is shown in Figure 7.5. As can be seen, there is a noticeable dip on the exit of the neutral section. The CW goes below its static position here, although there is no loss of contact as the force plot shows no negative values. This would appear to be a feature of the OCL installation generally, and the neutral section installation particularly, at Old Dalby. This is a consequence of using the ODTT neutral section as the basis for the 'baseline'.

Most of the movement takes place outside of the neutral section extent, and within the neutral section, only 5 mm of vertical displacement is observed.

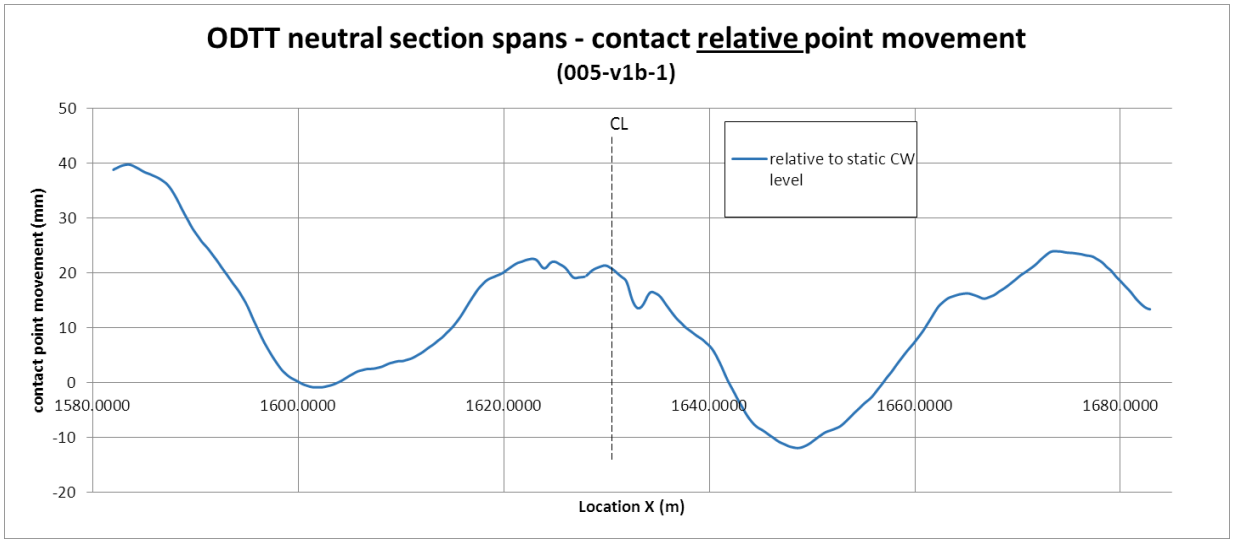

Figure 7.5 Baseline neutral section model: contact point vertical movement through the neutral section showing analysis zone 1 (two spans)

7.5 The results of the options tests

7.5.1 The choice of options

Considering the long list of possible modified neutral sections options shown in Table 7.1, the following were identified for investigation, as they represent a minimum of variants that can be most readily implemented in the baseline model. All models were created by incremental modifications to the baseline model.

1. A variant with the messenger insulators reduced in length, so that the messenger insulator is totally within the extent of the two spring dropper tubes;
2. A variant with the entry lever arm removed;
3. A variant with the centre short CW insulators replaced by a length of contact wire;
4. A variant with a duplicate of the entry lever arm installed at the exit end, prompted by the poor performance at the exit of the neutral section seen in the baseline model;
5. A variant with the centre short CW insulators replaced by a continuous flexible section (as an alternative to option 3);
6. A variant with the stiffness in all composite rods in all insulators increased.

The choice of which options to model and test took into account that the relevant research question centres around the ability of the analysis method described previously to undertake a parametric analysis. This requires a baseline model, and the options to be tested to be readily introduced into this baseline without extensive restructuring of the nodes and elements (other than for the form of the options itself), thus retaining the essence of the 'simulation method' intact.

All options have the merit of being close to modifications that either are or can be proposed in reality, and can answer the research questions.

The method adopted was to add the variation incrementally, and examine the output statistics, and compare to the baseline. Variations that show an improvement over the baseline are retained where considered appropriate, and any that do not are not perpetuated into the next variation.

The results for the options 1 to 6 (test 005-v2a to v2f) are shown in the figures and tables below, and the findings discussed individually. A comparative assessment is

made in section 7.6, and a review of the practicalities of implementing any of the modifications is in section 7.7.

7.5.2 Option 1

Test 1/option 01 reduces the length of the messenger insulators which causes the connection of the outer spring droppers to be directly to the messenger wire, rather than the messenger insulator (see Figure 6.3 top). In this implementation, the insulator is reduced in length from 2750mm to 2050mm, governed mainly by the arrangement of nodes in the baseline model. This is in fact the current arrangement for the AF single rod neutral section, and it has replaced the earlier arrangement (albeit the one used throughout this research), which was in force at the time the Old Dalby neutral section was installed.

	v2a								
	spans 8/9			N/S only			2 x half spans		
	target	value	diff.	target	value	diff.	target	value	diff.
Fm (N)	108.179	108.192	0.01%	116.96	116.969	0.00%	103.89	103.930	0.03%
sigma (N)	25.033	25.142	0.44%	36.68	36.899	0.60%	28.87	28.980	0.39%
Fmax (N)	182.966	183.274	0.17%	182.97	183.274	0.17%	182.97	183.274	0.17%
Fmin (N)	18.778	19.834	5.63%	23.21	24.1943	4.24%	18.78	19.834	5.63%

Figure 7.6 Parametric test 1 output data (20 Hz) (test 005-v2a) and statistical data compared to baseline target for the three analysis zones.

The contact force plots and statistical data for 20 Hz and 30 Hz filtered output are shown in Figure 7.6 and Figure 7.7.

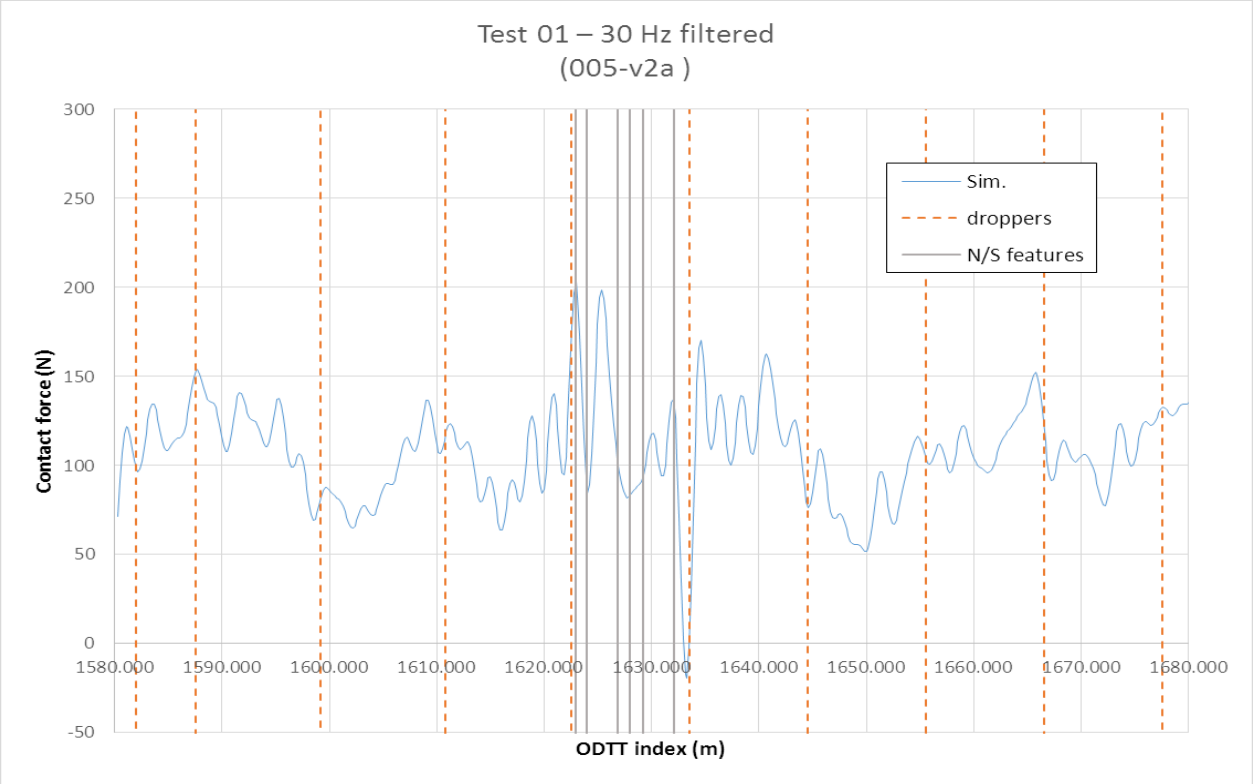

	v2a								
	spans 8/9			N/S only			2 x half spans		
	target	value	diff.	target	value	diff.	target	value	diff.
Fm (N)	108.176	108.189	0.01%	118.97	119.030	0.05%	103.87	103.91	0.04%
sigma (N)	27.588	27.737	0.54%	41.27	41.603	0.80%	32.66	32.84	0.55%
Fmax (N)	199.608	202.660	1.53%	199.61	202.660	1.53%	199.61	202.66	1.53%
Fmin (N)	-20.034	-19.613	-2.10%	0.46	2.156	366.7%	-20.03	-19.61	-2.10%

Figure 7.7 Parametric test 1 output data (30 Hz), (test 005-v2a) and statistical data compared to baseline target for the three analysis zones

Note that in these force plots (and all others in this chapter) the main neutral section features are also plotted (as vertical lines, in grey), and represent, from left to right: the start point of entry (lever arm), the first spring dropper, the second spring dropper, the centre registration point, the third spring dropper, the fourth spring dropper.

This test has demonstrated the effect of the change on the dynamics of the neutral section. As can be seen from the table in Figure 7.6, the change is marginal (as would be expected) with most values only moving by less than 1%, but the most noticeable improvement is an increase in the minimum force, thus contributing to avoiding losses of contact.

The plots of option 01 forces compared to the baseline(for both filtering frequencies) are shown in Figure 7.8. As can be seen, the approach to the neutral section is virtually

identical, but at the first spring dropper (which is the feature which has been altered in this test) the plots start to diverge.

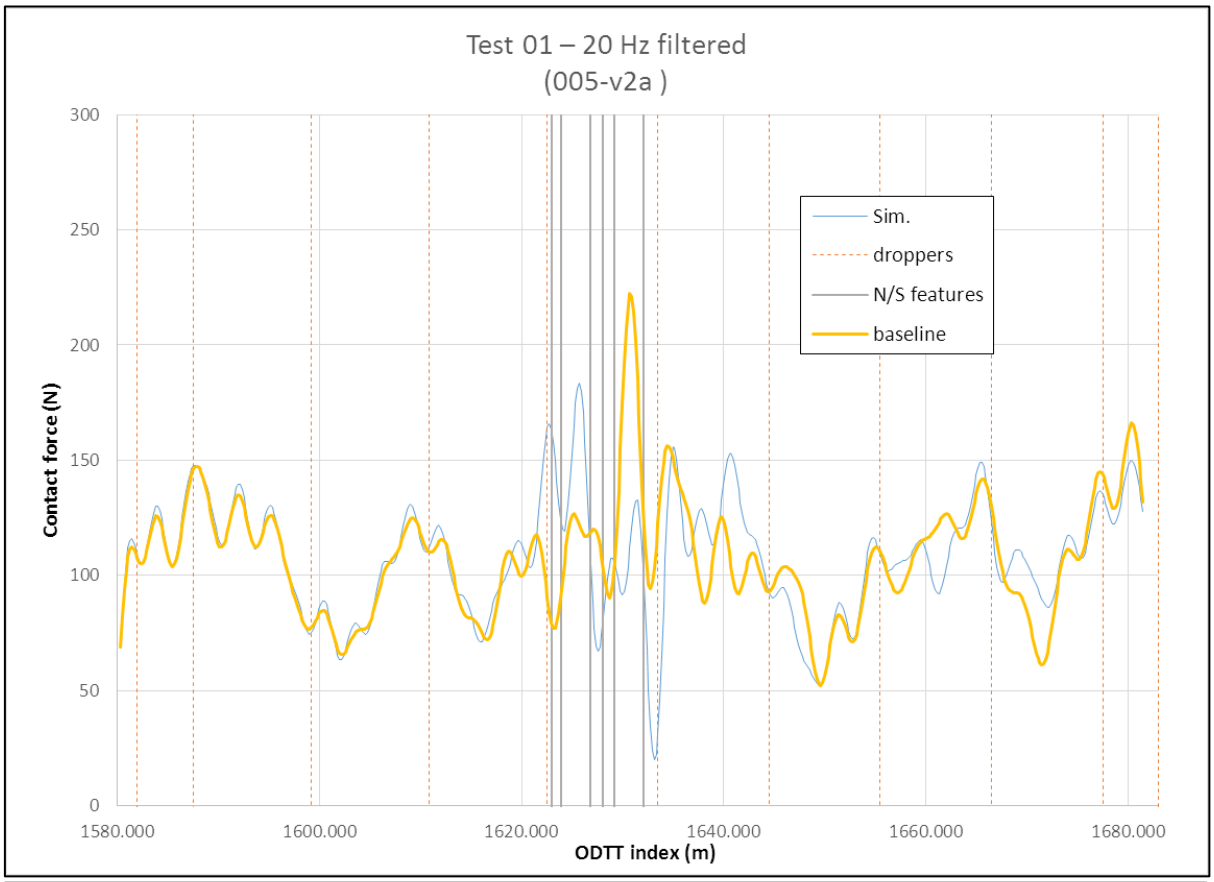

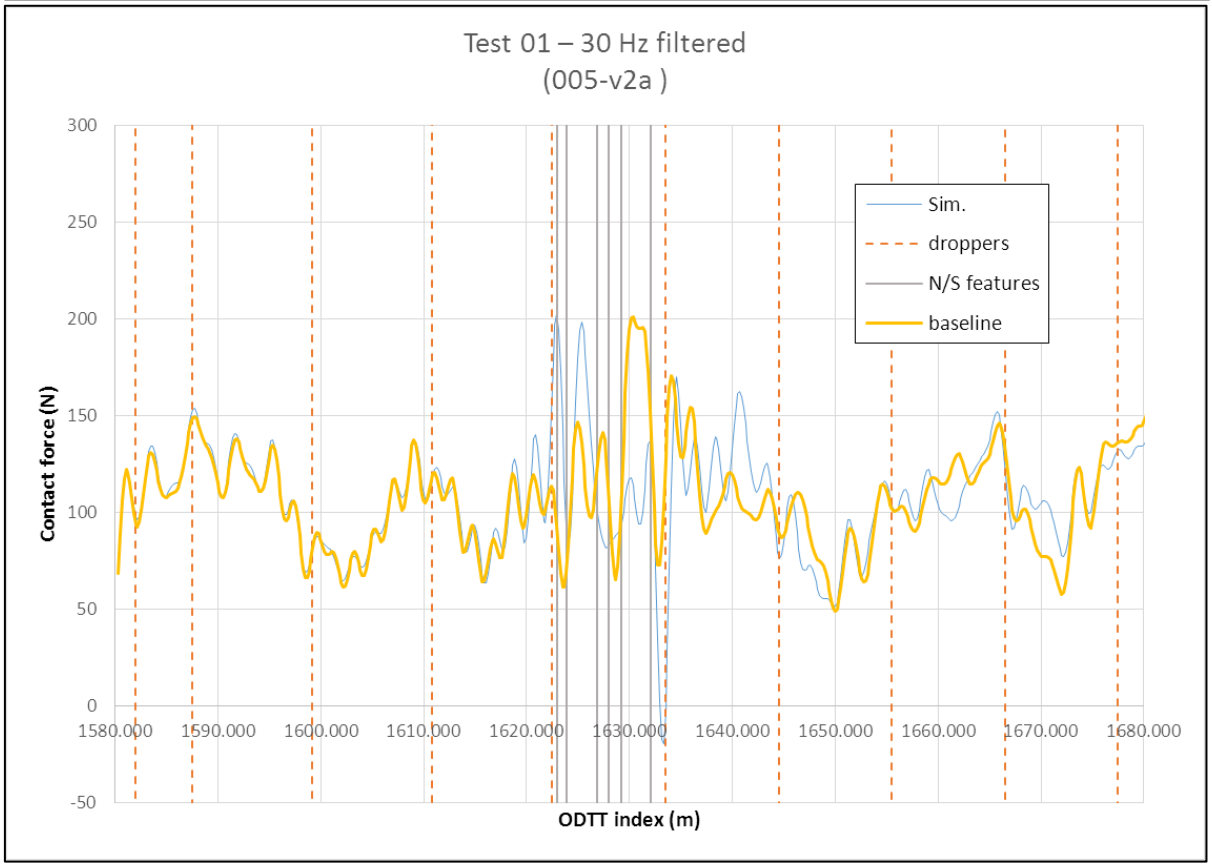

Figure 7.8 Parametric test 1 output data (20 and 30 Hz), (test 005-v2a) compared to baseline

This modification to the messenger insulator is included in all the remaining test options.

7.5.3 Option 2

In Test 2/option 2 the modification to remove the lever arm is prompted by the discussions with Network Rail engineers, and the appreciation that this feature of the neutral section is contentious (as has been described in Chapter 3). Some Network Rail zones have already removed the lever arm from the neutral sections in the line, in the belief that they are cause of failures. Lever arms have also been linked to CW fatigue failures in at least two neutral section incidents. The contact force plots and statistical data for 20 Hz and 30 Hz filtered output are shown in Figure 7.9 and Figure 7.10.

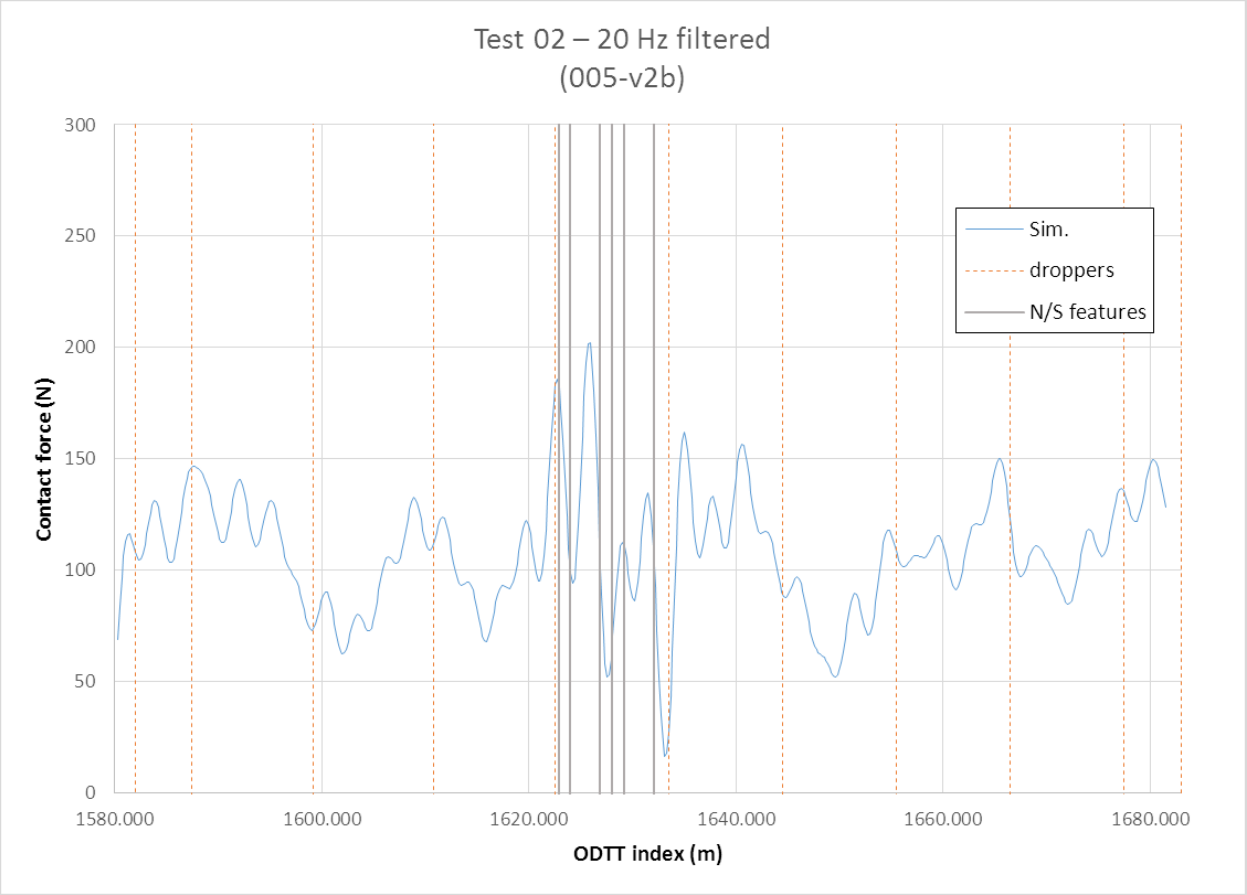

	v2b								
	spans 8/9			N/S only			2 x half spans		
	target	value	diff.	target	value	diff.	target	value	diff.
Fm (N)	108.179	108.169	-0.01%	116.96	116.808	-0.13%	103.89	103.913	0.02%
sigma (N)	25.033	26.739	6.82%	36.68	43.987	19.92%	28.87	31.549	9.28%
Fmax (N)	182.966	202.309	10.57%	182.97	202.309	10.57%	182.97	202.310	10.57%
Fmin (N)	18.778	16.167	-13.90%	23.21	22.012	-5.16%	18.78	16.168	-13.90%

Figure 7.9 Parametric test 2 output data (20 Hz), (test 005-v2b) and statistical data compared to baseline target

	v2b								
	spans 8/9			N/S only			2 x half spans		
	target	value	diff.	target	value	diff.	target	value	diff.
Fm (N)	108.176	108.159	0.02%	118.97	118.380	0.50%	103.87	103.87	0.00%
sigma (N)	27.588	29.638	7.43%	41.27	53.678	30.05%	32.66	35.90	9.92%
Fmax (N)	199.608	232.115	16.29%	199.61	232.115	16.29%	199.61	232.12	16.29%
Fmin (N)	-20.034	-14.159	-29.33%	0.46	1.156	150.2%	-20.03	-14.16	-29.33%

Figure 7.10 Parametric test 2 output data (30 Hz), (test 005-v2b) and statistical data compared to baseline target

The changes to the statistical data here are more pronounced than for test 1. Although mean forces are little changed, increase in standard deviation, especially in the neutral section zone, accompanied by a widening in the range between the maximum and minimum forces (as suggested by the SD increase) suggest that the lever arm does indeed fulfil its function of introducing the pantograph into the neutral section less 'brutally'. Interestingly, the movement in the values is across all zones of the analysis section.

The vertical displacement of the contact point between the pantograph head and the underside of the neutral section is shown in Figure 7.11. This shows virtually no difference to the baseline plot. The baseline is not shown as the two plots virtually

overlap and are not discernible at this scale. The only feature is a slight worsening of the smoothing at the entry point, as seen in the enlarged detail in Figure 7.12.

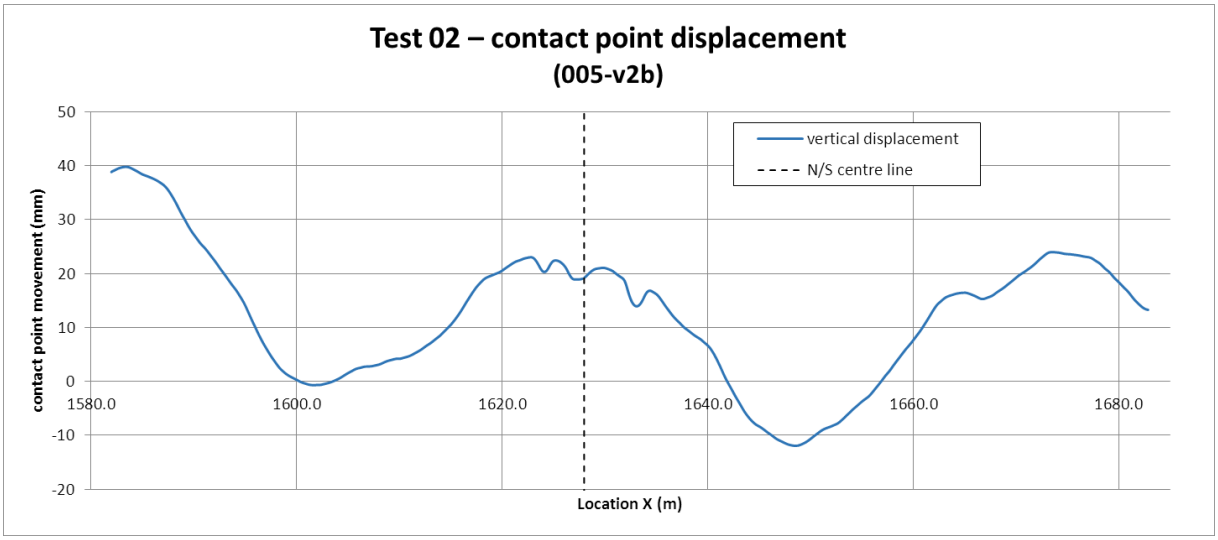

Figure 7.11 Parametric test 2 vertical displacement, (test 005-v2b)

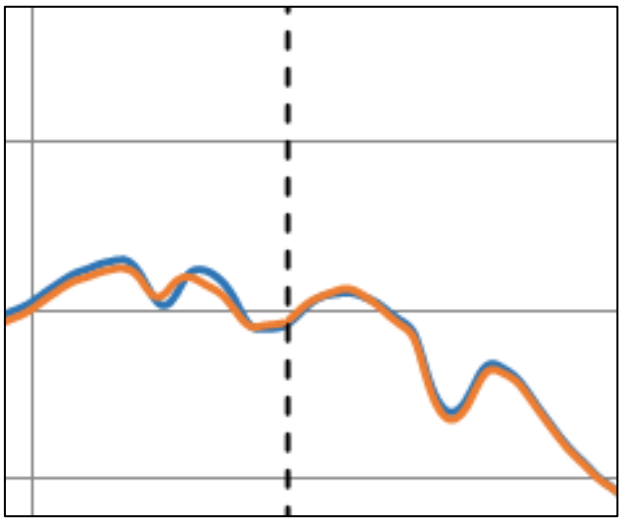

Figure 7.12 Detail of Parametric test 2 vertical displacement, at entry point. Orange line is baseline (test 005-v2b)

Based solely on this assessment of dynamics, retention of the lever arm seems a sensible action. The lever arm is retained in subsequent test options.

7.5.4 Option 3

Test 3/option 3 has retained the lever arm, and includes the shorter messenger insulators from the first test. The modification here is the replacement of the two centre short CW insulators with a length of contact wire. This is legitimate, as the two insulators here are not fulfilling the role of insulator, they are effectively part of the earthed section, but they provide a continuation from the long insulators either side,

with components of the same material and construction. One aspect of implementing this modification is that it requires two additional CW splice components to be introduced into the neutral section. The contact force plots and statistical data for 20 Hz and 30 Hz filtered output are shown in Figure 7.13 and Figure 7.14.

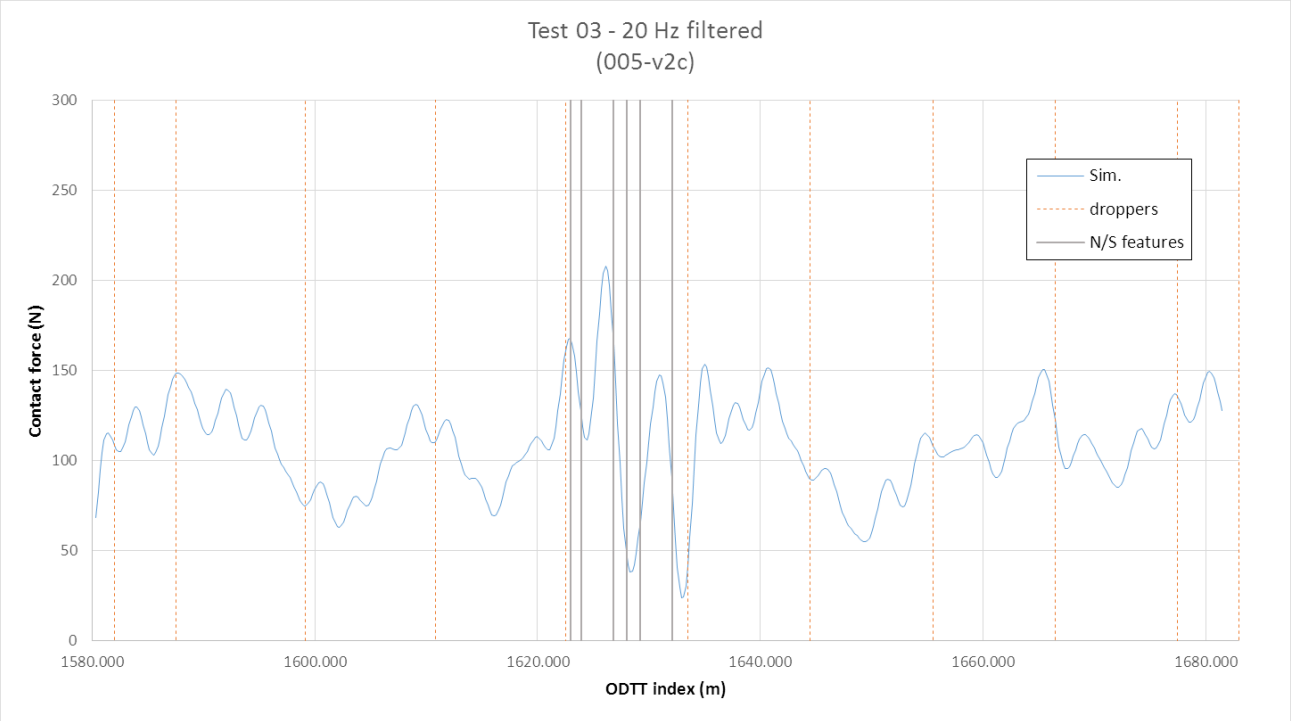

	v2c								
	spans 8/9			N/S only			2 x half spans		
	target	value	diff.	target	value	diff.	target	value	diff.
Fm (N)	108.179	108.400	0.20%	116.96	118.501	1.31%	103.89	104.441	0.53%
sigma (N)	25.033	27.184	8.59%	36.68	50.060	36.48%	28.87	32.301	11.89%
Fmax (N)	182.966	207.931	13.64%	182.97	207.931	13.64%	182.97	207.931	13.64%
Fmin (N)	18.778	23.933	27.45%	23.21	23.933	3.12%	18.78	23.933	27.45%

Figure 7.13 Parametric test 3 output data (20 Hz), (test 005-v2c) and statistical data compared to baseline target (red shaded cells differ from baseline target by over 20%)

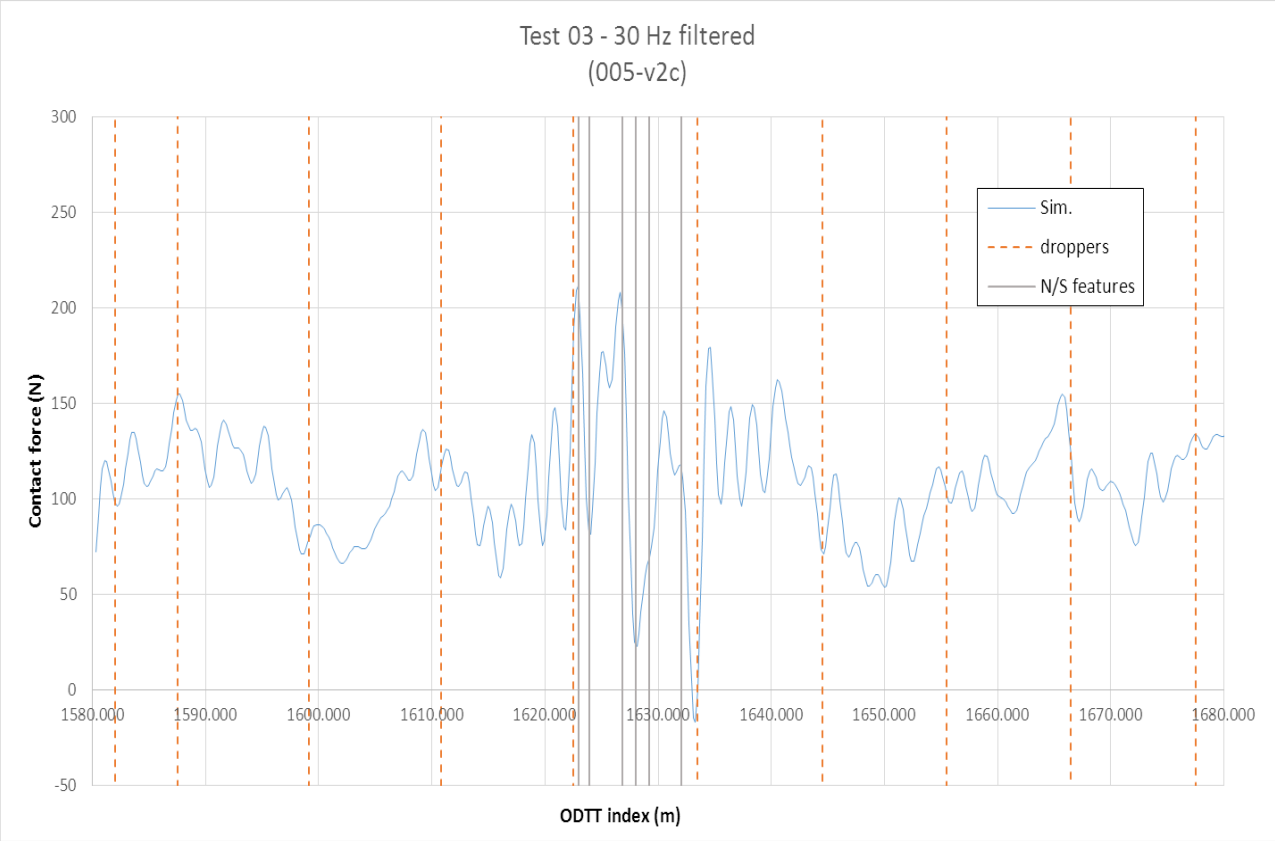

	v2c								
	spans 8/9			N/S only			2 x half spans		
	target	value	diff.	target	value	diff.	target	value	diff.
Fm (N)	108.176	108.400	0.21%	118.97	120.871	1.60%	103.87	104.425	0.53%
sigma (N)	27.588	30.361	10.05%	41.27	54.217	31.36%	32.66	36.998	13.27%
Fmax (N)	199.608	211.472	5.94%	199.61	211.472	5.94%	199.61	211.472	5.94%
Fmin (N)	-20.034	-16.838	-15.95%	0.46	4.616	898.9%	-20.03	-16.838	-15.95%

Figure 7.14 Parametric test 3 output data (30 Hz), (test 005-v2c) and statistical data compared to baseline target (red shaded cells differ from baseline target by over 20%)

The results show that the mean force is increased slightly in the neutral section zone, and the standard deviation of the force increase across all analysis zones, quite noticeably so in the neutral section zone (from 36.68N to 50.06N, a 36% increase). The increase in SD appears to be a symptom of higher forces generally, with the maximum force increasing by 25N. At the same time the minimum force does not change much. It appears that the inclusion of this modification will cause the behaviour to worsen.

The vertical displacement seen in Figure 7.15 also shows a noticeable rise either side of the centre line. The range of vertical movement through the neutral section zone is much higher, relatively, for this option, at 7.2mm compared to 4.6mm for the baseline.

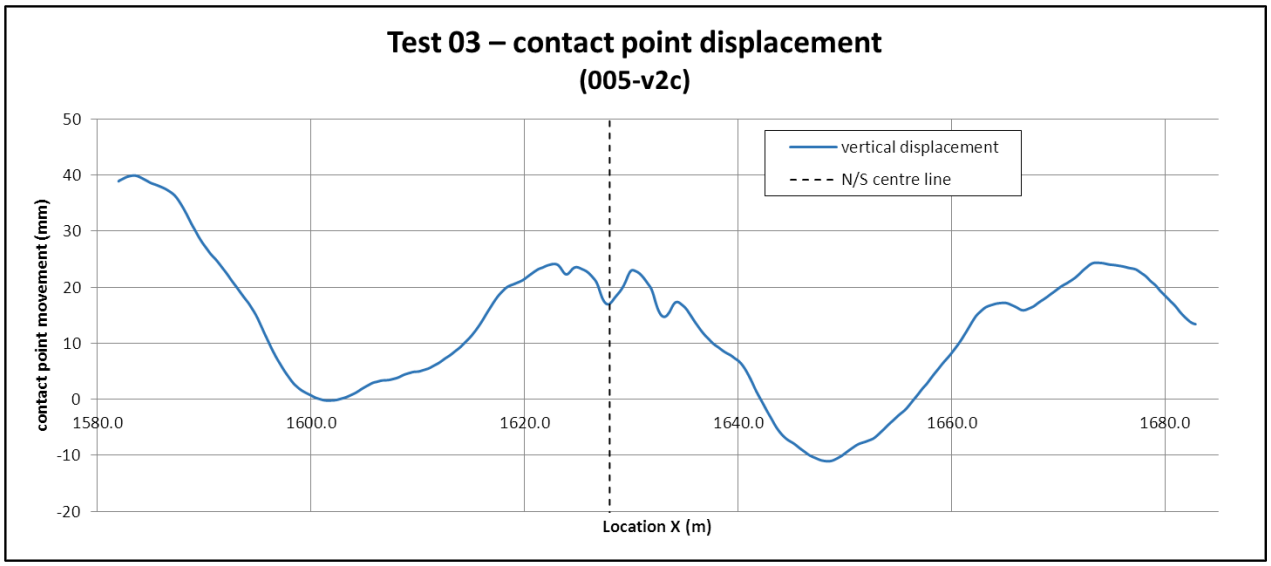

Figure 7.15 Parametric test 3 vertical displacement (test 005-v2c)

7.5.5 Option 4

Test 4/option 4 proposes the inclusion of an additional lever arm at the exit end, to create a fully symmetrical installation. This is based on the disturbed pattern of forces and displacements that are seen in the baseline, and all the previous 3 models, in the area at the end of the exit long CW insulator, and the associated outer connector to the final spring dropper and CW splices. The exit lever arm is modelled as an exact mirror image of the entry lever arm.

The contact force plots and statistical values are shown in Figure 7.16 and Figure 7.17. Across all the analysis zones, the standard deviation of force is much reduced (by between 12 and 22% in the 20 Hz results, although less so in the 30 Hz results), and the minimum force is a lot higher by over 30N, for both filtering frequencies. The peaks and troughs of the force plot show a much smoother profile, and in particular, the significant dip in contact force at the exit end seen in the baseline plot is not present. This is corroborated by the vertical displacement plot (Figure 7.18) where the profile at the exit of the neutral section does not show the pronounced dip that all others show, including the baseline. This is a significant improvement in neutral section performance, and its occurrence here in this option is a major contribution to the research question concerning the possibility of identifying design improvements.

Given the significant improvement made in the profile of the pantograph at the exit of the neutral section, the change introduced in this option is not carried forward into the two remaining options, 5 and 6, lest the inclusion of this improved behaviour might mask any effects that the particular details of those options might introduce.

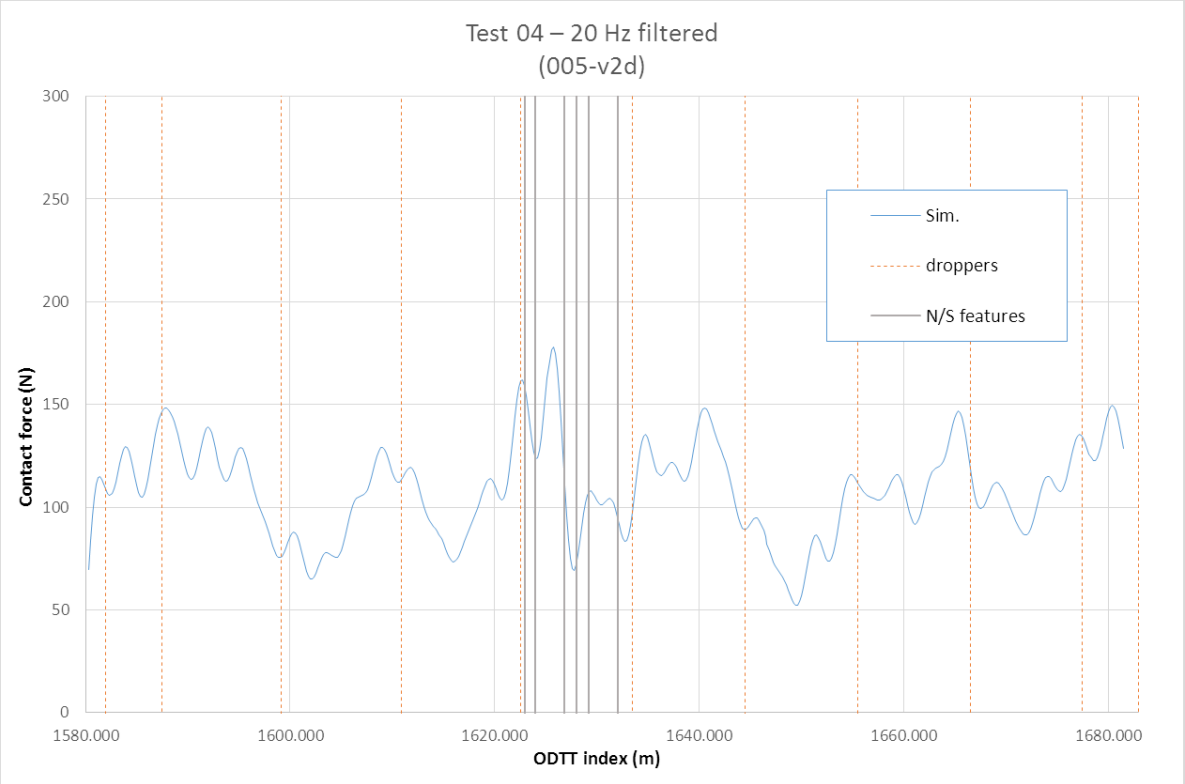

	v2d								
	spans 8/9			N/S only			2 x half spans		
	target	value	diff.	target	value	diff.	target	value	diff.
Fm (N)	108.179	108.631	0.42%	116.96	117.437	0.40%	103.89	104.814	0.88%
sigma (N)	25.033	22.824	8.83%	36.68	30.969	15.57%	28.87	25.285	12.42%
Fmax (N)	182.966	177.778	2.84%	182.97	177.778	2.84%	182.97	177.778	2.84%
Fmin (N)	18.778	52.167	178%	23.21	69.264	198.4%	18.78	52.167	177.8%

Figure 7.16 Parametric test 4 output data (20 Hz), (test 005-v2d) and statistical data compared to baseline target

	v2d								
	spans 8/9			N/S only			2 x half spans		
	target	value	diff.	target	value	diff.	target	value	diff.
Fm (N)	108.176	108.633	0.42%	118.97	119.090	0.10%	103.87	104.820	0.91%
sigma (N)	27.588	25.015	9.32%	41.27	37.874	8.24%	32.66	28.473	12.83%
Fmax (N)	199.608	202.952	1.68%	199.61	202.952	1.68%	199.61	202.952	1.68%
Fmin (N)	-20.034	50.915	-354%	0.46	80.376	1.7E+02	-20.03	50.915	354%

Figure 7.17 Parametric test 4 output data (30 Hz), (test 005-v2d) and statistical data compared to baseline target

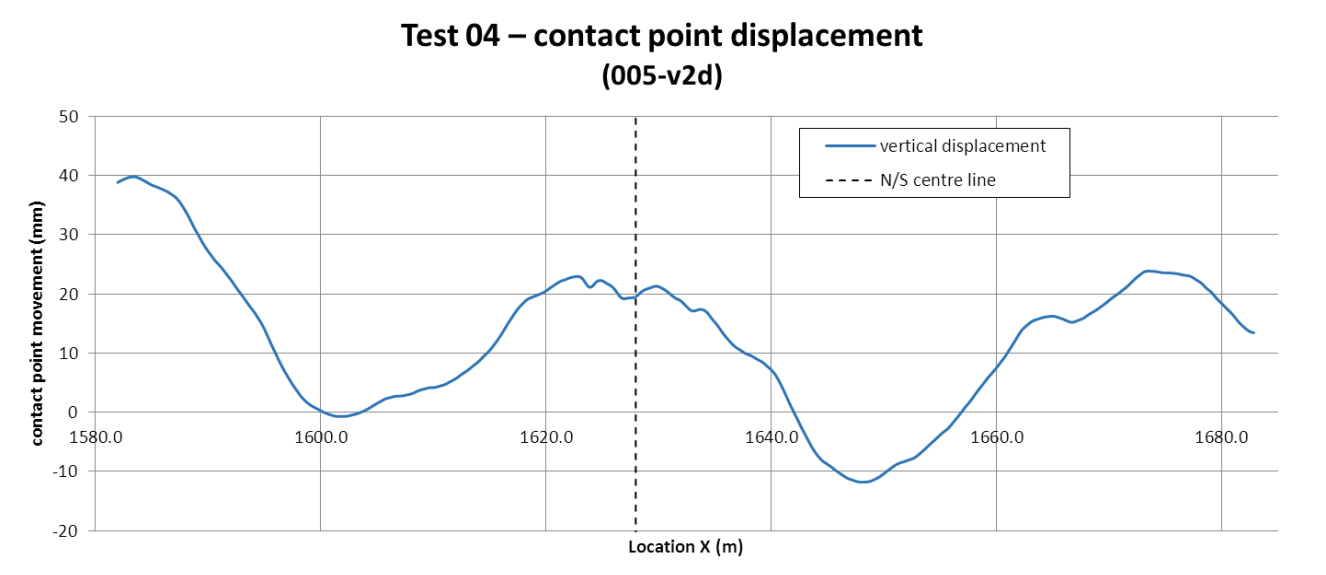

Figure 7.18 Parametric test 4 vertical displacement, (test 005-v2d)

7.5.6 Option 5

Test 5/option 5 is an attempt to eliminate the peak in stiffness that appear in the centre of the neutral section due to the stainless steel end ferrules on the end of the composite insulator rods. At the centre, and either side, where the insulators are connected to each other, two such ferrules are butted up, see the stiffness profile in Figure 6.22. This is achieved by replacing the material properties for the short CW insulators end ferrules with properties equivalent to the composite rod itself, so as to provide a continuity of bending stiffness though the centre section. This is clearly a theoretical option, as in practice some form of end fitting to the composite rod is required.

The contact force plots and statistical data for 20 Hz and 30 Hz filtered output are shown in Figure 7.19 and Figure 7.20.

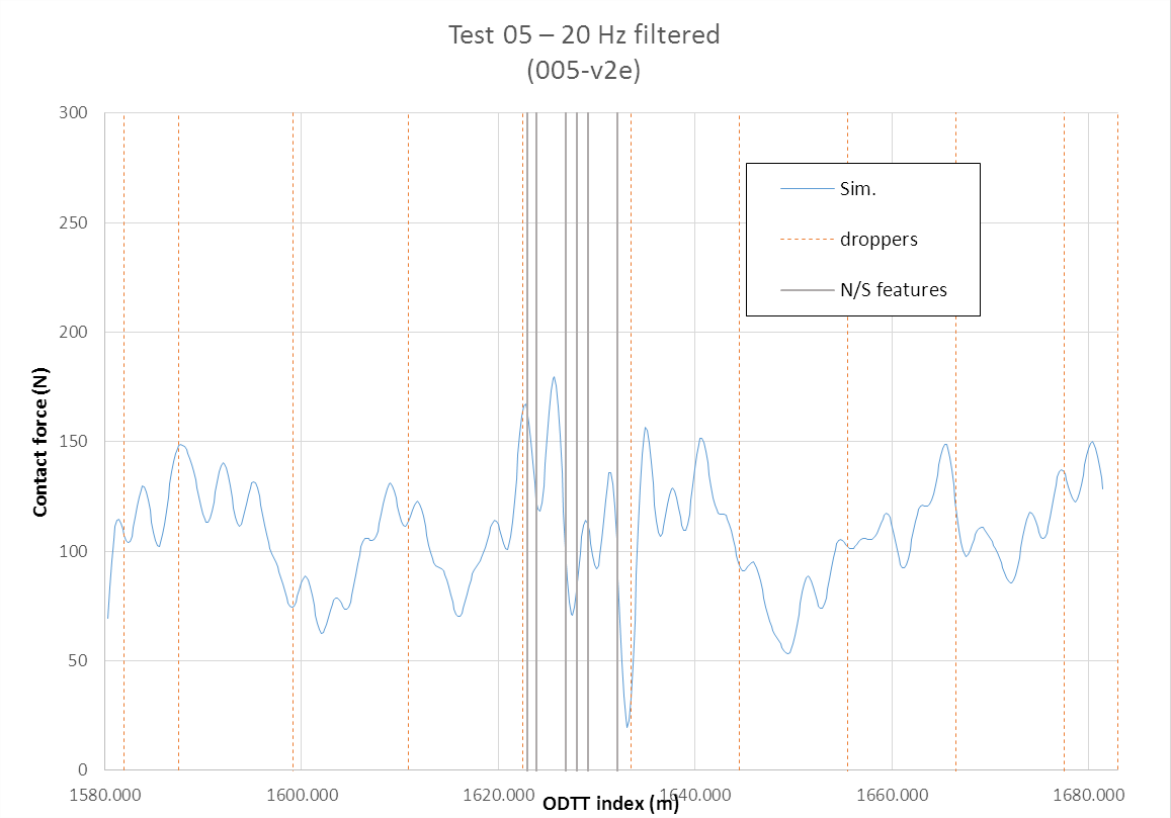

	v2e								
	spans 8/9			N/S only			2 x half spans		
	target	value	diff.	target	value	diff.	target	value	diff.
Fm (N)	108.179	108.056	0.11%	116.96	117.840	0.75%	103.89	103.711	0.06%
sigma (N)	25.033	24.998	0.14%	36.68	35.797	2.41%	28.87	28.532	0.34%
Fmax (N)	182.966	179.794	1.73%	182.97	179.794	1.73%	182.97	179.794	0.53%
Fmin (N)	18.778	19.637	4.57%	23.21	23.444	1.01%	18.78	19.637	2.84%

Figure 7.19 Parametric test 5 output data (20 Hz), (test 005-v2e) and statistical data compared to baseline target

	v2e								
	spans 8/9			N/S only			2 x half spans		
	target	value	diff.	target	value	diff.	target	value	diff.
Fm (N)	108.176	108.053	0.11%	118.97	119.801	0.70%	103.87	103.663	0.20%
sigma (N)	27.588	27.569	0.07%	41.27	40.765	1.23%	32.66	32.388	0.84%
Fmax (N)	199.608	204.665	2.53%	199.61	204.665	2.53%	199.61	204.665	2.53%
Fmin (N)	-20.034	-16.208	-19.10%	0.46	1.669	261%	-20.03	-16.208	19.10%

Figure 7.20 Parametric test 5 output data (30 Hz), (test 005-v2e) and statistical data compared to baseline target

Both at 20 and 30 Hz, there is very little difference seen in the statistical values. In the plot, in particular, there is no change in the two very high peaks at the entry, and the trough at the exit. In the centre portion, where this modification might be expected to have some effect, no significant improvement can be discerned. The maximum force at 30 Hz is slightly higher (5N), which on the criteria chosen makes this option a poorer performer than the baseline, although the 20 Hz force is slightly lower, suggesting only a short duration event. On inspection of the vertical displacement (Figure 7.21), around the centre line there is a slight smoothing of the trajectory, but the total range of movement, through the neutral section zone, is slightly higher than baseline at 5.5mm against 4.6mm.

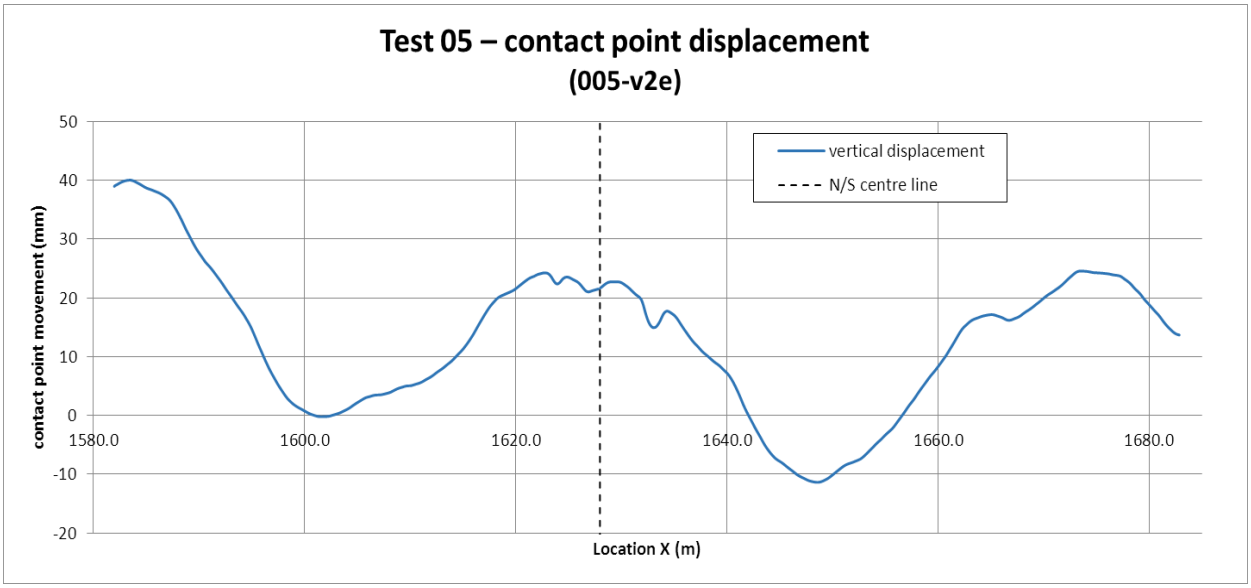

Figure 7.21 Parametric test 5 vertical displacement, (test 005-v2e)

7.5.7 Option 6

Test 6/option 6 is also a theoretical option. Referring again to Figure 6.22, the stiffness of the composite rods can be seen as being approximately half that of the CW it replaces. In this option, the material properties of the composite rod are replaced with values of the properties which have the effect of doubling the bending stiffness, i.e. adjusting the EI from 63,000 kNmm^2 to approx. 134,000 kNmm^2. This is achieved by adjusting the value of elastic modulus, E.

The contact force at 20 Hz and 30 Hz is shown in Figure 7.22 and Figure 7.23, and the vertical displacement in Figure 7.24.

For both the 20 and 30 Hz sets of results, the difference of the statistical values compared to the baseline are barely discernible, in fact of all the test made it is the most similar to the baseline. There is a small (2N) increase in maximum forces at 30 Hz. In some ways this is unexpected, as intuitively, it is the greater flexibility of the composite rods, compared to that of the regular CW, that is the most noticeable difference in a neutral section, and yet here it seems it makes just about no difference at all.

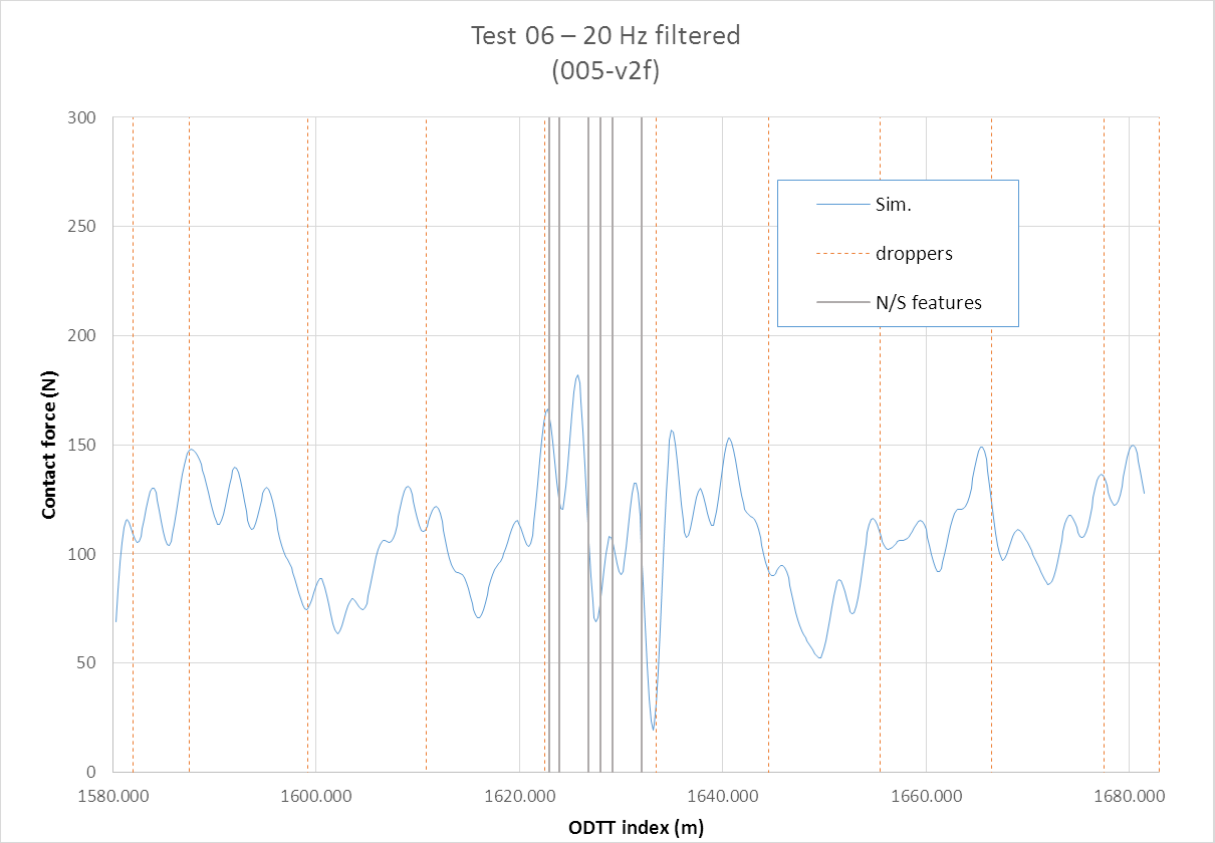

	v2f								
	spans 8/9			N/S only			2 x half spans		
	target	value	diff.	target	value	diff.	target	value	diff.
Fm (N)	108.179	108.209	0.03%	116.96	116.974	0.01%	103.89	103.959	0.06%
sigma (N)	25.033	25.126	0.37%	36.68	36.741	0.17%	28.87	28.967	0.34%
Fmax (N)	182.966	182.005	0.53%	182.97	182.005	0.53%	182.97	182.005	0.53%
Fmin (N)	18.778	19.311	2.84%	23.21	23.373	0.70%	18.78	19.311	2.84%

Figure 7.22 Parametric test 6 output data (20 Hz), (test 005-v2f) and statistical data compared to baseline target

	v2f								
	spans 8/9			N/S only			2 x half spans		
	target	value	diff.	target	value	diff.	target	value	diff.
Fm (N)	108.176	108.206	0.03%	118.97	118.949	0.02%	103.87	103.940	0.06%
sigma (N)	27.588	27.714	0.46%	41.27	41.708	1.05%	32.66	32.823	0.49%
Fmax (N)	199.608	202.845	1.62%	199.61	202.845	1.62%	199.61	202.845	1.62%
Fmin (N)	-20.034	-19.441	-2.96%	0.46	-1.232	367%	-20.03	-19.441	2.96%

Figure 7.23 Parametric test 6 output data (30 Hz), (test 005-v2f) and statistical data compared to baseline target

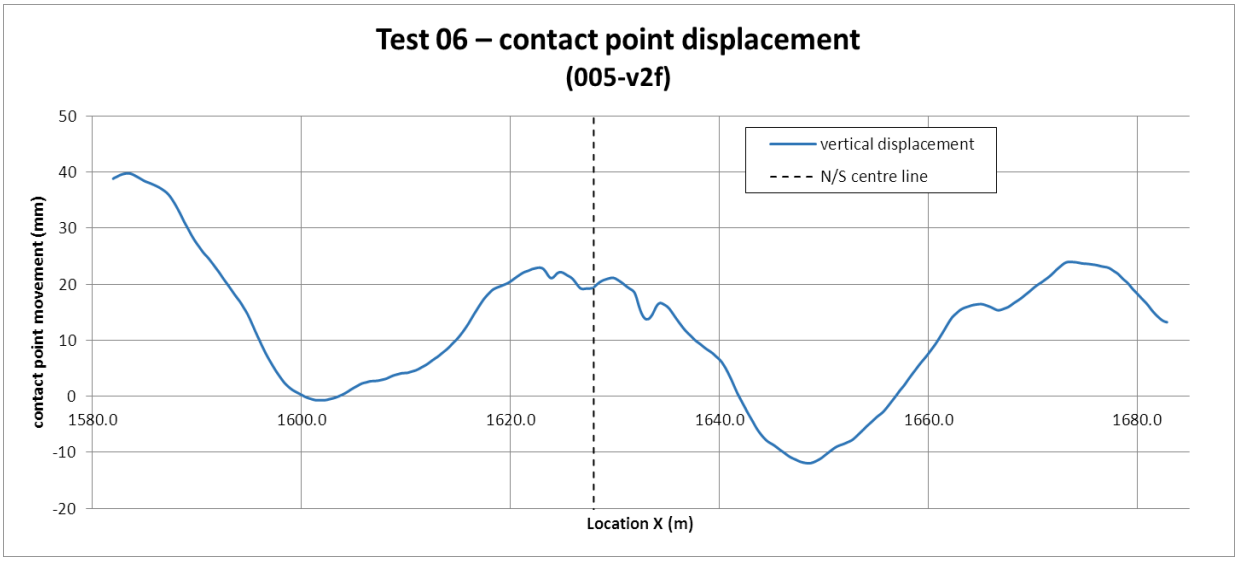

Figure 7.24 Parametric test 6 vertical displacement, (test 005-v2f)

7.6 The options compared

This comparative assessment of the options, tested by the method developed in this research, answers the last of the research questions. The basis of the comparison of the behaviour of the different options tested is the peak contact force (at both frequencies, 20 and 30 Hz), and the range of vertical movement of the contact point (pantograph head to underside CW) as it passes through the neutral section. The values are taken for the neutral section zone only (analysis zone 3).

The contact forces and statistical variations for both 20 Hz and 30 Hz filtering frequencies are shown in Table 7.4.

Table 7.4 Options 01-06 neutral section model: statistical values of contact force for the neutral section analysis zone 3, for both 20 Hz and 30 Hz filtering frequencies.

		01	02	03	04	05	06
		005-v2a	005-v2b	005-v2c	005-v2d	005-v2e	005-v2f
20 Hz	**baseline**						
Fm	**116.96**	116.969	116.808	118.501	117.437	117.840	116.974
σ	**36.68**	36.899	43.987	50.060	30.969	35.797	36.741
F max	**182.97**	183.275	202.310	207.931	177.778	179.794	182.005
F min	**23.21**	24.194	22.013	23.933	69.264	23.444	23.373
30 Hz							
Fm	**118.97**	119.030	118.380	120.871	119.090	119.801	118.949
σ	**41.27**	41.604	53.678	54.217	37.874	40.765	41.708
F max	**199.61**	202.661	232.115	211.472	202.952	204.665	202.845
F min	**0.46**	2.157	1.156	4.616	80.376	1.669	-1.232

Options 1, 5 and 6 are broadly neutral, although option 5 offers a slightly lower maximum force at 20 Hz. Options 2 and 3 are the worst performing, on both maximum force and standard deviation, with option 3 presenting a maximum force of 25N greater than the baseline at 20 Hz, and option 3 is 33N greater at 30 Hz.

Option 4 is clearly the best performer, at 20 Hz standard deviation is lower by almost 6N, and the maximum force is lower by 5N, but the minimum force is much greater than the baseline, by about 45N, showing a much more compact range of force throughout the neutral section. The results are mostly replicated at 30 Hz, with the minimum force moving significantly away from the very low to zero figures of the baseline, up to 80N.

The lower range of forces is corroborated by the vertical displacement of the contact point, where this option is the only one of the six that satisfactorily addresses the 'dip'

that occurs at the exit point, in the baseline, and in all other options tested. The range of vertical displacement for all options is shown in Table 7.5. Option 4 is lowest of all the options, and lower than the baseline. The improvement in this profile is shown in the enlarged comparison in Figure 7.25, particularly at the exit end, as would be expected, as this is the location of the modified parameter. This intervention is not intuitive, and its identification can be seen as a direct result of this form of analysis.

Table 7.5 Options 01-06 neutral section model: vertical displacement of contact point, in millimetres, for the neutral section analysis zone.

	01	02	03	04	05	06
	005-v2a	005-v2b	005-v2c	005-v2d	005-v2e	005-v2f
baseline						
4.624	5.299	5.271	7.208	4.323	5.508	5453

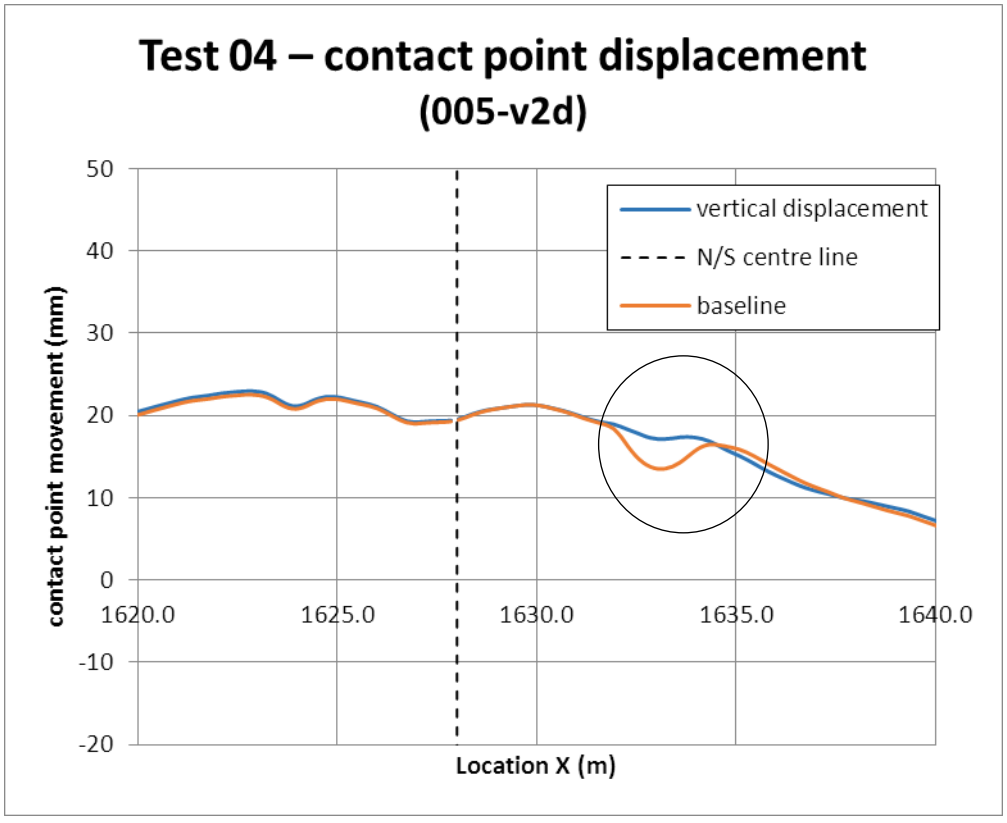

Figure 7.25 Option 4 vertical displacement compared to baseline, showing much improved profile at exit of neutral section (circled)

7.7 Practicalities of implementation

Test/options 1 to 4 are all clearly practical to achieve, as they represent an existing feature that is present in neutral section design.

Option 1 is merely a representation of an existing modification that has already been undertaken on many AF neutral sections in the line, subsequent to the installation at Old Dalby (which represents an earlier practice, see Figure 6.3). Option 2 also represents a current practice modification, albeit one that has been undertaken unilaterally by some local Network Rail engineers. Option 3 is not thought to have been undertaken, but can clearly be achieved, as the use of contact wire in the centre earthed portion of a neutral section is a common practice including in the twin rod version of the AF neutral section (see Figure 3.8). Although again not thought to have been previously undertaken, the installation of the lever arm at the exit end in option 4 merely replicates the arrangement at the entry end, and in fact makes the neutral section fully symmetrical. This intervention is not intuitive, and its identification can be seen as direct result of this form of analysis, and is a direct fulfilment of a research question.

Options 5 and 6 are 'theoretical' options, in that they propose a change to the physical properties of a component, which implies a change in material or form. Should either of these be progressed in further detail then the achievability of these modifications is the primary issue. For option 5, replacing the stainless steel end fitting of the composite rod requires an alternative material or form of construction which is less stiff than stainless steel, and yet which will adequately fulfil the functionality of terminating the composite PTFE/GRP rod. Equally the requirements of option 6, to increase the stiffness of the composite rod to the equivalent of the contact wire is also difficult to contemplate. Increasing the rod diameter would achieve this, but this would increase the offset of the neutral axis at the end point, increasing the local bending in the end fitting, and distorting the profile of the neutral section at this point.

However, as neither of these options appear to deliver any benefit in performance over the baseline case, there is no value in considering these issues further.

7.8 Summary

This chapter has described a limited number of modifications to the standard AF single rod neutral section, and simulated their behaviours using the validated dynamic simulation method whose development and validation has been described in previous chapters. This directly addresses the final research question. The behaviour of the various modifications proposed was compared to the baseline of the equivalent behaviour of the standard neutral section, under the same conditions. The assessment

criteria were peak force and vertical displacement, in accordance with the Network Rail performance requirements, and the published standards. A number of proposals were found to be marginally better or neutral, some others can be discounted for worsening performance, and one in particular, that of introducing a lever arm at the exit end of the neutral section, was found to significantly improve the performance. The baseline neutral sections model used was not perfect or clean, as it was based on the ODTT installation, with only minimal 'tidying up'. As was identified in the conclusions to Chapter 6 this may have imported certain anomalies into the model which may have in some sense contaminated the validation. This qualifies the results obtained, and prompts that a further exercise is undertaken with cleaner baseline data.

As modifications were able to be assessed to determine if they would improve or worsen the behaviour, so the method was demonstrated to be a useful tool for assessing such proposals as part of a more comprehensive programme of developments. It is believed that this form of design assessment of discrete features of the OCL has not been undertaken in this manner before. The identification of a design/performance improvement not previously identified (the exit lever arm) has demonstrated the utility and vindicated the research.

Chapter 8 Conclusions, Discussion, Lessons Learnt and Recommendations for Future Work

8.1 Summary

This chapter describes the work undertaken and the conclusions that can be drawn, together with a critique of the methodology, and suggestions for further work.

8.2 Overview of outcomes achieved

This research targeted a piece of UK railway overhead line electrification equipment known as a short neutral section that displays poor performance, and costs the UK rail industry a significant amount per year. Short neutral sections which use insulators inserted into the contact wire are used to separate the electrical phases and are known to cause problems. Notwithstanding the preference for longer 'carrier wire' types for (much) higher speeds, and the potential of inverter fed systems which might avoid the need for phase separation altogether, the existing requirement for a short neutral section which can be accommodated in the congested UK rail system infrastructure and which demonstrates better performance and reliability is still pressing.

This research briefly described the experience of British Rail with the introduction of the ceramic bead form of short neutral section, and its development during the 80s and 90s, and the subsequent introduction and development of a further (proprietary) type by Network Rail in the early 2000s, which was then assessed in detail in this research. Using information from Network Rail, the significant failures of the main types of neutral sections were analysed over the last 10 years, for which adequate data exists. European practice was also examined where relevant. This prompted the analysis of the dynamic behaviour of the neutral section, in particular the Arthur Flury single rod, using simulation. It was posited that a methodology for experimenting with variations in parameters might be derived, as a tool for optimising the behaviour.

An approach based around computer dynamic simulation was adopted. The methods currently in use by researchers for the dynamic analysis of the interaction of pantograph and overhead contact lines were investigated. An implementation, using the proprietary finite element and multi body software Ansys (rather than bespoke custom code as is current widespread practice) was developed and tested. The current European

standard benchmarks for such systems were used, and the Ansys simulation method developed here was shown to be accurate by these tests. Actual line test measurement data was obtained and the Ansys method successfully applied to simulating the test track OCL, and the output was validated, in accordance with current European practice and standards, providing a validated methodology for pantograph/overhead line interaction, which could then be adapted for investigating the neutral section. Such an application of these methods to the analysis of a neutral section was not known of elsewhere.

Mathematical models of a neutral section were constructed using their physical characteristics, data from drawings and captured in laboratory tests, and then included in the overhead contact line model. A hybrid of flexible finite elements and solid bodies and joint/force elements was used. The performance against real UK pantographs was simulated using the validated Ansys based methodology. Findings were again validated against real line test data, thus proving a robust methodology. Using this method a limited parametric analysis was undertaken, and the sensitivity of the neutral section performance to some particular parameters and characteristics of its construction was examined. The contribution of certain features of construction to its behaviour was noted and one particular improvement was identified which might be counter intuitive, thus demonstrating the value of this analytical approach. This demonstrated the value of this analysis technique as the basis of a more extensive development programme. The method was demonstrated to be a useful tool for assessing such proposals. It is believed that this form of design assessment by dynamic modelling of discrete features of the OCL has not been undertaken in this manner before, and could be seen as innovative.

This research has answered all the research questions set out at the commencement, outlined previously in 1.5, as shown below:

- Do short neutral sections have sufficiently similar characteristics that can be captured in a generic model;
    - Answered in Chapter 3
- Can the current state of art methods for simulating pantograph/OCL interaction be adapted to study the neutral section behaviour;
    - Answered in Chapter 5 and Chapter 6

- Can this simulation of behaviour be used to perform a parametric analysis on the neutral section;
    - Answered in Chapter 7
- Could this parametric analysis identify any improvements to the form of the neutral section.
    - Answered in Chapter 7

This research has not 'solved' the neutral section problem, but it has developed and tested a technique (which is, to the author's knowledge, novel) which can be applied to the problem and which has the capability to move the understanding forward. This has been demonstrated by successfully undertaking a limited number of tests of options to modify the parameters of neutral section components.

8.3 Critique of methodology

In establishing and creating the models described above (in Chapter 5), a number of simplifications, approximations, assumptions and compromises have, of necessity, been employed. It is appropriate to reflect critically on these, and their influence on the outcome.

a) An over-narrow definition of neutral section behaviour

Only a 'narrow' set of issues surrounding the neutral section has been chosen, that of the dynamic interaction with the pantograph. There are other issues, equally significant that are also in play that have been ignored here. Such as the electrical performance of the insulators, the specific material issues around the form of construction (e.g. the fatigue failures of the CW at the extreme end splices of the neutral section, as indicated by the incidents analysis), a wider consideration of short neutral sections in the context of the wider electrical feeding scenario (e.g. consideration of 'switched' forms of neutral section, 'meshed' system created by inverter fed systems). All are valid subject for further study, perhaps as a higher level wider ranging study. However, importantly, in the terms of the initial study proposal, this study has done exactly what it set out to do, and has resulted in a demonstration of a successful application of an existing methodology to identifying design improvement based on simulated behaviours. This is an extremely valuable contribution to knowledge

b) Limited view of the neutral section physical extent

It might be claimed that only a narrow parochial view of what constitutes the neutral section has been taken. The only parametric options which have been considered have been those to do with the construction of the neutral section itself. There is a view, based on experience, that the context of the neutral section in the OCL, i.e. the OCL arrangement in the spans leading into, and away from the neutral section, is an important factor (Network Rail, 2015c). Wire height is also an important factor, leading as it does to less linear pantograph behaviour. None of these have been considered. However none of this invalidates the work done. It may however be useful at a future point to widen the scope of the studies.

c) Reliance on 'emulating' the state of art techniques used for pantograph/OCL behaviour

An initial decision was to use the current state of art pantograph/OCL simulation techniques, which are in place in many industrial and research bodies throughout Europe and have proliferated recently as the Energy TSI requires the interoperable OCL to be validated using such methods. This decision may have restricted the outcomes. It may have been better to consider a novel, customised approach, specifically tailored to the neutral section problem, however it was within the spirt of the original proposal to benefit as much as possible from this work that had been undertaken. The initial proposal for the research, which was well thought through, was to use, or at least adapt, an existing approach, and this has been achieved.

d) Choice of Ansys

The decision to use Ansys was not made at the outset, and was a consequence of the sequential steps in the development of the research path. At each decision point, it seemed Ansys was the 'least worst' option. This was strongly influenced by the initial decision, subsequently abandoned, to use Universal Mechanism and import the flexible body models from Ansys.

As a consequence this decision became locked in, and probably influenced the achievability of (at least some) the subsequent objectives of the research.

The most immediately noticeable aspect of using Ansys was a loss of computational efficiency. Using a regular desktop PC, a specific CAD spec PC, or using a remote access

server over the VPN all had similarly (and similarly poor) performance. A typical simulation, of around 500-600m of OCL, at the standard 200 Hz sampling frequency could take from three to five hours. This clearly creates a practical limitation of the amount of iterative improvement to script and parameters that can be undertaken. It is highly likely that a more custom code would be much more efficient, and the parametric optioneering much less onerous.

This also required effort to be made to overcome the idiosyncrasies of Ansys itself. During the research, it was always important to remain mindful of which actions were directed towards achieving a realistic representation of real world physics, and which were merely workarounds to overcome an Ansys feature.

e) Reliance on techniques mainly used for TSI compliance verification

It might seem misplaced that the platform for the development of the DSM, although intended for ultimate use as a neutral section modelling tool, should be based on a process which is fundamentally created to support the OCL verification process under the ENE TSI. It has been shown that that TSI assessment for an OCL is based upon a very 'broad brush' and 'blunt instrument' approach using only mean contact force and standard deviation, being statistical values that can only really be considered useful or meaningful for a large population of data. This itself is not consistent with the neutral section situation, which is a single discrete feature, and could perhaps be reconsidered. It has been noted that the TSI based simulation methods concentrate on forces at the pantograph CW interface, and ignore other effects (strain, wear etc.) elsewhere in the OCL.

Having said that, little else exists in the way of a commonly accepted methodology, and the initial philosophy and one of the research questions was to consider if an adaptation of existing methodologies could be used.

f) Choice of creating a 'lumped parameter' neutral section model

An identification early in the research, was that in discussion with Network Rail that the manufacturers of the single rod neutral section were reluctant to disclose details of the construction, including material specifications and grades, and feedback was provided that FEM models had been attempted by other research institutes with minimal success.

In studying the work of other researchers, and in particular the PantoTRAIN work, the rationale for using the lumped parameter model of the pantograph is that the model can be retained even when minor details of the construction of the pantograph are changed. And the full MB representation requires full construction details of the pantograph. And it has been shown by these researchers, that the lumped parameter pantograph model produces adequate results.

On this basis, the analogous decision to use a similar lumped parameter model for the neutral section, which had the same obstacles to accessing explicit construction details, seems well justified. Additionally it contributes to knowledge in this area.

The issue might be that the model is being put to a different use here, than for the pantograph example. It has been seen that a detailed model of the OCL, coupled with a lumped parameter model of the pantograph, is effective in replicating the pantograph/OCL interaction, when conducted in a context aimed at studying and optimising the OCL. For those wanting to study and optimise the pantograph, then the explicit MB representation of the pantograph is required. On this basis it could be seen that to study, replicate and optimise the neutral section behaviour, then something more sophisticated than the lumped parameter model might be required. So the research was probably handicapped by the lack of manufacturer data into forcing the lumped parameter decision, no matter how attractive it seemed from a pragmatic view.

Having now received a large quantity of neutral section component parts, the possibility is now open for a more in depth analysis of the components themselves, an approach which was not envisaged at the outset.

g) Choice of (Ansys) modelling parameters

Once the decision to use Ansys was made, downstream of this, decisions about how the Ansys implementation would be undertaken were made. The use of the transient dynamic analysis, instead of say modal analysis, or use of LS DYNA can be examined.

Many of the model decisions were suggested by the interpretation of the state of art work reported such as in the Vehicle System Dynamics special issue on the pantograph catenary benchmark, however most of these 'clues' were tested independently in the research to uncover their usefulness. The results of the two EN 50318 'benchmark' validations vindicate this, as well as the comparison against measured line test data. In fact the quality of the validations output is sufficient to potentially allow the DSM here to

be approved for use under the ENE TSI, which at time of writing would make it one of only two or three such systems in the UK so approved. This is a highly successful outcome to one of the research questions.

The use of 2D vice 3D initially seemed sensible, as the ultimate neutral section model is essentially 2D, i.e. in a single plane. And the literature indicated that results (for the routine pantograph/OCL simulation of course) would be satisfactory. Ultimately it seems that the registration arm effects are more significant than first thought, and although eventually accommodated adequately, further work on replicating the effect in a 2D model would be required, if 2D were to be perpetuated.

The 2D decision also required a modified approach to pantograph head stiffness, as the pantograph of the line test data, the BW HSX 250 had pantograph head stiffness parameters that were non-linear in Y direction, and linear in Z. A workaround was required to accommodate these, although, in the event, no significant difference was seen to a more basic approach. This may have been due to pantograph state of maintenance issues, influencing the line test measurement data.

Assumptions and simplifications in model data, e.g. cylindrical beams for the two main OCL wires, the messenger and contact wire, the application of tension by initial stress, the springs for the droppers, and the 2D equivalent implementation of the registration arm effects, are a mixture of pragmatism and necessity, and seemed to not affect the outputs adversely, considering the successful validations.

h) Avoiding of custom code

Many, if not most, of state of art pantograph/OCL interaction systems certainly in Europe employ custom code written in a specialist language like Matlab or Mathematica. It was an early objective of this research that a more accessible approach using a proprietary FEM and MBS software would be used. This has been achieved, successfully, albeit in some respects the code is 'clunky', many workarounds have been necessary, and the computational efficiency is very poor (2-3 hours for an Ansys simulation, compared 5-10 minutes for a similar size simulation in a Matlab based custom system – in this case the IST/Huddersfield system 'TOPCAT' (Pombo and Antunes, 2018; Pombo and Antunes, 2019)).

Notwithstanding this other researchers using Ansys have chosen to persist in its usage (Sheffield University developed an Ansys based analysis tool (Beagles *et al.*, 2016), and

have chosen to continue to use it to study OCL bridge arrangements) (Beagles and Hayes, 2018).

i) Limited amount of lab testing of neutral section components

The decision above to use the lumped parameter neutral section model also then triggered an issue that to achieve this, some neutral section components needed to be obtained and tested in some way to extract the characteristics needed. This then created an issue with acquisition. It was not possible to purchase the components (at approx. 60,000 euros) as this was outside the budget for the research. No opportunity was available to seek a discount from the manufacturer (explored via Network Rail). The only possibility was to gain some ex-line materials from Network Rail. This put the access to the critical materials in the hands of a third party. Towards the end some material, and in fact, eventually quite a significant amount of material, was generously made available from Network Rail in Wembley; this arrived very late in the research timetable and naturally influenced the amount of lab testing that could be undertaken. The initial limited amount of material was too small to allow anything approaching destructive testing to be done, as only one sample of each component was available. Eventually a great many more components were acquired, but only later, and this is now available to support further work.

j) Choice of ODTT measurement data for validation

It is helpful, and in my opinion, vital, that a simulation method is validated against real results from the real system it is attempting to emulate. For this research, although EN 50318 was available for routine pantograph/OCL simulations, there was no precedent for a discrete feature like a neutral section.

The limited availability of UK line test measurement data is well known. The few items available are referenced in Chapter 6. It was fortuitous that the most recent available data, from the ODTT, actually included exactly the type of AF neutral section that was the subject of this research. The ability to validate against this was too good an opportunity to miss.

However, the data did not seem, on closer scrutiny, to be as good as would have been hoped. There was no absolute CW height measurement, no track side measurement of CW registration point uplift, the supposedly 'raw' data had in fact been already filtered (twice in fact), so losing some granularity, and the OCL was not as perfect as hoped – it is

expected running line OCL will be in a realistically degraded operational state, but it was recently installed, and had seen little usage – and some spans included anomalous force and acceleration events.

Although the validation was successfully completed, this achievement must be qualified; there remains a possibility that the simulation method merely produced a replication of a flawed OCL installation. This must be a fundamental drawback of any validation against field measurement data (as opposed to, say, lab test results). There is no obligation on the process to guarantee 'perfect' OCL as the target.

8.4 Considerations for further work

There are a number of areas where further work can be undertaken. These can be considered to be in three strands:

1. Revisiting this work, and addressing the areas which could benefit from further attention;
2. Taking this work 'as is' and going forward from its conclusion;
3. Taking the general approach described herein and applying it elsewhere in the field of pantograph/OCL interaction.

In any case, should the current Ansys method be perpetuated for any reason then a number of improvements can be made. Consideration should be given to:

- Tidying up and fully documenting the Ansys script;
- Making the code more 'compact';
- Making the method more 'universal' by using control files (text files) for control of process, with less specific data in the hard coded Ansys script;
- Investigating switching off some Ansys functions (and other things) to improve computational efficiency;
- Improving the formatting of output into a much more tidy and useable format, particularly to overcome the Ansys limit on 200 variables, which prevents much of the post processing being done in Ansys itself (which probably could be achieved by creating and then populating an array with all the output variables).

There will probably come a point when the computational inefficiency inherent in Ansys will prompt a consideration of producing custom code in, say, Matlab.

Under category 1, for further work especially on the neutral section, efforts could be directed to seek a better degree of granularity in the analysis:

- Consider looking at the pantograph collector strips separately;
- Consideration of energy and strain, as well as forces, particularly in the components and areas of the neutral section that are known to be weak;
- Create a 3D model to overcome some of the problems with the 2D registration arm effects;
- Extend the frequency range of interest, which might involve other forms of modelling for the contact;
- Create a baseline model for the parametric analysis that is more generic (i.e. not based on an existing installation, i.e. the ODTT) and that is constructed with the future options in mind, so that node/element placement is receptive to the changes from one option to the next;
- Explore many more combinations of options in the parametric analysis, the workload in this may be minimised by applying the techniques described by Grove and Davis (Grove and Davis, 1992);
- Explore these options hand in hand with the manufacturer or other industry partner;
- Test a full neutral section installation in the lab for resilience, and finesse the performance/failure criteria.

Under category 2, this work can be seen as a useful contribution to the wider issues surrounding the neutral section. It can be seen to sit alongside the investigations into specific areas and performances issues such as the fatigue cracking of the contact wire in the lever arm and approaches, and the failures of the ratchet bolts in the connections. This work offers a higher level view of the general behaviour of a pantograph passing through this type of neutral section, although it can be seen to be adaptable to other types due to the essentially same generic construction of neutral sections (as has been shown).

The characteristics examined in this work can be extended to bring out other features, in particular, in addition to the contact forces at the pantograph and neutral section interface, the forces, bending moments, stresses and displacements at significant points within the neutral section (or at least, in the contact wire level components of the neutral section) leading to a better understanding of the operating environment and therefore potential failures within those components.

The lumped parameter form of modelling used here has proved suitable for the intended form of analysis. For a more detailed examination of critical features of the construction, a less generic model is required (the lever arm and ratchet bolts mentioned above are particular features of the specific type of neutral section concerned after all) for which a detailed FEM model should be used. Such models require access to the manufacturers

drawings and technical data, and it is understood that this is not easily obtainable. However, once obtained, the form of modelling and analysis developed here can easily be adapted to include such a neutral section model into the dynamic simulation. (This is not restricted to neutral sections of course, other similar features of the OCL may be modelled in their dynamic context.)

The object of such an exercise would be the same as has been the case since the original short neutral sections were conceived, and which continues to this date, namely the passage of pantographs through a neutral section with minimum constraint. For UK classic lines, this would require passage at speeds of 200 km/h, at least, and possibly 225 km/h, this being the currently foreseen maximum speed on the UK classic network (although not implemented yet, but planned for West Coast and Great Western main lines).

Consider other forms of neutral section, e.g. ceramic bead and Siemens twin rod, and attempt a comparative analysis of these different forms.

Consider the effect of different situations in the approach spans (some Network Rail staff suggest it might be significant).

Should some of the above be achievable, then it might be appropriate to attempt a better optimised neutral section design, and move into prototyping and possibly real line testing of this, which may usefully involve work with industry and/or manufacturers.

Under Category 3, one could consider applying the methodology to other forms of discrete components in the OCL, e.g. section insulators which are known to be of interest to some parties.

8.5 Concluding remarks

This work has been extremely rewarding. It has answered all the research questions set out at the commencement (which wasn't a given), and has made a contribution to knowledge in this field, by providing a methodology for analysis of this type of discrete OCL feature which appears to be novel. The ability of this approach to identify a potential design improvement is a bonus, and indicates that further work using this method can be fruitful. Equally the fact that the dynamic simulation methodology developed here, although not unique, having the capability to become one of only three

UK systems to be authorised for validating pantograph/OCL interactions presented for assessment under the Interoperability regulations is a significant achievement. (The actual logistics and costs of achieving this – which are not insignificant – are not considered here.)

Appendix A Interoperability

"Interoperability" of the European rail system is a European Union initiative aimed at improving the competitive position of the rail sector so that it can compete effectively with other transport modes, and in particular with road. It is part of a series of legislative measures introduced over time by the EU to address the operation, regulation and competitiveness of the EU's railways, part of the goal of creating a 'Single European Railway Area'. This Appendix deals only with the technical aspects of interoperability, relevant to the research in this thesis, but a fuller description of all the related legislation is included in an informative House of Commons library briefing note on the subject (Butcher, 2013) and on ORR website (ORR, 2017a).

Early EU activity in the railway field dealt with the administrative and market aspects of opening up Europe's railways. Subsequent to a white paper in 1990, directives of the early 90s dealt with items such as separate accounting for infrastructure management and train operations, train operator licencing and capacity and access management and access fees.

Subsequently, the harmonisation of technical standards was addressed, under the heading of 'Interoperability'. The aim was to improve the economics of rail transport in Europe.

The objective of interoperability in particular is to create a harmonised European railway system that allows for safe and uninterrupted movement of trains, to:

- ensure compatibility between European railways to allow for through running of trains between Member States;
- harmonise Member State design assessment, acceptance and approval processes to prevent barriers to trade and promote a single European market for railway products and services; and
- deliver benefits of standardisation through economies of scale for railway components, improving the economic performance of European railways (and by implication the European railway supply chain) and the environmental performance of the whole European transport system.

(Department for Transport, 2012b) (EU, 2017b)

The first Directive on railway interoperability (the "High Speed Directive") of July 1996 (Directive 96/48/EC), came into force in 2002 and was followed by a further Directive in 2001 (2001/16/EC), applying the same principles to the 'Conventional' railway networks (the "Conventional Directive"). The particular high speed lines and conventional lines concerned were identified as part of the Trans European Network (TEN) and illustrated on a map drawn up by the European Commission (and contained in EC Decision 1692/96/EC, subsequently superseded by 661/2010/EU). TENs lines consisted of both 'high speed' and 'conventional' lines. Other lines are often referred to as 'domestic' or 'off-TENs' lines.

Subsequently a recast Interoperability Directive (2008/57/EC) has combined and replaced the Conventional Directive and the High Speed Directive. (EU, 2008). The recast directive included a mandate (2010/2576) to the ERA to consider the extension of the scope of the TSIs from TENs lines to the whole of the rail system in the European Union.

The earlier directives had been implemented in UK by the Railways (Interoperability) (High Speed) Regulations 2002 and the Railways (Interoperability) Regulations 2006. The current directive 2008/57/EC has been transposed into UK law as the Railways (Interoperability) Regulations 2011 ("RIR 2011"), and came into force on 12 January 2012 (*Railway (Interoperability) Regulations*, 2011).

The Interoperability Regulations provide for a common assessment and authorisation process for rail projects which are in scope. Generally speaking, assessment is the responsibility of the project entities, supported by Notified Bodies (NoBos) for assessment against TSIs (Dupas, 2010) and Designated Bodies (DeBos) for assessment against Notified National Technical Rules (NNTRs) (RSSB, 2014b); authorisation is granted by the National Safety Authority (the ORR in the UK), and decisions on projects being in scope, and derogations from the requirements, are made by the Competent Authority (see below) (Powell, 2015).

Technical Specifications for Interoperability (TSIs) support the Railway Interoperability Directive 2008/57/EC. They define the regulatory, technical and operational standards which must be met in order to satisfy the 'essential requirements' and to ensure the 'interoperability' of the European railway system (RSSB, 2012b). The 'essential requirements' can be summarised as:

- safety;

- reliability & availability;
- health;
- environmental protection; and
- technical compatibility.

The sub-systems (of the rail system) include both the structural sub-systems, which are (with their accepted acronyms):

- Energy (ENE);
- Infrastructure (INF);
- Control, Command & Signalling (On-board and Trackside) (CCS);
- Rolling Stock locomotives and passenger vehicles (LOC&PAS);
- Rolling Stock freight wagons (WAG)

And the functional sub-systems:

- Traffic Operation & Management (TOM);
- Maintenance;
- Telematics for freight applications (TAF); and
- Telematics for passenger applications (TAP).

Additional 'transverse' TSIs cover more than one sub-system: Persons with Reduced Mobility (PRM), Noise (NOI) and Safety in Railway Tunnels (SRT).

The TSI specifications are developed and revised by the European Railway Agency (ERA), with support from member states and introduced by the EC as Decisions or Regulations. (RSSB, 2012b) (Harassek, 2015) TSIs are generally published as EU Regulations.[26] Between them, the Interoperability Directive and the various TSIs describe a process for authorising new, upgraded or renewed rail infrastructure in accordance to its being assessed and demonstrated to be in accordance with the requirements of the TSIs. Assessment is undertaken by Notified Bodies (NoBos) (Dupas, 2010).

Where the TSI is incomplete for some reason or explicitly does not cover a subject (an 'open point'), the Member State (i.e. the DfT for the UK) is required to 'notify' to the EC what National Technical Rules are filling the gap. These rules are then called Notified National Technical Rules (NNTRs). NNTRs are also used to support a Member State's

[26] In the EU legal context, Directives apply only to Member States, who are obliged to transpose them into National law; Regulations apply directly to duty holders.

'specific cases' that apply to any part of the rail system that needs special provision in the TSI, for example (in the UK) relating to loading gauge. NNTRs are also used for the parts of the network that are in scope of interoperability, but are outside of the TENS network, and also for supporting derogations by demonstrating the satisfaction of the 'essential requirements'. Finally, and most extensively, NNTRs are used to ensure technical compatibility with existing systems and vehicles. (RSSB, 2014b)

Progress with the development of the TSIs continues. As of the end of 2016, updated and merged (i.e. including both conventional and high speed) TSIs exist (in separate versions) for all the subsystems listed above. In a separate exercise, the EU is concerned to eliminate as many open points and national specific cases as possible, seeing these as further barriers to harmonisation.

In particular, as far as relevance to this research is concerned, the updated and merged Energy TSI was published on 18 November 2014, for implementation from 1 January 2015 (EU, 2014a).

More recently, the Fourth Railway Package (4RP), has been introduced (June 2016) and includes both commercial and technical elements, known as the 'market pillar', and the 'technical pillar' respectively (Railway Gazette, 2016). Amongst other measures, the technical pillar includes for an enhanced role for the ERA (now renamed the European Union Agency for Rail) in authorisations, and derogations to TSIs (Fitch, 2017; ERA, 2018).

Appendix B Derivation of Detailed OCL Characteristics

B.1 Introduction

The purpose of this Appendix is to describe, in greater detail than given in the main text, how the data for the physical characteristics of the components of the OCL were determined, for use in the models described in Chapter 5. In particular how the data was 'triangulated' with data used in other studies, and raw technical elaborations. Mostly these are the specific applications of formulations found in standard texts on OCL fundamentals, e.g. (Bond, 1987; Keenor, 2016; Kiessling *et al.*, 2016) and are provided for completeness.

B.2 Section properties

B.2.1 General

Due to the Timoshenko/Euler Bernoulli equation for modelling the behaviour of a tensioned beam being used in the Ansys simulation, and as this equation (B.1a) includes bending stiffness, including the values of E (elastic modulus) and I (second moment of area) along with linear mass ρ as critical parameters, it is necessary for these to be represented accurately. The Euler Bernoulli equation relevant to this application, as identified in a number of papers in VSD 53-3 (e.g. Finner *et al.*, 2015), is:

$$\rho \frac{d^2z}{dt^2} + EI \frac{d^4z}{dx^4} - T \frac{d^2z}{dx^2} + c \frac{dz}{dt} + P(x,t) = 0 \qquad \text{Equation (B.1a)}$$

The Timoshenko beam equation, which is the beam formulation implemented in Ansys for the element types used, contains an additional second order term for shear deformation:

$$\frac{EI}{kAG} \frac{d^2z}{dt^2} \qquad \text{Equation (B.1b)}$$

Where A is section area, G is the shear modulus of the material, and k is the Timoshenko shear coefficient, which varies by section geometry, but for a circular section is normally

(but not universally) taken as 6/7 (*Timoshenko beam theory*, 2019). The shear modulus *G* is related to the elastic modulus by the value of Poisson's ratio, γ.

$$G = \frac{E}{2\,(1 + \gamma)} \qquad \text{Equation (B.1c)}$$

The exact formulation is not explicitly identified in the Ansys technical manuals. However, the input variables of linear mass, element section geometry, elastic modulus and Poisson's ratio are required, from which values of *I* and *G* might be determined internally in Ansys.

B.2.2 Catenary (messenger) wires

The catenary (messenger) wire is a stranded conductor (essentially a rope), made up of a number of strands, arranged in 'lays', typically for OCL purposes 19 identical strands in a 1:6:12 arrangement, see Figure B.1. The individual strands are typically either 2.1, 2.5 or 2.8 mm diameter (British Standards Institution, 1997; Liljedahl Bare Wire, 2014).

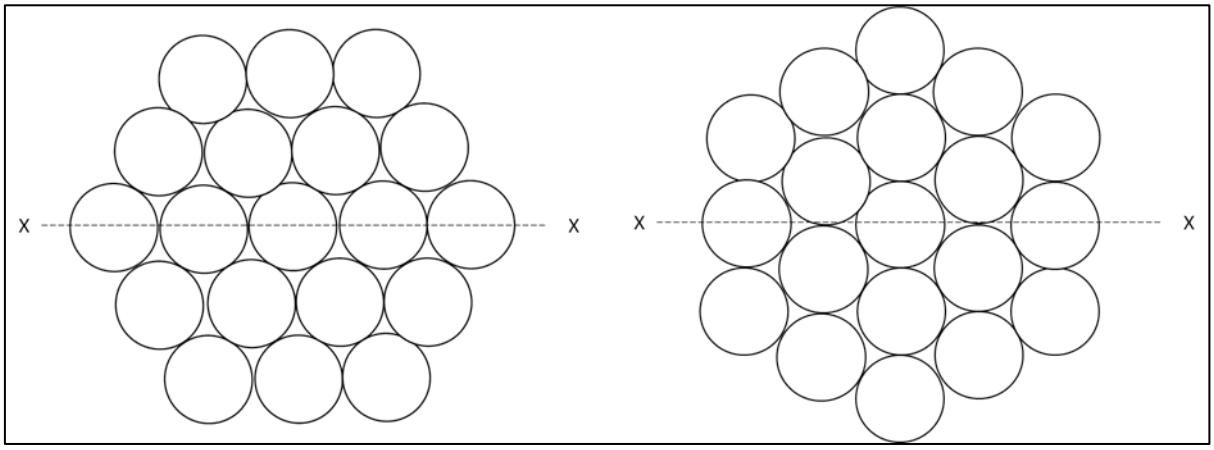

Figure B.1 19 x stranded conductor, major and minor axes

As the orientation of the entire conductor stranding rotates along its length, the actual section property, second moment of area, I, varies from its major to its minor axis value, linearly with length. The two values of I calculated use the maximum and minimum of this value, corresponding to the major and minor axes, shown on Figure B.1, dependent on the orientation of the strand pattern.

The value of I for the circular section of each individual strand of radius r is given by $I_{xx} = (\pi/4)\, r^4$, and the value of I of the whole stranded section is derived from the parallel axes theorem,

$$I_{x'x'} = I_{xx} + A\ O^2$$ Equation (B.2)

Where O is the offset between the x'x' and xx axes. For both the major and minor axes, maximum value of I is calculated:

$$I_{xx} = \sum_{j=1}^{n} I_j + A\ .\ O_j^2$$ Equation (B.3)

The effective value of I is taken as the mean of these two values.

For the purposes of the Ansys models of the OCL, the messenger wire is represented by a circular cross section of equivalent diameter to generate the same value of I. This is because the Ansys element type chosen, BEAM189, will generate section properties automatically from input data, and overriding these (using ASEC command) is unnecessarily complex. The equivalent circular diameter D_{eq} is thus given by:

$$D_{eq} = 2\ .\ \sqrt[\frac{1}{4}]{\frac{4\ .\ I}{\pi}}$$ Equation (B.4)

The values so developed for a range of commonly used messenger conductor sizes and stranding are shown in Table B.1 below. As can be seen, the refinement for the rotated axis makes only a very small effect on the actual value of I..

Table B.1 Derived section properties for typical messenger wires

Messenger wire (strands/strand diameter)	**I_{max} (mm⁴)**	**I_{min} (mm⁴)**	**I_{mean} (mm⁴)**	**Equivalent circular diameter D_{eq} (mm)**
	From equation 3	From equation 4		From equation 5
19/2.1	384.834	384.776	384.805	9.409
19/2.5	772.958	772.843	772.901	11.202
19/2.8	1216.265	1216.083	1216.174	12.546

B.2.3 Contact wires

The contact wire profile is a circular section with the inclusion of two grooves either side, for the clamps. The sections in common use are described in European standard EN 50149 (British Standards Institution, 2012c), see Figure B.2 for examples. As with the messenger wire, for the Ansys model an equivalent circular section is assumed, based on the actual value of I, second moment of area, as shown in Table B.2 below.

Table B.2 Derived section properties for typical contact wires

CW section area (mm^2)	**Actual diameter (mm)**	**I (mm^4)**	**Equivalent diameter (mm)**
			From equation 5
107	12.30	836.94	11.427
120	13.20	1118.70	12.287
150	14.80	1766.36	13.773

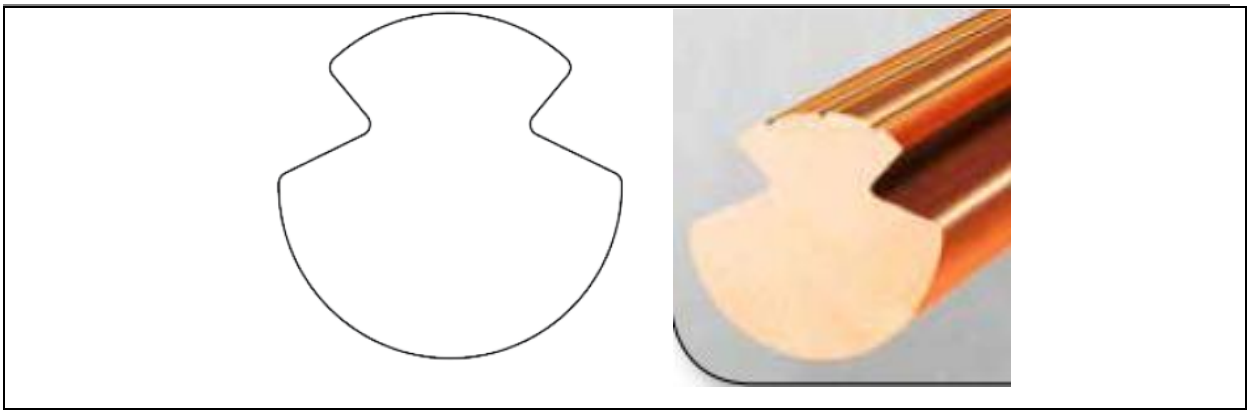

Figure B.2 Typical contact wire cross sections (Liljedahl Bare Wire, 2014)

B.3 Material properties

B.3.1 Elastic modulus (Young's modulus)

A stranded conductor (cable or rope) does not possess a real Elastic modulus, as it is in fact a mechanism rather than a homogeneous material. In technical literature it has been shown that stranded conductors display three phases of extension under load: an initial 'set', an elastic extension, and then a plastic extension (Bridon, 2013). However, an effective elastic modulus can be established for the middle phase, if it can assumed that the cable has been preloaded, and that the initial phase of a permanent set has been

undergone. For the OCL cable in the messenger wire, this is a realistic assumption, due to the nature of the installation procedure, and the tension in the wire (messenger wires can typically be tensioned to above 50/60% of breaking load). For the dropper wire, as noted below, this is not necessarily the case.

The technical literature detailing this value is very sparse, examples are (Welbourn, 1917; Copper Development Association, 2004; Beaty and Fink, 2013), however the Welbourn reference (notwithstanding its dating from 1917) gives a methodology for a 19/0.83" copper cable (which is the imperial equivalent of 19/2.1mm) and, after converting from imperial units, suggest a value of E of around 117 kN/mm^2. This is corroborated by Beaty and Donald. Values given in EN 50318:2018, which are taken from German railways (DB) practice, are slightly different.

For the contact wire, the value of Young's modulus, for all commonly used alloys of copper (Cu ETP, Cu Ag, Cu Sn), is given as E = 120 kN/mm^2 in all the major manufacturers technical literature (NKT, 2006; Liljedahl Bare Wire, 2014).

Table B.3 Commonly used stranded messenger wire make up, and elastic modulus from various sources: [1] (Welbourn, 1917; Copper Development Association, 2004; Beaty and Fink, 2013), [2] (British Standards Institution, 2018)

Nominal cross section mm^2	**No. strands/dia**	**Linear mass kg/m**	**Elastic modulus N/mm^2 [1]**	**Elastic modulus N/mm^2 [2]**
65	19/2.1	0.596	117,000.00	84,700
95	19/2.5	0.845		100,000.00
120	19/2.8	1.060		97,000.00

B.3.2 Dropper stiffness

The stiffness K (N/m) of a braided bronze wire, as used for the droppers, can be developed from the elastic modulus, which itself is determined by the method in B.3.1 above.

$$K_D = EA/L \qquad \text{Equation (B.5)}$$

Note that this is dependent upon length, and is not a 'material' property, and individual droppers of differing lengths will have a different stiffness.

There is no formal standard for dropper wires, although only a limited range are actually used within Europe, and can be considered as a de facto standard, and these wires and their properties can be identified from manufacturers literature. The general form is a multiple stranding, and the most common are shown below. The values of E are taken from a number of sources either directly or by inference but mainly the benchmark data in EN 50318:2018 (British Standards Institution, 2018). Note the disparity in values, varying by a factor of 10. It is possible some of these (the low values) are errors, as there is a mixture of elastic modulus and stiffness given. Stiffness is derived from elastic modulus as shown in equation (B.5).

Table B.4 Commonly used stranded dropper wire make up

Nominal cross section mm²	**No. strands/dia**	**Linear mass kg/m**	**Elastic modulus N/mm²**
10	7/7/0.5	0.089	10,000.00
12	7/7/0.56	0.117	84,700.00
16	7/7/0.65	0.155	10,000.00
25	19/7/0.5	0.246	

On consideration of the issue of stranded wires and 'apparent' elastic modulus, it has been seen above that the pre-loading of the messenger wire at a high (relative to breaking load at least) tension will put the wire into its middle phase where elastic modulus is conventionally found. For the dropper wires, as they are loaded at much lower values, only by a few kg as the weight of the CW as shown Table B.5, it cannot be considered they have entered the middle phase; the strands have not bedded in and been compacted, the 'initial set' has not been achieved. In this case, the apparent elastic modules is more associated with the effect of the individual strands compacting, and a much lower value obtains. The values quoted, from sources concerned with the same studies as reported here, can be considered indicative of these lower values.

Table B.5 Commonly used stranded dropper wire typical loadings

Nominal cross section mm²	**No. strands/dia**	**Typical load (N)**	**Typical stress (N/ mm²)**	**% of breaking stress**
10	7/7/0.5	100	10.000	1.70%
12	7/7/0.56	100	8.333	1.41%
16	7/7/0.65	100	6.250	1.06%

25	19/7/0.5	100	4.000	0.68%

B.4 OCL static geometry

B.4.1 General approach

The OCL is a highly elastic system, subject to tensions and self-weight (gravity) loads, and is consequently subject to large deformations to arrive at its steady state position. To create the Ansys model accurately, it is necessary to create an unloaded OCL geometry that will, under application of the static loads (tensions, point masses and self-weight), deform into the recognisable loaded geometry of the steady state OCL, that is familiar. By establishing this with a high degree of accuracy reduces the amount of displacement during the equilibrium finding stage in Ansys, and hence minimises the strains that might be so introduced.

B.4.2 Steady state (loaded) OCL geometry

The principle of the catenary suspension, as outlined in Chapter 2, is that the desired profile of the contact wire (whether level or 'pre-sagged') is delivered by the accurate calculation of dropper lengths, based upon the known masses of the wires and components, and the tensions in the two conductors. The following is based upon an adaptation of the method shown in (Bond, 1987), and is also referred to as the 'separated model system', described in (Cho, 2015), relating to the separate models of CW, generating dropper loads, and messenger wire model using the dropper loads. Although the common formulation of the 'catenary' curve is as a hyperbolic cosine, in this case the effective profile is that of a parabola with point loads. The actual profile of the wire between the point loads, is assumed linear here, and the Ansys process will generate the catenary hyperbolic profile.

In the following derivation, the following legend is used, (note the subscript *m* is used for the messenger wire for clarity):

R_A, R_B reactions at supports A and B

T_m, T_c tension in catenary wire (messenger) and contact wire

W_m, W_c, W_e, W_r, linear weight of catenary wire (messenger), CW, effective CW, and relaxed CW

n number of droppers

W_{dj} weight of dropper j

P_j point load at dropper j

X_j distance from left support point of dropper j

F_j distance below support point (fall) of top of dropper j

OCL component weights are usually expressed in kg, and are converted to consistent units, N, by the gravitational acceleration g = 9.806 m/s^2

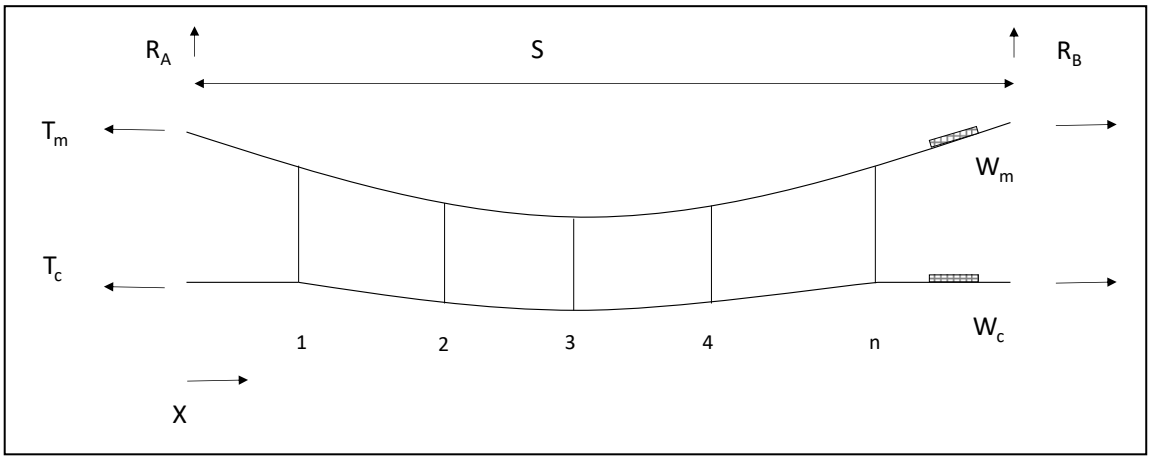

Figure B.3 Steady state OCL geometry for a typical span and legend

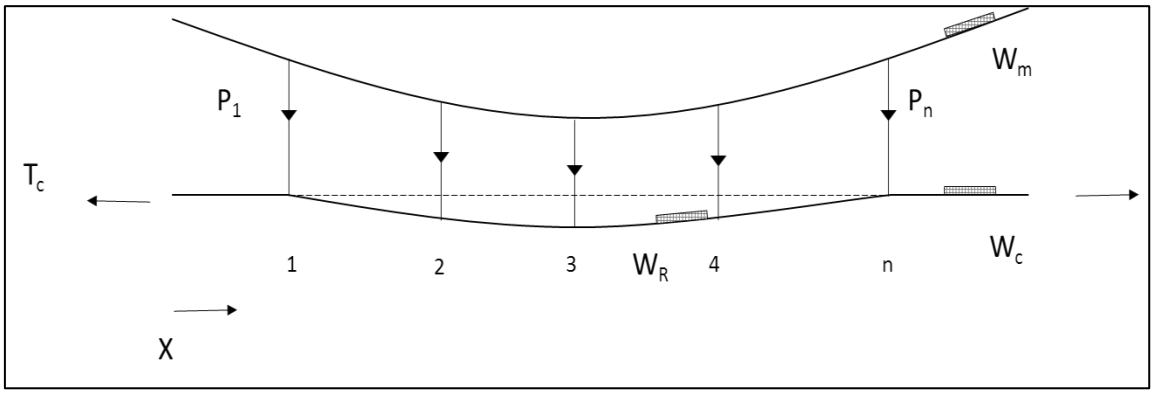

Figure B.4 Steady state OCL geometry showing imposed loads

The geometry is shown in Figure B.3 and the imposed loading in Figure B.4. The approach is to take moments about the dropper/catenary connection (i.e. 'top of dropper'), on the principle that at steady state, moments to left of this point equal the moments to the right of this point, and both equal zero.

$$M_L = M_R = 0$$

The unknown in this equation is the offset (fall, F) of top of dropper from (i.e. below) the suspension point, and the equations can be solved for this. See Figures B.5.

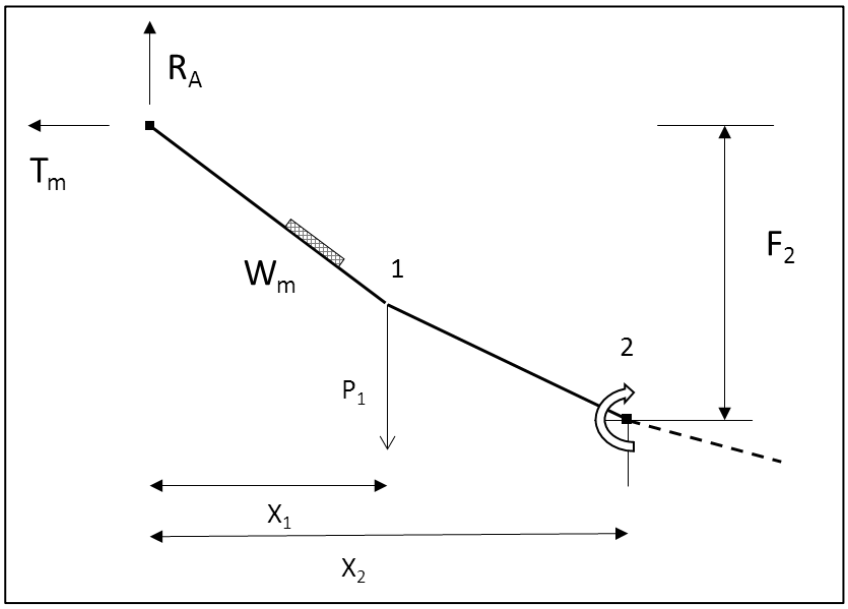

Figure B.5 moments acting about top of dropper 2

M_L = R_A moment – T_m moment – W_m moment – P_1 moment = 0 Equation (B.6)

Expanding, we have

$$(R_A.X_2) - (T_m.F_2) - \left(W_m.X_2.\frac{X_2}{2}\right) - P_1\,(X_2 - X_1) = 0 \qquad \text{Equation (B.7)}$$

Which can be rearranged to solve for F_2 as

$$F_2 = \frac{\left\{(R_A.X_2) - \left(W_m.X_2.\frac{X_2}{2}\right) - P_1\,(X_2 - X_1)\right\}}{T_m} \qquad \text{Equation (B.8)}$$

And can thus be expressed in generalised form for all such points 1 to j to be solved:

$$F_j = \left\{(R_A.X_j) - \left(\frac{W_m.X_j^2}{2}\right) - \sum_{k=1}^{j-1} P_k\,.(X_j - X_k)\right\} / T_m \qquad \text{Equation (B.9)}$$

The actual dropper length is the system height (messenger – contact wire separation at the support) less the fall F, plus the contact wire sag at that point. Also note that all

calculations are from assumed centre lines of messenger and contact wire, but conventionally dropper length (and system height) is measured from catenary centre line to underside of contact wire, therefore a correction of half a contact wire diameter needs to be made.

W_m and T_m are known, and the reactions (for a symmetrical span with equal system heights at each support) are given by:

$$R_A = R_B = \left\{ X_B \,.\, (W_m + W_c) + \sum_{j=1}^{n} W_{dj} \right\} / 2 \qquad \text{Equation (B.10)}$$

The additional complexity is in an iteration for derivation of the mass of the dropper itself (required for reactions and dropper point loads), as this is dependent upon dropper length, which is itself part of the solution. Additionally there needs to be an understanding of the effect of contact wire pre-sag. This is dealt with below.

Contact wire pre-sag, where utilised, is an attempt to improve current collection by equalizing compliance at mid span with that at the support, see Chapter 2. Conventionally this is parabolic in form, and around 1/1000 of the span length. Pre-sag is implemented between the first and last droppers, as typically there is no dropper at the support point. The effect of pre-sag on dropper loads is to relieve the intermediate droppers (2 to n-1) of some load, and transfer this to the extreme droppers, 1 and n.

The sag of a tensioned wire acting under its own self weight is a hyperbolic cosine function, but for the spans and sags considered here, it can approximated to a parabola (Bond, 1987), and is given by:

$$Sag = W_{.} L\,(L\text{-}x)^2/2T \qquad \text{Equation (B.11)}$$

Inverting, the *effective* self-weight (reduced weight) of the contact wire (W_R) forced to a given sag (the pre-sag, PS) is given by:

$$W_R = PS\,.\,T_c\,/\,L^2 \qquad \text{Equation (B.12)}$$

Consequently the intermediate droppers (2 to n-1) are loaded by the effective weight, and the end droppers (1 and n) additionally see the balance of the effective weight to the actual weight. As shown in Figure B.6 and equations (13 and 14).

$$P_2 = (W_R \,.\, L_2) / 2 + (W_R \,.\, L_1) / 2 + W_d \qquad \text{Equation (B.13)}$$

$$P_1 = W_C \,.\, X_1 + (W_R \,.\, L_1) / 2 + (W_R - W_C)\,(Xn - X_1) / 2 + W_d \qquad \text{Equation (B.14)}$$

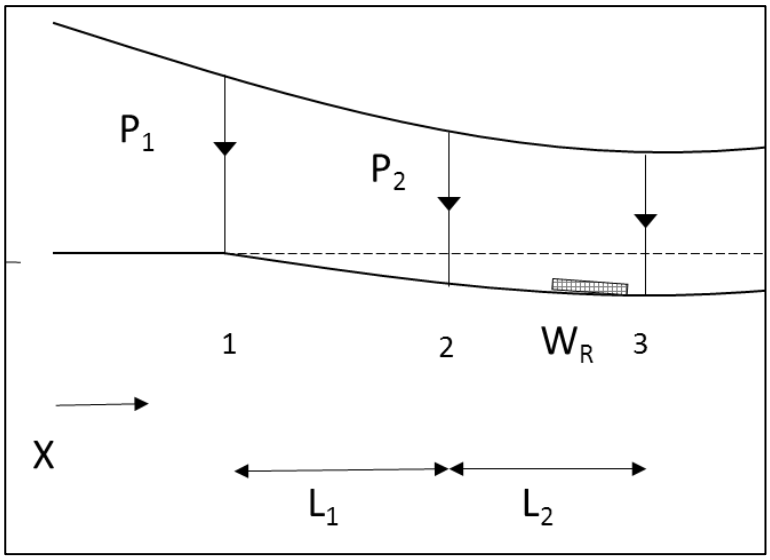

Figure B.6 Dropper load calculation notation

Dropper weight W_d is then part of the calculation. Typically droppers are formed of three elements: a messenger clamp, a contact wire clamp, and a length of wire or braid connecting them. The expression for the weight (W_d) of a dropper can be given by:

$$W_d = W_{cm} + W_{cc} + (L_d \,.\, W_{dw}) \qquad \text{Equation (B.15)}$$

Where

W_{cm} = the weight of the catenary (messenger) clamp

W_{cc} = the weight of the contact wire clamp

L_d = the length of the dropper wire

W_{dw} = the linear weight of the dropper wire

The length of dropper wire included in a dropper is taken as the dropper length, plus an additional allowance for the 'tails' of the wire at the end of the clamps, see Figure B.7, for a typical example of an Arthur Flury dropper used in Network Rail Series 1 OCL. For this work, this value has been taken as 0.150m. Consequently the wire length in a dropper, is:

$$L_d = D_L + 0.15$$ Equation (B.16)

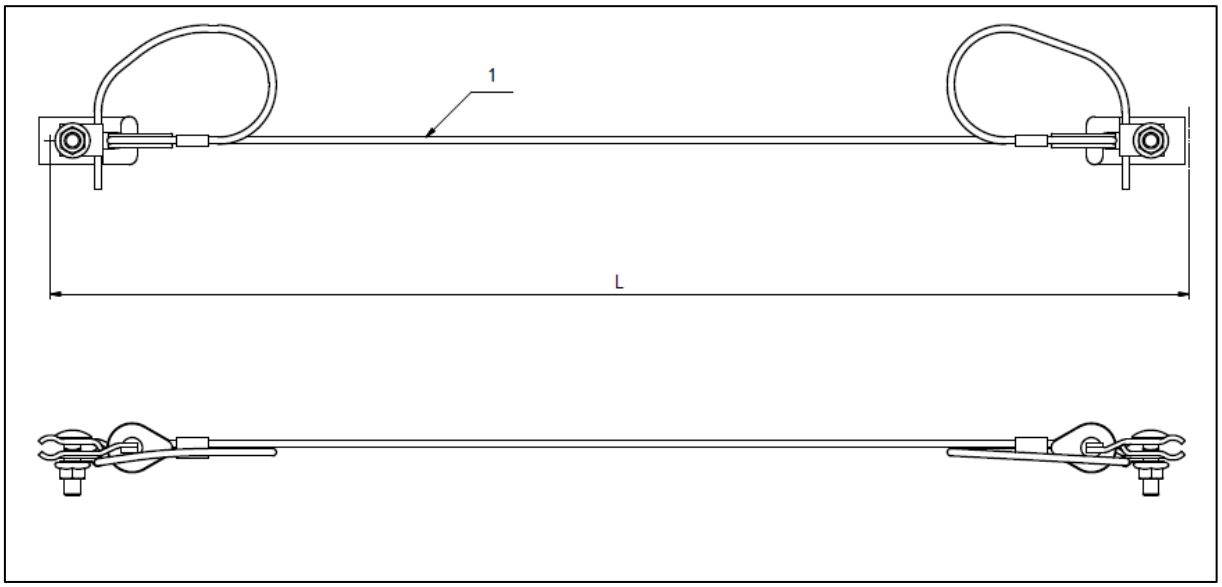

Figure B.7 Flexible dropper by Arthur Flury from the F+F series 1 catalogue (Furrer + Frey, 2016c)

Registration arms

There is no contact wire support or dropper at the support and registration points, and hence the mass imposed by the registration arm must be accounted for as well. Therefore for each end dropper, i.e. droppers 1 and n, the load also includes one quarter of the weight of a registration arm, on the assumption that half of the registration arm weight applies on the CW, and that this is distributed to the two spans either side. Additionally one half of the weight of a CW clamp is included, under the same principle

The radial load uplift force created by the heel setting of the registration arm (see Figure 5.7 in Chapter 5) is applied at the support point, as it affects the geometry of the CW. Using the notation in the figure, the uplift force F_R is given by

$$F_R = \text{Rad} \,.\, \text{Heel} \,/ L_{arm}$$ Equation (B.17)

The radial load is derived from the stagger and track curvature, and is described later in this Appendix.

In calculating the dropper weight to be included in equations 13 and 14 above, for calculation of support reactions and dropper loads P_j, a starting dropper weight

assuming dropper length is zero, is used. Due to weight of clamps, this gives a non-zero dropper weight, and due to greater relative weight of clamps to wire, is a reasonable starting point for the iteration. After a first iteration of calculations, the calculated dropper lengths can be substituted for the initial zero assumptions, and a new set of dropper lengths thus calculated. The iteration can be repeated until the error between the calculated and the input dropper lengths is sufficiently small. For an accuracy of 0.1 mm it is found that convergence can be achieved in 4 or 5 iterations. Note that normal dropper manufacture accuracy is of the order of 5 mm.

B.4.3 Application of point loads

The effect of the neutral section in the span will cause the normal dropper lengths and profile calculation to require adjustment, as they assume constant linear mass of the main conductors, and do not account for the point loads of the individual neutral section components.

This is achieved by the application of conventional 'point load in span' adjustments, described in (Furrer + Frey, 2016b) and confirmed by (Bond, 1987). In this case in a span of length L, the sag d, at a point load P, at position x, is given by:

$$d = \frac{x\,(L-x)}{T\,.L}\,.\;(Pg + \frac{W.g.L}{2}) \qquad \text{Equation (B.18)}$$

And the reduction in dropper length R_x at each point x, (where y = L-x) is

$$R_x = \frac{P.g.x.y}{T.L} \qquad \text{Equation (B.19)}$$

In our case, as the neutral section is an assembly of point loads, the full affect will be derived by the overlay of the individual effects of 3 sets of point loads:

- The centre insulators (and associated fittings);
- The long CW insulators and spring droppers (and associated fittings);
- The messenger wire insulators (and associated fittings).

Additionally, in each case, the mass of the elements will be the net mass, i.e. excluding the mass of messenger and CW wires they replace, and which has already been taken into account in the initial dropper calculations.

B.5 Stagger and radial load

The radial load at the registration point is the load in the registration arm that is the component of the CW (or messenger) tension caused by the angle the tensioned wire makes as it is 'pulled off' to the required lateral offset, known as 'stagger'. This can be calculated from the angle subtended at the registration point, as RL = 2 T tan α/2, but this is redundant as the trigonometry used to derive the angle α can be used directly to derive the radial load. See Figure B.8.

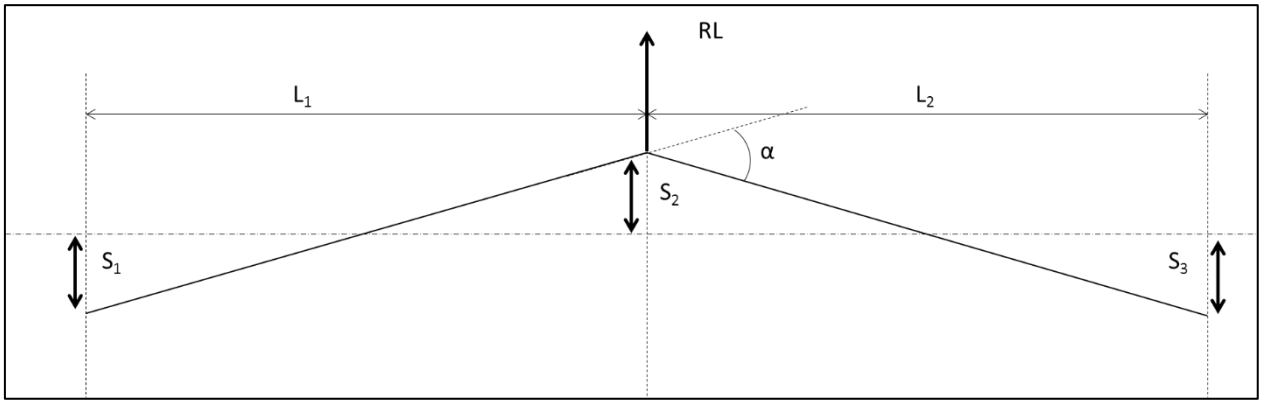

Figure B.8 Radial load on tangent (straight) track

For tangent (straight) track, the radial load RL_C in the CW is given by comparing the triangles created by the track centreline, the stagger and the path of the contact wire to that of the tension and radial load, so that

$$RL_C = T_C \, . \, [\, (S_2 + S_1)/L_1 + (S_2 + S_3)/L_2 \,] \qquad \text{Equation (B.20)}$$

For curved track, a different approach is employed. The curvature of the track is usually given by reference to the 'versine' of the curve, rather than its radius. The versine is the offset of the chord representing the span between the successive registration points, and is the common way of expressing a curve in UK railway track survey, design and setting out, and so is also then used on OCL layout plans and drawings. The versine of an angle θ is v = 1 – Cos θ and so the approximation $v = L^2 / 8R$ can be made (as in our case radius is much larger than versine).

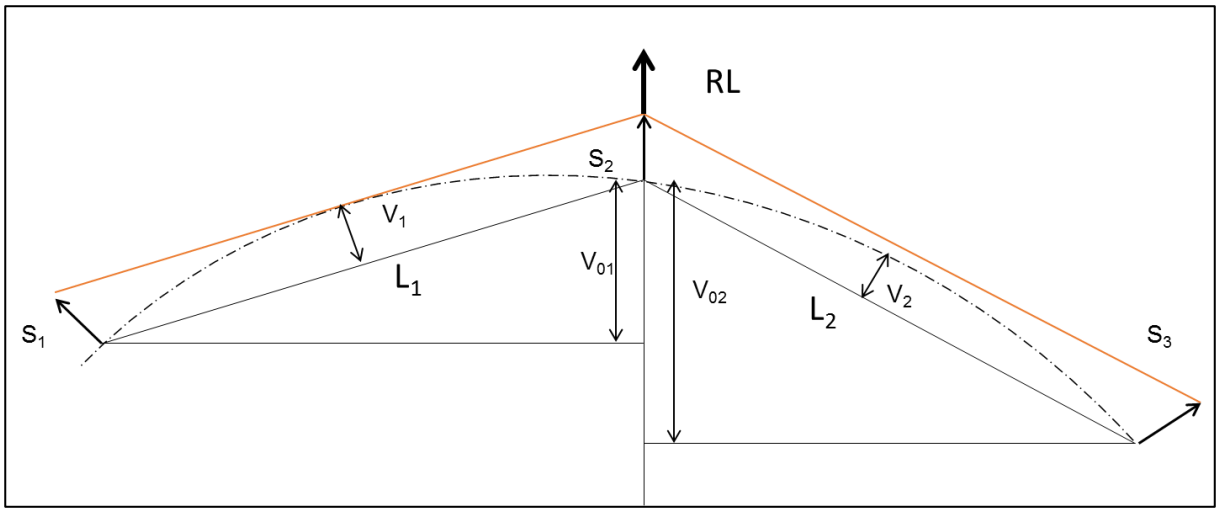

Figure B.9 Radial load on curved track

For the case of curved track, see Figure B.9. We can also make the approximations that $V_{01} = 4 \times V_1$, $V_{02} = 4 \times V_2$ and that staggers are essentially parallel, so the derivation of CW radial load on a curved track is given by

$$RL_C = T_C \,.\, [(S_2 - S_1 + 4.V_1)/L_1 + (S_2 - S_3 + 4.V_2)/L_2] \qquad \text{Equation (B.21)}$$

making appropriate adjustments for the sign of stagger and versine where necessary. The same expressions are used for the messenger wire, substituting the messenger tension.

B.6 Assumptions

Some simplifying assumptions made in the OCL geometry calculation in B.4 have a minor impact on accuracy of the results.

The messenger and contact wires are considered to act as strings rather than beams.

Dropper elasticity and extension – droppers are assumed to be 'stiff' and that the dropper load does not contribute to any extension of the dropper.

Messenger elasticity and extension –messenger wires are assumed to be 'stiff' and that the messenger tension does not contribute to any extension of the messenger.

Plane vs 'staggered' OCL geometry – the staggering OCL increases to length of the OCL segments in the span compared to the 'plane' span length.

In the calculation of mass of the messenger segments (between droppers) the length of the segment is considered only the difference in the x-coordinate locations, not the developed length of the inclined messenger wire (greater at the ends of the spans).

Assumptions about stagger and radial load are included in the calculation for each span, notwithstanding the actual stagger and radial load.

Appendix C Detail of Line Test Measurements and Data

C.1 Summary

This Appendix describes the detail of the provenance, collection and processing of the pantograph/OCL line test data. This was provided by Furrer + Frey for both regular OCL and neutral section elements, and was used for comparison with the simulation results, to achieve validation of the model and simulation method.

C.2 Introduction

The data for these tests was sought so that the pantograph/OCL simulation methodology, developed for the neutral sections study, could be validated for credibility before being used to analyse and critique the neutral section. The validation of results of simulation methods against line test data is a fundamental requirement of the ENE TSI and is specified in relevant European standard EN 50318 (British Standards Institution, 2002), and in turn the requirements for the line test measurement themselves are also subject of European standard EN 50317 (British Standards Institution, 2012a).

C.3 Background to tests

In line with the application of the relevant UK legislation (*Railway (Interoperability) Regulations*, 2011), the new Hitachi built IEP trains (Hitachi Rail Europe, 2018), and the Furrer + Frey designed new OCL (known as Series 1) (Dolphin, 2014; Furrer + Frey, 2014) had to be tested for acceptance as part of the commissioning of the newly electrified Great Western Electrification Project (GWEP) (Network Rail, 2011b). Pantograph and OCL interaction tests are a component part of the testing in accordance with the relevant Energy and Locomotive TSIs (for TSI details see Appendix A).

Some of the dynamic tests were undertaken at Network Rail's Melton test track (formerly called Old Dalby, and still referred to as such in some reports) (Network Rail, 2017), undertaken by Hitachi, and for which purposes a portion of the test track's OCL

electrified section was converted to Furrer + Frey Series 1 type equipment. The tests were undertaken during June 2016.

The tests were conducted using instrumented pantographs mounted on an Hitachi IEP class 800 train set. The instrumentation of the pantographs, and the recording and processing of the data, was carried out by DB Systemtechnik (DBST) (DB Systemtechnik, 2016b). Test were undertaken in accordance EN 50317 (DB Systemtechnik, 2016a). The data was supplied to myself by Furrer + Frey, who had received it from Hitachi (Bryan, 2016).

C.4 Test protocols, and data collected

The Old Dalby Test Track (ODTT) has OCL erected over a section of the Up (northbound) line (see Figure C.1). This OCL is a mixture of many different types. The Series 1 section extends from 10.428km to 13.318 km (first and last in-running registrations) a length of approx. 2.8 km. The types of OCL outside this are Mk3D to the south and UK1 to the north. The Series 1 section is shown on two layout plans 118049-FAF-REP-EOH-000015 (rev02) and 118049-FAF-REP-EOH-000016 (rev02), an extract from which is shown in Figure C.2.

Figure C.1 Hitachi IEP train on test at Old Dalby. Furrer+Frey Series 1 OCL installed on Up (northbound) track, on LH side in the photo (Photo credit Barry Duffin)

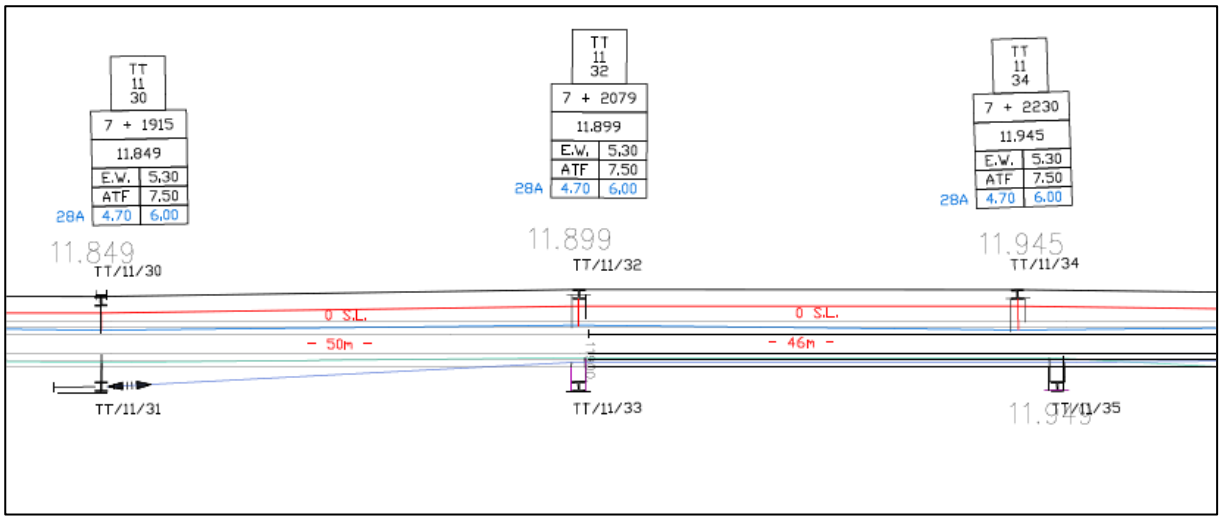

Figure C.2 Extract from Old Dalby OCL layout plan (drawing 118049-FAF-REP-EOH-000015 (rev02))

The Series 1 OCL over this section is a widely varying sequence of specific OCL features, and its close spacing is not typical of a normal OCL installation on a running line. This is because all these features, bridges, overlaps, crossovers, neutral sections of both types, needed to be included for testing and validating as part of the Series 1 OCL development, and TSI assessment process.

DBST instrumented pantograph measurement data is available for the whole of the Series 1 section. Several test runs were made over several days, and the data chosen as the basis for this research element is in file A015167026_0001.SA1. This is as shown in Table C.1 below. Train formations and types are shown in Figure C.4.

In addition a video (of varying quality, but mostly poor) of the pantograph during the test, indexed with certain output data, is available, see sample screen shot in Figure C.3.

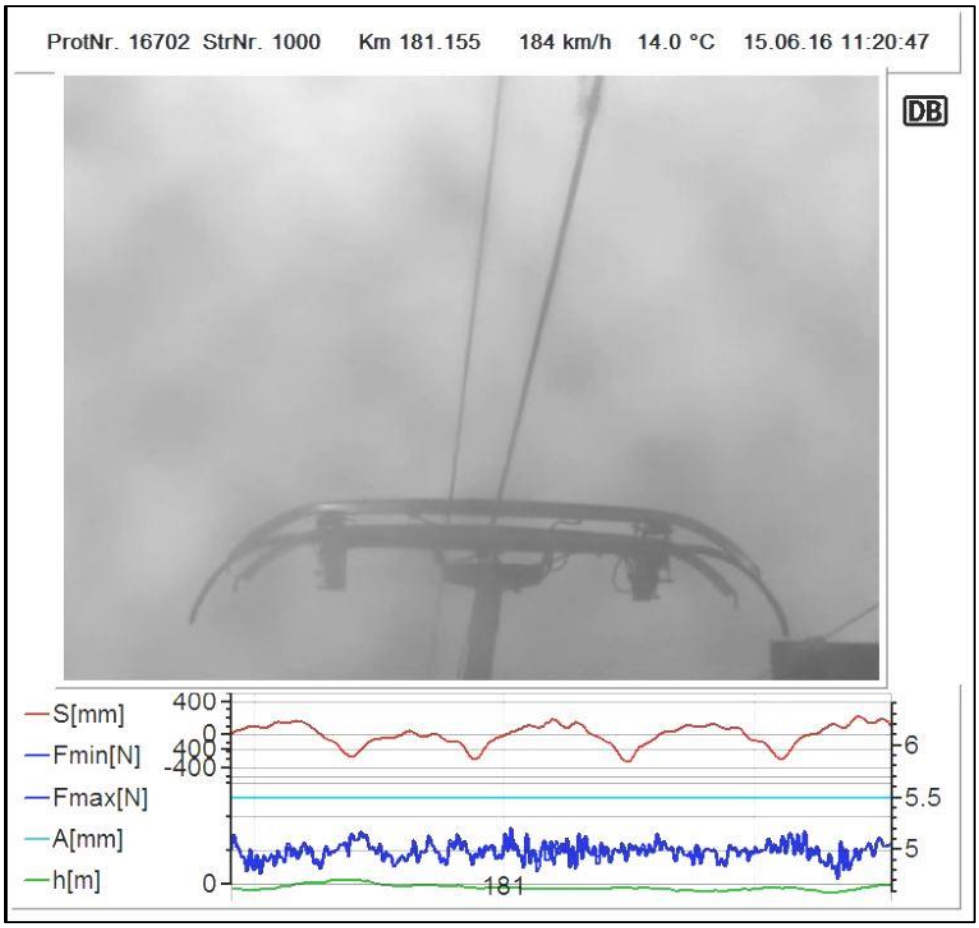

Figure C.3 Screen shot from ODTT test run DBST video showing data output

The Speed of the test train varies from 195 to 202 km/h throughout the section.

Table C.1 Old Dalby test run data

Run no.	8
Data file	A015167026_0001.SA1
Date	15 June 2016
Direction	Northbound
Train formation	5 + 5 (formation type 01)
No. of pantographs raised	2
Pantograph measured	Trailing
Pantograph spacing	200m
Pantograph Fs	Leading = 70N Trailing = 90N
Pantograph type	HSX 250

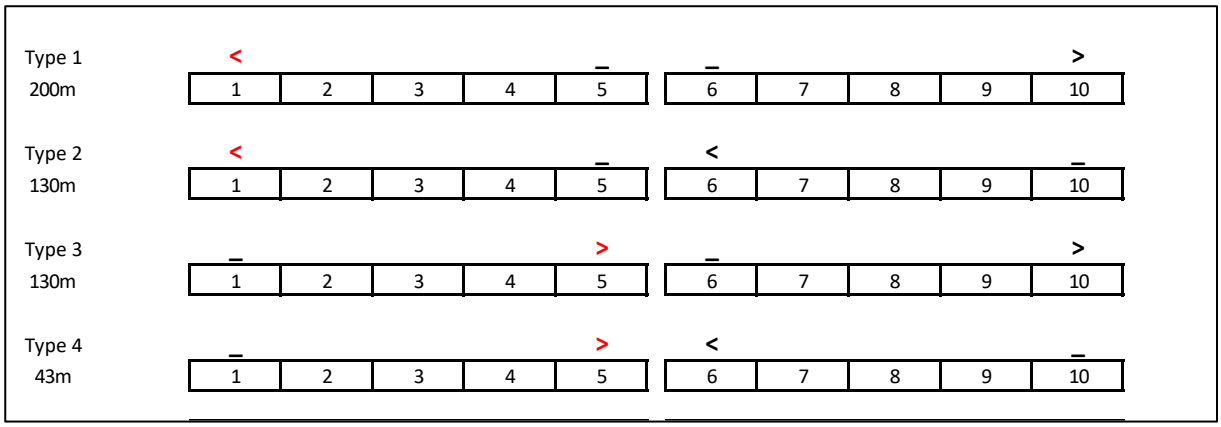

Figure C.4 IEP test train formations showing pantograph locations and spacing (instrumented pantograph shown red). (Bryan, 2016)

C.5 Data analysis

C.5.1 Data channels definitions

The data was extracted from the raw data file and formatted into an Excel spreadsheet, from which an example is shown in Figure C.5, and the explanation of the (German language) column headings is given in Table C.2 (Bryan, 2017) with further clarification provided by DBST themselves directly (DB Systemtechnik, 2018). Some of this output data is also presented graphically in the video screen shot (Figure C.3), where *inter alia* red is stagger (mm), dark blue is contact force (N) and green is CW height (m).

Str.km	v [km/h]	Fz1 [N]	az1 [m/s²]	Fz2 [N]	az2 [m/s²]	Fz3 [N]	az3 [m/s²]	Fz4 [N]	az4 [m/s²]	Winkel_Y [°]	Winkel_X [°]	ax1 [m/s²]	Höhe [m]	az_Dach [m/s²]	ay_Dach [m/s²]	Fzlu [N]	Fzllu [N]	Fzu [N]	Fzlb [N]	Fzllb [N]	Fzb [N]	Fzla [N]	Fzlla [N]	Fza [N]	Seitenlage [m]	az34 [m/s²]	az12 [m/s²]
183.0000	195	57	-5.33	-8	-2.22	60	-3.41	-2	0.24	1.3	1.66	-1.44	4.722	0.42	-0.3	49	58	107	41	54	95	57	57	114	-0.4153	-3.77	-1.56
183.0002	195	55	-6.17	-9	-1.92	59	-3.95	-2	1.32	0.83	1.86	-3.65	4.721	0.48	-0.06	46	57	103	37	54	91	53	56	110	-0.4215	-4.01	-1.26
183.0004	195	52	-6.71	-10	-1.26	57	-4.97	-3	2.57	0.51	2.18	-6.41	4.721	0.6	0.24	43	54	97	34	52	85	50	54	104	-0.4276	-3.95	-1.2
183.0006	195	49	-6.59	-10	-0.54	55	-6.05	-4	3.59	0.54	2.53	-8.92	4.72	0.72	0.48	39	51	90	31	49	80	47	51	98	-0.4334	-3.53	-1.2
183.0008	195	46	-6.17	-10	-0.06	53	-6.77	-4	4.01	0.77	2.78	-10.54	4.72	0.72	0.48	36	49	85	29	46	75	45	48	94	-0.4392	-3.11	-1.38
183.0010	195	43	-5.15	-10	0.24	52	-7.24	-5	4.25	1.33	3.04	-12.03	4.719	0.66	0.42	33	46	80	28	43	71	44	46	89	-0.4449	-2.45	-1.5
183.0012	195	40	-3.77	-9	0.24	50	-6.95	-6	3.95	2.11	3.17	-12.21	4.719	0.42	0.24	31	44	75	27	41	68	43	43	87	-0.4503	-1.74	-1.5
183.0014	195	38	-2.57	-8	0	49	-6.05	-6	3.41	2.77	3.16	-11.44	4.718	0.3	0.12	30	43	73	27	40	68	43	43	86	-0.4555	-1.26	-1.32
183.0016	195	36	-0.9	-6	-0.36	47	-4.07	-5	2.28	3.67	2.98	-9.22	4.718	0.12	0	30	42	72	29	40	68	45	42	87	-0.4603	-0.6	-0.9
183.0018	195	35	0.78	-5	-0.78	45	-1.5	-5	1.02	4.48	2.6	-6.05	4.718	0.12	0	30	40	71	30	40	70	46	42	89	-0.4648	0	-0.24
183.0020	195	35	2.51	-4	-1.2	43	1.26	-4	-0.3	5.06	2.07	-2.69	4.718	0.3	0.06	31	39	70	32	40	73	48	43	91	-0.4688	0.66	0.48
183.0022	195	35	3.83	-3	-1.44	41	3.05	-3	-1.26	5.27	1.58	-0.42	4.718	0.48	0.12	32	38	70	34	40	75	50	43	93	-0.4725	1.2	0.9
183.0024	195	36	5.63	-3	-1.62	39	5.03	-2	-2.28	5.19	0.88	2.04	4.718	0.84	0.18	33	37	70	38	40	78	54	43	96	-0.4759	1.98	1.38
183.0026	195	37	7.72	-2	-1.74	37	6.29	-1	-3.05	4.66	0.17	3.77	4.718	1.08	0.24	35	36	71	41	40	81	57	42	99	-0.4789	2.93	1.62
183.0028	195	38	9.58	-2	-1.8	36	6.95	0	-3.59	3.97	-0.33	4.73	4.718	1.14	0.18	36	36	72	44	40	84	60	42	103	-0.4815	3.89	1.68
183.0029	195	39	12.21	-2	-1.68	36	7.66	0	-4.37	2.76	-0.94	5.51	4.719	0.96	0.06	38	36	74	49	40	89	65	42	107	-0.4837	5.27	1.62
183.0032	195	41	14.79	-2	-1.56	36	8.8	1	-5.27	1.33	-1.44	6.05	4.719	0.6	-0.12	40	37	77	54	41	95	70	43	114	-0.4855	6.59	1.74
183.0034	195	43	16.35	-2	-1.56	37	9.94	2	-6.17	0.25	-1.72	6.35	4.719	0.24	-0.24	41	38	80	57	43	100	73	45	119	-0.4869	7.36	1.86
183.0036	195	45	17.54	-1	-1.68	39	11.86	2	-7.42	-1.04	-1.97	6.65	4.72	-0.12	-0.36	43	41	85	61	46	107	77	49	125	-0.4879	7.9	2.22
183.0038	195	46	17.24	-1	-2.22	42	13.71	3	-8.44	-1.93	-2.05	6.89	4.72	-0.36	-0.36	45	45	90	62	51	113	78	53	131	-0.4886	7.48	2.63
183.0039	195	47	15.63	0	-2.93	45	14.55	3	-8.92	-2.26	-1.98	6.95	4.72	-0.36	-0.3	47	48	95	61	54	115	77	57	134	-0.489	6.29	2.81
183.0042	195	47	11.74	1	-4.25	49	14.31	4	-8.62	-2.14	-1.7	6.77	4.72	-0.12	-0.18	48	53	101	56	59	115	72	61	133	-0.4893	3.71	2.81
183.0044	195	46	6.05	2	-5.93	53	12.03	4	-7.19	-1.43	-1.19	6.23	4.72	0.24	0	48	57	105	48	62	110	64	64	129	-0.4895	0.06	2.4
183.0046	195	44	0.96	3	-7.24	56	8.92	3	-5.21	-0.57	-0.65	5.57	4.72	0.48	0.06	47	59	106	40	63	104	56	66	122	-0.4897	-3.11	1.86
183.0048	195	41	-6.05	4	-8.8	59	3.17	2	-1.86	0.8	0.25	4.61	4.721	0.72	0.18	45	61	106	29	63	91	45	65	110	-0.4901	-7.42	0.66
183.0049	195	39	-10.78	4	-9.46	61	-1.86	1	1.14	1.85	1.04	4.01	4.721	0.78	0.12	43	62	104	20	61	81	36	63	100	-0.4904	-10.12	-0.36

Figure C.5 Extract from DBST data

Table C.2 Legend to DBST data column headings (data channels)

Column heading	Units	Description
Strecke		Number of route (used in Germany, in UK only a virtual number)
Str.km	km	"Milestone" (in km)
Latitude		geographical Information, not used in UK
Longitude		geographical Information, not used in UK
vkmh	km/hr	Speed in km/h
Fz1	N	Vertical force Sensor 1...4
Fz2	N	
Fz3	N	
Fz4	N	
az1	m/s^2	Vertical acceleration Sensor 1...4
az2	m/s^2	
az3	m/s^2	
az4	m/s^2	
ax1	m/s^2	Acceleration in x direction (longitudinal)
ay1	m/s^2	Acceleration in y direction (lateral)
Höhe	m	Extraction of panto (height)
az_Dach	m/s^2	Acceleration on roof of train in z-direction (vertical)
ay_Dach	m/s^2	Acceleration on roof of train in y-direction (lateral)
FzIu	N	Force strip 1 (without aero and acceleration correction)
FzIIu	N	Force strip 2 (without aero and acceleration correction)
Fzu	N	Total force (without aero and acceleration correction)
FzIb	N	Force strip 1 (without aero but with acceleration correction)
FzIIb	N	Force strip 2 (without aero but with acceleration correction)
Fzb	N	Total force (without aero but with acceleration correction)
FzIa	N	Force strip 1 (with aero and acceleration correction)
FzIIa	N	Force strip 2 (with aero and acceleration correction)
Fza	N	Total force (with aero and acceleration correction)
Seitenlage	m	Lateral position - stagger
az12	m/s^2	Acceleration strip 1
az34	m/s^2	Acceleration strip 2

C.5.2 Note on kilometrage and indexation.

The data kilometrage for the pantograph instrumentation output is not correlated with the Old Dalby test track datum. A mechanism for indexation of the distance measurement – in the data legend, 'Strecke km' – against the actual Old Dalby route layout, structures and features, was required.

There are in fact three distinct sets of along track chainages in use at Old Dalby, as follows:

- The original Old Dalby track chainage in kilometres in the range 10 – 13 km;
- A separate kilometres chainage used in the recent OCL surveys, in metres, in the range 1000 – 2000m (the 'ODTT index');
- The chainage used in the test train odometry (by DBST) in the range 184 – 189 km (the DBST index').

The first listed is not used here. The other two need to be synchronised against each other, as one indexes the pantograph measurement data, the other indexes the OCL features. Two approaches were used: one was the manual indexing by using the test train's pantograph video (Figure C.3) at a very slow playback speed, and the points at which the pantograph passed the registrations being interpreted visually using single frame advance. The accuracy of this method is around ±1m, separate to the accuracy of the actual odometer readings. The second approach was to use the recorded data itself, and to identify the structure locations from the stagger reading (legend 'Seitenlage' in the data), particularly, the points where the stagger changes direction, an example of which is shown in Figure C.6.

Two points emerged. First the two readings were out of step by around 8 or 10m, far too much for the inaccuracies of the methods employed. It seems likely that the odometer reading from the on board instrumentation is probably GPS based, and the receiver is located remotely from the actual centre line of the pantograph. The problem of indexation was exacerbated also by the apparent unreliability of the Old Dalby OCL layout plans. It was found that several occasions the given OCL structure location (in km) (see Figure C.2) did not correlate with the shown span lengths. This was not thought to be a curvature issue, as there is virtually no curvature through the relevant section.

The correlation between the ODTT and DBST indices is indicated in columns 3 and 4 of Table C.5.

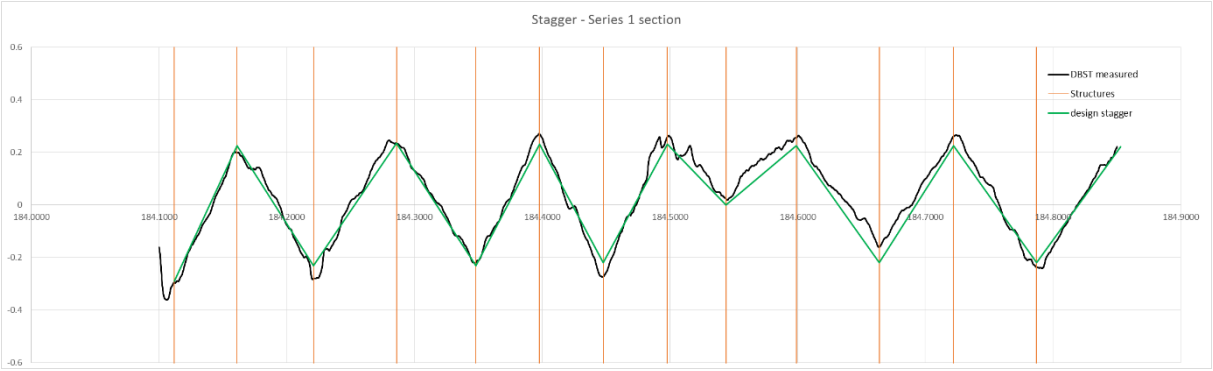

Figure C.6 overlay of measured stagger points from DBST data, with layout plan design stagger, showing correlation

The solution adopted was to use the indexing synchronisation based on the 'best fit' of the stagger readings compared to the OCL layout plan data, but with the OCL layout plan data 'modified' by the actual span lengths. This hybrid adjustment was used to prepare the OCL nodes data for the simulation, and to relate to the measured data.

C.5.3 Selecting the 'analysis section'

The OCL layout plans, and the longitudinal profile data of the whole of the Series 1 section of ODTT indicates that there was only one length of uninterrupted 'open route' OCL available. This was the 13 span section from 1196.00 (using ODTT index) to 1937.00, a total length of 741m. Either side of this section, were installed specific OCL features such as multiple overlaps, carrier wire neutral sections and bridge arrangements, as part of the extensive testing regime for Series 1. Within these 13 spans was incorporated the AF single rod neutral section, at location1628.00 (between spans 8 and 9). Out of necessity these 13 spans were chosen as the analysis section. See Figure C.8.

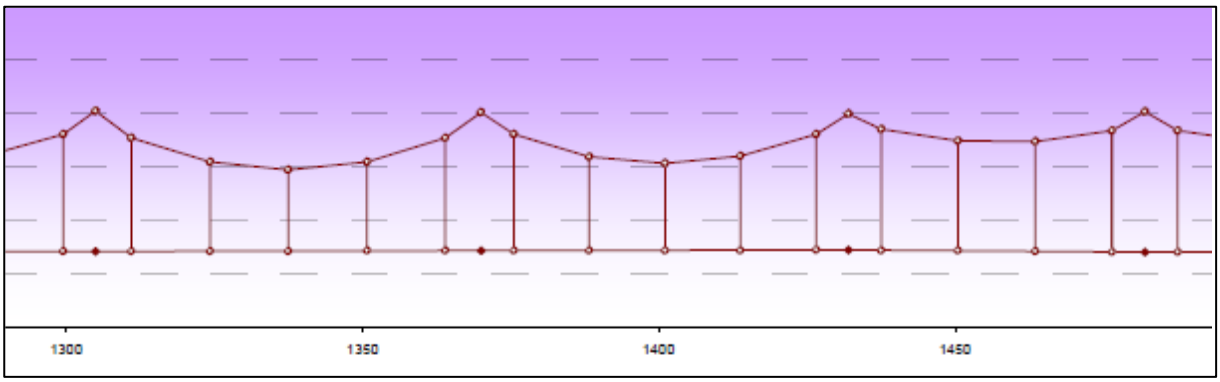

Figure C.7 Longitudinal profile of the OCL within the analysis section (extract) (Bryan, 2016)

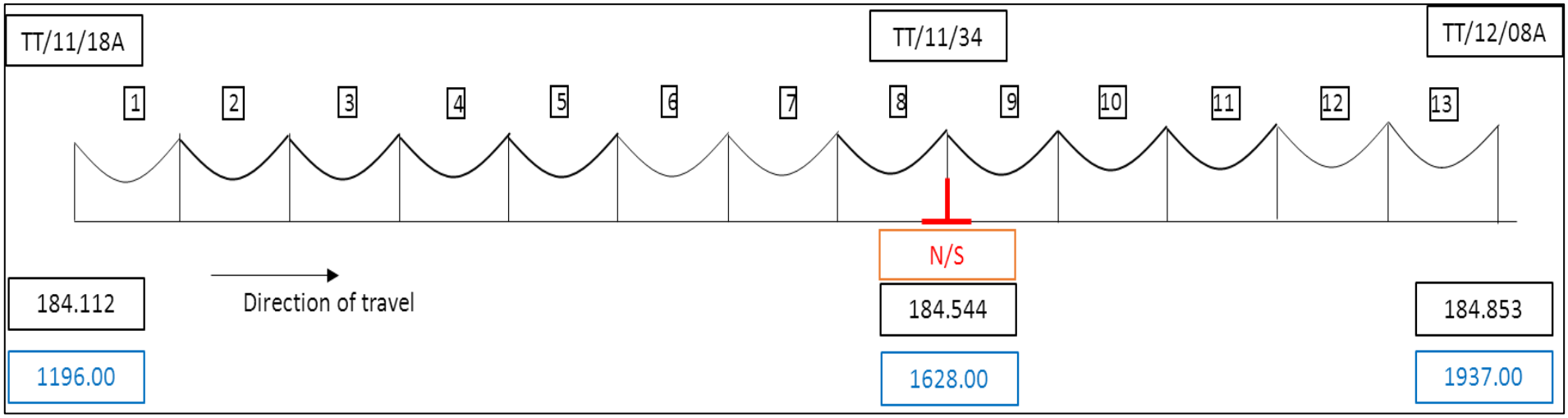

Figure C.8 The 13 span analysis section of the ODTT. Showing the ODTT and DBST chainages. Neutral section location shown in red

The OCL data for the 13 spans chosen is summarised in Table C.5.

The data sources by column number are:

Column	Source
1, 2, 4, 5	from OD layout plans 118049-FAF-REP-EOH-000015 (rev02) and 118049-FAF-REP-EOH-000016 (rev02)
3	from DBST data and interrogation of DBST video
6, 7, 8, 9	from F&F ODTT OCL data 'as fitted'
10	from authors own calculation spreadsheet, in line with Appendix B
11, 12, 13	from F&F Series 1 Manual 06 (allocation design) (Furrer + Frey, 2016b)
12	from F&F drawing 442.00119, and 444.0055 (Furrer + Frey, 2016d)

C.6 Data scrutiny

C.6.1 Cleansing the data

The data, as can be seen from the extract, is a channel by channel output from the instrumentation on the pantograph, in a text (CSV) file.

As can be expected from such a large quantity of data, taken in real world on-site conditions, there are some anomalies in the continuity of the data. This is mainly presented in duplication or skipping of the regular 20cm distance interval. In order to prepare the data for analysis, a certain amount of 'cleansing' had to be undertaken. This mainly involved the regularisation of the 20cm interval. In all, over the 750m of the chosen analysis section, 21 spurious data entries, and 314 irregular intervals were found. (Representing 0.56% and 8.37% of the total data entries of 3750).

Spurious entries were simply deleted. The irregular distance step entries were all of the form 10 cm followed by 30 cm, and then reverting to the standard pattern. The approach here was to delete the two entries and replace with a 'replacement' entry at the 20cm interval, with all data values taken as the mean of the values in the distance steps either side.

C.6.2 Analysing the data

The force data is plotted for the analysis section, both raw (effectively 35 Hz filtered, see Figure C.11) and 20 Hz filtered. As the DBST data is by distance interval sampling (0.02m) the data was converted to time interval sampling by using the speed data. As the speed is mostly consistent throughout the analysis section (~200 km/h) this

produces a robust time interval based data which can be processed and filtered conventionally. This is an accepted practice with distance interval sampled data (Brodkorb, 2018).

On inspection, it seems that the force data is disturbed around span 3. These forces may be caused by anomalies in the OCL, or in the vehicle pantograph. The vehicle anomalies may be in turn caused by track irregularities. This is corroborated by the pantograph head data, shown in Figure C.12. Here it is also supported by a plot of the train roof vertical acceleration (the field 'az_Dach' in the DBST data). It can be seen that the pantograph head vertical displacement rises suddenly in and around span 3, accompanied by a downward train roof acceleration. The force -displacement plot is also shown in greater detail in Figure C.13. Track irregularities are the likely cause, but however caused, this cannot be replicated in the OCL model.

Consequently it seems prudent and legitimate to exclude these anomalous data associated with span 3 from the benchmark target data for comparison with the simulated results, as they appear to arise from sources that cannot be modelled.

C.6.3 Notes on the ODTT series 1 FFT

The unfiltered data has been analysed by Fourier transform, and the force data in the frequency domain is shown in Figure C.9 and the PSD is shown in Figure C.10.

There are three peaks shown in the PSD, at approx. 1.4, 3.3 and 4.6 Hz. These can perhaps be associated with regular periodic features of the OCL, i.e. dropper and span (i.e. registration) passing frequencies.

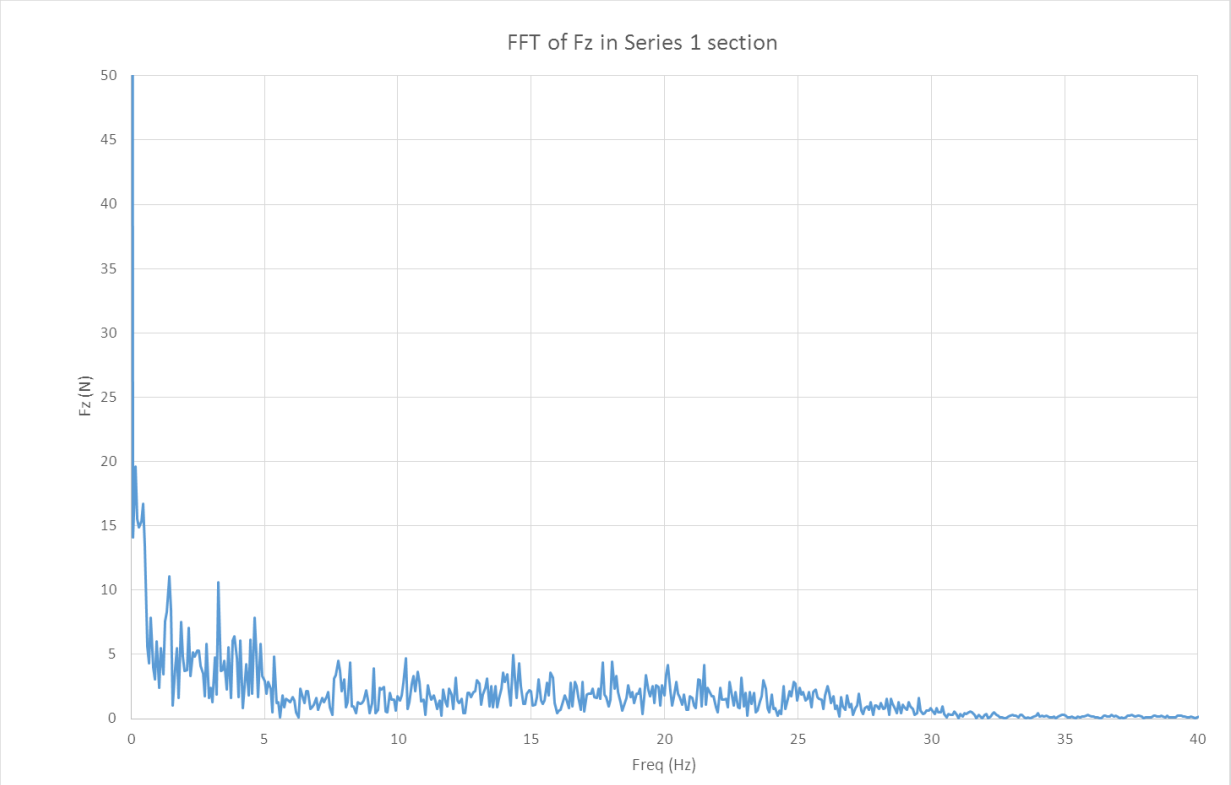

Figure C.9 ODTT measured force data in the frequency domain

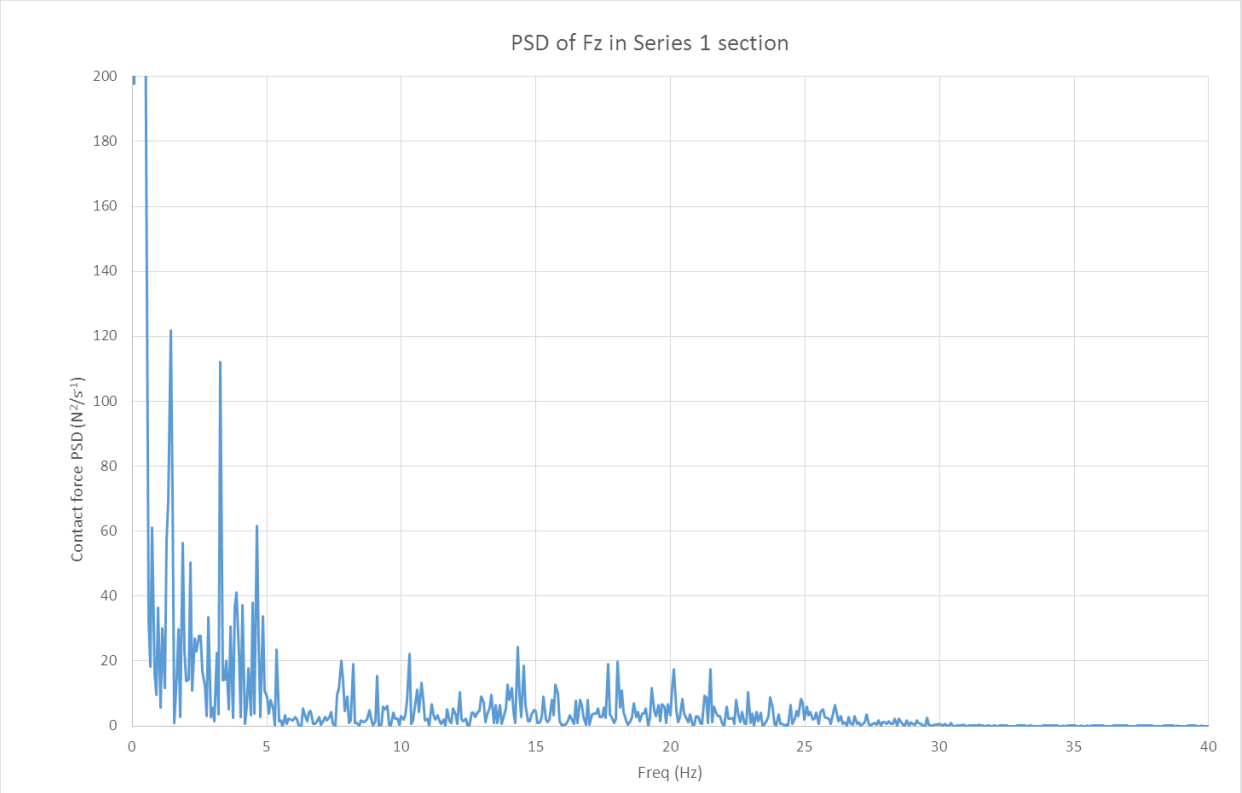

Figure C.10 PSD of ODTT data

The dropper spacing is irregular in different spans, but varies from 11m to 14m. At 200 km/h this equates to a dropper passing frequencies of 5.05 Hz to 3.56 Hz. This can be identified to the third peak at around 4.6 Hz. Span lengths also vary, less regularly, from 46m to 65m. This is probably the cause of the first peak at 1.4 Hz. The middle peak at around 3.28 Hz has unknown cause.

This data also shows very little presence of frequencies above around 35 Hz, even though the sampling frequency of the data is around 277 Hz (based on 0.2m interval at 200 km/h), and should in theory show frequencies up to half this, i.e. 135 Hz.

Information from DBST (DB Systemtechnik, 2019a; DB Systemtechnik, 2019b) has indicated that although nominally sampled at ~277 Hz, there is a 200Hz filter in the instrumentation, and additionally, a selectable software filter which is usually set to 20 Hz, but this was not confirmed for these tests, although it would seem in this case it was set higher at around 35 Hz. It is assumed that the 200Hz referred to is a filter on the sampling rate, whereas the 20Hz is the processed signal.

Consequently it seems that the best that can be extracted from the data is at 35 Hz, which is essentially the raw data.

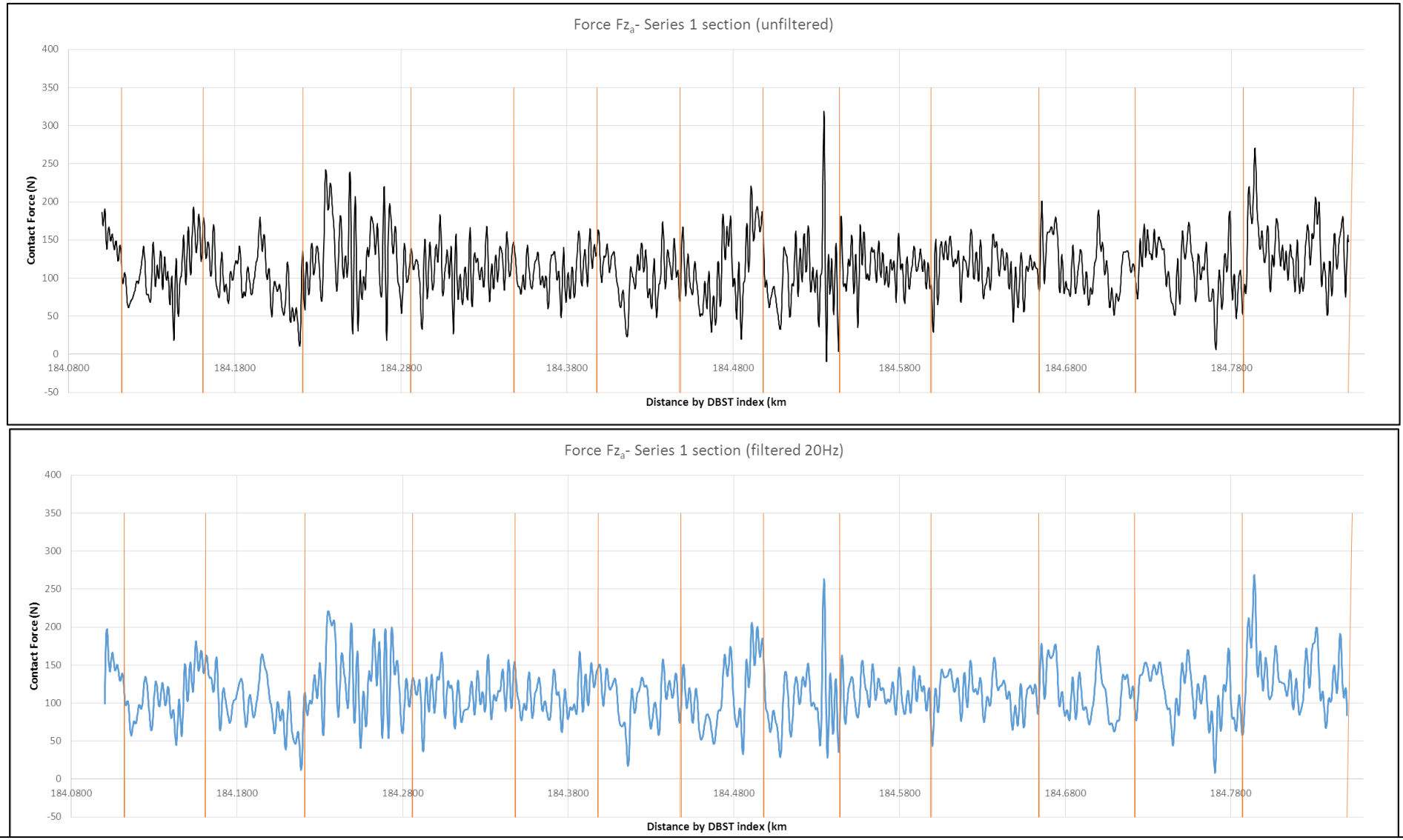

Figure C.11 ODTT test data, pantograph contact force plot through analysis section (top, unfiltered) (bottom filtered)

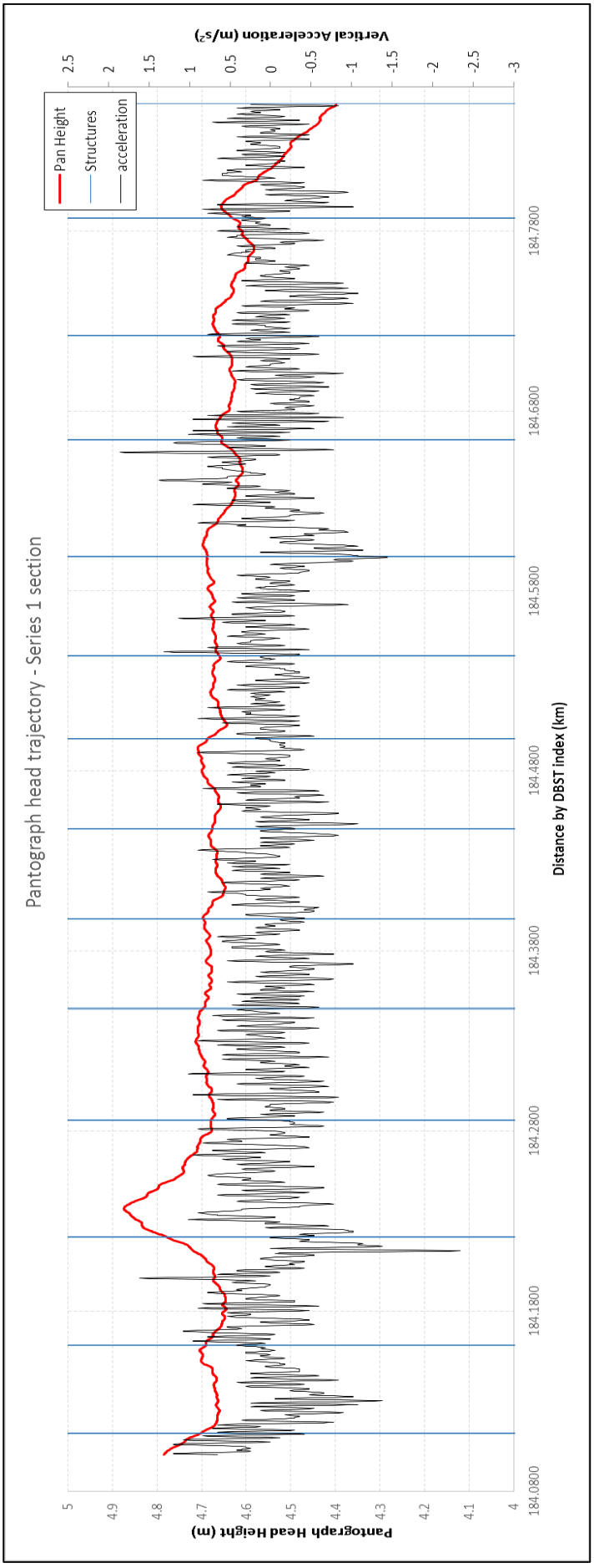

Figure C.12 ODTT test data, pantograph head trajectory, and vehicle vertical acceleration

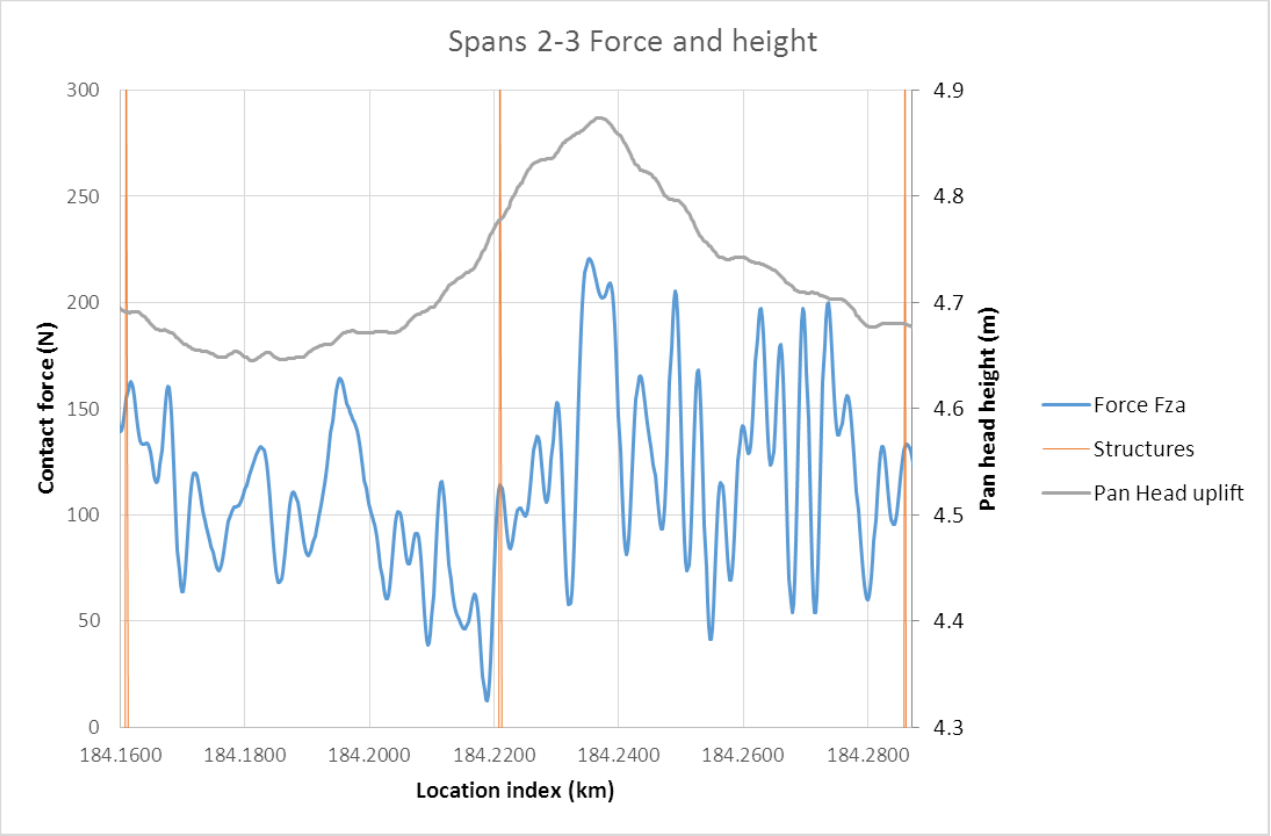

Figure C.13 Detail of anomalous force and pantograph height data in spans 2 and 3

C.6.4 Geometrical profile check

Dropper calculation by the method described in Appendix B was compared to actual measured 'as built' CW and messenger profile as delivered in the OCL surveyed data and good correlation was achieved. A typical example is shown in Table C.3 below, for span 3. The errors are in messenger height, as the CW height was taken as the datum for the calculations. The greatest difference is 12 mm, which represents a 1.14% error in dropper length.

Table C.3 Span 03 geometrical profile check

	measured		calculated			differences	
X	Y	Y	Y	Y			
	Messgr.	CW	Messgr.	CW		Messgr.	drop lngth
1305.00	6.01200	4.70600	6.01200	4.70600		0.00000	
1311.00	5.75928	4.70628	5.77130	4.70628		0.01202	1.14%
1324.25	5.53389	4.70689	5.54301	4.70689		0.00912	1.10%
1337.50	5.46250	4.70750	5.46504	4.70750		0.00254	0.34%
1350.75	5.53511	4.70811	5.53730	4.70811		0.00219	0.27%
1364.00	5.76172	4.70872	5.75988	4.70872		-0.00184	-0.17%
1370.00	5.99800	4.70900	5.99800	4.70900		0.00000	

C.7 Choice of target data

The choice of the data for which the test values would be used as the targets for the simulation results, for the purposes of validation of accuracy and representative-ness, was based on the above analysis.

In accordance with the requirements of the current standard EN 50318 this is based on Table 2 of that standard, requiring the values of mean contact force, standard deviation, filtered at a 'frequency range of interest', and pantograph head range of displacement, and CW registration point uplift to be simulated within a given tolerance of a measured result.

The data was taken for the spans 1 to 7, i.e. to exclude the neutral section spans, and additionally, as already identified, excluding some of the apparently anomalous data associated with span 3. The statistical values are shown in Table C.4 below. No value is included for maximum uplift at the support as this (trackside measurement) was not recorded on these tests (DB Systemtechnik, 2019a).

Table C.4 Target values of pantograph/OCL interaction from ODTT

Parameter	**ODTT measured values**
Mean contact force, Fm (N)	109.61
Standard deviation of the contact force, σ	30.574
Maximum uplift at the support (mm)	*Not included*
Range of vertical position of the point of contact (mm)	64.0

Table C.5 details of the OCL installation within the ODTT analysis section

stru	ODTT location	INDEX	DBST index	span north	Track	curvature north (mm)	Structure type	CW ht	Catenary ht	system ht	stagger	rad load (N)	Arm length (mm)	Arm mass (kg)	Heel setting (mm)	Note
dummy (C)				*49*	*Dn Main*	*5*					*-0.230*					
TT/11/18A	11.513	1196.00	184.103	49	Dn Main	5	STC	4.711	5.995	1.284	0.290	349	1000	2.203	80	
TT 11/20A	11.562	1245.00	184.152	61	Dn Main	-29	STC	4.700	5.999	1.299	-0.225	296	1000	2.203	80	
TT 11/22	11.622	1305.00	184.213	65	Dn Main	-5	STC	4.706	6.012	1.306	0.230	241	1000	2.203	80	
TT 11/25A	11.687	1370.00	184.278	63	Dn Main	5	STC	4.709	5.998	1.289	-0.235	240	1000	2.203	80	
TT 11/26	11.749	1432.00	184.341	50	Dn Main	0	STC	4.715	5.985	1.270	0.230	274	1000	2.203	80	
TT 11/28	11.799	1482.00	184.391	51	Dn Main	0	STC	4.699	6.007	1.308	-0.230	297	1000	2.203	80	
TT 11/30	11.849	1532.00	184.442	50	Dn Main	0	STC	4.703	6.003	1.300	0.220	294	1000	2.203	80	
TT 11/32	11.899	1582.00	184.492	46	Dn Main	0	STC	4.697	6.002	1.305	-0.230	231	1000	2.203	80	
TT 11/34	11.945	1628.00	184.538	55	Dn Main	0	STC	4.695	5.990	1.295	0.000	150	1000	2.203	80	neutral section
TT 12/01	12.000	1683.00	184.593	65	Dn Main	-10	STC	4.704	5.992	1.288	-0.225	180	1000	2.203	80	
TT 12/03	12.065	1748.00	184.658	60	Dn Main	10	portal	4.702	6.010	1.308	0.220	235	1000	2.203	80	
TT 12/04	12.123	1806.00	184.718	65	Dn Main	70	STC	4.658	5.954	1.296	-0.225	235	1000	2.203	80	
TT 12/06	12.188	1871.00	184.783	64	Dn Main	-70	STC	4.617	5.934	1.317	0.220	227	1000	2.203	80	
TT 12/08A	12.254	1937.00	184.847	64	Dn Main	0	anchor portal	4.434	6.077	1.643	-0.222	230	1000	2.203	80	
dummy (D)					*Dn Main*						*0.230*					

Appendix D Brecknell Willis HSX 250 Pantograph

D.1 Introduction

The Brecknell Willis HSX 250 pantograph model data published by RSSB required certain additional work to extract all the necessary data to create the pantograph model, for use in simulating the Old Dalby IEP tests.

The BW HSX 250 was developed by UK pantograph manufacturer Brecknell Willis for the Hitachi IEP train (Hartland and Cullingford (2013); (Hitachi Rail Europe, 2018), known now as class 800. See photos Figure D.1.

Figure D.1 BW HSX 250 pantograph (left) on IEP (class 800) train (LNER Azuma), (right) from (Hartland and Cullingford, 2013)

The data for the pantograph was initially taken from RSSB report T1105 (RSSB, 2016) which had been commissioned to provide lumped mass data for all commonly used UK pantographs. See Figure D.2. However, not all the information provided was clear and interpretations had to be made, and further clarifications were sought from RSSB. This Appendix describes how those interpretations were made, and their implications for the simulations.

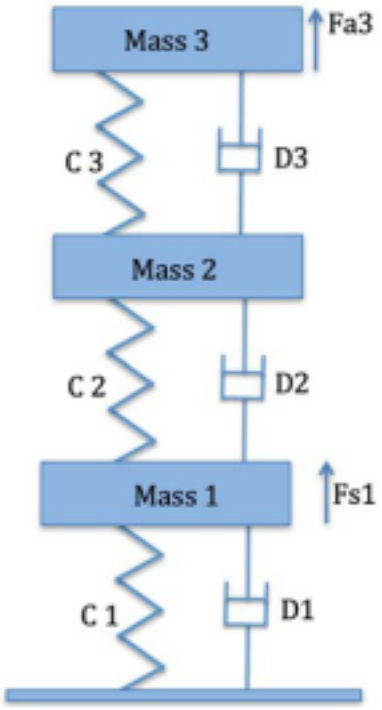

Parameter	Value
Masses	
M1	3.53 kg
M2	7.50 kg
M3	5.30 kg
Damping	
D1	32.6 Ns/m
D2	0 Ns/m
D3	70.0 Ns/m
Springs	
C1	0 N/m
C2	5000 N/m
C3	See manufacturers data below
Externally Applied Forces	
Fs1	70 to 120N
Fa3	0.006 Ns^2/m^2 (Variable if required)

Manufacturers data for secondary suspension	
Preload (vertical force required before suspension displacement)	Approximately 20N
Spring rate	Effective rate at head centre-line increases with displacement approximately as per $0.07(x^2+50x)$ N/mm (reducing to 50 % of this value at the suspension assembly)
Total available displacement	Approximately 60mm

Figure D.2 Lumped parameter data of BW HSX 250 pantograph, from RSSB T1105 (RSSB, 2016)

D.2 Pantograph head stiffness

The comments associated with the reference to the pantograph head spring stiffness (C3 in the diagram) required further explanation. The clarification response from RSSB (RSSB, 2018a) is quoted below:

> *"The effective vertical spring rate of the panhead varies according to where the vertical load is applied. It is a minimum stiffness directly above the head suspension assembly (either side) and a maximum stiffness at the panhead centreline where the effective stiffness is double that of a single suspension unit.*

Because the spring assemblies which support the panhead are not vertical their effective vertical stiffness varies with displacement.

A more accurate approximation for the displacement of a single suspension unit is as follows:

Each suspension unit responds to $F=0.06x^2 + 1.7x + 6$ where F is the additional vertically applied load directly above the suspension unit and x the subsequent vertical displacement due to force F. Hence there is a total 12N vertical force on head centreline required before the head assembly moves downwards from its up stop."

A spreadsheet demonstrating the calculation of the effective stiffness of the pantograph head suspension at any point, and under any load (force) was also provided.

The particular construction of the pantograph head suspension makes the head stiffness variable, non-linearly with force, and additionally also variable, linearly, with position across the pantograph head. This has been interpreted as shown in Figure D.3 below.

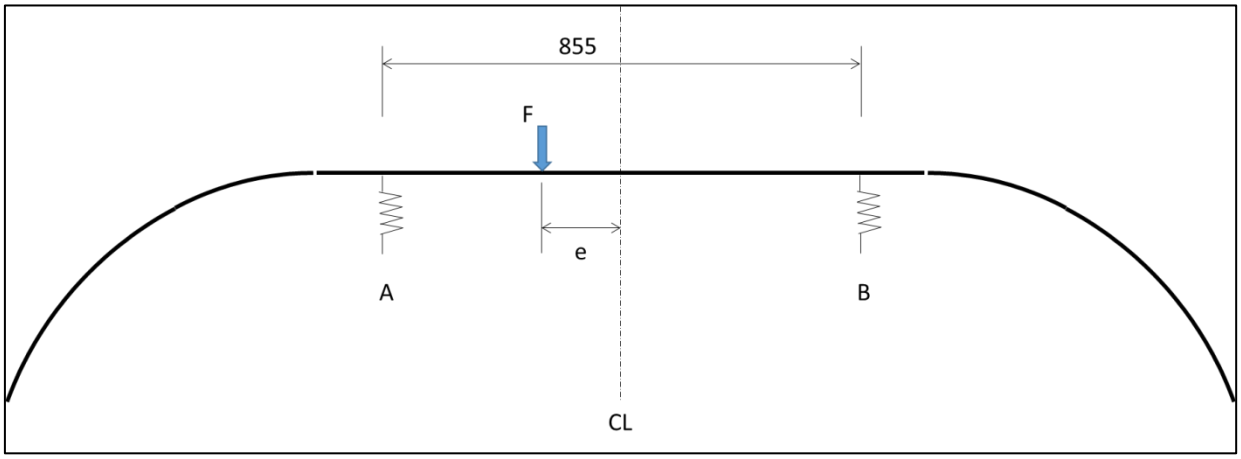

Figure D.3 HSX 250 arrangement of pantograph head suspension geometry

The following calculation is extracted from the above referenced RSSB provided spreadsheet. The relationship between the displacement x and the applied force F of ***each*** suspension point is:

$$F = 0.06\,x^2 + 1.7\,x + 6 \qquad \text{Equation (D.1)}$$

This can be expressed as a general quadratic equation, where a = 0.06, b = 1.7 and c = (6 – F), so the displacement *x* at each suspension point, for a force F at that suspension point, is as

$$x = \frac{-1.7 + \sqrt{1.7^2 - (2.9 - 0.24(6 - F))}}{0.12} \qquad \text{Equation (D.2)}$$

The forces F_A and F_B at each suspension point, for a total force F applied at an offset e from the centre line of the pantograph head (see Figure D.3) is

$$F_A = \frac{F \cdot \left(\frac{855}{2} + e\right)}{855} \qquad \text{Equation (D.3)}$$

and where

$$F_B = F - F_A \qquad \text{Equation (D.4)}$$

The displacement at the point of application for forces which are offset from the pantograph head centre line can be calculated from the suspension point displacements by substituting F_A and F_B for F in equation D.2 and by linear interpolation between the suspension point displacements X_A and X_B for the force application point displacement X_F.

$$x_F = x_A - \left[\left\{\frac{x_A - x_B}{855}\right\} \cdot \left(\frac{855}{2} - e\right)\right] \qquad \text{Equation (D.5)}$$

and this can be tabulated and plotted for a range of expected forces and offsets as shown in Figure D.4. The data can be plotted, for the same range of forces, for a series of offsets, up to 400mm, which represents the largest dynamic stagger of the CW encountered in the ODTT data for the Series 1 section used for comparison and validation purposes (see Appendix C), and is shown in Figure D.4.

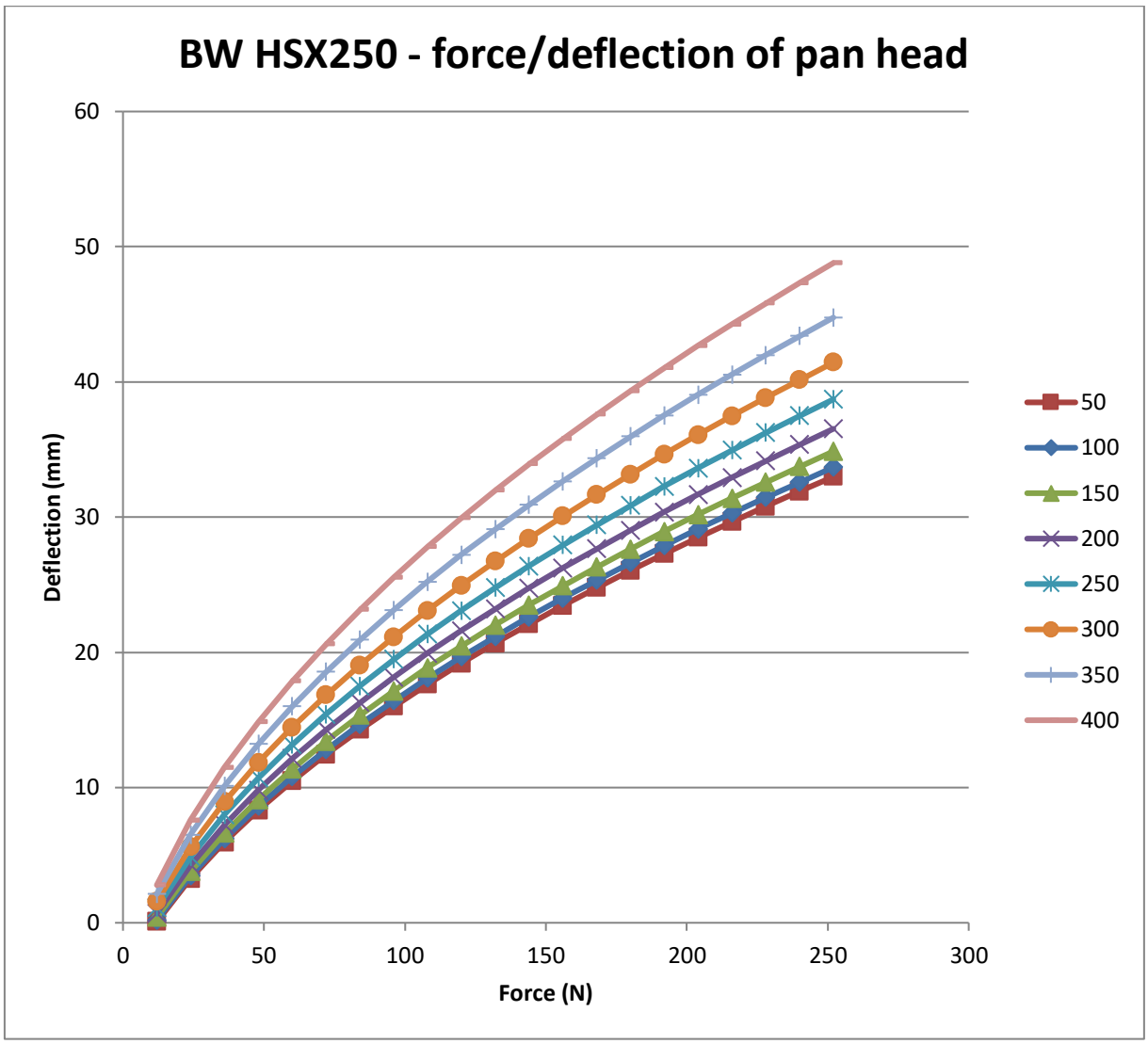

Figure D.4 Force deflection plot of HSX 250 pantograph for a range of force application point offsets

However, as the analysis proposed in this research is a two dimensional analysis, where the Z axis of the across track dimension is not considered, then this particular non-linearity cannot be coded in the data. A choice is made as to which value of data corresponding to which offset shall be taken. The Ansys model is essentially a 2D model, and the stagger of the CW (offset in Z coordinate direction) is not implemented, neither is the Z direction width of the pantograph head. It is for this reason that the registration arm is replaced by its 2D effects. Similarly the 2D effect of the variation in pantograph head stiffness must be equally accommodated.

Given the analysis section chosen from the ODTT is largely on straight (tangent) track, where the staggers are conventionally offset alternately from one side to the other (see Figure C.5 and Table C.4 in Appendix C), and in particular where the feature of interest,

the neutral section, is on a zero stagger, it seems appropriate assumption to use the panhead centre line characteristic as the chosen one for the analysis.

The displacement at the pantograph head centre line, for a force at the pantograph head centre line is therefore a specific form of D.5 where e = 0, and

$$F_A = F_B = \frac{F}{2} \qquad \text{Equation (D.6)}$$

Which can be tabulated and plotted for a range of expected forces as shown in Figure D.5.

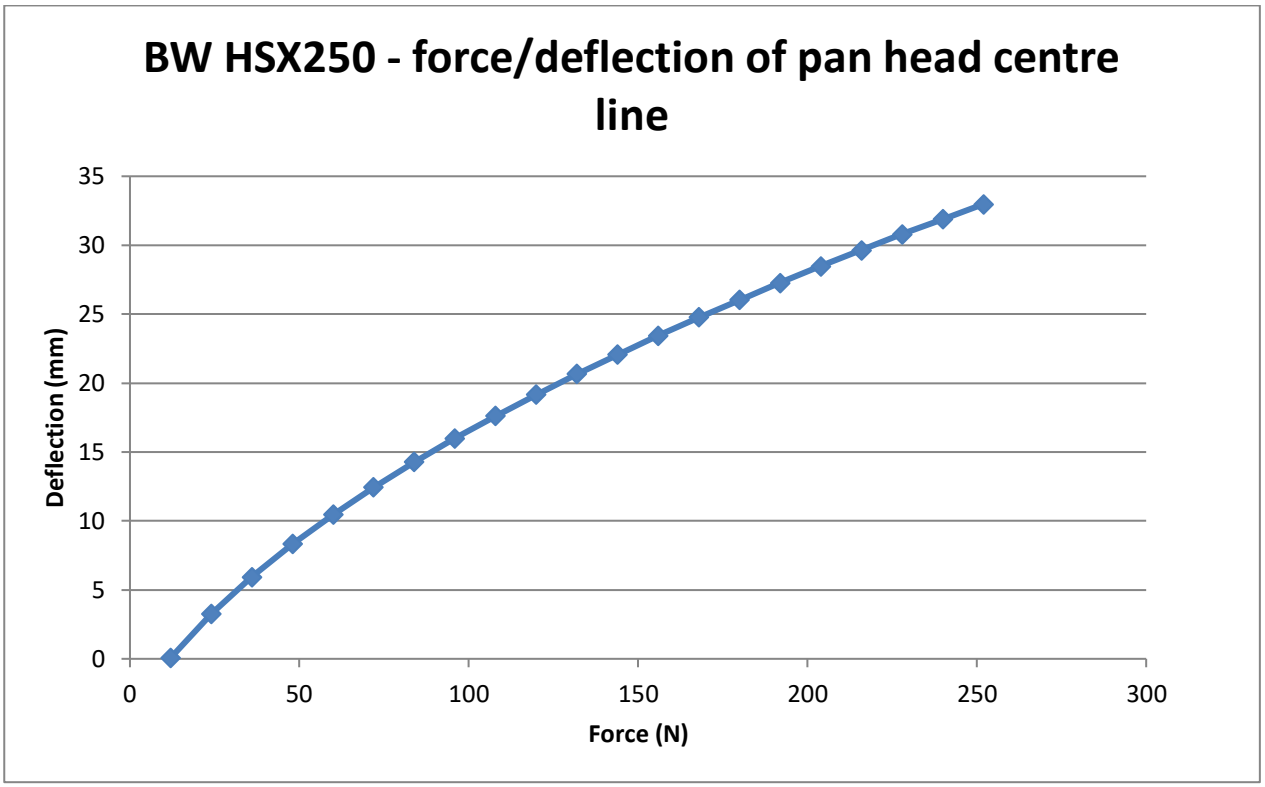

Figure D.5 Suspension displacement of HSX 250 pantograph for a force at the centre line

The issue is how to apply this to the Ansys model. In particular, the opportunity is taken to combine this non-linear stiffness with the inclusion of the bump stops, the limit on vertical movement of 60mm. This is applied in the Ansys model by the same non-linear stiffness, but by applying a stiffness of near infinity (or at least a very high value – computers do not like values of infinity) beyond the extremes of the 60mm suspension

travel. The full force deflection plot for this non-linear stiffness data is shown in Figure D.6.

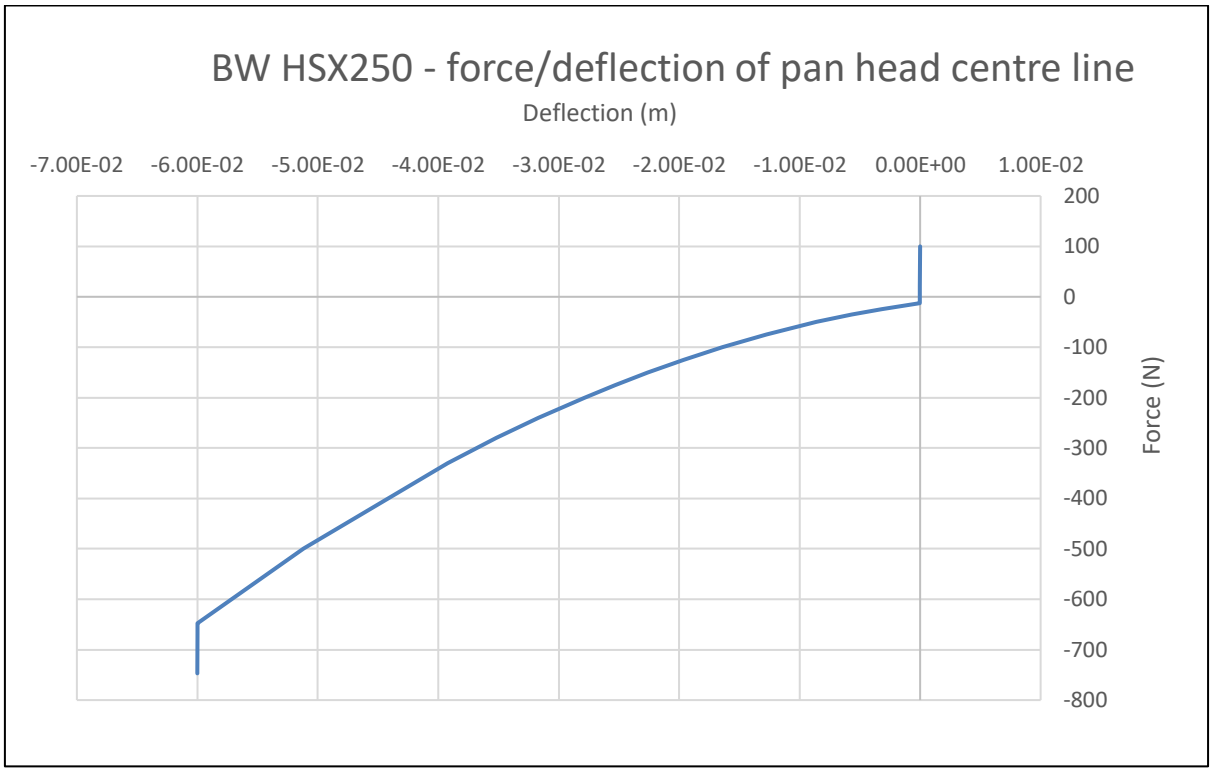

Figure D.6. Force deflection plot of HSX 250 pantograph including bump stops, as applied in Ansys model

D.3 Interpretation of 'preload'

Most pantographs of this type using springs have the initial extension/compression of the main springs which is set so as to counter balance the mass of the pantograph frame. The term 'preload' here is interpreted as being the shortfall of the spring extension/compression forces against the sum of the masses, and hence the additional force to be applied to complete the balance of the masses, before the Fs1 contact force can take effect and act upon the CW as the static contact force.

$$\sum K \,.\, x = \sum m \,.\, g - P_L \qquad \text{Equation (D.7)}$$

In the pantograph models used in this research, in all cases the pantograph spring extension/compression cannot be assessed as the pantograph construction data is not known, and so is ignored, and is replaced by a discrete force equivalent to the sum of the relevant pantograph frame masses.

The static contact force range of 70 – 120 N refers to the range within which the static contact force can be set for any given application, or operator requirement. On the Hitachi IEP the pantograph has two settings of 70N and 90N which are selectable. The proposed practice (and that employed for the ODTT tests) is that the leading pantograph is set to 70N and the trailing to 90N (Bryan, 2016).

D.4 Force aerodynamic augment

The force shown as aerodynamic force Fa in the diagram, is, by inference from the units, actually the coefficient k in the expression for the aerodynamic force augment:

$$F_{aero} = k \,.\, v^2 \qquad \text{Equation (D.8)}$$

where v is in m/s

As the speed throughout the test section in question is essentially constant at 200 km/h (in fact 201.75 through the analysis section), the aerodynamic force augment is fixed at F_{aero} = 18.85 N

This is applied as an augment to the static contact force when undertaking the dynamic load steps of the simulation.

D.5 Pantograph head mass

The pantograph head mass, M3 in the diagram, is shown as 5.30kg. Information from DBST (DB Systemtechnik, 2018) indicates that a value of 4.8kg was used in extracting the pantograph head force from the accelerometers fitted. In the simulation studies reported in 5.5, corroboration with the simulation results was only obtained with a value of 5.30 plus 0.50kg, being an allowance for the instrumentation attached to the pantograph heads during the tests, was used.

Appendix E Dynamic Simulation Method Ansys Script

Set directory and file name conventions

Start PREP7

- Read in variables, and calculate internal variables for CW properties, messenger properties, dropper properties, registration support properties, pantograph properties
- Define element types and key option parameters
- Create variables for run properties, run length, pantograph separation, start & end locations for each pantograph
- Read in multi functional array data file(s)
  - Create and populate dropper data array
  - Create and populate registration data array
  - Create and populate support data array
- Read in OCL nodes coordinate data text file
- Define material properties and section properties for messenger. Create BEAM189 messenger elements from nodes data.
- Apply messenger tension by initial stress
- Define real properties for messenger springs. Create messenger springs elements COMBIN14
- Define material properties and section properties for CW. Create BEAM189 CW elements from nodes data
- Apply CW tension by initial stress
- Define real properties for CW spring. Create single CW spring element COMBIN14
- DO-LOOP for dropper real properties and parameters creation from array data
- DO-LOOP to create dropper COMBIN39, messenger clamp MASS21 and CW clamp MASS21 elements
- DO-LOOP for registration real properties and parameters creation from array data
- DO-LOOP for support real properties and parameters creation from array data
- Create pantograph nodes
- Set real properties for pantograph mass, spring and damper, including table of values for non-linear pan head stiffness. Create both pantograph elements using MASS21, COMBIN39 and BEAM189
- Create initial contact gap by setting pantograph head heights

Set real properties for penalty contact parameters. Create pantograph head (x2) TARGE170 and CW CONTA176 contact elements. Match each pantograph head to a set of CW contact elements by real properties

Create component for pantograph head nodes, for later output results definition

DO-LOOP to create registration spring COMBIN39, force and CW clamp MASS21 elements

Create component for CW registration point nodes, for later output results definition

DO-LOOP to create mast support COMBIN14 spring and damping elements

Create component for all CW contact elements, for later output results definition

Set boundary conditions:

Fix all nodes in UZ, ROTX, ROTY

Fix all messenger and CW ends in UX, UY

Fix 'ground' ends of registration arms and mast supports in UX, UY, ROTZ

Start SOLUTION

Set analysis type is transient dynamic analysis

Start load step 1

Set time integration is OFF

Constrain pantograph nodes in all DoFs

Set convergence tolerance values for U, F, TOT, M to 1.0E-2.0 to aid convergence

Solve in 5 sub-steps

Start load step 2

Un-constrain both sets pantograph nodes (except base) DoFs in Y

Apply relevant uplift force to each pantograph

Solve in single sub-step

Start load step 3

Set time integration is ON

Select full Newmark integration, and set an amplitude decay factor (numerical damping) of 0.2

Set load step time is 1.0 second

Solve in 10 sub-steps

Start load step 4

Select full Newmark integration, and set an amplitude decay factor (numerical damping) of 0.1

Un-constrain pantograph #1 nodes in X DoF, and set velocity = simulation speed

Set pantograph #1 aerodynamic uplift force

Turn auto time stepping off

Set load step time to first time interval (for two pan hybrid case)

Set sub step integration time step to 1/sampling frequency

Output results only for the defined components

Start load step 5

Select full Newmark integration, and set an amplitude decay factor (numerical damping) of 0.1

Un-constrain pantograph #2 nodes in X DoF, and set velocity = simulation speed

Set pantograph #2 aerodynamic uplift force

Turn auto time stepping off

Set load step time to second time interval (for two pan hybrid case)

Set sub step integration time step to 1/sampling frequency

Output results only for the defined components

Solve all load steps

Start POST26

Generate nodal solution variables for X and Y displacement of pantograph #1 head

Generate nodal solution variables for X and Y displacement of pantograph #2 head

Print all solutions to output

Increased allowed number of variables to 200 (Ansys maximum)

DO-LOOP for generating element solution variables for contact pressure for first 200 CW contact elements for pantograph #1, and output results

Clear variables and repeat do-loop for a further 200 CW contact pressure variables, and repeat until all CW contact pressure variables for pantograph #1 have been output to file

DO-LOOP for generating element solution variables for contact pressure for first 200 CW contact elements for pantograph #2, and output results

Clear variables and repeat do-loop for a further 200 CW contact pressure variables, and repeat until all CW contact pressure variables for pantograph #2 have been output to file

Generate nodal solution variables for Y displacement of CW registration arm connection, print to output.

Finish

Bibliography

15 kV AC railway electrification (2016). Available at: https://en.wikipedia.org/wiki/15_kV_AC_railway_electrification?oldid=716082622 (Accessed: 20 May 2016).

Abbott, M.R. (1968) *Calculation of the dynamic behaviour of a trolley wire overhead contact system for electric railways* (Technical Report 68103). Farnborough: Royal Aircraft Establishment, Royal Aircraft Establishment.

Acevedo, J.C.M., Guerra, C.T., Almenara, L.F., Díaz, J.I., Álvarez, J.C., Villalba, A.B., Nieva, T. and Aiarzaguena, M. (2011) 'IFZONE project: improving circulation in neutral sections', *World Congress on Railway Research*. Lille, France, 22-26 May, 2011.

Ambrósio, J., Pombo, J., Antunes, P. and Pereira, M. (2015) 'PantoCat statement of method', *Vehicle System Dynamics*, 53(3), pp. 314-328.

Ambrósio, J., Pombo, J., Facchinetti, A., Bruni, S., Massat, J.-P. and Dupuis, H. (2011) *Key parameters for pantograph/catenary numerical models* (PantoTRAIN Technical Report D1.1). Brussels, Belgium: UNIFE.

Ambrósio, J., Pombo, J., Pereira, M., Antunes, P. and Mósca, A. (2012a) 'A computational procedure for the dynamic analysis of the catenary-pantograph interaction in high-speed trains', *Journal of Theoretical and Applied Mechanics*, 50(3), pp. 681-699.

Ambrósio, J., Pombo, J., Pereira, M., Antunes, P. and Mósca, A. (2012b) 'Recent developments in pantograph-catenary interaction modelling and analysis', *International Journal of Railway Technology*, 1(1), pp. 249-278.

Ambrósio, J., Pombo, J., Rauter, F. and Pereira, M. (2008) 'A memory based communication in the co-simulation of multibody and finite element codes for pantograph-catenary interaction simulation', in Bottasso C.L (ed.) *Multibody Dynamics*. Dordrecht, The Netherlands: Springer, pp. 211-231.

ANSYS Mechanical APDL Multibody Analysis Guide (2013). Release 15.0 edn. Canonsburg, PA: Ansys, Inc.

ANSYS Mechanical APDL Structural Analysis Guide (2013). Release 15.0 edn. Canonsburg, PA: Ansys, Inc.

ANSYS Mechanical User's Guide (2013). Release 15.0 edn. Canonsburg, PA: Ansys, Inc.

Antunes, P., Ambrósio, J., Pombo, J. and Facchinetti, A. (2020) 'A new methodology to study the pantograph–catenary dynamics in curved railway tracks', *Vehicle System Dynamics*, 58(3), pp. 425-452.

Antunes, P.C. (2012) *Development of multibody pantograph and finite element catenary models for application to high-speed railway operations*. IST, Instituto Superior Técnico, Technical University of Lisbon.

Apiwattanalunggarn, P., Shaw, S. and Pierre, C. (2005) 'Component mode synthesis using nonlinear normal modes', *Non Linear Dynamics*, 41(1-3), pp. 17-46.

Arthur Flury (2011) *Neutral section NS 25 web catalogue entry* Available at: http://www.aflury.ch/en/ProductOverview.aspx?ctgyName=L5-NS25&parentCtgy=L4-Phasentrennung_konventionell&path=WebHome/Bahn/L1-BahnKatalog/L2-Phasentrenner/L3-Phasentrenner/L4-Phasentrennung_konventionell (Accessed: 3 March 2015).

Arthur Flury (2014) 'NSR lever arm introduction, presentation slides'. 19 Sep 2014.

Arthur Flury (2017) *Installation instruction NSR25 (MA NSR ENG 00 2017 03)*. Available at: http://www.aflury.ch/en/getAttachment.axd?attaName=MA_NSR_ENG_00_2017_03 (Accessed: 18 Jan 2019).

Arthur Flury (2019) *On-line product catalogue* Available at: http://www.aflury.ch/de/CategoryOverview.aspx?ctgyName=L1-BahnKatalog&path=WebHome%2fBahn%2fL1-BahnKatalog (Accessed: 18 Jan 2019).

Arthur Flury (UK) (2016) Email from Paul Culnane to John Morris, 1 Dec 2016.

Arthur Flury (UK) (2018) Email from Paul Culnane to John Morris, 17 Aug 2018.

AUS Ltd (2019) Email from Danny Richards (AUS Ltd) to John Morris, 22 July 2019.

Bampton, M.C.C. and Craig Jr, R.R. (1968) 'Coupling of substructures for dynamic analyses', *AIAA Journal*, 6(7), pp. 1313-1319.

Bastian, A., Courtois, C. and Machet, A. (2011) 'Phase separation sections - passing with minimum constraints', *Elektrische Bahnen*, 109(4/5), April 2011, pp. 197-203.

Baxter, A. (2015) *Network Rail: A Guide to Overhead Electrification* (132787-ALB-GUN-EOH-000001). London: Alan Baxter & Associates.

Beagles, A., Fletcher, D., Peffers, M., Mak, P. and Lowe, C. (2016) 'Validation of a new model for railway overhead line dynamics', *Proceedings of the Institution of Civil Engineers - Transport*, Volume 169 (Issue 5, October 2016), pp. 339-349.

Beagles, A. and Hayes, S. (2018) Informal meeting with John Morris, 27 Nov 2018.

Beaty, H.W. and Fink, D.G. (2013) *Standard Handbook for Electrical Engineers, Sixteenth Edition*. 16th edn. New York: McGraw-Hill Education.

BICC (c.1966/67) 'Brochure 27A, Railway Electrification'. Liverpool: BICC.

Bobillot, A., Cléon, L.M., Collina, A., Mohamed, O. and Ghidorzi, R. (2008) 'Pantograph-catenary: a high-speed European couple', *World Congress on Railway Research*. Seoul, Korea, May 2008.

Bobillot, A., Delcourt, V., Demanche, P. and Massat, J.P. (2006) 'Pantograph-Catenary: three paths to knowledge', *World Congress on Railway Research*. Montreal, Canada, June 2006.

Bobillot, A., Massat, J.-P. and Mentel, J.-P. (2011) 'Design of pantograph-catenary systems by simulation', *World Congress on Railway Research*. Lille, France, May 2011.

Bond, R.W. (1987) *The Overhead Contact System Design Manual*. unpublished manual. Balfour Beatty Power Construction Ltd (Traction & General Division).

Bradwell, A. and Wheeler, J.C.G. (1974) *Investigation of recent fractures of ceramic collar neutral section insulators in service* (TM-ETR-024). Derby: British Rail Research, British Rail Research.

Bridon (2013) 'Steel rope techncial information'. Bridon,. Available at: www.bridon.com (Accessed: 2 Jan 2017).

British Standards Institution (1997) *BS 7884:1997 Copper and copper-cadmium stranded conductors for overhead electric traction and power transmission systems*. London: British Standards Institution.

British Standards Institution (2002) *BS EN 50318:2002, Railway applications. Current collection systems. Validation of simulation of the dynamic interaction between pantograph and overhead contact line*. London: British Standards Institution.

British Standards Institution (2004) *BS EN 50163:2004 Railway applications. Supply voltages of traction systems*. London: British Standards Institution.

British Standards Institution (2009) *BS EN 50119:2009: Railway applications. Fixed installations. Electric traction overhead contact lines*. London British Standards Institution,.

British Standards Institution (2010) *BS EN 50206-1:2010 Railway applications. Rolling stock. Pantographs. Characteristics and tests. Pantographs for main line vehicles*. London: British Standards Institution.

British Standards Institution (2012a) *BS EN 50317:2012, Railway applications. Current collection systems. Requirements for and validation of measurements of the dynamic interaction between pantograph and overhead contact line*. London: British Standards Institution,.

British Standards Institution (2012b) *BS EN 50367:2012, Railway applications. Current collection systems. Technical criteria for the interaction between pantograph and overhead line (to achieve free access)*. London: British Standards Institution,.

British Standards Institution (2012c) *BS EN 50149:2012: Railway applications. Fixed installations. Electric traction. Copper and copper alloy grooved contact wires*. London British Standards Institution,.

British Standards Institution (2016) *Draft for Public Comment of BS EN 50318 Railway applications - Current collection systems- Validation of the dynamic interaction between pantographs and overhead contact line*. London: British Standards Institution.

British Standards Institution (2017) *BS EN 50124-1:2017, Railway applications - Insulation coordination. Part 1: Basic requirements — Clearances and creepage distances for all electrical and electronic equipment*. London: British Standards Institution.

British Standards Institution (2018) *BS EN 50318:2018, Railway applications. Current collection systems. Validation of simulation of the dynamic interaction between pantograph and overhead contact line*. London: British Standards Institution.

British Transport Commission (1955) *Modernisation of British Railways: The system of electrification for British Railways*. London: British Transport Commission.

British Transport Commission (1960) 'Adoption of 25kV railways electrification at industrial frequency', *British Railways Electrification Conference*. London, 3-6 Oct 1960. BTC.

Brodkorb, A. (2018) Conversation with John Morris, 5 June 2018.

Brown, L. (2012) 'On course, in motion - the pantograph-catenary system', *EURAILmag*, 25(1, 2012), pp. 126-129.

Bruni, S., Ambrosio, J., Carnicero, A., Cho, Y.H., Finner, L., Ikeda, M., Kwon, S.Y., Massat, J.-P., Stichel, S., Tur, M. and Zhang, W. (2015) 'The results of the pantograph–catenary interaction benchmark', *Vehicle System Dynamics*, 53(3), pp. 412-435.

Bruni, S., Ambrósio, J., Pombo, J. and Kolbe, M. (2011a) *Pantograph models based on laboratory tests* (PantoTRAIN Technical Report D1.2). Brussels, Belgium: UNIFE.

Bruni, S., Bucca, G., Collina, A. and Facchinetti, A. (2011b) 'Numerical and Hardware-in-the-Loop Simulation of Pantograph-Catenary Interaction', *PACIFIC*. Amiens, France, 8 Dec 2011.

Bryan, C. (2016) Email to John Morris, 24 Oct 2016.

Bryan, C. (2017) Email to John Morris, 24 Feb 2017.

Butcher, L. (2013) 'Railways: EU Policy (SN00184)' [Briefing Paper]. 14 Feb. 2013. London: House of Commons Library.

Butcher, L. (2015) 'Rail electrification (SN05907)' [Briefing Paper]. 17 Dec. 2015. London: House of Commons Library.

Capitaine, A., Bianchi, J.-P., Constant, P. and Genest, F. (2019) 'Tension variability in contact wire and messenger wire of auto tensioned catenaries ', *World Congress on Railway Research*. Tokyo, Japan, Oct. 2019.

Cau, G., Delooz, F., Dupuis, H. and Massat, J.-P. (2011) *Collection of pantographs and catenary data base at European level* (PantoTRAIN Technical Report D3.1). Brussels, Belgium: UNIFE.

CENELEC (2016) *Cenelec: who we are*. Available at: https://www.cenelec.eu/aboutcenelec/whoweare/index.html (Accessed: 03 Nov. 2016).

Cho, Y.H. (2015) 'SPOPS statement of methods', *Vehicle System Dynamics*, 53(3), pp. 329-340.

Collina, A. and Bruni, S. (2002) 'Numerical simulation of pantograph-overhead equipment interaction', *Vehicle System Dynamics: International Journal of Vehicle Mechanics and Mobility*, 38(4), pp. 261–291.

Collina, A., Bruni, S., Facchinetti, A. and Zuin, A. (2015) 'PCaDA statement of methods', *Vehicle System Dynamics*, 53(3), pp. 347-356.

Collina, A. and Zuin, A. (2014) *Validation of the performance of rigid overhead conductor bar on ballasted track*. Polimi/Furrer+Frey.

Computational Mechanics Limited (2017a) Conversation with Roman Kovalev and John Morris, 29 Nov 2017.

Computational Mechanics Limited (2017b) Email from Gennady Mikheev to John Morris, 15 Feb 2017.

Cook, M. (1996) *Dynamic performance simulations of the neutral section designs proposed for the North London line* (RR-TRS-96-028). Derby: British Rail Research, British Rail Research.

Copper Development Association (2004) 'Copper and copper alloys: compositions, applications and properties'. Hemel Hempstaed, UK: CDA Publication 120. Available at: https://www.thenbs.com/PublicationIndex/documents/details?Pub=CDA&DocID=278784 (Accessed: 27 Sep. 2016).

Dahlberg, T. (2006) 'Catenary, pantograph, and their interaction', *Vehicle System Dynamics*, 44(8), pp. 591-593.

DB Systemtechnik (2016a) *DB Overhead Equipment (OHE) Measurement Systems*. Available at: https://www.db-systemtechnik.de/file/dbst-en/11848860/_GnXCxKmJq5uaetCw1K1TBcBzC0/12203980/data/product_measurement_system_ohe.pdf (Accessed: 25 Jan 2018).

DB Systemtechnik (2016b) *Testing programme for the next generation of intercity trains for UK*. Available at: http://www.db-systemtechnik.de/dbst-en/news/news/11862680/pi_pruefungen_iep-express_hitachi_rail_europe.html (Accessed: 25 Jan 2018).

DB Systemtechnik (2018) Email (18/9/18) from Michael Kolbe to John Morris, 18 Sep 2018.

DB Systemtechnik (2019a) Email (7/8/19) from Michael Kolbe to John Morris, 7 Aug 2019.

DB Systemtechnik (2019b) Email (21/6/19) from Michael Kolbe to John Morris, 21 June 2019.

Department for Transport (2009) *Britain's Transport Infrastrucure: Rail Electrification*. London: DfT Publications,.

Department for Transport (2012a) *Low cost electrification for branch lines* (DeltaRail-ES-2010-003). London: DeltaRail, DfT. [Online]. Available at:

https://www.gov.uk/government/uploads/system/uploads/attachment_data/file/3872/low-cost-electrification-report.pdf (Accessed: 11 July 2016).

Department for Transport (2012b) *Rail interoperability and standards*. Available at: https://www.gov.uk/government/policies/expanding-and-improving-the-rail-network/supporting-pages/rail-interoperability-and-standards (Accessed: 29 January 2013).

Department for Transport (2012c) *Railways Act 2005 Statement in respect of Control Period 5*. Available at: https://www.gov.uk/government/uploads/system/uploads/attachment_data/file/3641/railways-act-2005.pdf.

Dolphin, N. (2014) 'Series 1', *Railway Electrification: The journey in planning tomorrow's railway*. London, UK, 21 Oct. 2014. IET.

Doughty, P. (2015) 'The UK master series development', *Railway electrification: updating the network for the 21st century*. London, UK, 25 June 2015. IMechE.

Duffy, M.C. (2003) *Electric Railways, 1880-1990*. Institution of Engineering and Technology.

Dupas, J.-M. (2010) 'NoBos – providing competent, independent and impartial assessments for the railway industry', *European Railway Review*, 2010(4), 3 Aug 2010.

Elkins, J.A. (1976) *A method for predicting the dynamic response of a pantograph running at constant speed under a finite length of over-head equipment* (TN-DA-36). Derby: British Rail Research, British Rail Research.

ERA (2018) *Frequently Asked Questions about the 4th Railway Package*. Available at: http://www.era.europa.eu/Document-Register/Documents/FAQ-4RP.pdf (Accessed: 29 June 2018).

EU (2008) 'Council Directive 2008/57/EC on the interoperability of the rail system within the Community'. OJ L 191/1, pp. 1-46. Available at: http://eur-lex.europa.eu/eli/dir/2008/57/oj (Accessed: 24 June 2016).

EU (2014a) 'Commission Regulation (EU) No 1301/2014 on the technical specifications for interoperability relating to the 'energy' subsystem of the rail system in the Union'. OJ L 356/179, pp. 179-227. Available at: http://eur-lex.europa.eu/eli/reg/2014/1301/oj (Accessed: 24 June 2016).

EU (2014b) 'Transport in Figures, Statistical Pocketbook 2014'. Luxembourg: Publications Office of the European Union.

EU (2015) *Research and Innovation: Sixth Framework Programme*. Available at: https://ec.europa.eu/research/fp6/index_en.cfm (Accessed: 03 Nov. 2016).

EU (2016) *Research and Innovation: FP7*. Available at: https://ec.europa.eu/research/fp7/index_en.cfm (Accessed: 03 Nov. 2016).

EU (2017a) *Electrification of the Transport System: Studies and reports*. Brussels, Belgium: European Commission EU. [Online]. Available at:

https://ec.europa.eu/programmes/horizon2020/en/news/electrification-transport-system-expert-group-report-0 (Accessed: 25 Aug. 2019).

EU (2017b) *European Commission DG Mobility & Transport: Rail: Interoperability*. Available at: https://ec.europa.eu/transport/modes/rail/interoperability/interoperability_en (Accessed: 23 Apr. 2017).

EU (2019) 'Transport in Figures, Statistical Pocketbook 2019'. Luxembourg: Publications Office of the European Union.

EUROPAC Consortium (2008) *Publishable Final Activity Report* (FP6-012440). Paris: EUROPAC Consortium.

European Copper Institute (2012) *CuNi1Si data sheet*. Available at: http://www.conductivity-app.org/alloy-sheet/1 (Accessed: 22 Aug 2019).

Evans, J. (1980a) *Guide to program RCJEN for calculating impact forces between pantographs and neutral section skids* (IM-ETR-039). British Rail Research, British Rail Research.

Evans, J. (1980b) *Prediction of forces between pantographs and neutral section skids* (IM-ETR-038). British Rail Research, British Rail Research.

Facchinetti, A. and Bruni, S. (2015) 'Special issue on the pantograph-catenary benchmark', *Vehicle System Dynamics*, 53(3), pp. 303-435.

Finner, L., Poetsch, G., Sarnes, B. and Kolbe, M. (2015) 'Program for catenary–pantograph analysis, PrOSA statement of methods and validation according EN 50318', *Vehicle System Dynamics*, 53(3), pp. 305-313.

Fitch, K. (2017) 'The technical pillar of the 4th Railway Package', *Single European Railway Area (SERA) Regional Conference North Sea*. Amsterdam, The Netherlands, 14 June 2017. Available at: http://www.era.europa.eu/Document-Register/Documents/EC_Technical_pillar%20of%20the%204th%20Railway%20Package%20A.pdf (Accessed: 20 Dec. 2017).

Furrer + Frey (2014) 'Series 1: the Great Western railway electrification project'. 2014. Furrer + Frey,. Available at: https://www.furrerfrey.ch/dam/jcr:98f3522c-51ff-4d89-9fd7-dc16601d1db3/140918_F%20F_Series1_pamphlet_onlinePub.pdf (Accessed: 3 Apr 2018).

Furrer + Frey (2016a) *Series 1 OLE System: Manual 001 - System Description* (118049-FAF-MAN-EOH-000004, Issue 5.2 DCP5f). Bern, Switzerland: Furrer + Frey.

Furrer + Frey (2016b) *Series 1 OLE System: Manual 006 - Allocation Design Rules* (118049-FAF-MAN-EOH-000001, Issue 6.2 DCP5f). Bern, Switzerland: Furrer + Frey.

Furrer + Frey (2016c) *Series 1 OLE System: Manual 007B - Assembly Drawings* (118049-FAF-MAN-EOH-000015, Version 9.0 DCP5f). Bern, Switzerland: Furrer + Frey.

Furrer + Frey (2016d) *Series 1 OLE System: Manual 007C - Component Drawings* (118049-FAF-MAN-EOH-000016, Version 9.0 DCP5f). Bern, Switzerland: Furrer + Frey.

The Future Railway, The Industry's Rail Technical Strategy (2012). London: RSSB.

Galland-SAS (2016) 'Galland Product Brochure'. France: Galland-SAS. Available at: https://www.galland-sas.com/en/ (Accessed: 27 Jun 2019).

GE/RT8000/AC Railway Rule Book: Module AC; AC Electrified Lines (2003). London: RSSB.

Goerguelue, U. (2011) *Beam Theories: The difference between Euler-Bernoulli and Timoschenko*. unpublished paper.

Goldring, A.G., Hartshorn, P.R., Ricketts, C.E. and Robinson, W. (1969) 'Insulation for high voltage a.c. railway electrification in Great Britain', *Proceedings of the IEE*, 116(8), pp. 1377-1386.

Gordon, S. (1999) *The Craig-Bampton Method*. Available at: https://femci.gsfc.nasa.gov/presentations.html (Accessed: 6 Nov 2017).

Gostling, R. and Hobbs, A. (1981) *The interaction of pantograph and overhead equipment: practical applications of a new theoretical method* (TM-DA-37). Derby: British Rail Research, British Rail Research.

Gostling, R. and Hobbs, A. (1983) 'The interaction of pantograph and overhead equipment: practical applications of a new theoretical method', *Proceedings of the Institution of Mechanical Engineers*, 197C, pp. 61-69.

Gregori, S., Tur, M., Tarancón, J.E. and Fuenmayor, F.J. (2019) 'Stochastic Monte Carlo simulations of the pantograph–catenary dynamic interaction to allow for uncertainties introduced during catenary installation', *Vehicle System Dynamics*, 57(4), pp. 471-492.

Grove, D.M. and Davis, T.P. (1992) *Engineering, Quality & Experimental Design*. Harlow, Essex, UK: Longman.

Hajianmaleki, M. and Qatu, M.S. (2011) 'Mechanics of Composite Beams', in Tesinova, P. (ed.) *Advances in Composite Materials - Analysis of Natural and Man-Made Materials*. InTech. Available at: http://www.intechopen.com/books/advances-in-composite-materials-analysis-ofnatural-and-man-made-materials/mechanics-of-composite-beams.

Hanley, R., Licciardello, R., Martin, S. and Rose, K. (2014) *TrioTRAIN: bringing research and standardisation closer together*. Available at: http://tra2014.traconference.eu/papers/pdfs/TRA2014_Fpaper_18213.pdf (Accessed: 13 June 2016).

Harassek, A. (2015) 'European Railway Agency and development of the TSIs for European High Speed Railway System', *Transport Technology Systems (Technika Transportu Szynowego)*, 2015(6-Eng), 6 May 2015, pp. 10-13.

Harell, P., Drugge, L. and Reijm, M. (2005) 'Study of critical sections in catenary systems during multiple pantograph operation', *Proceedings of the Institution of Mechanical Engineers, Part F: Journal of Rail and Rapid Transit*, 219(4), pp. 203-211.

Hartland, D. and Cullingford, S. (2013) *The Development of High Speed Pantographs in Great Britain*. unpublished paper. Brecknell Willis.

Haugland, F.H. (2015) *Dynamic behavior of a full scale laboratory model of a catenary system by measurements and numerical analysis*. NTNU, Norwegian University of Science and Technology, Trondheim.

Hendy, P. (2015) *Report from Sir Peter Hendy to the Secretary of State for Transport on the replanning of Network Rail's Investment Programme*. London: Network Rail. [Online]. Available at: http://www.networkrailmediacentre.co.uk/resources/hendy-report-on-replanning-network-rail-s-investment-programme-november-2015 (Accessed: 13 March 2017).

Hetzel, P.G. and Smith, W.R. (1978) *Assessment of the quality of current collection,* (TM-ETR-108). Derby: British Rail Research, British Rail Research.

Hewings, D. (2015) 'Great Western traction system design', *Railway electrification: systems engineering and integration of a major construction project*. London, UK, 22 Oct. 2015. IET.

Hitachi Rail Europe (2018) *Class 800/801 (IEP)*. Available at: http://www.hitachirail-eu.com/products/projects/class-800/801-iep (Accessed: 09 Mar 2018).

Holmes, R. (1982) *The quality of current collection* (IM-ES-089). Derby: British Rail Research.

Howard, M. (2013) 'High Speed 2', *Railway electrification - lessons for the future*. London, UK, 3 Dec. 2013. IET.

Infrastruturas de Portugal (2019) Email from Marco Felipe Santos (Infrastruturas de Portugal) to John Morris, 7 Aug 2019.

Institute of Transportation (CIP) Belgrade (2019) Email from Andreja Mijalcic (CIP) to John Morris, 9 Aug 2019.

International Energy Agency (2019) *The Future of Rail: Opportunities for energy and the environment*. Paris, France: International Energy Agency, IEA. [Online]. Available at: https://webstore.iea.org/the-future-of-rail (Accessed: 30 Jan. 2019).

IXC (2014) *OLE Neutral Section Reliability Review - Final Report* (INV-1-2012). Birmingham: IXC UK Ltd.

Jones, C.R. (1984a) 'Further reductions in cost of overhead line equipment on British Railways', *Rail International*, April 1984.

Jones, C.R. (1984b) 'Implications of increased speed for the design of overhead equipment', *Beyond 200km/h: Engineering options*. London, 1984. Railway Engineers Forum.

Jönsson, P.-A., Stichel, S. and Nilsson, C. (2015) 'CaPaSIM statement of methods', *Vehicle System Dynamics*, 53(3), pp. 341-346.

Kalsbeek, G.V., Avronsart, S. and Meyer, F. (2013) 'Design and preparation of homologation of pantograph-catenary systems by dynamic simulation', *World Congress on Railway Research*. Sydney, Australia, Nov 2013.

Keenor, G. (2016) *Overhead Line Electrification for Railways*. Available at: http://www.railwaysarchive.co.uk/OLE/ (Accessed: 27 Feb. 2017).

Kerr, D.A. (2009) *The Fourier analysis tool in Microsoft Excel* (iss. 1). Available at: http://dougkerr.net/Pumpkin/articles/Excel_Fourier.pdf (Accessed: 4 Apr 2018).

Khayyamim, S., Monti, A., Bagliano, V. and DeKeyzer, I. (2015) 'MERLIN: Making energy management in the railway system smarter', *European Railway Review*, Sustainable rail developments supplement 2015, pp. 4-7.

Kiessling, F., Puschmann, R., Schmieder, A. and Schneider, E. (2016) *Contact lines for electrical railways: planning, design, implementation, maintenance* 3rd edn. Erlangen, Germany: Publicis.

Kim, N.-H. (2015) *Introduction to Nonlinear Finite Element Analysis*. New York, USA: Springer, US.

Kobayashi, T., Shimizu, M. and Oya, A. (2008a) 'Transition structures between rigid conductor line and catenary overhead contact line', *World Congress on Railway Research*. Seoul, Korea, May 2008.

Kobayashi, T., Shimizu, M. and Oya, A. (2008b) 'Transition Structures between Rigid Conductor Line and Catenary Overhead Contact Line', *Quarterly Review of RTRI* 49 (2), pp. 103-107.

Kolpakhchyan P.G., Pogorelov D.Yu., Badikova L.V., Ponasenko O.N. and Popov P.V. (2006) 'Mathematical modelling of the system "electric current collector - contact network" (in Russian)', *Bulletin of VELNII*, 2006(3), pp. 32-42.

Laurent, C., Massat, J.P., Nguyen-Tajan, T.M.L., Bianchi, J.P. and Balmès, E. (2013) 'Pantograph catenary dynamic optimisation based on advanced multi body and finite element co-simulation tools', *23rd IAVSD symposium*. Qingdao, China.

Leouatini, M., Ambrósio, J., Pombo, J. and Facchinetti, A. (2011) *Validation requirements for pantograph/catenary simulation tools* (PantoTRAIN – Technical report D1.3). Brussels, Belgium: UNIFE.

Levy, S., Bain, J.A. and Leclerc, E.J. (1968) 'Railway overhead contact systems catenary-pantograph dynamics for power collection at high speeds', *Transactions of ASME: Journal of Engineering for Industry*, Paper No. 58-RR-2, pp. 692-699.

Liljedahl Bare Wire (2014) 'Contact wire and stranded conductors for overhead catenary systems'. Liljedahl Bare Wire. Available at: http://www.elektrokoppar.se/images/pdf/train_eng2014.pdf (Accessed: 19 Sep. 2016).

Massat, J.-P., Balmes, E., Bianchi, J.-P. and Van Kalsbeek, G. (2015) 'OSCAR statement of methods', *Vehicle System Dynamics*, 53(3), pp. 370-379.

Massat, J.-P., Laurent, C., Bianchi, J.-P. and Balmes, E. (2014) 'Pantograph catenary dynamic optimisation based on advanced multibody and finite element co-simulation tools', *Vehicle System Dynamics: International Journal of Vehicle Mechanics and Mobility*, 52(1), pp. 338-354.

Materials Data Book. (2003) Cambridge University Engineering Department. Available at: http://www-mdp.eng.cam.ac.uk/web/library/enginfo/cueddatabooks/materials.pdf (Accessed: 19 Jul 2019).

Meddins, B. (2000) *Introduction to digital signal processing*. Oxford: Boston : Newnes.

MERLIN (2015) 'Final issue of the Merlin Newsletter '. 8 Jan 2016. Merlin. Available at: http://www.merlin-rail.eu/wp-content/uploads/2016/01/Merlin_Newslette_2nd_issue_Dec_2015.pdf (Accessed: 14 July 2016).

Morris, J.C. (2013) 'Considerations for improved design of phase-break sections ', *Railway Engineering 2013, 12th International Conference and Exhibition*. London, UK, 10th – 11th July 2013.

Morris, J.C. and Giddins, G. (2015) 'Application of RAM techniques to OLE reliability prediction on Great Western Electrification', *Railway electrification: updating the network for the 21st century*. London, UK, 25 June 2015. IMechE.

Morris, J.C., Robinson, M. and Palacin, R. (2017) 'Railway electrification: considerations for the improvement of design of short neutral sections', *The Stephenson Conference: Research for Railways*. London, UK, 25th - 27th April 2017. IMechE, pp. 297-305.

Morris, R.B. (1965) 'The application of an analogue computer to a problem of pantograph and overhead line dynamics', *Proceedings of the Institution of Mechanical Engineers*, 179 Pt1(25), pp. 782-808.

NeTIRail (2015) *Deliverable D 3.1: Power supply technologies and practices of low and high-density railways, identifying learning points and future opportunities* (H2020-MG-2015-2015 GA-636237). Brussels, Belgium: NeTIRail.

Network Rail (2006) *NR/SP/ELP/21088 issue 02, General maintenance parameters for 25 kV overhead line electrification equipment*. London: Network Rail.

Network Rail (2009) *Network RUS – Electrification*. London: Network Rail.

Network Rail (2010a) *NR/SIN/111 issue 1.0, Special Inspection Notice: Lever modification upgrade to Arthur Flury Single Rod Neutral Sections*. London: Network Rail.

Network Rail (2010b) *Series 1 OLE Specificiation, NR-1-2010*. London: Network Rail.

Network Rail (2011a) *Internal memorandum, 2006-2010 Reportable traction power incidents*. London: Network Rail.

Network Rail (2011b) *Modernising the Great Western*. Available at: http://www.networkrail.co.uk/uploadedFiles/networkrailcouk/Contents/Improvements/The_Great_Western/WesternVision.pdf (Accessed: 24 Aug 2016).

Network Rail (2011c) *NR/L1/ELP/27000 issue 01, Asset management policy for Electrical Power assets*. Network Rail,.

Network Rail (2012a) *Internal memorandum, AF neutral section design development, draft 0.3*. London: Network Rail.

Network Rail (2012b) *Paper to ORR, West Coast South Reliability Programme: Final Report and Recommendations*. London: Network Rail.

Network Rail (2012c) *Safety Bulletin IGSB263: AF Neutral Section - Contact wire splice component failure*. Milton Keynes, UK: Network Rail.

Network Rail (2012d) *Western Route Electrification: Major Feeding Schematic* (124101-NWR-DRG-EP-0100). London: EPDG.

Network Rail (2013a) *GWEP: FMEA – Carrier Wire Neutral Section Workshop*. Swindon: GWEP LDO,.

Network Rail (2013b) *GWEP: Neutral section positioning report* (118049-IED-REP-EOH-00135). London: EPDG,.

Network Rail (2013c) *GWML Electrification: Sectioning Diagram Route Sections 1 - 7* (118049-IED-DRG-EOH-000103). London.

Network Rail (2013d) Informal meeting Nick Snell (NR)/John Morris, 18 July 2013.

Network Rail (2013e) *NR/OLE D10 issue 02, Installation of Arthur Flury Single Rod Neutral Section*. London: Network Rail.

Network Rail (2013f) *Retford feeder station – contact wire failure within splice of Arthur Flury neutral section on the Up Main, 29 Aug 2013* (Report 13153). London: Atkins.

Network Rail (2014a) *Annual return to ORR, 2013/14*. London: Network Rail. [Online]. Available at: http://www.networkrail.co.uk/publications/Annual-return/ (Accessed: 10 July 2015).

Network Rail (2014b) Email Phil Doughty (NR) to John Morris, 4 July 14, 4 July 2014.

Network Rail (2014c) *Historical record of Network Rail stewardship*. London: Network Rail. [Online]. Available at: http://www.networkrail.co.uk/publications/annual-return/stewardship.xls (Accessed: 18 March 2015).

Network Rail (2014d) Informal meeting Phil Doughty (NR)/John Morris 3 Dec 14, 3 Dec 2014.

Network Rail (2014e) Informal meeting Phil Doughty (NR)/John Morris 7 Aug 14, 7 Aug 2014.

Network Rail (2014f) *Tallington - OLE Dewirement, 21 October 2013, Final Report* (Report 13182). London: Atkins.

Network Rail (2015a) 'Freedom of Information response FOI/2015/01013' [FOI response]. 18 Nov. 2015. Network Rail.

Network Rail (2015b) Incident information from Phil Doughty (NR) at informal meeting with John Morris, 10 Aug 2015.

Network Rail (2015c) Informal meeting with Richard Ollerenshaw (NR York), 26 Aug 2015.

Network Rail (2015d) *NR/L2/ELP/21087 issue 06, Risk Based Maintenance for Overhead Line Assets*. London: Network Rail.

Network Rail (2015e) *Specification for In-Line Neutral Sections, Issue 0.5 Draft*. London: Network Rail.

Network Rail (2016) Informal meeting with Nawaz Ahmad, re: Network Rail 'Whole Life Product Management' initiative, 26 Jan 2016.

Network Rail (2017) *Melton Rail Innovation & Development Centre*. Available at: https://www.networkrail.co.uk/industry-commercial-partners/research-development-technology/ridc/ridc-melton/ (Accessed: 11 Jan 2018).

Network Rail (2018) *National Electronic Sectional Appendices*. Available at: https://www.networkrail.co.uk/industry-commercial-partners/information-operating-companies/national-electronic-sectional-appendix/ (Accessed: 6 Nov 2018).

NKT (2006) 'NKT Railway Product Brochure'. Köln, Germany: NKT. Available at: www.nktcables.com (Accessed: 19 Sep. 2016).

Ockendon, J.R. and Tayler, A.B. (1971) 'The dynamics of a current collection system for an electric locomotive', *Proceedings of the Royal Society of London. Series A, Mathematical and Physical Sciences*, Vol. 322,(No. 1551), pp. 447-468.

ORR (2015a) *Electrification failures, overhead line, by operating route, table 2.38, 2004/05 – 2013/14*. Available at: http://dataportal.orr.gov.uk/displayreport/report/html/c420e676-3b9c-45fa-8968-fbee7850af65# (Accessed: 18 March 2015).

ORR (2015b) *ORR's Policy on Third Rail DC Electrification Systems*. Available at: http://orr.gov.uk/__data/assets/pdf_file/0017/17621/dc-electrification-policy-statement.pdf (Accessed: 22 July 2015).

ORR (2017a) *EU law*. Available at: http://orr.gov.uk/about-orr/what-we-do/the-law-and-our-duties/eu-law (Accessed: 21 September 2017).

ORR (2017b) *Monitoring Network Rail performance*. Available at: http://orr.gov.uk/what-and-how-we-regulate/regulation-of-network-rail/monitoring-performance (Accessed: 27 February 2017).

Palfreyman, T. and Hewings, D. (2013) 'The smart grid applied to railway traction systems: a vision for integration', *acrps: ac rail power supply. 6th international conference*. Leipzig, Germany, 7-8 March 2013.

Pantograph (2019). Available at: https://en.wikipedia.org/wiki/Pantograph_(transport).

Pappalardo, C.M., Patel, M.D., Tinsley, B. and Shabana, A.A. (2015) 'Contact force control in multibody pantograph/catenary systems', *Proceedings of the Institution of Mechanical Engineers, Part K: Journal of Multi-body Dynamics*.

Pombo, J. and Antunes, P. (2018) 'Recent developments in the pantograph-OLE interface', *RIA Electrification Technical Interest Group*. London, 2 Oct 2018. RIA.

Pombo, J. and Antunes, P. (2019) Informal meeting with John Morris at Huddersfield University, 17 Jan. 2019.

Powell, A. (2015) 'Assessment of TSI compliance on projects', *Railway electrification: updating the network for the 21st century*. London, UK, 25 June 2015. IMechE.

Rachid, A., Walters, S. and Mpanda, A. (2011) 'Pantograph Catenary Interaction Framework for Intelligent Control (PACIFIC)', *Railway Pro Magazine*, 2011(Nov), 24 Nov 2011.

Railway (Interoperability) Regulations (SI 2011/3066).

Railway Codes (2018) *Overhead line electrification neutral sections (OHNS)*. Available at: http://www.railwaycodes.org.uk/electrification/neutral.shtm (Accessed: 6 Nov 2018).

Railway Gazette (2016) *The Fourth Railway Package explained*. Available at: http://www.railwaygazette.com/news/policy/single-view/view/the-fourth-railway-package-explained (Accessed: 03 May 2017).

Ren, W.-X., Chen, G. and Hu, W.-H. (2005) 'Empirical formulas to estimate cable tension by cable fundamental frequency', *Structural Engineering and Mechanics*, 20(3), pp. 363-380.

ResearchGate (2014) *Basic difference between Euler-Bernoulli and Timoshenko beam theory* [Discussion forum]. Available at: https://www.researchgate.net/post/Whats_the_basic_difference_between_Euler-Bernoulli_and_Timoshenko_beam_theory (Accessed: 7 Aug).

Resta, F., Facchinetti, A., Collina, A. and Bucca, G. (2008) 'On the use of a hardware in the loop set-up for pantograph dynamics evaluation', *Vehicle System Dynamics: International Journal of Vehicle Mechanics and Mobility*, 46(S1), pp. 1039–1052.

RIA (2016) Circulation of archive of Network Rail electrical power incidents, 2006 - 2016, 7 June 2016.

RSSB (2009) *Simulation and verification of results from 125mph current collection modelling for two pantographs – Technical report* (T841). London: SNCF RSSB.

RSSB (2011a) *'Energy Game Changer': Low cost and discontinuous electrification study: Potential to reduce the costs for electrifying GB railways report (ITLR-T27095-003)* (T966). London: Interfleet Technology, TSLG.

RSSB (2011b) *'Energy Game Changer': Low cost and discontinuous electrification study: Route to market report (ITLR-T27095-002)* (T966). London: Interfleet Technology TSLG.

RSSB (2011c) *Investigating the economics of the 3rd rail dc system compared to other electrification systems* (T950). London: RSSB RSSB.

RSSB (2012a) *PantoTRAIN summary report* (T849). London: RSSB RSSB.

RSSB (2012b) 'Technical Specification for Interoperability - leaflet'. 28 May 2012. RSSB. Available at: https://www.rssb.co.uk/library/standards-and-the-rail-

industry/technical%20specification%20for%20interoperability%20-%20leaflet.pdf (Accessed: 25 Apr 2017).

RSSB (2014a) *GL/RT1210: AC Energy Subsystem and Interfaces to Rolling Stock Subsystem*. London: RSSB.

RSSB (2014b) 'National Technical Rules - leaflet'. 11 Dec 2014. RSSB. Available at: https://www.rssb.co.uk/library/standards-and-the-rail-industry/2014-12-leaflet-national-technical-rules.pdf (Accessed: 25 Apr 2017).

RSSB (2016) *Lump mass models for legacy pantographs on GB mainline* (T1105). London: RSSB RSSB.

RSSB (2018a) Email from Shamil Velji to John Morris, 13 Aug 2018.

RSSB (2018b) *ENE TSI UK Mirror Group minutes - 19 July 2018*. London: RSSB RSSB.

Sánchez-Rebollo, C., Carnicero, A. and Jiménez-Octavio, J.R. (2015) 'CANDY statement of methods', *Vehicle System Dynamics*, 53(3), pp. 392-401.

Saxena, A. and Gilgen, M. (2011) 'Insulated overlap type neutral section for rigid overhead catenary in underground system', *PACIFIC*. Amiens, France, 8 Dec 2011.

Seddon, A.E. and Lester, J. (1992) 'Prediction as a tool', *High Speed Current Collection Seminar (S079)*. London, 24 September 1992. Institution of Mechanical Engineers.

Simanek, J. (2019) Email from Jiri Simanek (Secheron, Czech) to John Morris, 19 July 2019.

SNCF (2019) Email from Guido van Kalsbeek (SNCF) to John Morris, 22 July 2019.

The IET (2010) *Electric Traction Systems*. London, UK The Institution of Engineering and Technology.

Thelisson, G. (2012) 'Overhead line from start to finish', *Railway Gazette International*, 168 (July 2012), pp. 48-49.

Thieffry, P., Chawla, V. and Sharma, S. (2007) 'Flexible Multibody Dynamics', *ANSYS Advantage*, 1(4), pp. 32-34.

Timoshenko beam theory (2019). Available at: https://en.wikipedia.org/wiki/Timoshenko_beam_theory (Accessed: 4 May 2019).

Tur, M., Baeza, L., Fuenmayor, F.J. and García, E. (2015) 'PACDIN statement of methods', *Vehicle System Dynamics*, 53(3), pp. 402-411.

UIC (2015) 'Railway statistics 2014 synopsis'. 19 June 2015. Paris: UIC.

UIC (2019) 'Railway statistics 2019 synopsis'. 5 Aug 2019. Paris: UIC.

UNIFE (2011) 'TrioTRAIN: PantoTRAIN presentation to ERA Meeting'. 15 April, 2011. ERA Lille.

Unipart Rail (2015) *Unipart Overhead Line Catalogue Listings*. Available at: https://www.unipartrail.com/WebPDF/StockPDF/Overhead%20Line%20Catalogue%20Listings.pdf (Accessed: 7 Aug. 2015).

Vera, C., Suarez, B., Paulin, J. and Rodríguez, P. (2006) 'Simulation model for the study of overhead rail current collector systems dynamics, focused on the design of a new conductor rail', *Vehicle System Dynamics*, Volume 44(8), pp. 595-614.

Welbourn, B. (1917) 'The properties of electrolytic copper – modulus of elasticity', *Proceedings of the Institution of Electrical Engineers*, 1917, pp. 53-54.

Wheeler, J.C.G. (1975) *The development of a new design of ceramic collar insulator* (TM-ETR-059). Derby: British Rail Research, British Rail Research.

Wheeler, J.C.G. (1980) *The initial development of a skidless design of neutral section* (TM-ETR-132). British Rail Research, British Rail Research.

Wheeler, J.C.G., Bradwell, A. and Billinge, R.H. (1979) *The high speed filming of pantograph passages though Leighton Buzzard neutral section* (TM-ETR-117). Derby: British Rail Research, British Rail Research.

Wheeler, J.C.G., Bradwell, A. and Billinge, R.H. (1980) *The interaction of APT and service pantographs with neutral sections* (IM-ETR-034). Derby: British Rail Research, British Rail Research.

Wheeler, J.C.G., Bradwell, A. and Tansley, J. (1978) *Recent failures of 40,000 series ceramic bead insulators* (TM-ETR-105). Derby: British Rail Research, British Rail Research.

Zhou, N., Lv, Q., Yang, Y. and Zhang, W. (2015) '<TPL-PCRUN> Statement of methods', *Vehicle System Dynamics*, 53(3), pp. 380-391.